Dissertation submitted in fulfilment of the requirements for the degree

Master of Science in Engineering

Department of Mechanical Engineering

University of Cape Town

Analysis of carbonaceous solid deposits from thermal stressing of FAMEs and FAME/diesel blends at different temperatures in a continuous flow reactor

---

Uyuenendiwannyi Mandavha

September 2015

PLAGIARISM DECLARATION

1. I know that plagiarism is wrong. Plagiarism is using another's work and to pretend that it is one's own.

2. Each significant contribution to, and quotation in, this project from the work, or works of other people has been attributed and has been cited and referenced.

3. This project is my own work.

4. I acknowledge that copying someone else's work, or parts of it, is wrong, and declare that this is my own work.

Uyuenendiwannyi Mandavha

SIGNATURE: Signed by candidate

signature removed

DATE: 06-12-15

ACKNOWLEDGEMENTS

First and above all, the author would like to thank God for giving her strength and protection while working on this project.

I would like to extend my gratitude to my sponsors; the National Research Foundation of South Africa and Sasol Technology; this project would not have been possible without the financial support you provided.

I would like to thank my supervisor, Dr Chris Woolard: firstly for granting me the opportunity to pursue my master's degree at Sasol Advanced Fuels Laboratory (SAFL). I am grateful for his guidance and much appreciated advice during the course of this project. Last but not least, I would like to thank him for the time he dedicated into hosting journal clubs. I really learnt a lot and this was a good foundation for my thesis. It provided a platform to share ideas with other people within your field gave me more knowledge about my project.

I also would like to thank Mrs Miranda Waldron, Mr Mohamed Jaffer and Dr Innocent Shuro from the Electron Microscope Unit (EMU) at the University of Cape Town (UCT) for helping me with microscopy images for my samples. Their patience and willingness to assist was greatly appreciated.

I would like to extend my gratitude to Mr Fletcher Hiten from the Central Analytical Facilities (CAF) at Stellenbosch University for performing ESI-MS on my samples.

I would like to extend my heartfelt gratitude to Mr Gerhard Lourens for helping me whenever the flow reactor was giving me problems.

I would like to thank Irénée Kaminuza for taking time from his Masters studies to show me how to operate the flow reactor and sand bath. I am truly grateful for your friendship. I would like to thank you for the time you sacrificed to proof read my thesis.

I would like to extend my gratitude to Marvelous Vukeya for assisting me with the GC-MS. Thank you for your friendship.

I would like to thank my colleagues at SAFL for the advice and support they offered me during my MSc studies.

I would like to thank my friends: Livhuwani Tessa Magidi, Rabelani Rofhiwa Masindi and Akhona Vava for being such amazing friends. Thank you for your motivational words and always being there to cheer me up during hard times.

I would like to thank Koketso Charles Aphane for his support throughout this thesis. Thank you for being my pillar of strength when I felt defeated. I am grateful for the love and patience you showed me.

I would like to thank my siblings, Mandavha Rivhatshinyi, Mandavha Mbiludziavhavha, Mandavha Hudivhannyi, Mandavha Musatondwa and Mandavha Justice. I would have never made it without the unconditional love and support they gave me.

Last but not least, I would like to thank my mother Mrs Mandavha Tshiphiri Rose. Thank you for being such a wonderful mother, my rock and pillar of strength. I am grateful for the wise words that you always gave me whenever I was feeling discouraged. Thank you for supporting me and encouraging me to pursue my dreams. Thank you for giving me more love that I could ever imagine, thank you for your selfless heart. Your words will forever be embedded in my mind and in my heart.

TABLE OF CONTENTS

LIST OF FIGURES

LIST OF TABLES

LIST OF ABBREVIATIONS

amu	Atomic Mass Unit
ASTM	ASTM International (formerly the American Society for Testing and Materials)
B20	A diesel blends which contains 20% fatty acid methyl esters (v/v)
B100	100% FAME (biodiesel)
CAF	Central Analytical Facilities
CEN	European Committee for Standardisation
CFPP	Cold Filter Plugging Point
CR	Common Rail
DCA	Deposit Control Additive
DRIFTS	Diffuse Reflectance Infrared Fourier Transform Spectroscopy/Spectrometry
EBSD	Electron Backscattered Detection
EDS	Energy Dispersive Spectrometry
EMU	Electron Microscope Unit
EN 590	European Union automotive diesel fuel quality specification
ESI-MS	Electrospray Ionisation-Mass Spectrometry
ESI (-) MS	Negative Electrospray Ionisation-Mass Spectrometry
ESI (+) MS	Positive Electrospray Ionisation-Mass Spectrometry
FAME	Fatty Acid Methyl Ester
FIE	Fuel Injection Equipment
FTIR	Fourier Transform Infrared Spectroscopy
GC-MS	Gas Chromatography-Mass Spectrometry
GIF	Gatan Tridiem Image Filter
GTL	Gas to Liquids
HFRR	High Frequency Reciprocating Rig
HPDI	High Pressure Diesel Injector
HPLC	High Performance Liquid Chromatography
HRTEM	High-Resolution Transmission Electron Microscopy
JET A1	Civil aviation turbine fuel used outside the United States of America
m/z	Mass to charge ratio
PAH	Polyaromatic Hydrocarbon

PLOM	Polarised Light Optical Microscopy
ppm	parts per million
QCM	Quartz Crystal Microbalance
RME	Rapeseed Methyl Ester
RME20	20% RME, blended with 80% EN590 reference diesel (v/v)
SAFL	Sasol Advanced Fuels Laboratory
SEM	Scanning Electron Microscopy
SME	Soybean Methyl Ester
SME7	7% SME, blended with 93% EN590 reference diesel (v/v)
SME20	20% SME, blended with 80% EN590 reference diesel (v/v)
SME50	50% SME, blended with 50% EN590 reference diesel (v/v)
SMORS	Soluble Macromolecular Oxidatively Reactive Species
SS 316	Stainless Steel 316
syn air	synthetic air
TEM	Transmission Electron Microscopy
TGA	Thermogravimetric Analysis
TGA-MS	Thermogravimetric Analysis-Mass Spectrometry
TPO	Temperature Programmed Oxidation
UCT	University of Cape Town
UHP	Ultra High Purity
USA	United States of America
UV – Vis	Ultraviolet-Visible (spectroscopy)
v/v	percentage/fraction by volume
wt.%	mass (or weight) percentage

ABSTRACT

Fuel deposits are carbon-rich high molecular weight species that are formed from the degradation of fuel. Diesel deposits may form on vital parts of a vehicle's engine or fuel system such as the fuel injectors. Once these deposits have formed, they can block the spray holes of the injector and may also cause moving parts within the injector to stick. Diesel deposits can cause engine failure, engine malfunction and affect engine performance.

This study aims to investigate early stage deposits, formed in laboratory reactors, in particular a flow reactor. This was performed in order to gain insight into the processes by which these deposits form and what factors influence their formation. A flow reactor and closed sand bath reactor were employed to produce carbonaceous deposits, with the aim being that these might be similar to those formed in diesel injectors. The solid deposits were analysed using a Temperature Programmed Oxidation (TPO), Transmission Electron Microscopy (TEM) and Scanning Electron Microscopy (SEM). Soluble deposit precursors from the stressed fuels were assessed using ultraviolet visible spectroscopy (UV-Vis) and electrospray ionisation-mass spectroscopy (ESI-MS) in order to provide further insight into the chemical processes preceding deposit formation.

The test fuels stressed in this study were an EN 590 reference diesel and two fatty acid methyl esters (FAMES), *viz*. rapeseed methyl ester (RME100) and soya methyl ester (SME100). Binary blends of 80 % EN 590 diesel and 20 %RME (RME20), 80 % EN 590 diesel and 20 % SME(SME20), 50 % EN 590 diesel and 50 % SME (SME50) and 93 % EN 590 diesel and 7 % SME (SME7) (v/v) were also investigated. Aerated fuels were thermally stressed at 300°C and 400°C for 5h in the presence of oxygen in a continuous flow reactor.

This study represents the first application of the flow reactor methodology to systems that contain fatty acids methyl esters (FAMEs). The flow reactor results conducted at 300°C for 5h yielded deposits from EN 590 diesel and SME20 whereas SME100, RME20 and SME20 did not show any discernible deposits. The low deposition in FAME and FAME/diesel blends was attributed to the high solvency of the fuels. The TPO profile and microscopy images suggested the deposits were formed from nucleation and growth in the fluid phase owing to their spherical morphology.

Results from experiments conducted at 400°C in the flow reactor indicated that the test fuels had different deposition tendencies relative to each other. The amount of deposits formed from each fuel was as follows: 68 μg/cm^2 for the tube section from the top of the reactor stressed with EN590 diesel, 131 μg/cm^2 (the tube section from the middle section of the flow reactor stressed with EN590 diesel), 112 μg/cm^2 (B100, RME), 33 μg/cm^2 (B100, SME), 212 μg/cm^2 (B20, RME) and 380 μg/cm^2 (B20, SME).The high deposition of B20 blends was ascribed to the unsaturated double bonds along the fatty acid backbone of these FAMES which makes them prone to oxidation. The carbonaceous deposits displayed spherical morphology. The presence of graphene sheets is strongly suggested by the interference fringes observed. The morphology of the spheroidal deposits seemed to suggest that they were formed by homogeneous nucleation and growth in fluid phase. Large polyaromatic molecules were suggested to have been the basic building blocks of the spherical deposits.

The effect of different percentages of FAME on the solvency of the bulk fuel was investigated using SME7, SME20, SME50 and SME100 at 400°C for 5h in a flow reactor. The results showed that the deposition propensity increases with a decrease in the FAME concentration of the blend. The presence of the non-polar EN 590 in the blend reduces the polarity of the bulk fuels and consequently the polar oxidation products precipitate out of solution.

Zinc neodecanoate was added to the test fuels to assess the effect of trace metal dissolved in the fuel of the deposit formed. Adding zinc to the test fuels was found to increase deposition. The effect was more pronounced in B100 (rapeseed and soybean) fuels that for the EN 590 reference diesel. The quantities of deposits formed were 425 μg/cm^2 (EN590 diesel top), 377 μg/cm^2 (EN590 diesel middle), and 2970 μg/cm^2 (RME100), 2625 μg/cm^2 (SME100). The pronounced deposition in B100 was attributed to the catalytic effect of zinc on the oxidation of FAME.

No discernible deposits were observed to form in closed bomb reactors which contained fuel and synthetic air at 300°C. The test fuels, however, showed distinct colour changes that were accompanied by an increase in absorbance when analysed in the UV-Vis spectral range.

1. INTRODUCTION

1.1 Background and motivation for this study

Deposit formation, within diesel fuel injection equipment (FIE), is a phenomenon that has been in existence since the inception of FIE over 100 years ago (1) . It was, however, not as large a concern as today where there is an increased demand for lower emissions and better fuel economy.

In order to meet emission regulations many measures have been taken, such as the use of fuels that produce lower CO_2, greenhouse gas and particulate matter emissions per kilometre driven. This has led to the introduction of fatty acid methyl esters (FAMEs), commonly known as biodiesel (2).

In addition to changes in the fuel, changes have also been implemented in the fuel systems, in particular the FIE technology. The reason for this technology change was to improve fuel atomisation which facilitates complete combustion. This was achieved by increasing the injection pressure and implementing high efficiency nozzles with smaller holes (3,4).

These changes have helped meet emission regulations. These changes, however, have been accompanied by some drawbacks. FAMEs contain large quantities of methyl esters of unsaturated fatty acids which make them more prone to oxidative degradation when compared to petroleum-derived diesel (5). It is possible that these FAMEs can degrade to form solid deposits that are detrimental to vital engine and fuel system components.

Once formed, deposits tend to accumulate and block the injector nozzles in FIE. The smaller injector holes in modern common rail injection systems are sensitive to even the smallest amount of deposit formed. Deposits may also form within the injector body. This causes the moving parts to stick which then delays the response of the injector (3).

The injector nozzle deposits affect the fuel spray pattern and the amount of fuel that is injected into the combustion chamber. This consequently has an effect on the engine performance, *i.e.* loss of power and eventually these deposits may lead to engine failure (1) (3).

How fuel degrades to form insoluble deposits within the fuel injection system and other vital engine components is a very complex topic, which is not well understood (1). It involves bulk liquid-phase reactions, nucleation of particles through polymerisation or clustering reactions, solubility, transport phenomena, and surface reaction (1,6,7).

Many studies have characterised deposits formed on FIE parts during field tests (8) and using simulation test bed engines (9) in an attempt to understand how they form. In addition, deposits formed during short duration accelerated degradation tests have also been analysed. Understanding the reactions by which deposit formation occur in the short period of time after fuel has been exposed to degradation conditions, is a key step in preventing early stage deposits (10).

In accelerated degradation tests, the fuel is exposed to conditions that favour deposit formation, for a short period of time. Different reactors have been employed in previous studies. These include flow reactors (8,10,11,12,13), quartz crystal microbalances (QCM) (14,15,16), closed bomb reactors (15,17) and glass flasks (15,16,18,19).

A thorough investigation of the literature revealed that, degradation studies using flow reactors have predominately focused on jet fuel. Very little work has been done on diesel fuel and, in particular, FAMEs. The aim of this study is thus to analyse carbonaceous solid deposits formed from thermal stressing of FAMEs and FAMEs blends at different temperatures in a flow reactor for a short period of time.

1.2 Objectives

The primary objective of this study was to:

- develop a technique using continuous flow reactor to mimic the formation of deposits in diesel injectors.

In addition to this, specific objectives were set in order to test the applicability of the developed technique. These objectives included:

- an evaluation of the role of fuel composition (FAME type and FAME concentration) on the amount and type of deposits formed;

- an evaluation of the effect of temperature on the amount and type of deposits formed;
- a characterisation of the chemical and morphology of the deposits formed; and
- an assessment of the effect of zinc doping the deposition potential of diesel and FAME.

1.3 Scope and limitations of the study

The primary focus of this study was to develop a technique using continuous flow reactor to mimic the formation of deposits in diesel injectors. This study, however, also evaluated the effect of FAME blending concentration, temperature and a trace metal (Zn) on the amount of deposits formed.

Test fuels used in this study were: an EN 590 reference diesel, RME20, SME20, RME100, and SME100. SME7 and SME50 were used together with SME20 and SME100 to assess the effect of blending concentration on the amount of deposits formed.

The thermal stressing temperatures evaluated in this study were 300°C and 400°C. Temperatures lower than 300°C were not evaluated in this study because preliminary experiments, conducted at 250°C, using EN 590 reference diesel generated no deposits. Kaminuza *et al.* also conducted experiments in the flow reactor at 250°C for 24 h and generated no deposits (15).

To evaluate the effect of metal on deposit formation, zinc neodecanoate was used to dope the fuels. The fuels were doped with 10 ppm zinc neodecanoate with the purpose of exacerbating conditions to promote greater deposition in the test fuel (20). These experiments were only conducted on pure diesel and FAMES and not on blends.

All the test fuels were thermally stressed using a SS 316 metal tube. Since very little deposits were formed using this tube, which is an active metal that catalyses the deposition process (12,21), no experiments were conducted using an inert metal tube such as alumina-coated SS 316 metal tube.

The solid deposits that formed on the metal surface were analysed using multiphase carbon analysis, SEM, TEM and optical microscopy. Some of the deposits, that formed on the metal

surface, had closely adhered to the surface and could not be scrapped off for analysis and as a result characterisation techniques that required deposit powder sample such as TEM could not be conducted on all the stressed tube samples.

The degraded fuel was analysed using UV-visible spectrophotometry, Fourier Transmission Infrared (FTIR) Spectroscopy, Gas Chromatography-Mass Spectroscopy (GC-MS) and Electron Spray Ionisation-Mass Spectroscopy (ESI-MS). Only UV-Vis spectroscopy and ESI-MS results proved useful techniques for monitoring oxidation products in stressed fuel. GC-MS and FTIR were found not to be useful as the changes that had occurred were too subtle to be observed when the spectra of the stressed and unstressed fuels were compared

2 LITERATURE REVIEW

2.1 Diesel

2.1.1 Diesel fuel composition

Diesel refers to a liquid fuel that is used to power diesel engines. Middle distillates with carbon number ranging from C_{10} and C_{22} and a boiling point between 250°C-370°C, produced from fractional distillation of crude oil are suitable for diesel production (22,23). Diesel comprises a complex mixture of hydrocarbons. Chemical structures of some of these hydrocarbons are illustrated in Figure 2-1 (23).

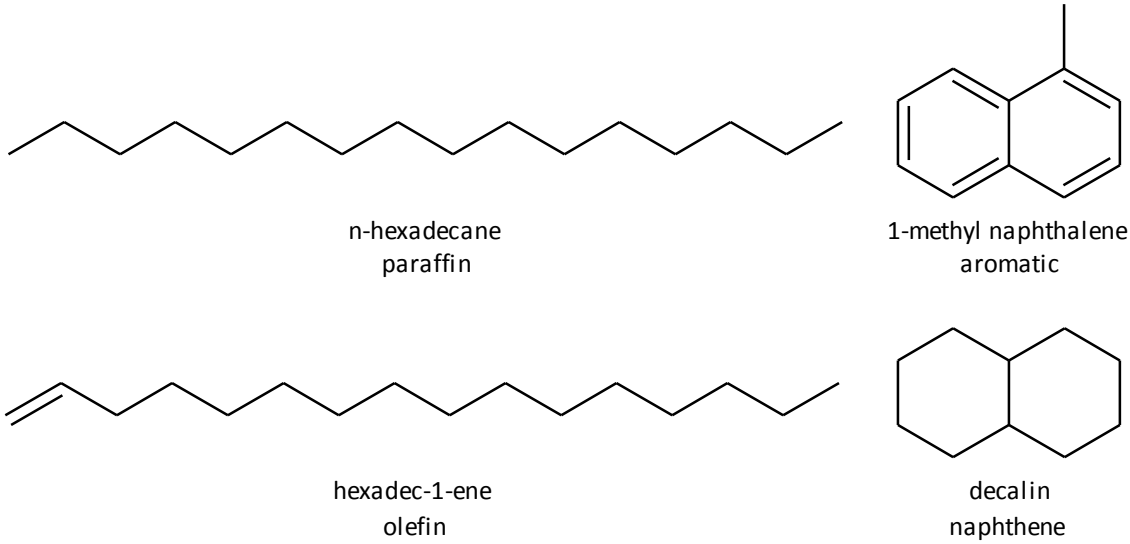

Figure 2-1: Chemical structure of hydrocarbon found in diesel fuel **(24)**.

In addition to hydrocarbons, crude oil from which diesel is made, contains small amounts of nitrogen, sulfur and oxygen, elements referred to as heteroatoms (24). Some heteroatom-containing compounds that are commonly found in diesel fuel include dibenzothiophene, carbazole and phenol. Their molecular structures are illustrated in Figure 2-2 (1) (23).

Even though heteroatom-containing compounds make up a small percentage of the molecules that are found in diesel fuel, they play a major role in determining certain fuel properties such as the stability of the fuel. This will be evaluated in the succeeding sections (1,23).

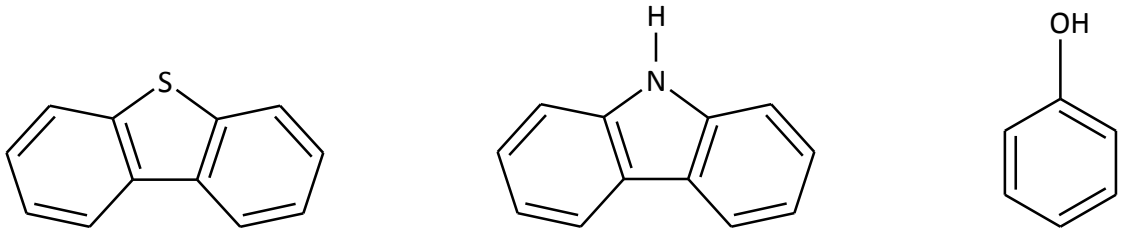

dibenzothiophene carbazole phenol

Figure 2-2: Molecular structure of heteroatom-containing compounds commonly found in diesel fuel (23).

2.1.2 Diesel engines

Diesel engines were traditionally used in heavy duty applications such as trucks, buses; farm equipment and underground mining equipment (22,25). More recently, however, diesel engines have proved to be popular in light duty applications. A major reason for this being diesel's high efficiency compared to petrol. Diesel engines are approximately 15-25 % more fuel efficient than petrol engines with the same capacities (26).

The performance of a diesel engine relies mainly on the fuel injection system which is made up of fuel injector and fuel filter amongst other parts as indicated in Figure 2-3. Fuel injection systems have been systematically modified in an attempt to control emissions, fuel consumption and driving performance (27).

Some of the changes that were made to the fuel injection equipment include the introduction of a common rail (CR) fuel injection system which has a high injection pressure. The high pressure in the common rail allows for effective air -fuel mixing which provides high power output and reduced the smoke generation (28).

Unlike traditional injection systems that rely on an engine's diesel injection pump to deliver required fuel pressure at the correct time, the common rail system does not depend on the engine's speed and load to obtain high pressure. Instead of a mechanical injection system, the amount of injected fuel is controlled by means of an electrically controlled solenoid valve (28). Furthermore, common rail systems are made of high precision components with high efficiency nozzles with smaller spray holes with dimensions of approximately 100µm (29).

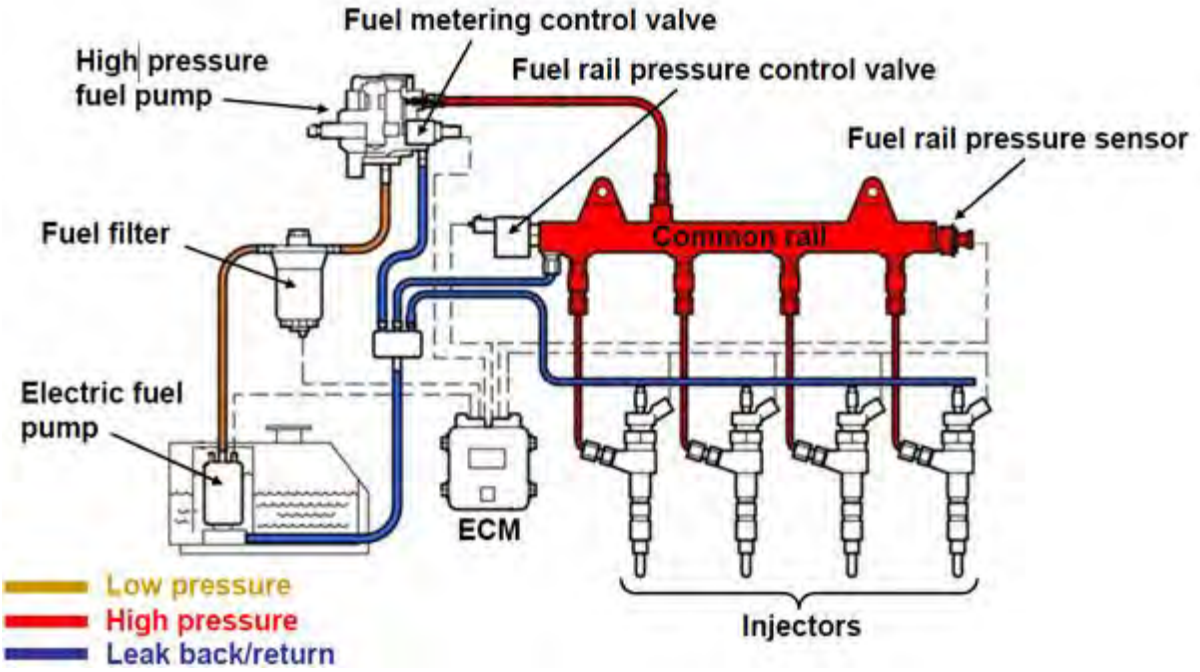

Figure 2-3: Components of the common rail injection system (reproduced from (30)*).*

There are some drawbacks associated with the common rail fuel injection systems. The higher temperature and pressure that the fuel is exposed to favour hydrogen redistribution reactions in the hydrocarbons which may lead to the formation of solid carbonaceous deposits (10). The small spray holes are sensitive to even the smallest amount of deposit.

2.2 Biodiesel composition and properties

Fuel quality has also changed in response to environmental pressures. Alternative, renewable fuels with lower carbon footprints than petroleum diesel have been introduced to power diesel engines (2,31,32). Among the alternatives for fossil diesel, biodiesel has been widely investigated due to its renewability, comparable properties to fossil fuel derived diesel and the reduction in primary emission products such as particulate matter, carbon monoxide, hydrocarbons and sulfurous oxide (32,33).

Biodiesel refers to a fuel that comprises a monoalkyl ester of long chain fatty acids, derived from renewable feedstock, such as vegetable oil, animal fat or used cooking oil (31,34). Biodiesel is produced by a transesterification process which involves the reaction of a short chain alcohol such as methanol/ethanol with a triglyceride source in the presence of a

catalyst to give a mono-alkyl ester (biodiesel) and glycerol as a by-product as shown in Figure 2-4 (31,35). Biodiesel that is produced by reacting triglyceride in the presence of methanol, are commonly used and they are referred to as Fatty Acid Methyl Esters (FAME) (32,33).

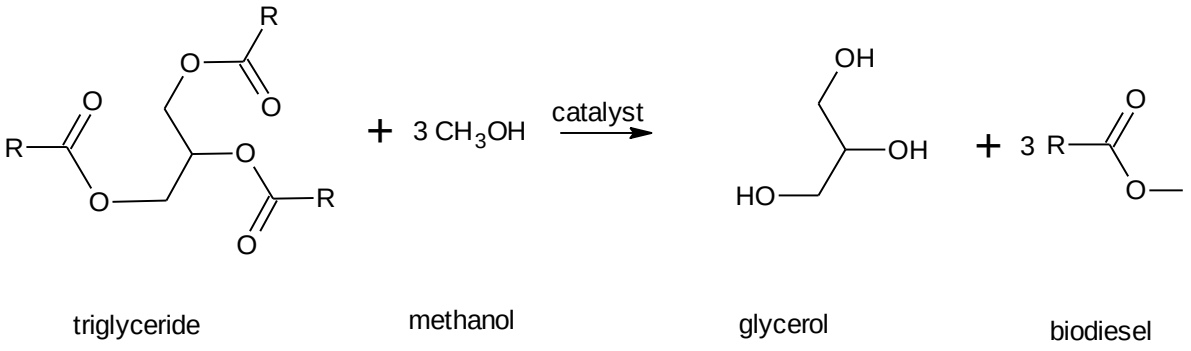

Figure 2-4: Transesterification reaction with methanol as alcohol (31).

The composition of fatty acids in FAME varies, depending on the feedstock from which it was produced from, as indicated in Table 2-1. The numbers before the colon in Table 2-1 refers to the carbon number whereas the number after the colon refers to the number of double bonds

Table 2-1: Typical chemical composition of vegetable oils commonly used in biodiesel (adapted from (22)*.*

Vegetable oil	Fatty acid distribution in wt. %				
	16:0	18:0	18:1	18:2	18:3
Rapeseed	3	1	64	22	8
Soya bean	12	3	23	55	6

In the United State of America (USA) soya bean vegetable oil is the most common feedstock and the biodiesel produced from this feedstock is referred to Soya Methyl Ester (SME) (22). In Europe the majority of the biodiesel is produced from rapeseed vegetable oil and the biodiesel produced from that is Rapeseed Methyl Ester (RME) (22,32,34).

Depending on the feedstock used, the composition of fatty acids varies in a wide range from 12 to 22 atoms. Over 90% of these fatty acids contain between 16 and 18 carbon atoms (33). The molecular structures of these fatty acids are depicted in Figure 2-5.

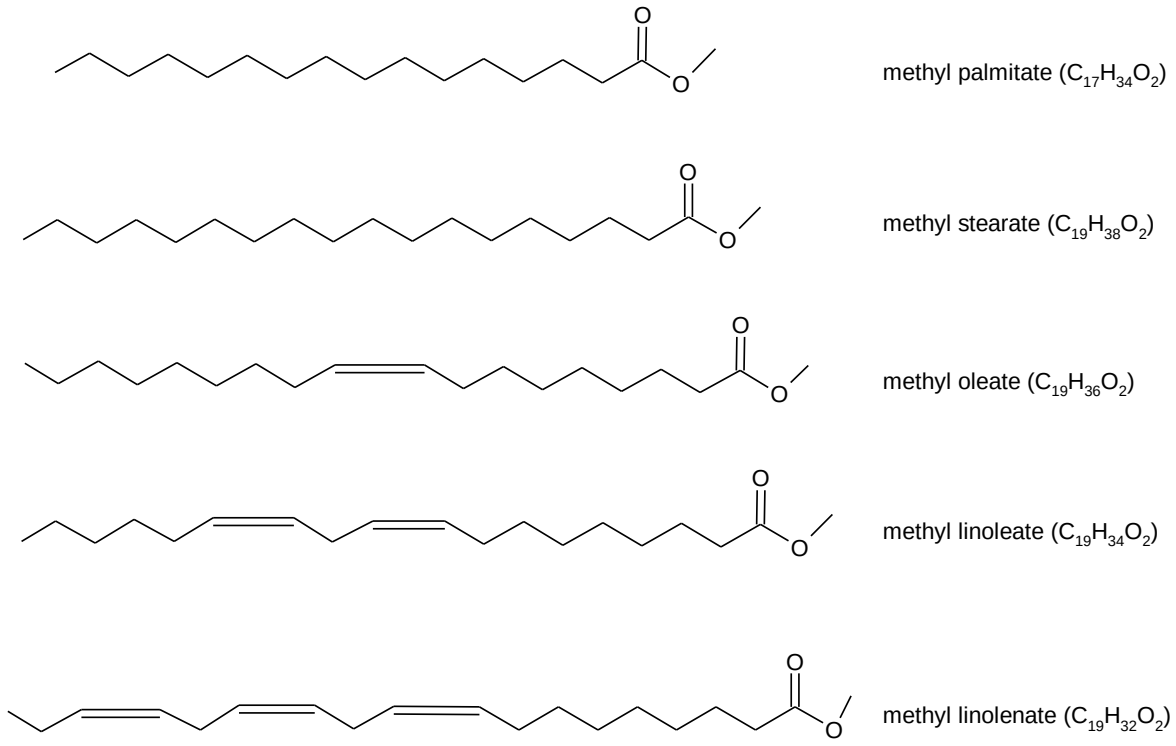

Figure 2-5: Fatty acids commonly found in SME and RME (adapted from (34)*).*

Biodiesel can be used as a pure component containing no petroleum base diesel fuel or as a blend with conventional diesel at varying levels. ASTM International and the European Committee for Standardization (CEN) have established specifications that should be met by biodiesel and biodiesel blends before they are made commercially available (32).

In Europe the EN 14214 standard has been developed for B100 (34). Another standard specification developed by the Europe standard setting organisation is the CEN TS 15940:2012. This specification allows for petroleum diesel (including gas to liquid (GTL) diesel) to be sold commercially as a neat fuel or as a blend, containing up to 7% FAME. Many market fuels in the European community contain up to 7 % FAME (36).

The ASTM D7467 standard in the USA allows for B6 to B20 (where B stands for Biodiesel) (34). In the USA the most commonly used biodiesel blend is B20. This blend is also the most commonly used blend overall due to its good balance between material compatibility, cold weather operability, performance, emission benefits, and cost (37).

2.3 Fuel stability

The problem of fuel instability exists throughout the life cycle of fuel; from when it is produced in the refinery until it is used to power the engine. Fuel is considered unstable when it undergoes chemical changes that produce undesirable consequences such as deposits, increased acidity and changes in colour (1).

The stability of fuel can be divided into two general classes: storage stability and thermal stability (38). When fuel is kept in storage for an extended period of time, it may undergo what is known as storage instability. Fuel becomes unstable because of interactions it has with the environment it is exposed to. This might include contaminants and light (38).

During engine operation, fuel can degrade via thermal degradation, depending on the temperature to which the fuel is exposed (39). Thermal degradation can be divided into three temperature regimes; (i) the thermal oxidative regime, (ii) a transition regime and (iii) the pyrolysis regime (40).

***Thermal oxidative regime**:* Degradation occurs when the fuel is exposed to temperature in the range of 150°C-300°C in the presence of oxygen (40,41,42). Fuel decomposition occurs by autoxidation and increases with increasing fuel temperature. The temperature of this regime is largely dependent on the fuel's properties (40).

***Transition regime**:* The temperature range for this regime ranges from 300°C-500°C. Under this condition both autoxidation and pyrolysis reactions contribute to decomposition. The decomposition rate decreases with increasing fuel temperature. This may be attributed to transition from the liquid phase to the supercritical phase which enhances the ability of the solvent to keep the species in solution or due to depletion of hydroperoxide (40).

Pyrolysis reaction regime: Thermal instability is experienced when the fuel is exposed to very high temperatures > 500°C in the absence of oxygen (40,42). Pyrolysis proceeds through a free-radical chain reaction process yielding many products. These free radicals are produced by breaking of the carbon-carbon bonds. At such high temperatures, direct pyrolysis dominates and decomposition is enhanced when the temperature of the fuel increases (40).

Instability of fuel is a major concern for fuel and engine manufacturers because it leads to the formation of solid deposits. Once formed, the deposits restrict and disrupt fuel injected into the combustion chamber. As a result there is a loss in power and an increase in fuel consumption.

Figure *2-6* illustrates injector tip deposits formed after an engine had been running for 1000 h (25). It is evident from that the injector nozzle fuelled with SME100 formed more deposits compared to that fuelled with petro diesel.

Figure 2-6: An example of deposits on injector tips from an engine fuelled with petroleum diesel (left) and SME (right) (25).

How fuel degrades to form insoluble deposits within the fuel injection system and other vital engine components is a very complex topic which is not well understood (1). It involves bulk liquid-phase reactions, nucleation of particles through polymerisation or clustering reactions, solubility and transport phenomena, as well as surface reactions (6,7). The succeeding sections discuss some of the mechanisms that have been proposed to lead to deposit formation in both diesel and FAMEs.

2.4 Mechanism of diesel deposits formation in the thermal oxidative regime

Several factors affect the stability of diesel fuel. These include temperature, oxygen content fuel composition and the composition of the metal to which the fuel is exposed (10,38). With regards to fuel composition, stability generally decreases in the order paraffins > naphthenes (cycloparaffins)> aromatics > olefins (alkenes) when oxygen is present in the stressing environment. Petroleum-derived diesel is more stable under storage and thermo-oxidative conditions than biodiesel because biodiesel contains a greater amount of molecules with double bonds (1).

Oxidative degradation of diesel fuel has been proposed to occur by a set of reactions categorised as initiation, propagation and termination as indicated in

Figure 2-7: Oxidation of hydrocarbon by free-radical chain reaction .

It is suggested that when the hydrocarbon species present in diesel are exposed to oxygen (dissolved in the fuel or from the atmosphere) at high temperatures, the fuel then, undergoes a free radical chain reaction that results in hydroperoxide formation .

Once formed, the hydroperoxides are likely to decompose to form polar low molecular weight species such as aldehydes, ketones, acids, and alcohols. The low molecular weight products undergo further condensation and polymerisation through the reactions depicted in Figure 2-8 to form high molecular weight species referred to as oligomers. These condensation reaction cycles continue and eventually the oligomers precipitate out of solution to form gums and deposits formation on vital engine parts .

.

Initiation

$$RH \xrightarrow{\Delta} R^{\bullet} + H^{\bullet}$$

Propagation

$R^{\bullet} + O2 \longrightarrow ROO^{\bullet}$

$ROO^{\bullet} + RH \longrightarrow ROOH + R^{\bullet}$

Chain branching

$ROOH \longrightarrow RO^{\bullet} + HO^{\bullet}$

$RO^{\bullet} + RH \longrightarrow ROH + R^{\bullet}$

$HO^{\bullet} + RH \longrightarrow H_2O + R^{\bullet}$

Termination

$R^{\bullet} + R^{\bullet}$

$ROO^{\bullet} + R^{\bullet}$

$ROO^{\bullet} + ROO^{\bullet}$ $\longrightarrow$ *alcohol, aldehyde, ketones, acids*

$RO^{\bullet} + R^{\bullet}$

Figure 2-7: Oxidation of hydrocarbon by free-radical chain reaction (43).

It is suggested that when the hydrocarbon species present in diesel are exposed to oxygen (dissolved in the fuel or from the atmosphere) at high temperatures, the fuel then, undergoes a free radical chain reaction that results in hydroperoxide formation (29,43).

Once formed, the hydroperoxides are likely to decompose to form polar low molecular weight species such as aldehydes, ketones, acids, and alcohols (10,29,43). The low molecular weight products undergo further condensation and polymerisation through the reactions depicted in Figure 2-8 to form high molecular weight species referred to as oligomers. These condensation reaction cycles continue and eventually the oligomers precipitate out of solution to form gums and deposits formation on vital engine parts (43,44).

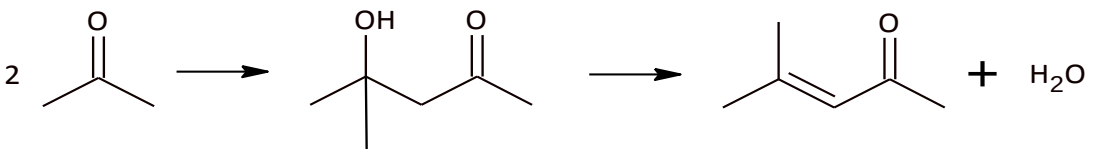

Figure 2-8: Reaction showing condensation and polymerisation reactions of primary oxidation products (43).

2.4.1 Soluble macromolecular oxidatively reactive species (SMORS) mechanism

Thermal oxidative deposits in middle distillates do not result from hydrocarbon species only. Heteroatom-containing species have also been proposed as precursors of thermal oxidative deposits in middle distillates (18,19,45). A different reaction pathway has been proposed to account for the influence of heteroatomic species in deposit formation (46). The reaction mechanism which was developed is referred to as SMORS mechanism. The process involves the reacting of low-molecular-weight heteroatomic molecules, such as phenol and indoles into higher molecular weight structures.

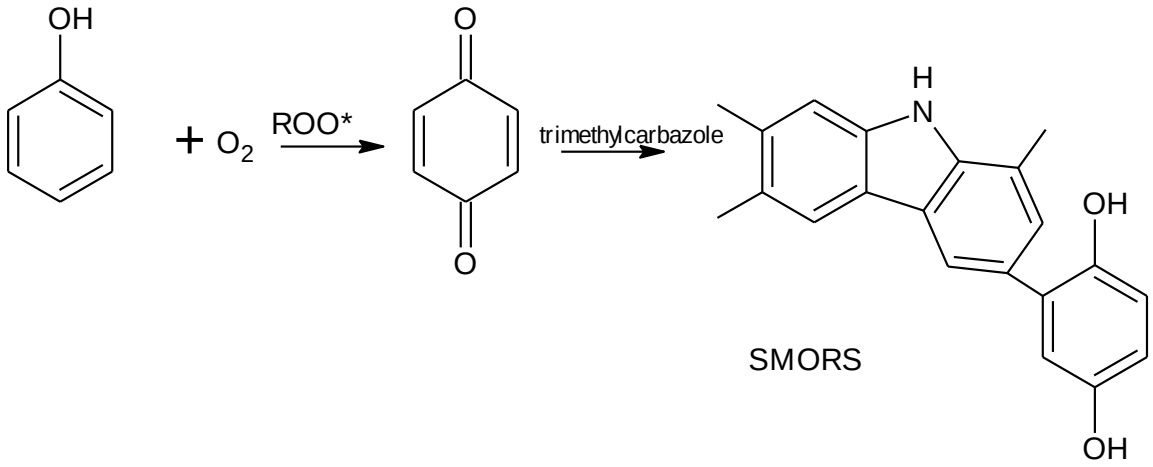

Figure 2-9: SMORS mechanism for thermal oxidation of middle distillates (reproduced from (45)*).*

An example reaction, showing the formation of a SMORS molecule, is shown in Figure 2-9. A heteroatom-containing compound, phenol, which is often found in middle distillates, reacts with oxygen and a hydroperoxide to form 1, 4-benzoquinone. The quinone readily reacts with an electron rich heterocycle such as trimethylcarbazole to produce low molecular weight SMORS as indicated in Figure 2-9 (45). It is important to note that the reaction scheme shown in Figure 2-9 and the SMORS mechanism is meant to be generic and is applicable to a variety of other compounds in addition to the ones shown in Figure 2-9 such as carbazoles, quinones, pyrroles, anisoles and indoles (45).

SMORS have higher polarity and are highly reactive compared to the phenol compounds from which they are produced. As a result they readily undergo oxidation and coupling cycles until high molecular weight species (> 900 Da) with high polarity are produced. These compounds are insoluble in fuel and are they precipitate out to form what are referred to as thermal oxidative deposits (19).

2.5 Mechanism of FAME deposit under the thermo-oxidative regime

The presence of a high amount of unsaturated fatty acid methyl esters in FAMEs makes them more prone to oxidation compared to diesel. The degree of FAME oxidation is dependent on the amount and configuration of the unsaturated fatty acid esters (29,47,48,49,50)

The configuration of the polyunsaturated olefins in the fatty acid chain is typically methylene interrupted instead of conjugated as shown in Figure 2-5 (51,52). The methylene carbon atoms between two double bonds are referred to as *bis*-allylic carbon atoms. The higher the number of double bonds in the fatty acid chains the more *bis*-allylic carbon atoms present. The relative rate of oxidation for C_{18} methyl esters is linolenic (18:3) > linoleic (18:2) >> oleic (18:1) (47).

It has been proposed that the site of first attack during FAME oxidation is at a *bis*-allylic carbon. The hydrogen located at this position is weakly bonded and can be easily abstracted (49,52). A proposed mechanism for methyl linoleate degradation is depicted in Figure 2-10. Once the hydrogen is abstracted a free radical is formed. In the presence of excess oxygen the radical rapidly reacts with oxygen to form conjugated peroxide radical. The peroxy radical reacts with a hydrogen atom to form hydroperoxide which is the primary oxidation product and a precursor for deposit formation (48).

The hydroperoxide decomposes to form secondary oxidation products such as aldehydes, alcohols and acids which can participate in condensation reactions to form oligomers (53). The peroxide radicals can also interact to form high molecular weight dimers and oligomers (9,48,52).

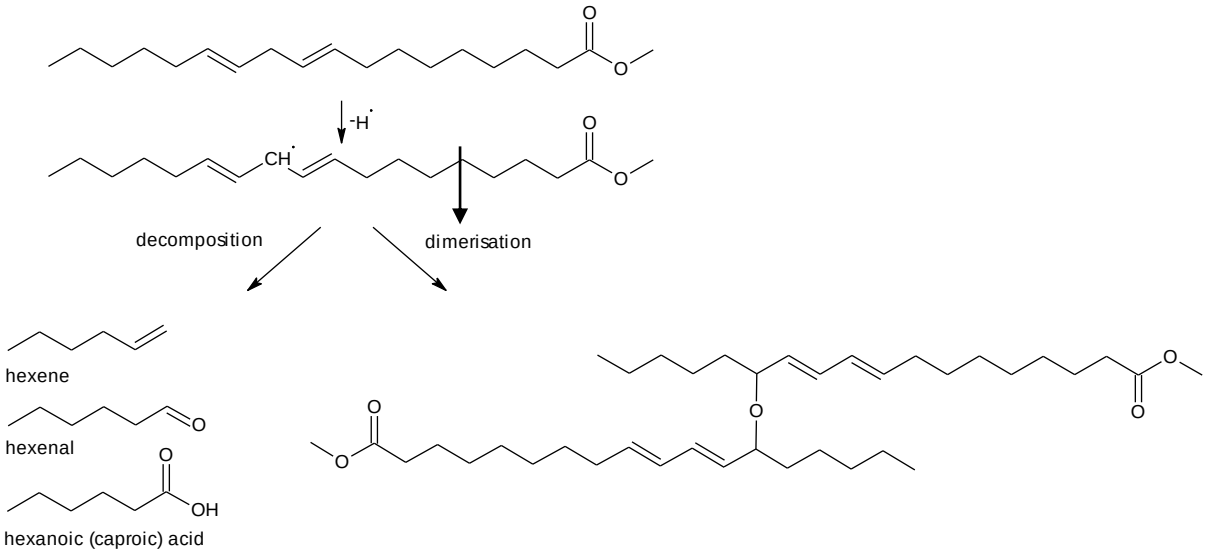

Figure 2-10: Proposed reaction pathway for the thermo-oxidative degradation of methyl linoleate; (a) decomposition, and (b) dimerization (48).

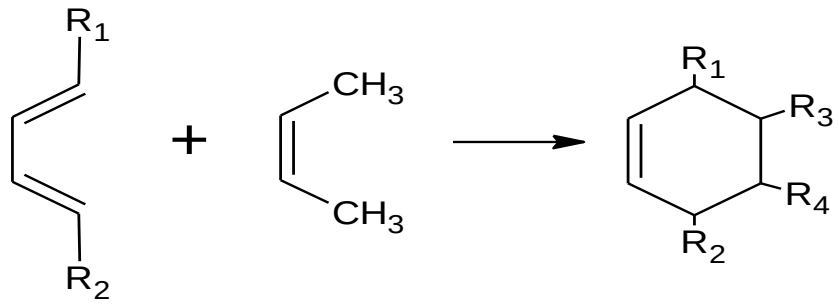

Figure 2-11: Mechanism for the formation of high molecular weight species via Diesel-Alder reactions.

At higher temperatures, between 250 and 300°C, or above, the methylene-interrupted configuration begins to isomerise to form a stable conjugated structure (38). Conjugated dienes are primary products from this reaction. They can further react with a single olefin group from the fatty acid chain to form a cyclohexene as indicted in Figure 2-11. The reaction is referred to as a Diels-Alder reaction (38,51,53).

The products from these reactions are usually dimers although trimers can also be formed when isolated double bonds from a dimer side chain react with a conjugated diene from another fatty acid chain (38).

2.6 Effect of fuel solvency on the formation of diesel deposits

When the polarity and molecular weight of the fuel degradation products exceeds the solubility barrier imposed by bulk the polarity of a fuel, the oligomers precipitate out of solution to form gums and solid deposits (54,55). The extent to which the bulk fuel is able to retain the high molecular weight polymers in solution is known as the solvency effect (55).

The high molecular weight species that are produced from the reaction mechanism in the preceding sections consists of a wide variety of polar oxygenated products (28 (54)). The high molecular weight products tend to stay in solution when formed from highly polar fuel such as FAME, which is inherently polar and an excellent solvent for polar species (51).

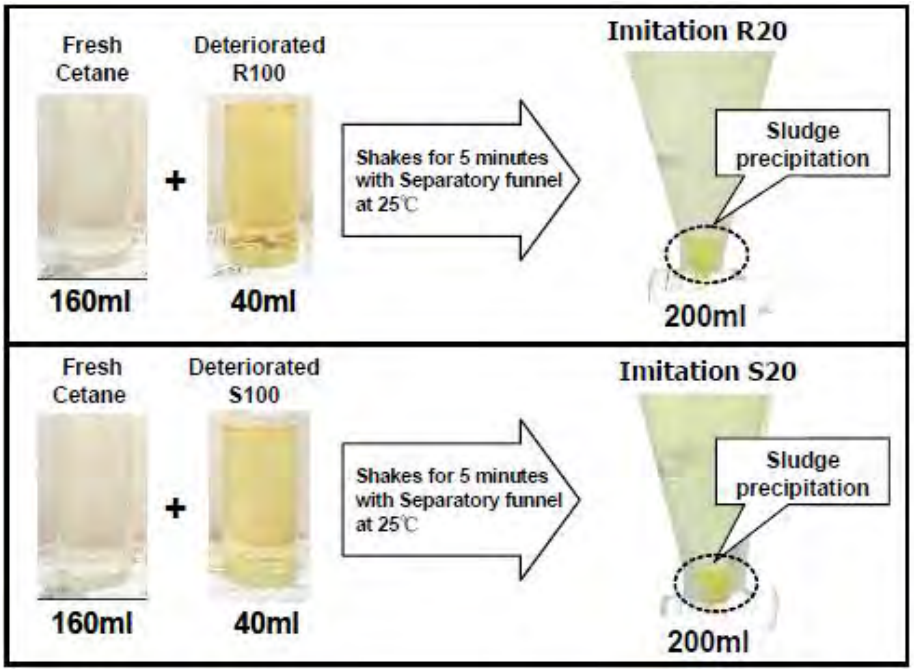

Figure 2-12: Deposit precipitation caused by the mixing of a fresh petroleum diesel model compound, n-hexadecane, and deteriorated biodiesel (56).

Blending pure biodiesel with petroleum diesel has been found to decrease the bulk polarity of the fuel, due to the low solvency of petroleum diesel (51,54,55). As the level of biodiesel in the blend decreases the bulk polarity of the fuel decreases, the reduced solvency may facilitate soluble material in biodiesel portion to become insoluble and precipitate out of solution (54,55).

Osawa *et al.* blended deteriorated rapeseed methyl esters (RME) and deteriorated soybean methyl esters (SME) with *n*-hexadecane (a model compound for fresh petroleum diesel). The FAMEs had previously been heated for 16h at 115°C in an FIE simulation test rig. No precipitates were noted from the heated fuels. Colour changes were, however, observed. After mixing the degraded FAME with n-hexadecane, however, a sludge layer precipitated out of solution and two layers with different colours were observed as in Figure 2-12 (56).

Vukeya investigated the solvency effects of the fuel by stressing biodiesel/diesel blends of different percentages in the QCM. The mass accumulation was found initially to rapidly increase when FAME was added but then to decrease with as increase in biodiesel percentage as can been seen in Figure 2-13. The lowest mass was accumulated from RME100 and the highest mass was accumulated from RME10 (16).The result from this study imply that as the concentration of FAME increases in the blend, the mass of deposits that accumulates/deposits decreases.

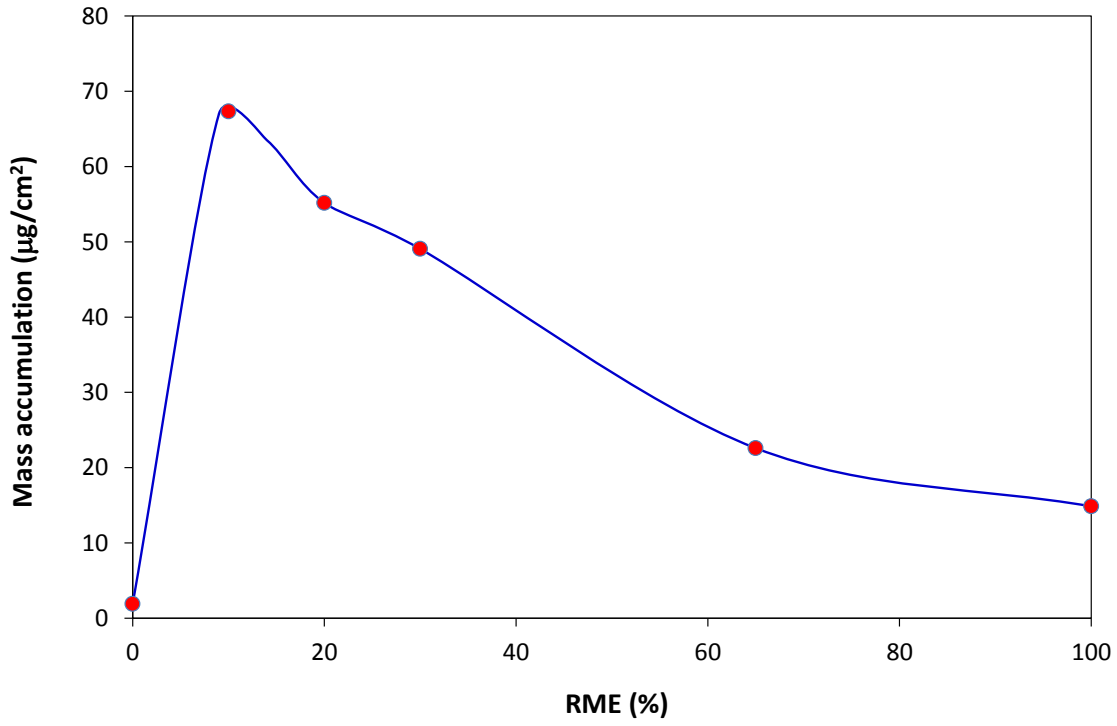

Figure 2-13: Biodiesel percentage versus mass accumulation for biodiesel/diesel model compounds blends (reproduced from **(16)***).*

2.7 Characterisation of soluble deposit precursor

High molecular weight species that are present in the fuel can manifest through changes in the colour of the degraded fuel. It is important to note that, colour on its own does not give a clear guide of the extent of oxidation. Analysis of the other factors such as viscosity, fuel composition and molecular weight of the degraded fuel, can be used to evaluate the extent of oxidation of a fuel (1). The changes in molecular weight and composition of the fuel can be monitored using spectroscopic techniques.

2.7.1 Ultraviolet-visible (UV-Vis) spectroscopy

Ultraviolet visible spectroscopy is a useful technique that is commonly used in analytical chemistry for the quantitative determination of different analytes, such as transition metal ions, highly conjugated organic compounds, and biological macromolecules. Recently this technique has been employed in characterising FAME and monitoring oxidation products of degraded FAME (57,58).

UV-Vis spectrophometers uses electromagnetic radiation between the wavelength of 190 and 800 nm which is divided into the ultraviolet (190-400 nm) and the visible (400-800 nm) regions. A quartz cell containing solution is placed in the path of a light beam and the spectrum is recorded by varying the wavelength of the incident light (59,60).

Different light source are used depending on the regions being studied; in the ultraviolet region a deuterium arc lamp is used as a light source whereas in the visible region a tungsten-halogen lamp is used as a light source (61).

When the light passed through the solution is absorbed, the energy from the light causes changes in the electronic energy levels within molecules present in solution. Electrons are transferred from a bonding (π, σ) or non- bonding (n) orbital into an empty anti-bonding (π^*, σ^*) orbital. The possible electron transfers that the light might cause are depicted in Figure 2-14 , with those common with the UV-Vis region highlighted by the red arrows (59,60,61).

The σ- σ^* transition depicted by the black arrow in Figure 2-14 is a high-energy transitions that involves very short wavelength ultraviolet light (< 150 nm). As a result it usually falls

outside the generally available measurable range of UV-visible spectrophotometers (200-1000 nm) (59).

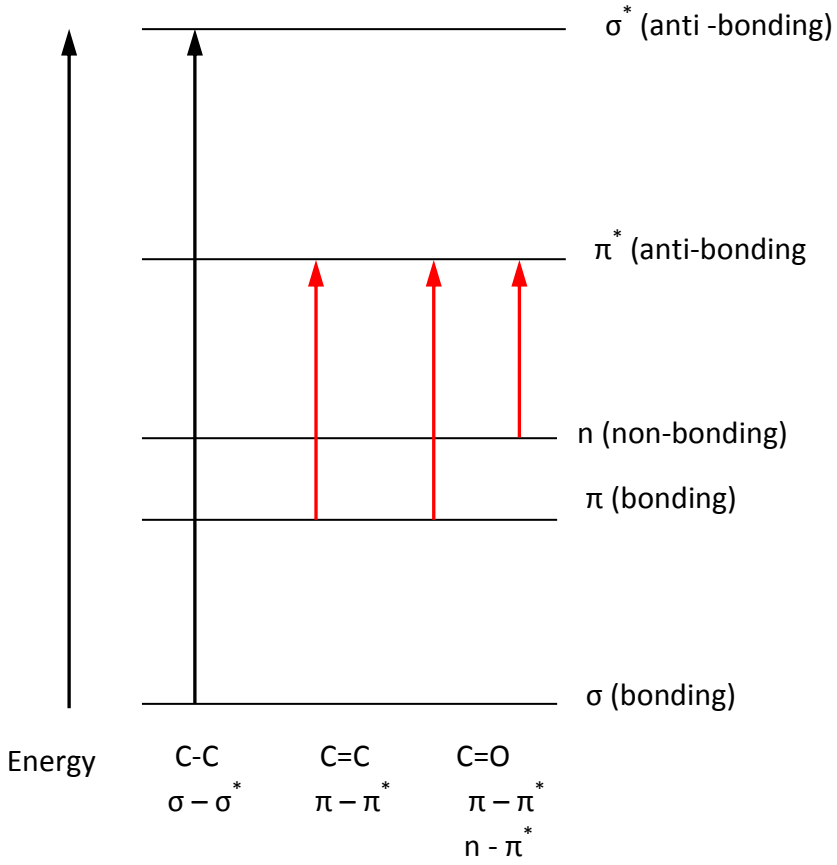

Figure 2-14: Electron transitions in ultraviolet/visible spectroscopy.

If the molecules in solution contain chromophores, a narrow absorbance bands will occur at a wavelength that is highly characteristic of the difference in energy levels of the absorbing species (61). A chromophore refers to a light absorbing species in a molecule. Some chromophores that absorb light in the UV-visible region include conjugated unsaturation (C=C-C=C), aromatics compounds (C=C) and unsaturated non-bonding electrons (C=O) which may be present in ester group in FAMEs (59,61).

There is typically a linear relationship between the number of molecules that absorb light at a given wavelength and the absorbance according to the Beer-Lambert Law. It follows that the higher the concentration of light absorbing species in a molecules the higher the absorbance intensity at a given wavelength (59,61). Additional information on the principles of UV–visible spectroscopy can be found in (59,61).

In fuel stability experiments, this technique has been used primarily to characterise biodiesel changes and monitor the presence of primary (peroxides and conjugated dienes) and secondary products (ketone, acids and alcohols) present in the fuel after thermal degradation (60).

Singer *et al.* used UV-Vis spectroscopy to monitor deposit precursors, formed after mineral diesel and diesel/biodiesel blends were degraded at varying temperatures and for different stressing times. The colour of the degraded fuel changed after stressing for 5h. Furthermore the absorbance of the stressed fuel increased when compared to the unstressed fuel.

Absorption peaks were noted around 225-235 nm, 240-275 nm and 280-400 nm. The absorption at 225-235 nm was attributed to the presence of π-π^* transitions of conjugated dienes whereas the peak at 240-275 nm was attributed to diketone and unsaturated ketones which indicated the formation of secondary products. The peak at 280-400 nm was assigned to n-π^* transition due to carbonyl groups (29). Similar oxidation behaviour has been observed in other studies (57,58,60,62,63,64).

The absorption peaks around 232 nm and 279 are often used to monitor thermal-degradation of FAMEs as these wavelengths are said to be strongly affected by primary and secondary oxidation products, *i.e* ketones, aldehydes and acids (58).

Li *et al.* used this technique to monitor oxidation rate in hydrocarbons. Most of the fuels showed absorption bands at 280-400 nm which were attributed to transition of C=O group formed as a results of thermal oxidation (65). Commodo *et al.*, also observed C=O absorptions in degraded jet fuel (42). Absorption peaks observed at lower wavelengths in the range of 200-300 nm have been attributed to the presence of C=C transitions in aromatic hydrocarbons present in the fuel (63,66). Vukeya used UV-Vis spectroscopy to monitor colour changes brought about by oxidation. It was found that, the more vulnerable the FAME was to oxidation, *i.e. the* greater degree of unsaturation the darker the colour of the stressed fuel after extended stressing at 140^{o}C. The darkening in colour and the increase in absorption was suggested to be due to the presence of oxygenated species (ketone and carboxylic acids) in the stressed fuel. The absorption peaks in this study were also in the range 270-320 nm (15).

2.7.2 Electrospray ionisation-mass spectroscopy (ESI-MS)

The ESI-MS technique has been mostly used to determine molecular weights of macromolecules such as intermediate molecular mass polymers, biomolecules and inorganic and organometallic complexes (7). The use of this technique in petroleum characterisation is relatively new, the reason being that this technique is traditionally considered suitable for characterising molecules that have polar functionalities. Petroleum, however, is largely composed of a mixture of non-polar hydrocarbons (67). Nonetheless, the heteroatoms (nitrogen, sulfur and oxygen), contained in the fuel, are polar and can be ionised by ESI-MS. Furthermore the products that are formed when fuel degrades are polar in nature and can also be ionised using ESI-MS.

ESI-MS uses electrical energy to assist the transfer of ions from solution into the gaseous phase. A sample of solution is injected into a capillary tube and drawn to the tip where a high voltage is applied to the solution, thereby producing fine charged droplets. As the droplets move, the solvent from the droplets is evaporated and smaller charged droplets are formed due to electrostatic repulsion of like charges. The evaporation of solvent and fission to smaller droplets is repeated until the droplets become small enough that the sample ions are liberated in the gas phase. Figure 2-15 shows a scheme of how the electron spray is ionised (68).

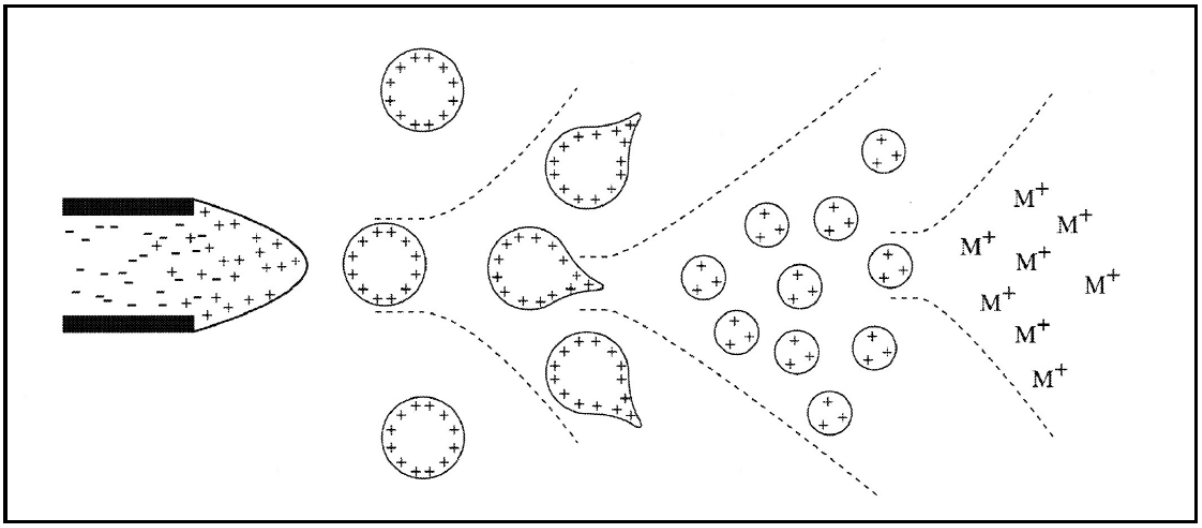

Figure 2-15: Scheme of electrospray ionisation (68).

The gas phase ions are passed through a mass spectrometer where they are detected according to their mass/charge (m/z) ratio. Depending on the mode that the ESI-MS is being operated in, ions will either undergo protonation $[M + nH]^{n+}$ or deprotonation $[M - nH]^{n-}$.

ESI-MS is a soft ionisation technique when compared to more traditional fuel diagnostic techniques such as GC-MS. As a consequence macromolecules can be ionised using this technique with little or no fragmentation of the target molecules (69). In addition, the low volatility and thermal instability of highly polar compounds is not an issue with this technique (70).

In recent years, ESI−MS has been employed for the analysis of many complex hydrocarbon mixtures, including diesel (69,70) and jet fuel (7,71). The technique's sensitivity to polar species, present in diesel, has been evaluated in previous studies. Rostad *et al.* used this technique to differentiate between different fuels types based on their polar components (70). Hughey *et al.* also used the technique to investigate polar species present in diesel fuel (69). Adams et al. used HPLC coupled with ESI-MS detection to identify heteroatom-containing species in jet fuel (71).

The aforementioned studies investigated polar species present in as-received fuel. Commodo *et al.* used positive ESI-MS to identify polar compounds formed from thermal stressing Jet A-1 in the presence of oxygen as well as polar compounds in neat unstressed Jet A-1 (7). ESI-MS allowed Commodo *et al.* (7) to propose a mechanism for jet fuel degradation. The soluble polar species in the m/z 250-400 range were suggested to be deposits precursors which had aggregated, polymerised and/or clustered to form insoluble precursors leading to the precipitation of solid deposits.

Compared to petroleum-derived fuels, biodiesel is inherently more polar and ESI-MS has been widely used to evaluate biodiesel fuel (47). Catharino *et al.* used ESI-MS in both positive and negative mode to identify the alcohol used in the transesterificaton process, monitor biodiesel degradation products and also to detect and estimate the residual amount of glycerine and mono-, di-, tri-glycerides (72). In negative ion mode, characteristic sets of ions corresponding to de-protonated fatty acids were detected in the unstressed biodiesel. Furthermore negative ESI-MS was employed to identify oxidation products (oxidised fatty acids) that formed after the fuel was degraded under thermal-oxidative conditions (120°C,

8h in excess air). Positive ion ESI-MS mode detected protonated fatty esters present in the fuel. This was useful in revealing the oil source and the alcohol used for transesterification (72).

Ogawa *et al*. have used positive ion ESI-MS to track the oxidation of a number of FAME model compounds. The formation of dimers which contained ketone functionalities was noted (48). Abdelnur *et al.* used positive ESI-MS to identify characteristics sets of ions found in petroleum diesel and biodiesel. Furthermore the technique was used to quantify and identify FAME/petroleum blends and detect contamination of the blends with biodiesel oil (73). FAME blends in this study were readily recognised due to the presence of characteristic FAME ions m/z 295 and m/z 589 which were attributed to protonated molecules of linoleic acid methyl esters and its proton bound dimer respectively (73).

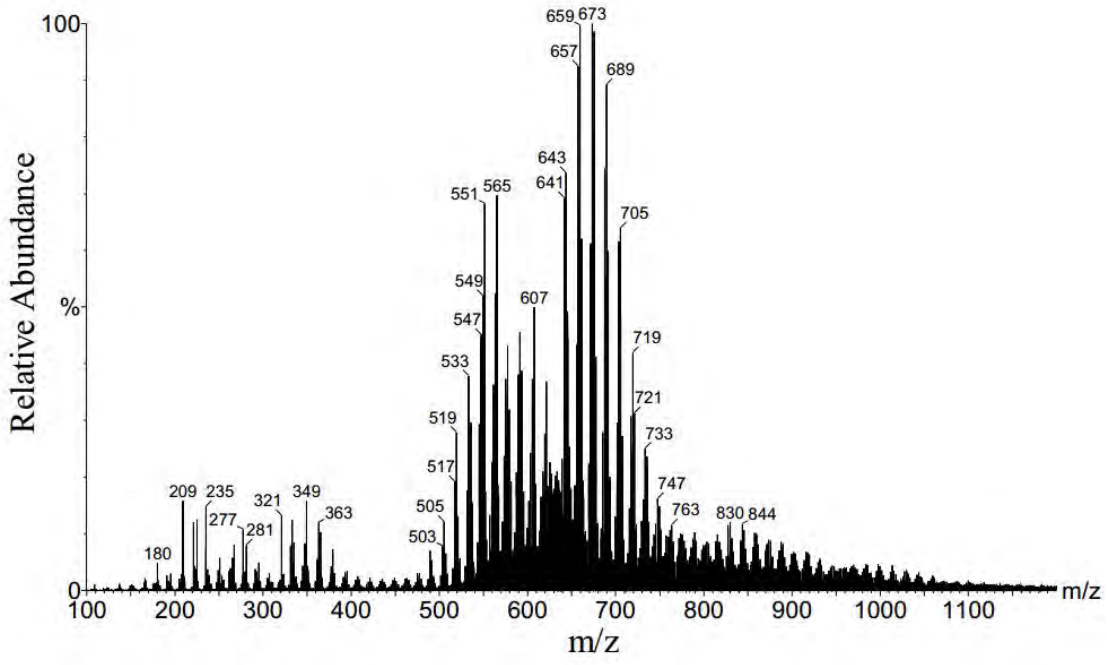

Figure 2-16: ESI-MS of high molecular fraction, fractioned from oxidised waste cooking oil methyl esters (reproduced from **(48)***) Species are* $[M+Na]^+$.

A recent study, conducted by Kaminuza, evaluated the relative stability of petroleum diesel blended with rapeseed and soya bean diesel. The oxidation products detected after thermal oxidation showed homologous series that indicated the addition of an oxygen atom with increasing m/z. In addition to this, the presence of ions with m/z ions (580-700 amu)

suggested that dimerization reaction between esters were also taking place. Figure 2-17 shows the ESI-MS spectra of the stressed SME100 at 140°C for 15h in the presence of excess air (15). Dimers are highlighted by the red box in Figure 2-17.

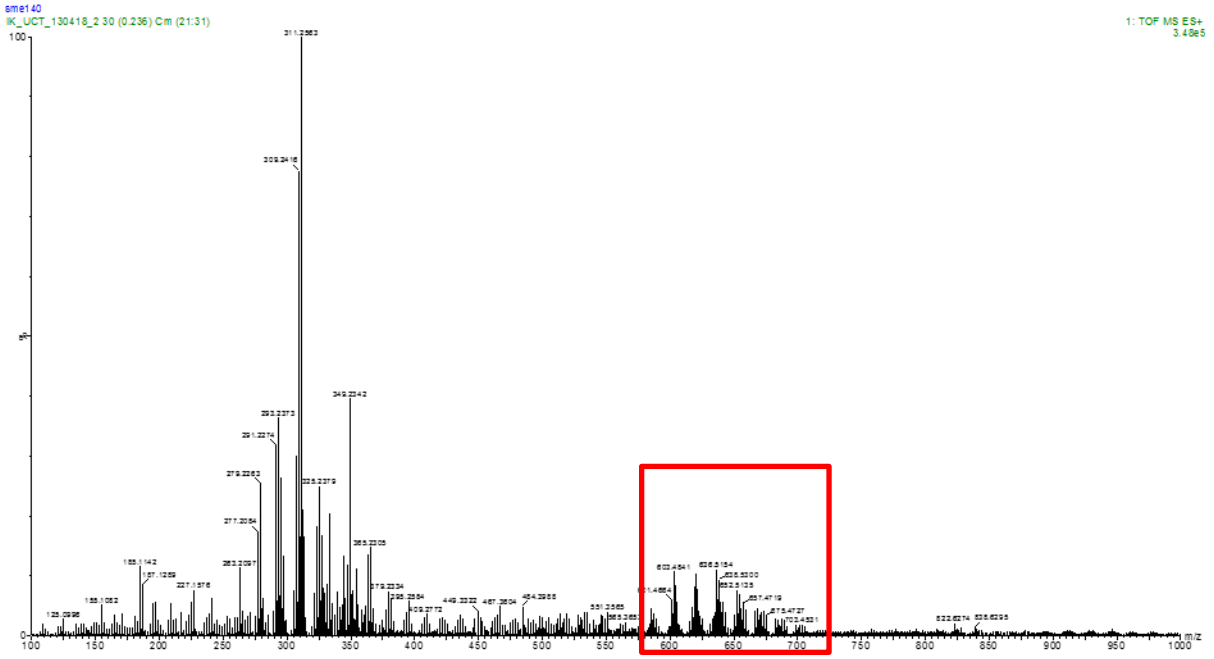

Figure 2-17: ESI-MS(+) spectrum (m/z range 100-1000) of SME, stressed in flowing air at 140°C for 15h (adapted from (15)*).*

2.8 Characterisation of carbonaceous deposits

Soluble condensation products are the principal source of deposits that eventually precipitate out of solution to form insoluble deposits (44). In order to understand how solid deposits sediment on vital engine parts, it is important to evaluate the reaction mechanism by which they form. Knowledge about the morphology and chemical nature of the deposits is useful in postulating mechanisms by which these deposits form and can help in the development of solutions to inhibit their formation (10).

Studies have been conducted using simulation apparatus such as flow reactors (8,11,12,13), fluidised sand bath reactors (15,17), quartz crystal microbalances (14,15,16) and flask reactors (15,18,19). These studies subject the fuel to high temperature, high pressure and an oxygen-rich environment for extended periods of time in order to produce deposits,

which are then characterised to gain knowledge on their morphology. Other approaches used to sample deposits, include simulation, using test bed engines. The test bed engine is operated for extended period of time, until deposits have formed on engine parts, *i.e.* injector (9). Deposits are also sampled from different engine parts of a vehicle that has been in the field for thousands of hours (8).

In order to understand early stage deposits, short duration experiments are most useful. Many of these studies, however, have investigated the morphology of jet fuel deposits produced in flow reactors for short duration experiments (10,74,75,76). Where flow reactors have been used to form diesel deposits for characterisation, the work has been restricted to petroleum diesels or model compounds (*n*-hexadecane) (10,77) as far as this author could ascertain. With the exception of some preliminary experiments by Kaminuza (15), no work has been done on FAME and FAME blends using a flow reactor.

Several types of carbon deposits have been observed when different metal-fuel combinations were investigated under thermal oxidative (10), transition (78) and pyrolytic (11,12) conditions in a flow reactor. Common deposits that have been identified in previous research include amorphous deposits and filamentous deposits (10).

AMORPHOUS DEPOSITS:

These kinds of deposits are formed when hydrocarbons degrade at relatively low temperatures (below 500°C) (10). Amorphous deposits have been suggested to form by polymerisation/condensation of hydrocarbon species to larger polynuclear aromatic hydrocarbons (PAHs) which then nucleate and grow to become carbonaceous deposit (39,79). These deposits are believed to be thermally produced and the reaction mechanism is referred to as a homogeneous reaction. The deposits forming process for amorphous deposits is believed not to be initiated by the metal surface to which the fuel is exposed (10).

FILAMENTOUS DEPOSITS:

These deposits form by catalytic decomposition of a hydrocarbon on a metal surface. Most of the metals that give rise to filamentous deposit are transition metals. A mechanism has

been proposed to account for the growth of filamentous carbon on some transition metals (79).

According to this model, filamentous carbon growth on a metal particle occurs by adsorption of the hydrocarbon on the metal surface followed by dehydrogenation and diffusion of the remaining carbon through the metal particle and precipitation out of the metal in the form of a filament (79). This type of deposit forms via a heterogeneous reaction mechanism.

2.8.1 Deposit Characterisation Techniques

Various analytical techniques have been used to characterise deposits formed from short duration simulation experiments. Some of these techniques are discussed below.

2.8.1.1 Scanning electron microscopy

Scanning electron microscope has been useful in fuel studies; to investigate the surface morphology of carbonaceous deposits (80). Venkataraman and Eser used SEM to characterise the microstructure of surface deposits stripped from a high pressure diesel injector (HPDI), which had been in the field for several hours (8). The SEM micrographs displayed in Figure 2-18, showed deposits that consisted of agglomerated spherical particles.

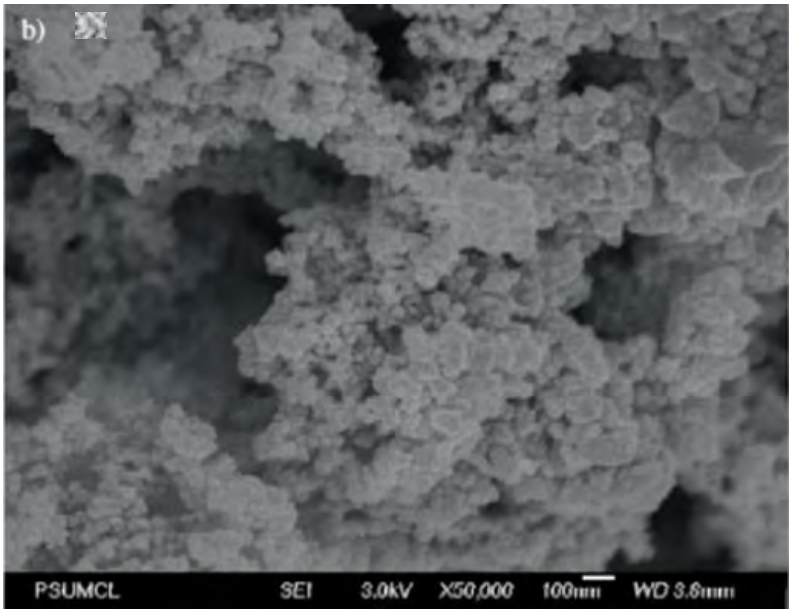

Figure 2-18: Morphology of deposits formed at the tip of a high pressure fuel injector nozzle (8) .

The individual spheroids that could be resolved in the clusters were found to have uniform size distribution. Similar morphology was observed from deposits formed from thermal stressing jet A at a furnace temperature of 260°C for 2.5h. The average size observed for individual spherical particle was reported to be approximately 90 nm (81).

Ram Mohan and Eser analysed deposits formed from thermal stressing Jet A over iron and nickel-based alloy surfaces at 350°C for 5h. SEM micrographs of the solid deposits stressed on SS316 showed four distinct morphologies indicated by the red circles in Figure 2-19. These morphologies included, metal sulfides in the form of a faceted crystallite denoted as (P), fibres denoted by (F), layers of carbonaceous thin films (A1) scattered along the length of filamentous structure and spherulitic carbon denoted by (S) (78).

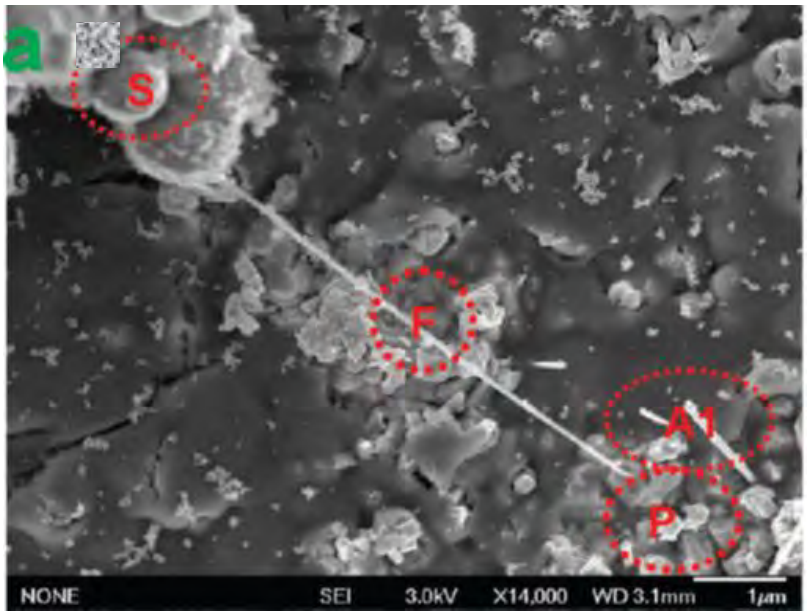

Figure 2-19: SEM micrographs of deposits formed from thermal stressing Jet A on SS 316 surface for 350°C at 5h in a flow reactor (78).

Deposits with different morphologies were also observed from the SEM results of deposits formed from thermal stressing Jet A on SS 316 foil for 10h at 470°C in the absence of oxygen. The SEM micrographs of these deposits showed deposits with a spherical morphology and filamentous deposits which were surrounded by a carbonaceous layer. It was argued that the different morphologies, suggest deposits were formed by both a heterogeneous (catalytic) and homogeneous mechanism (thermal) (80).

2.8.1.2 Transmission electron microscopy

Venkataraman and Eser (8) used transmission electron microscopy (TEM) to obtain more information on the internal structure of the deposits formed from HPDI. The TEM results were compared to those formed from thermal stressing n-hexadecane at 160°C for 2. 5h in a flow reactor TEM results confirmed the presence of deposits with a spherical agglomerated morphology which was observed on the SEM micrographs of HPDI deposits (Figure 2-20a). The *n*-hexadecane deposits also showed spherical particles when viewed under TEM (Figure 2-20b).

The individual particles were then further analysed using high resolution TEM (HRTEM). This was done to obtain more information on the difference in morphology which was not observed in TEM (8). The HPDI deposits did not show any interference patterns when viewed under TEM (see Figure 2-21a). The *n*-hexadecane deposits, however, showed lattice fringes with a short fringe length towards the edges of the particle as indicated by the red arrow in Figure 2-21b. Lattice fringes were also observed in HRTEM micrographs of jet fuel deposits (see the red arrow in Figure 2-21c).

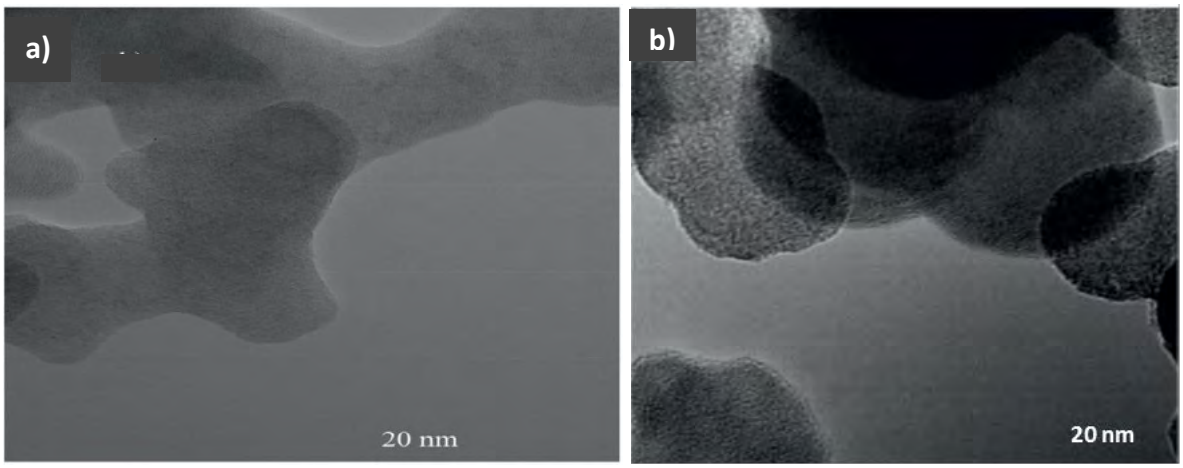

Figure 2-20: TEM images of deposits from (a) an HPDI (high pressure diesel injector) (b) thermally stressed n-hexadecane at 160°C for 2.5h.

It was proposed that fringes observed on these deposits, demonstrated layers of planar poly-aromatic structures. Deposits with lattice fringes were suggested to have a higher fraction of ordered carbonaceous material than those without fringes. Venkataraman and Eser (8) inferred that, deposits with a higher fraction of ordered carbonaceous material,

were observed when n-hexadecane was stressed than with commercial diesel. A suggested reason was that simpler model systems have fewer interfering molecules which may disrupt ordered growth (8).

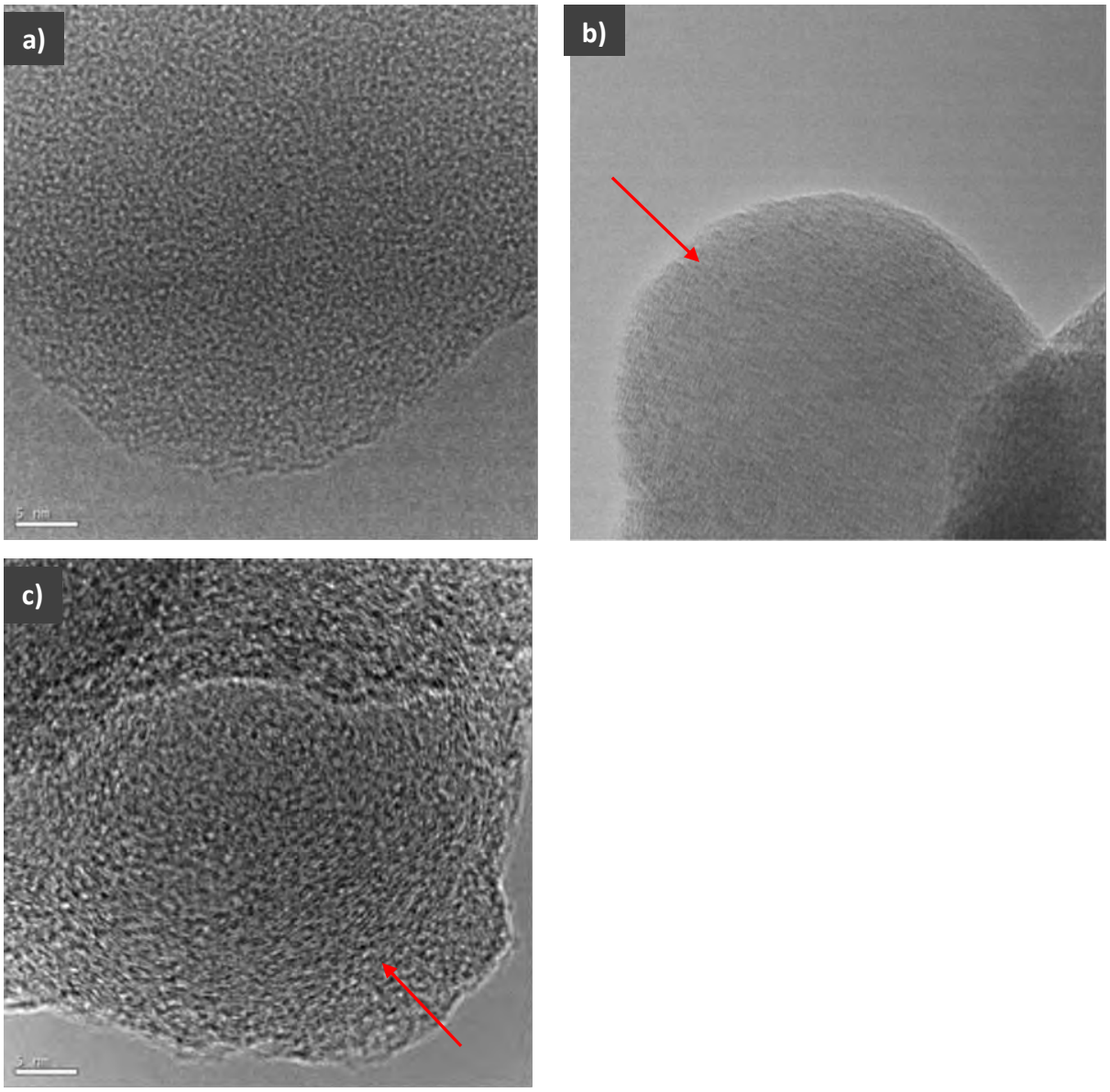

Figure 2-21: HRTEM images of particle deposits obtained from a) HPDI b)thermal stressing n-hexadecane in flow reactor at 160°C for 2.5h c) thermal stressing Jet A in flow reactor at 260°C for 2.5h.

2.8.1.2.4 Moiré Fringe Patterns

When deposits are viewed under transmission electron microscope, it is possible that artefacts are seen on the micrographs which appear to be lattice fringes. These artefacts are referred to as moiré fringe patterns.

A moiré fringe pattern can formed by superimposing two gratings: one undistorted and one distorted due to specimen deformation (82).

Gratings are arrays of dark and light lines which are usually straight, parallel and equally spaced. When two line gratings of different pitch (line spacing) are superimposed without rotation, then moiré fringes will be formed that represents different pitch. Examples of moiré fringes have been depicted in Figure 2-22.

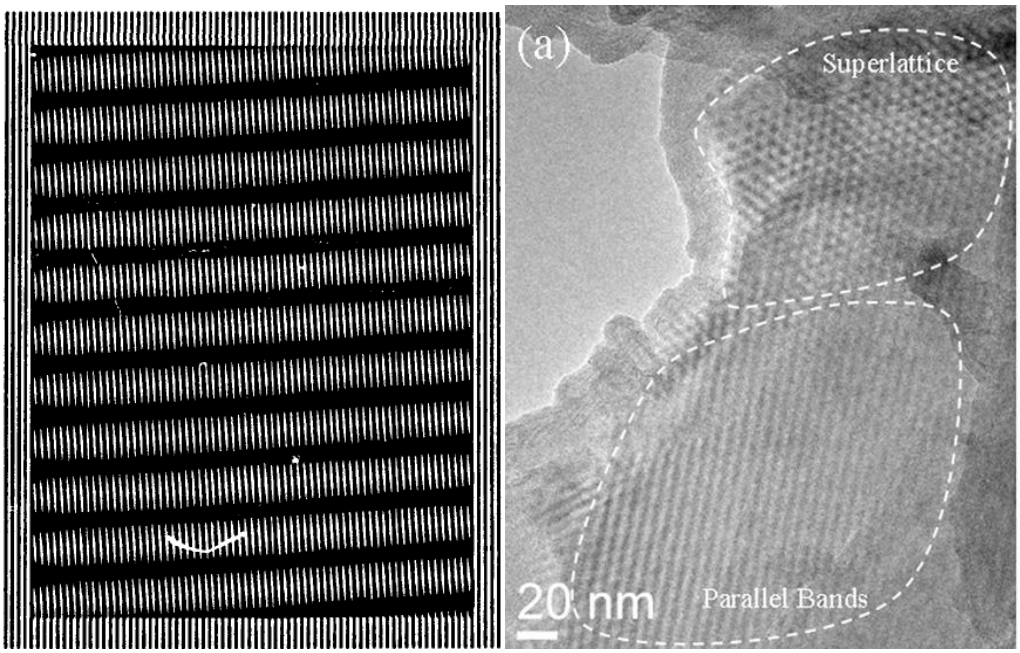

Figure 2-22: a) Schematic of the moiré fringes produced by pure rotation (82) *b) moiré pattern of parallel bands seen in TEM images* (83)*.*

Where a crystalline lattice structure is rotated in relation to another, moiré fringes may also be observed in TEM micrographs.

2.8.1.3 Temperature Programmed Oxidation (TPO)

Temperature programmed oxidation is an analytical technique which can be used to determine the oxidative reactivity of carbonaceous deposits (12,84). The TPO profiles show quantity of CO_2 (and H_2O) evolved as function of temperature. Depending on the reactivity of the deposits, these will oxidise at different temperatures.

Compared to other analytical techniques such as the thermogravimetric analysis-mass spectrometry (TGA-MS), TPO has proven to be more useful in quantifying even the smallest amount of deposits (81). Unlike TGA, a carbon analyser (the instrument which produces TPO profiles), can analyse heavier tube segments up to 10 cm in length (85). This kind of weight is heavy and beyond the mass that typical TGAs can measure which is 100 mg (15).

Several authors have used temperature programmed oxidation to characterise carbon deposits on metal surfaces (10,11,12,13). The carbon burn-off temperatures provide valuable information about the reactivity of the carbon present on the metal tube surface (13). The less reactive a carbon structure is, the higher its burn-off temperature will be.

Carbonaceous deposits with high hydrogen and oxygen species bonded to them have been found to oxidise at lower temperature. This carbon structure is thought to be a less ordered carbon structure. Carbonaceous deposits that contain more carbon and less hydrogen species oxidise at high temperature. These are structurally more ordered deposits (12,13).

Eser and co-workers proposed that TPO peaks that evolve at low temperature (<350˚C) could be attributed to amorphous, hydrogen-rich deposits or secondary deposits that form on the catalytically formed carbon (12,86). TPO peaks, evolving at temperatures between 350˚C-450˚C, were assigned to oxidation of thicker carbonaceous filaments that contain metal sulfides. The peaks at high temperatures (> 500˚C) were attributed to highly ordered carbonaceous deposits, with crystalline patterns. These are likely produced from catalytic reactions on an active metal surface (12). These results were obtained from carbonaceous deposits formed by stressing jet fuel at 470°C on different metal surfaces (12).

Venkataraman used TPO to analyze diesel injector deposits. The TPO profile of deposits scrapped from a diesel injector is depicted in Figure 2-23. The deposits oxidized over a wide temperature range (150-750°C). The peak that evolved between 150-200°C was assigned to

the oxidation of lighter hydrocarbons physisorbed on the deposits. The CO_2 peak at 580°C was attributed to the oxidation of polyaromatic hydrocarbons. The temperature, associated with the CO_2 evolution from this component of the HPDI deposits, is similar to that of the less ordered polyaromatic components of the jet fuel deposits. This suggests that the structural order and corresponding oxidative reactivity of this component of the deposits from the two fuels is similar (10).

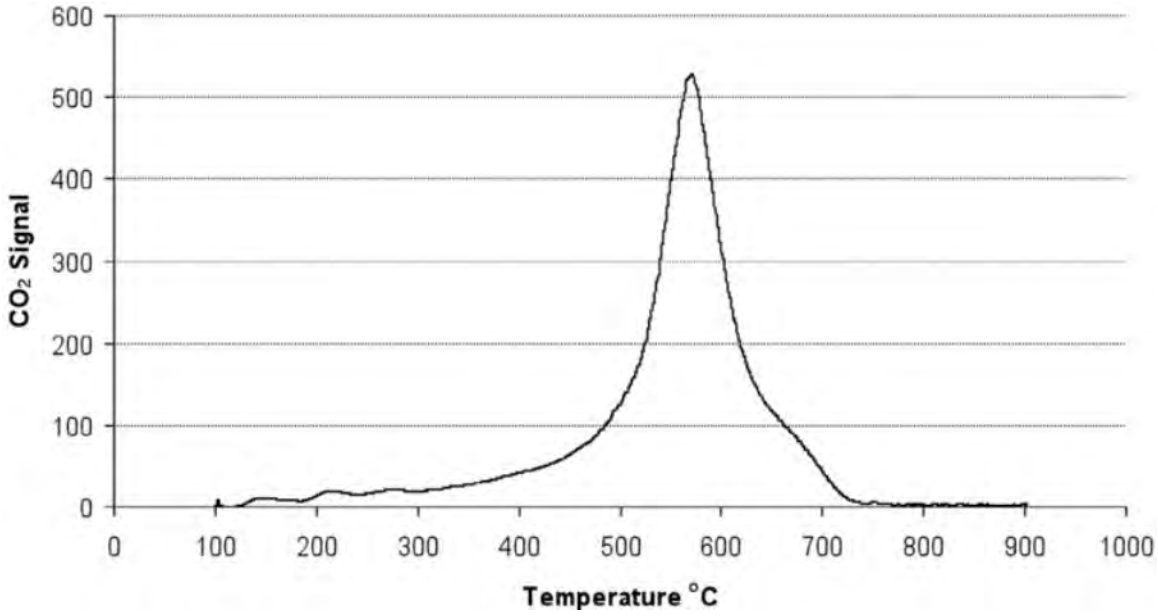

Figure 2-23: TPO profile of HPDI deposits from the oxidation of carbon species in HPDI deposits from 100-1000°C (8).

3 EXPERIMENTAL SECTION

3.1 Materials used

3.1.1 Test fuels

Different fuels were used in this study; namely an EN 590 reference diesel and two fatty acid methyl esters (FAMEs): RME100 and SME100. Binary blends of; RME20, SME20, SME50 and SME7 were used in this study.

The fuels used were provided by Sasol Technology. Properties of EN 590 diesel, RME20 and SME20 are listed in Table 3-1.

Table 3-1: Characteristics of fuels used and their properties.

	EN 590 diesel	RME20	SME20
EN 590 (%)	100	80	80
Density @ 15 (g/cm^3)	0.8358	0.8417	0.8419
Density @ 40 (g/cm^3)	2.79	3.05	2.49
CFPP (^oC)	-20.0	-22.0	-17.0
Derived cetane number	56.5	51.2	54.2
Flash point (^oC)	84.0	85.0	88.0
Acid number	0.06	0.08	0.09
HFRR	327	-	-
S content (ppm)	< 1	1.0	< 1
I value (Br number)	<0.01	10.50	10.70
Carbon residue (wt. %)	0.02	0.03	0.10
Ash content (wt. %)	<0.01	<0.01	<0.01
Oxidation stability (Rancimat)(h)	168.0	30.82	13.79

3.1.2 Metal alloy tubes

The fuels were thermally stressed in iron (Fe) rich SS 316 tubes with an outer diameter of 0.32 cm (⅛ "), inner diameter of 0.2 cm and a length of 110 cm. These tubes were provided by Swagelok (Johannesburg, South Africa).

Energy dispersive spectroscopy (EDS), using an Oxford Xmax detector and INCA software at the Electron Microscope Unit (EMU) of the University of Cape Town (UCT), were used to obtain the composition of the SS 316 tubes. Table 3-2 shows the composition of the exterior and interior of the metal tubes obtained from an average of three spots on the sample.

Table 3-2: Composition of SS 316 metal tube.

	Fe	**Ni**	**Cr**	**C**	**Si**
Exterior (wt. %)	58 ± 0.72	11 ± 0.72	16 ± 0.19	14 ± 0.98	-
Interior (wt. %)	46± 1.38	11± 0.80	13± 0.50	25± 2.16	5

3.2 Thermal stressing

3.2.1 Flow reactor

Figure 3-1 shows a schematic of the laboratory non-recirculating loop flow reactor system. A similar reactor has been used in previous studies to investigate deposits formed as fuel degrades (10,13). The flow reactor comprised a vertical furnace, a Carbolite temperature controller, a Waters HPLC pump and a Van Waters and Rogers (VWR) chiller. The purpose of the chiller is to circulate coolant to the condensing unit in order to cool the heated fuel. The HPLC pump is used to ensure there is a constant fuel delivery rate throughout the run.

The fuel was pumped from the fuel reservoir so that it flowed vertically up the SS 316 tube heated by furnace. It is important to note that only 97 cm of the 110 cm tube inserted was heated. Conditions in the reactor were non-isothermal because the temperature inside the reactor varied with axial distance. The temperature profile along the reactor was measured. Temperature measurements were made at three different points along the length of the

reactor tubes; at 15, 45 and 75 cm. 15 cm was measured from the bottom of the furnace tube section and not the bottom of the tube as not all the tube was heated.

Measurements of the fuel exit temperatures were also made. K-type thermocouples were used to monitor the temperature output from the four sections. Temperature outputs from these thermocouples were recorded hourly for the duration of the experiment.

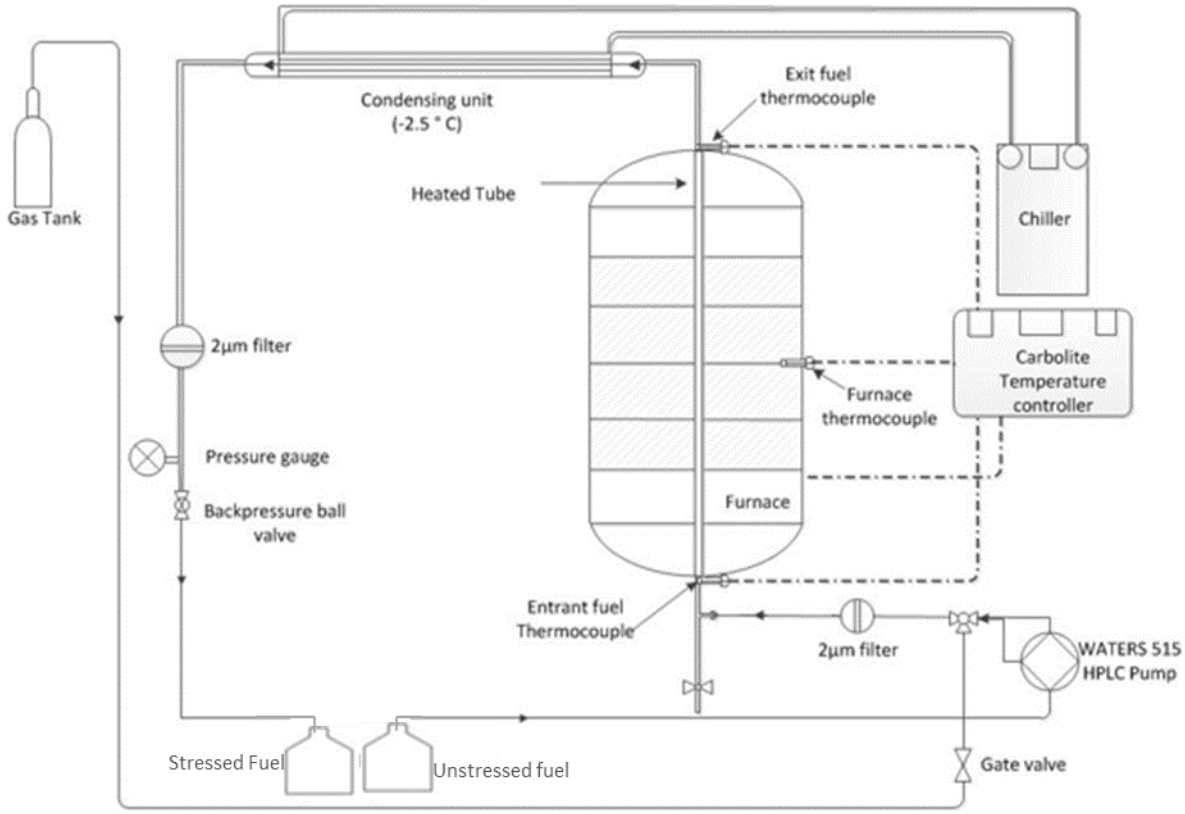

Figure 3-1: Schematic representation of the flow reactor set up used for the thermal stressing.

The flow reactor was operated in a non-recirculating system as indicated in Figure 3-1. This set up was chosen because the operating temperatures in this study were > 300 °C. In a real engine it is likely that the fuel is exposed to such high temperatures at the injector tip (87) (88). Once the fuel reaches the injector tip, it is sprayed into the combustion chamber and is not recirculated back to the fuel tank. Another reason for conducting the experiments using a non-recirculating flow reactor was for comparative reasons as most of the previous studies were conducted using a similar set up (10,13). Some of the experimental parameters

that were used when running the flow reactor have been depicted in Table 3-3. The reasons for the selected operating parameters are also outlined.

Table 3-3 : Experimental parameters employed when running the flow reactor.

Experimental parameter	Set point	Reason
Fuel tested	EN 590 diesel	In studies where the behaviour of commercial diesel is evaluated; EN 590 diesel is often used as a reference.
	SME and RME	In an attempt to meet the stringent emissions, diesel fuels are being blended with biodiesel. To investigate the effect of neat FAMEs and their blends on deposit formation SME and RME were used as they are the leading sources of biodiesel (32) .
Furnace temperature	300 °C. It should be noted that the thermal stressing temperatures reported in this study were measured from the thermocouple placed in the middle section along the flow reactor.	The temperature is within the thermal oxidative region. This temperature is similar to those that injector tips are exposed to (87,88).
	400°C	Experiments conducted at 300°C revealed that most test fuels had not formed carbonaceous deposits. Since the objective of the study was to characterise

		carbonaceous deposits formed, higher temperatures were employed in an attempt to accelerate the formation of deposits.
Fuel flow rate	1 mℓ/min	This flow rate is lower than the range of flow rates used in previous studies which range from 1.2 mℓ-10 mℓ/min (10,13). This was chosen to allow the fuel more residence time in the metal tube.
Metal Tube	SS 316	The effect of Fe and Fe-rich alloys such as SS 316 on deposit has been extensively investigated by Venkataraman (10). In order to compare results from this study with results from those studies this metal alloy was selected.

Other experimental conditions used for the thermal stressing experiment	
Sample size	500 mℓ
Experiment duration	5h
Fuel state	Aerated
Tube length exposed to furnace	97 cm
Fuel resident time	7.44 min
Coolant temperature	-2.3 °C

As received 6 m tubes were sectioned into 110 cm long tubes prior to stressing. Afterwards, these were cleaned in an ultrasonic bath with water to get rid of any dirt that could have accumulated during manufacture and storage of the tubes. The appropriate tube fitting

procedure was carried out to ensure that the tubes could be tightly fastened to the flow reactor without any leakages. The procedure followed during thermal stressing is described below:

Experimental technique:

1. The HPLC pump was primed using a syringe to get rid of any air bubbles in the fuel line.
2. The system was checked for leaks by setting the pump at a flow rate of 10 mℓ/min and letting it run for 30min with the reactor open.
3. The flow rate was set to the desired flow rate.
4. The back pressure valve was set to the desired pressure.
5. The desired temperature on the carbolite TVS 12/60/900 three-zone temperature controlling unit was set.
6. Both thermocouple readers were switched on in order to monitor the temperature profile across the furnace. K-type thermocouples were used in this study because they can withstand the elevated temperatures used in this study.
7. After setting all the experimental conditions, the experiment was started. For the duration of the experiment all the experimental parameters listed in Table 3-3 were kept constant.
8. Once the experiment was completed, the system was switched off and the furnace allowed to cool down completely. The metal tube was removed and sectioned into 22 evenly sized pieces (5 cm length each).
9. The sections were washed with *n*-hexane (Kimix, Cape Town, South Africa) and allowed to dry overnight. This was done to remove of any non physisorbed residual fuel.
10. Once the samples were dry, they were analysed using a LECO-RC612 multiphase carbon analyser and optical microscopy.

3.2.1.1 Zinc doping

Thermal stressing at 300°C did not form deposits on tubes stressed with pure FAME and diesel/FAME blends so in an attempt to drive the reaction to form deposits the test fuels were doped with zinc neodecanoate from Alfa Aeser (Karlsruhe, Germany). Previous studies have shown that zinc has an effect on a fuel's stability (20,89,90). The doping procedure is described below.

***Doping procedure**:*

1. 31.25 mg of zinc neodecanoate (Alfa Aeser, Karlsruhe, Germany) was added to 500 g of the base fuel to make up a solution of 10 ppm zinc (m/m) doped fuel.

3.2.1.2 Pre-stressing test fuel in the flask reactor

In an attempt to form solid deposits at 300°C the test fuels were stressed in a flask before at 140°C for 6h before being thermally stressed in a flow reactor. The experimental set up used has been described by Kaminuza (15) and Vukeya (16). 6h was chosen for the thermal stressing time for the flask study as Vukeya showed that by this time appreciable deposit precursors had started forming (16).

1. 500 mℓ of SME 100 was placed in a 500 mℓ three-neck round bottom flask equipped with a reflux condenser, thermocouples and gas delivery pipette.
2. The heating mantle was switched on, the gas line was opened and the flow of gas was adjusted to 50 mℓ/ min.
3. The temperature was then allowed to stabilize at 140°C.
4. The test fuel was stressed for 6 h.
5. Afterwards the pre- stressed fuel was thermally stressed in the flow reactor at 300°C for 5h.
6. The procedure describe in steps 8-10 for the thermal stressing procedure were repeated

3.2.1.3 Increase in thermal stressing temperature

Experiments conducted at 300°C even after zinc doping and pre-stressing in the flow reactor did not form carbonaceous deposits on SS 316 tube when stressed with FAME. In order to drive the reaction to form deposits faster, the thermal stressing temperature was increased to 400°C. The same thermal stressing procedure outlined in section 3.2.1 was followed.

The effect of metal contamination on the deposition tendency was investigated by doping EN 590 reference diesel, RME100 and SME100 with 10 ppm zinc. The fuels were stressed in the flow reactor at 400°C for 5h. The doping procedure outlined in 3.2.1.1 was followed.

The effect of biodiesel blend percentage on the amount of deposits formed was also evaluated at 400°C in a flow reactor; SME blends of 7, 20, 50 and 100 % were tested.

3.2.2 Closed bomb reactor (fluidised sand bath)

The test fuels were also thermally stressed in a closed bomb reactor under similar conditions to those employed in the flow reactor. This was done in order to evaluate if the deposition rate between the two reactors differs and also to characterise and compare degraded fuels and degraded tubes. A similar comparison was conducted by Li and Eser in their study of copper surface effects on deposits formed in bath and flow reactor (17).

A 5 cm SS 316 tube segment was inserted in the bomb reactor before the reaction. This was done in order to evaluate if any deposits would adhere to the surface after thermal degradation. Fuels were degraded in metallic bombs which were externally heated by being submerged in a fluidised sand bath. The reactor bombs were also constructed of 316 stainless steel cylinder with 60 mℓ volume capacity.

Figure 3-2 shows a schematic of the major components making up the sand bath system. The reactor bomb/vessel is clamped onto the rotor shaft sand bath and submerged in the sand for the duration of the experiment.

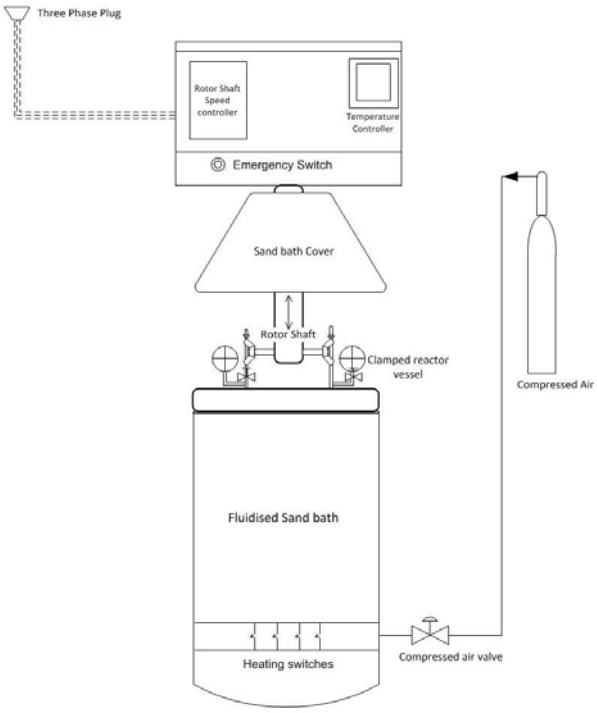

Figure 3-2: Schematic of the fluidised sand bath system used to degrade fuel.

3.3 Characterisation of degraded fuel

3.3.1 Ultraviolet- visible (UV-Vis) spectroscopy

A T80+ double beam UV-VIS (PG Instruments, Lutterworth, Ltd, United Kingdom) was used in this study to monitor colour changes brought about by oxidation. The extent of absorption in the stressed fuel was monitored and compared to that of the unstressed fuel. The changes in composition were then deduced from the absorbance measurements.

The presence of aromatics in diesel and unsaturated fatty acids in biodiesel causes these fuels to have a high absorbance in the UV range. In order to bring the absorbance to a measurable range [0-2], the test fuels were diluted twice with *n*-hexane (Kimix, Cape Town, South Africa). An absorbance of less than 2 minimises errors in the absorbance measurement (63). *n*-Hexane was selected as a solvent because it has it does not absorb UV-Vis radiation above 200nm. Hence any absorbance observed should be exclusively due to the sample being measured (62).

The experimental parameters and the specifications of the instrument are outlined in Table 3-4. The procedure followed to dilute the test fuel is described below.

Table 3-4: UV-Vis specifications and experimental parameters.

Instrument specifications	
Cell holder	8
Wavelength range	190nm-1000nm
Wavelength accuracy	±0.3nm
Experimental parameters	
Mode	Absorbance
Wavelength range	200nm-360nm
Scanning speed	Middle
Interval	1.0
Absorbance range	0.0-2.0
Lamp source	W lamp and D_2 lamp

Dilution protocol:

1. 0.4 mℓ fuel was sampled using an autopipette.
2. To that 9.6 mℓ of *n*-hexane was added to make up 10 mℓ solution.
3. The procedure was repeated once more until the absorbance of the mixture was within the measurable absorbance range (0-2). The dilution factor in each run was 25×25 = 625.

3.3.2 Gas chromatography–mass spectroscopy (GC-MS)

A Shimadzu QP 2010 Plus GC-MS was used to analyse the deposit precursors present in the liquid state of the fuel. The GC-MS had a high performance quadrapole mass spectrometer that allowed mass detection at a range of 1.5 to 1090 m/z.

The degraded fuel samples were analysed by GC-MS using the conditions listed in Table 3-5.

Table 3-5: GC-MS parameters used to analyse thermally stressed fuel.

Instrument	**Shimadzu QP 2010 Plus GC-MS**
Column	BPX5 MS Column (fused silica) with a temperature range: -60°C to 360°C and dimensions of 25m (axial length), 0.32 mm (internal diameter) and 0.25µm (film thickness).
Gas	Helium (Air Product, Cape Town, South Africa)
GC injection program	
Injection temperature	270°C
Injection mode	Splitless
Injection volume	1 µℓ
GC pressure program	
Flow control mode	Linear velocity
Pressure	53.1 kPa
Total flow	38.3 mℓ/min
Column flow	3.21 mℓ/min
Purge flow	3.0 mℓ/min
GC temperature program	
Ramp	50°C/min
Temperature	20°C/min to 270°C
Hold	5.5 Min

3.3.3 Fourier transform infrared spectroscopy (FTIR)

FTIR was used to evaluate changes in the composition of the fuel after thermal degradation. This was done by analysing the fuel before and after thermal degradation and comparing the spectra. The specifications of the instrument together with the parameters employed when analysing the fuels are listed below in Table 3-6.

Table 3-6: FTIR specifications and experimental parameters.

Instrument specifications	
Instrument type	Nicolet 6700 FTIR
Spectral range	7800 - 350 cm^{-1}
Optical resolution	0.09 cm^{-1}
Wavenumber precision	0.01 cm^{-1}
Experimental parameters	
FTIR mode	Absorbance
Number of sample scans	100
Number of background scans	32
Resolution	4.00
Optical velocity	0.63
Aperture	100
Detector	DTGS KBr
Beam splitter	KBr
Source	IR

3.3.4 Electrospray ionisation-mass spectrometry (ESI-MS)

Positive and negative mode ESI-MS was used to evaluate the structure and molecular masses of soluble deposit precursors present in the test fuels after thermal oxidation. The ESI analysis was at the conducted at the Central Analytical Facilities (CAF) of Stellenbosch University, South Africa. Both stressed and unstressed test fuels were analysed for comparison purposes. Sample preparations for ESI-MS as well as instrumental parameters are outlined below:

***Samples preparation*:**

1. 5 mℓ of stressed fuel/unstressed fuel was mixed with 2 mℓ methanol (Kimix, Cape Town, South Africa) (fuel: methanol 5:2 by volume) in a separating funnel.
2. The fuel-methanol mixture was shaken and left in the separating funnel for 30 min to ensure adequate separation of the methanol fraction from the fuel.

3. The methanol layer was collected in GC vials for ESI-MS analysis at the CAF, Stellenbosch University.

The mass spectra of the methanol extract were collected in the range of m/z 100-1500 using parameters indicated in Table 3-7.

Table 3-7: Instrumental parameters used in the acquisition of ESI-MS data.

Instrument	**Waters Synapt G2**
Source	ESI positive/ negative
Cone voltage	15 V
Lock mass (reference)	Leucine enkaphalin (555.6 g/mol)

3.4 Characterisation of solid deposits

3.4.1 Temperature programmed oxidation

The stressed metal tubes were analysed using a LECO model RC-612 multiphase carbon analyser. Carbon analysers have been used to in previous studies to measure the amount of carbonaceous deposits formed on metal surfaces after thermal degradation (10,13,84,86). The instrument reacts the carbon formed in the deposit with medical oxygen (Air Products, Cape Town, South Africa) in a furnace over a copper oxide (CuO) catalyst bed and oxidises the hydrocarbons/carbon/carbon monoxide to carbon dioxide. The carbon dioxide is quantitatively measured by a calibrated infrared (IR) detector as a function of temperature in the furnace.

Table 3-8 contains the systematic conditions that were employed to analyse the deposits formed on the metal surface. The experimental conditions used in this study were similar to those employed in previous studies. This was done to facilitate comparison (10,86).

Table 3-8: Systematic conditions of the carbon analyser.

Sample size	5 cm
Gas	Medical oxygen
Heating rate	30 °C/min
Gas flow rate	750 mℓ/min
Furnace temperature	100°C-900°C

Procedure:

1. After the instrument was switched on and a system check performed, a blank calibration was conducted.
2. The blank calibration was performed by inserting an empty nickel combustion boat in the furnace and analysing it. The empty combustion boat was analysed three times before a standard calibration was conducted. The purpose of the blank calibration was to remove any residual carbon from the combustion boat.
3. After the blank calibration, a standard calibration was performed using a reference powder containing synthetic carbon at wt. % 1.03 ± 0.02. This standard was provided by LECO (Johannesburg, South Africa). It was chosen because the amount of carbon on the exposed tubes was expected to be low. This standard is suitable when measuring samples with low levels of carbon.
4. Three different masses of the standard sample, 0.25g, 0.5g and 1.0g were analysed. Thereafter a calibration curve was produced
5. Following the standard calibration, a blank metal tube that had not been thermally stressed was analysed.
6. The mass and surface areas of the stressed tube were measured.
7. Then, the thermally stressed tube sections were placed in a heated furnace.
8. The samples were heated in an oxygen environment, which caused the carbon on the surface to be oxidised and converted to CO_2.
9. The CO_2 was then quantified using an infrared detector and results were provided as weight % C.

10. The resultant carbon burn-off from the carbon deposited on the metal surface was quantified by temperature-programmed oxidation. The TPO provides valuable information about the structure of carbon present on the surface.

3.4.2 Microscopy

3.4.2.1 Optical

In order to compare evaluate whether any deposits had formed, the thermally stressed tubes were sliced in half lengthwise using a carbide cutter at the Mechanical Engineering workshop at the University of Cape Town.

Bright field photomicrographs of the sliced deposits were taken using a Nikon Shuttlepix P-MFSC microscope.

Polarised light optical microscopy (PLOM) was used to assess the presence of anisotropy in the deposits that were formed on the tube surfaces. Micrographs were collected using a Nikon Eclipse MA200 polarised light microscope.

3.4.2.2 Scanning Electron Microscopy

The surface morphology of the deposits formed was investigated using an FEI Nova NanoSEM 30 series with digital micrograph software at the Electron Microscope Unit (EMU) at the University of Cape Town (UCT).

The microstructure of the samples was observed in scanning mode as well as with Electron Back-scattered Detection (EBSD). The acquisition parameters used to obtain each micrograph are displayed on the each micrograph in the results section. In addition to image analysis the, composition analysis on the deposits was conducted using Energy Dispersive Spectroscopy (EDS) with an Oxford Xmax detector and INCA software at the Electron Microscope Unit (EMU) of the University of Cape Town.

3.4.2.3 Transmission Electron Microscopy

A FEI Tecnai G^2 20 TEM from the EMU at UCT was used to evaluate the internal structure of the carbonaceous deposits that were produced. The TEM was equipped with a lanthanum hexaboride (LaB_6) filament and a Gatan Tridiem Image Filter (GIF).

Sample preparation procedure:

1. Deposits formed on the metal surfaces were scrapped off and placed in a small test tube containing approximately ± 2 mℓ high purity ethanol (Kimix, Cape Town, South Africa).
2. Thereafter the vial was centrifuged for 5min or until sufficient deposits were visible in the vial.
3. Using a dropper, a few drops of the deposits were transferred onto a 3 mm carbon-coated copper grid.
4. The 3 mm grid containing the sample was held under a UV light (250W xenon lamp source) until the ethanol completely evaporated.
5. The dry copper grid was then inserted into the TEM grid holder.

4 AUTOXIDATIVE DEPOSITS

4.1 Fuel degradation in flow reactor

This study evaluated the effect of thermal stressing five different test fuels on the quality and quantity of deposits formed. The fuels were stressed in a flow reactor at 300°C for 5h over a SS 316 surface. The five fuels that were assessed were EN 590 reference diesel, RME100, SME100, RME20 and SME20.

4.2 Visual observations

Samples of the five test fuels were observed pre and post thermal stress; Figure 4-1 depicts the test fuels with the top row representing the fuel pre-thermal stressing and the bottom row representing the test fuel post thermal stressing. Significant colour changes were evident with some fuels.

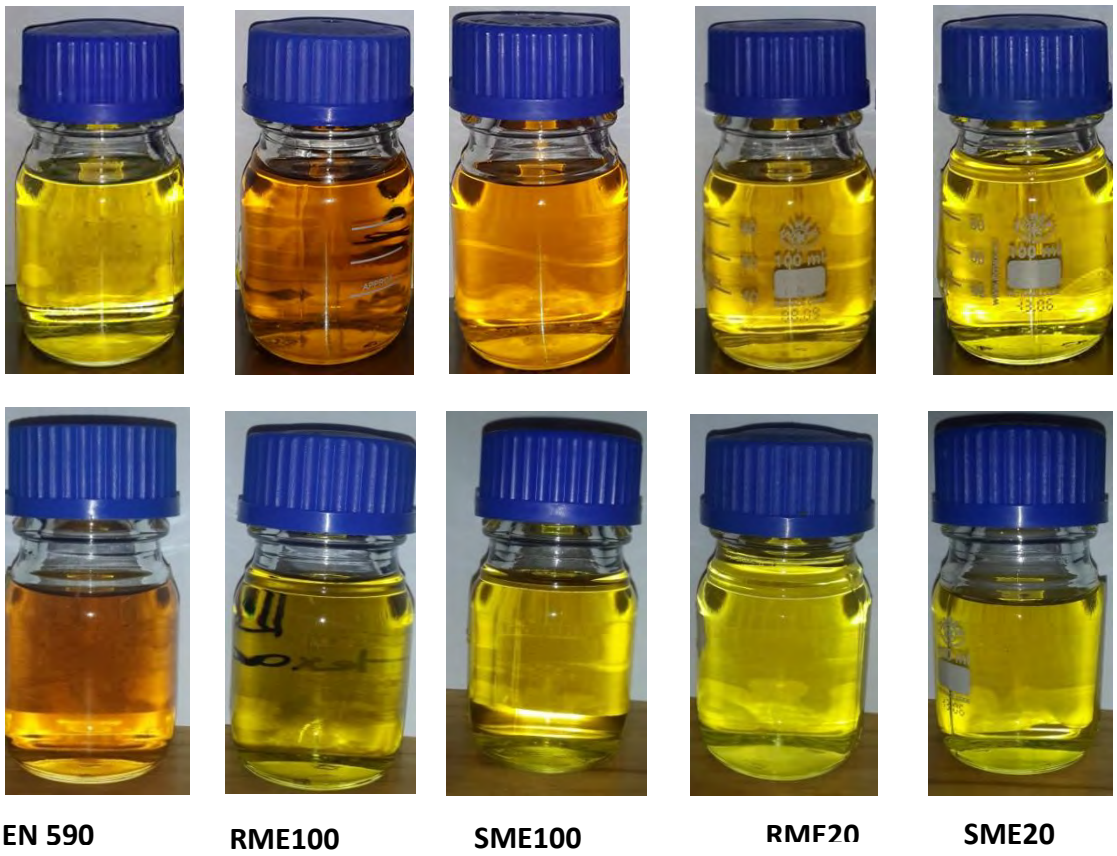

Figure 4-1: Photographs of test fuel pre (top) and post (bottom) thermal stressing at 300°C for 5h on a SS 316 tube in a flow reactor.

The initially yellow EN 590 diesel turned orange after thermal stress whereas the initially orange RME100 and SME100 turned yellow after thermal oxidation for 5h.

RME20 and SME20 did not display a significant change in colour. The fuels did, however, appear slightly lighter in colour compared to the respective unstressed fuel samples. The lightening in colour observed with pure FAME and FAME/diesel blends was unexpected and does not appear to have been reported in previous studies. A repeated run also showed the same observations as can be seen in the Figure 10-1 in Appendix A.

In order to gain insight into compositional changes that are associated with the changes in colour of the fuel, the stressed and unstressed fuels were analysed using different analytical techniques viz: GC-MS, FTIR, UV-Vis and ESI-MS. UV-VIS and ESI-MS proved to be the most useful techniques in identifying fuel changes as very little difference could be discerned from the GC-MS and FTIR results (see Figure 10-2 and Figure 10-3 in appendix A). No sediment was observed.

4.3 UV-Visible investigations on the test fuels

RME100, SME100 and EN 590 diesel showed significant colour changes after thermo-stressing. The UV-Vis spectra of these fuels in the visible region are in Figure 4-2 to Figure 4-4. The UV absorption of stressed EN 590 diesel is higher compared to the unstressed fuel. This is consistent with the darkening of the fuel upon stressing.

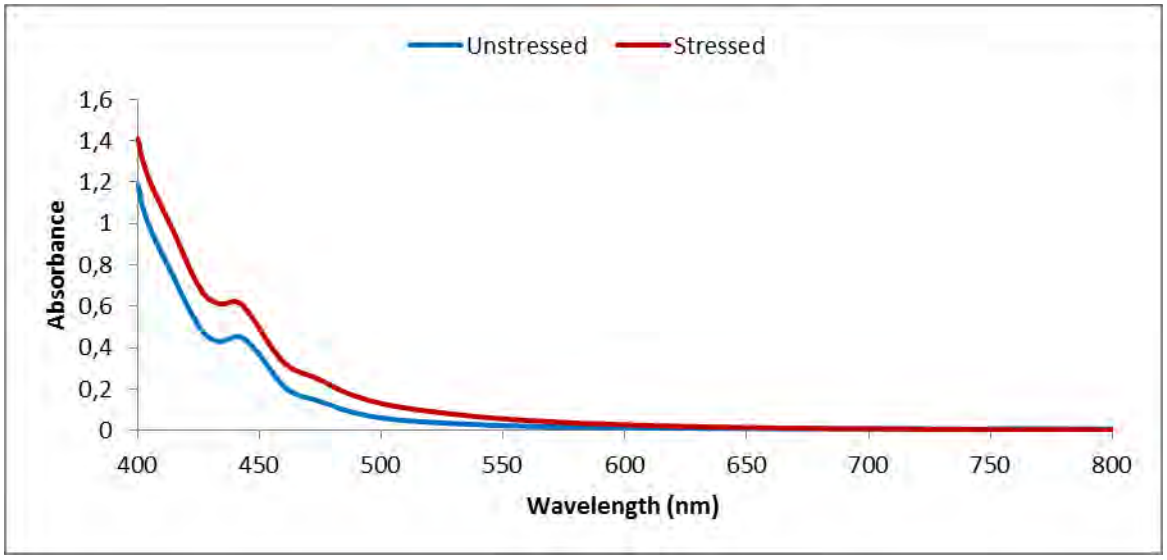

Figure 4-2: UV-Vis spectra of unstressed and stressed EN 590 diesel analysed in the visible region.

The extent of absorption for RME100 and SME100, which changed to a lighter colour after oxidation, in the visible spectrum decreased compared to the unstressed fuel. Again, these

results are consistent with the visual observations. SME20 and RME20 did not show a significant colour change and as a result these fuels were not analysed in the visible region.

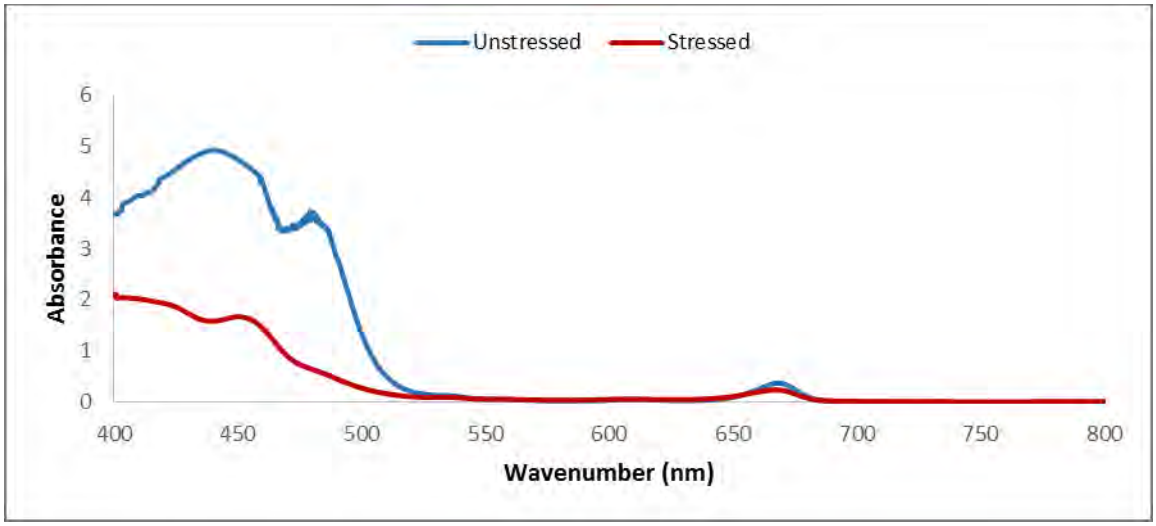

Figure 4-3: UV-Vis spectra of unstressed and stressed RME 100 analysed in the visible region.

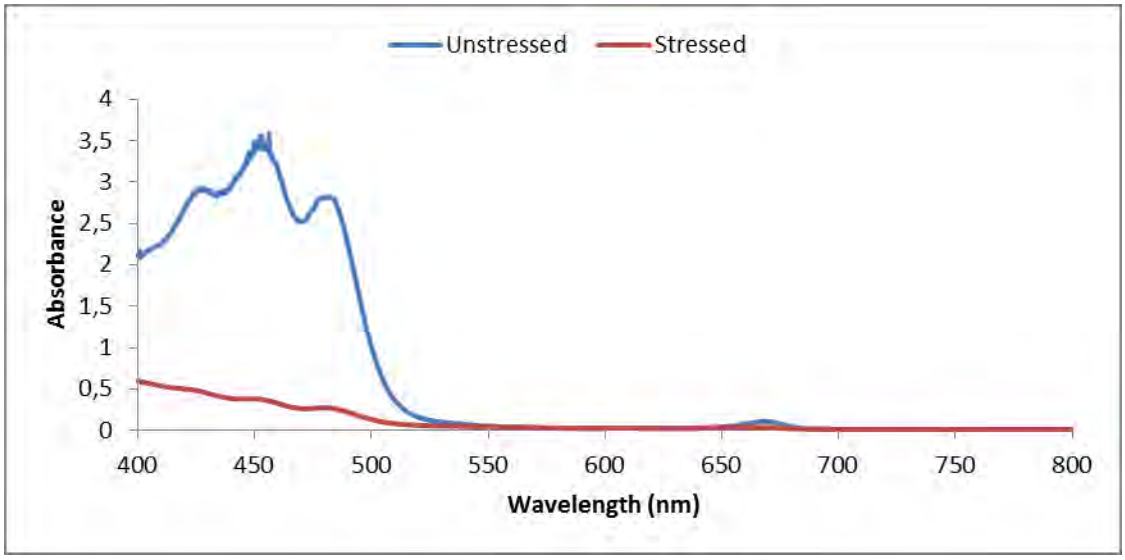

Figure 4-4: Figure 4 2: UV-Vis spectra of unstressed and stressed SME 100 analysed in the visible region.

The UV-Vis spectra of all five test fuels showed an increase in absorbance after thermal oxidation (See Figure 4-5 to Figure 4-9). An assessment of the repeatability of the UV-Vis results has been provided in Figure 10-4. The results show that the results are repeatable in terms of the wavelength at which the peak absorbs light and the extent of absorbance. All

five fuels showed an absorbance peak maximum between 280 and 270nm. An increase in absorbance at these wavelengths is likely due to the formation of secondary oxidation products such as diketones or unsaturated ketones ($\pi - \pi^*$ transitions) (29,58).

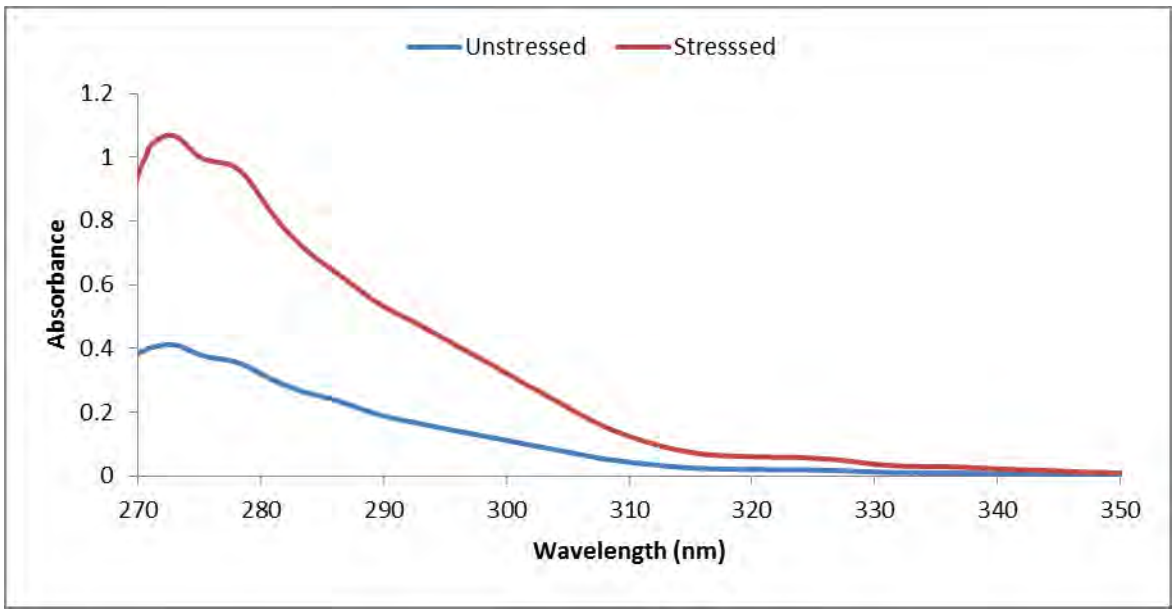

Figure 4-5: UV spectra of unstressed EN 590 diesel and stressed EN 590 diesel measured after 625× dilution in n-hexane.

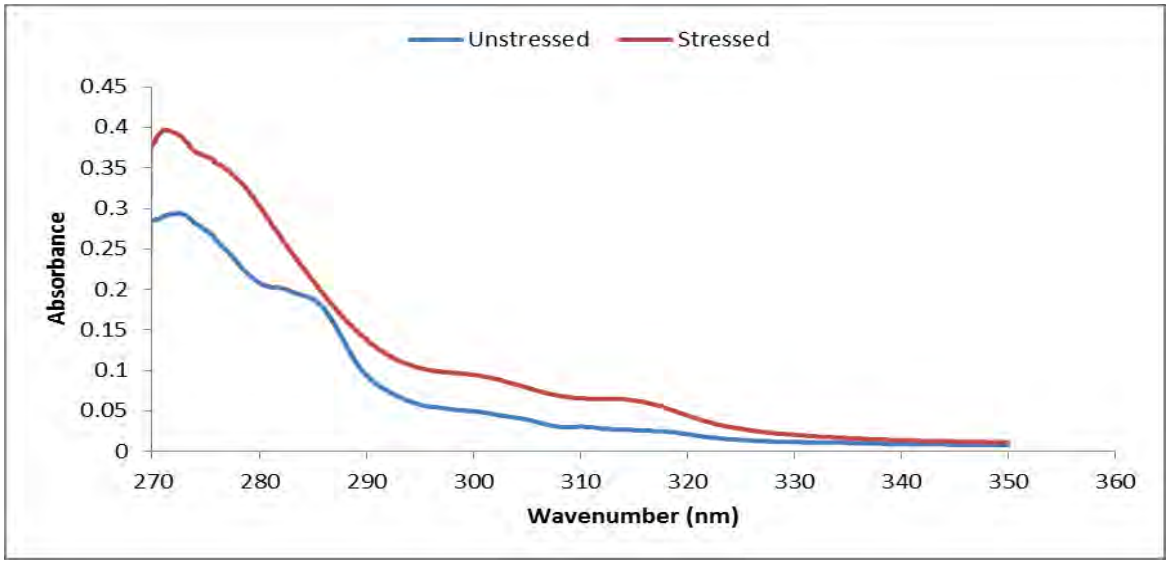

Figure 4-6: UV spectra of unstressed RME100 and stressed RME100 measured after 625× dilution in n-hexane.

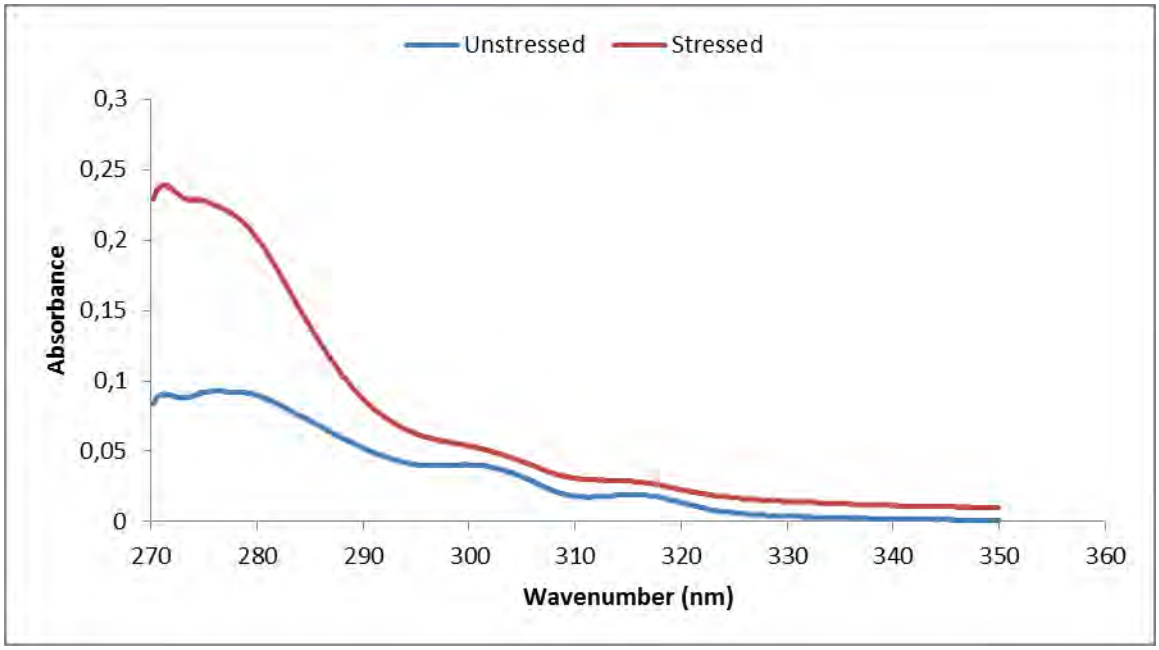

Figure 4-7: UV spectra of unstressed SME100 and stressed SME100 measured after 625× dilution in n-hexane.

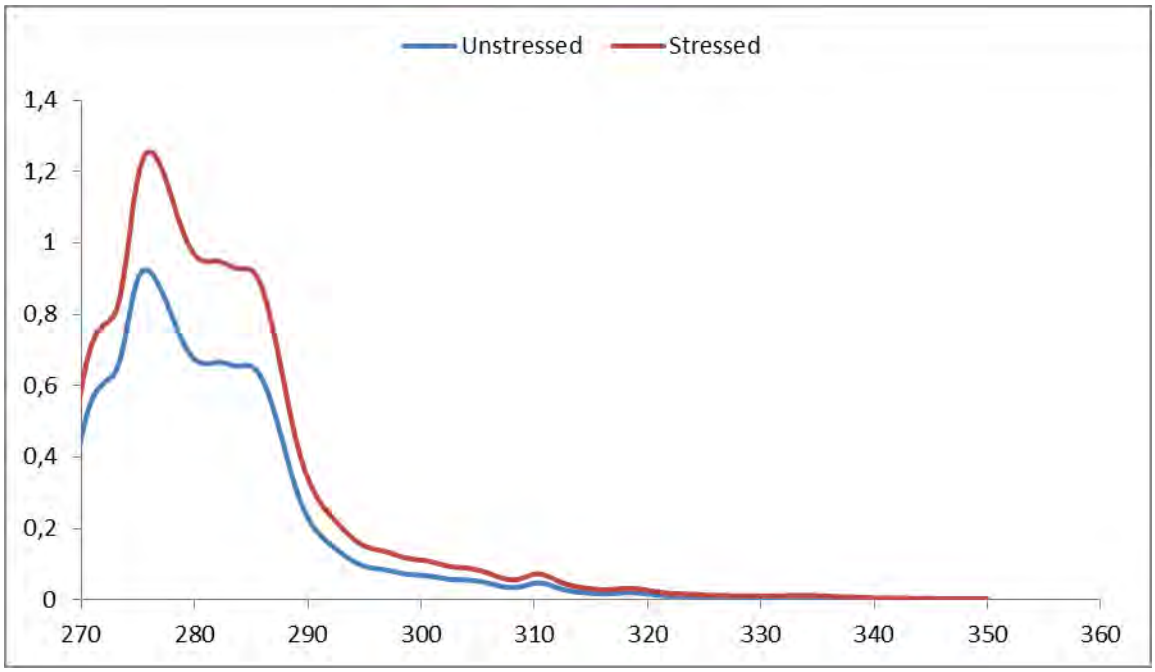

Figure 4-8: UV spectra of unstressed RME20 and stressed RME20 measured after 625× dilution in n-hexane.

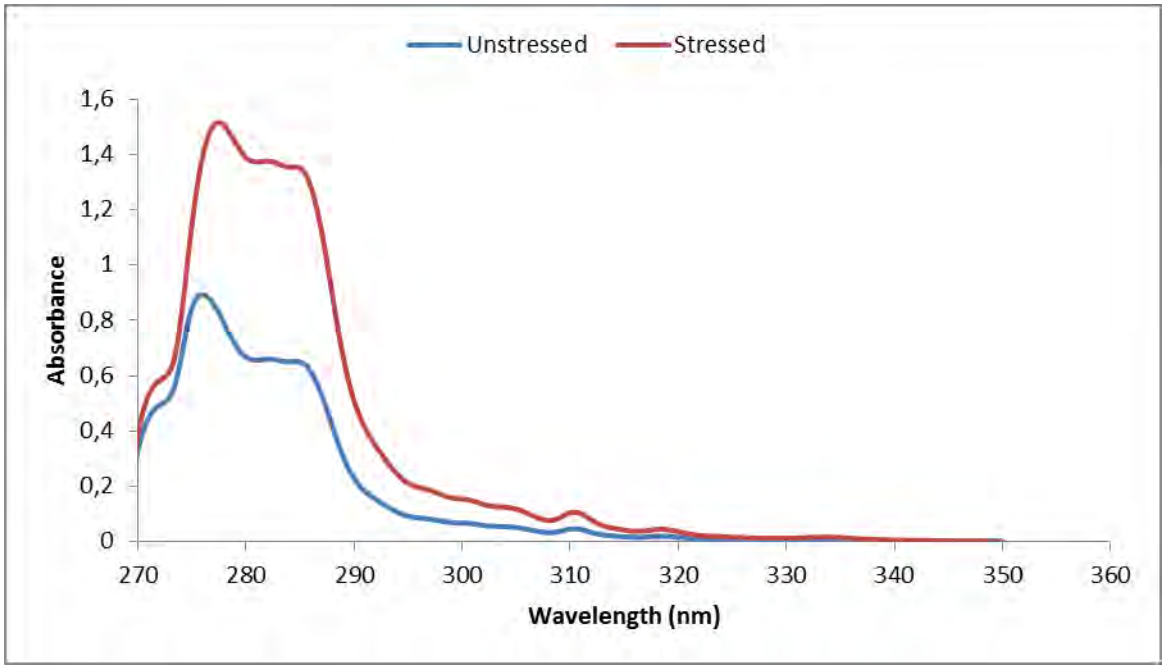

Figure 4-9: UV spectra of unstressed SME20 and stressed SME20 measured after 625× dilution in n-hexane.

4.4 ESI-MS analysis

To study the compositional changes in more detail, ESI-MS was performed on the five stressed fuels. The spectra of the stressed and unstressed fuels are depicted with the spectrum of unstressed fuel on top and stressed fuel's spectrum at the bottom.

4.4.1 EN 590 diesel

The ESI (+) MS spectra of an EN 590 reference diesel, before and after thermal stressing are depicted in Figure 4-10. The majority of the peaks are concentred in the m/z < 400 range. However upon stressing there is a decrease in peak intensity and concentration of peaks in the range 150-400 when compared to the ESI-MS spectrum of the unstressed fuel (see Figure 4-10). Furthermore the peak intensity of species with m/z 600 and m/z ranging from 700-800 amu increased relative to peaks observed in the unstressed fuel. This was accompanied by high molecular weight species with m/z > 1200 amu (see red box in Figure 4-10).

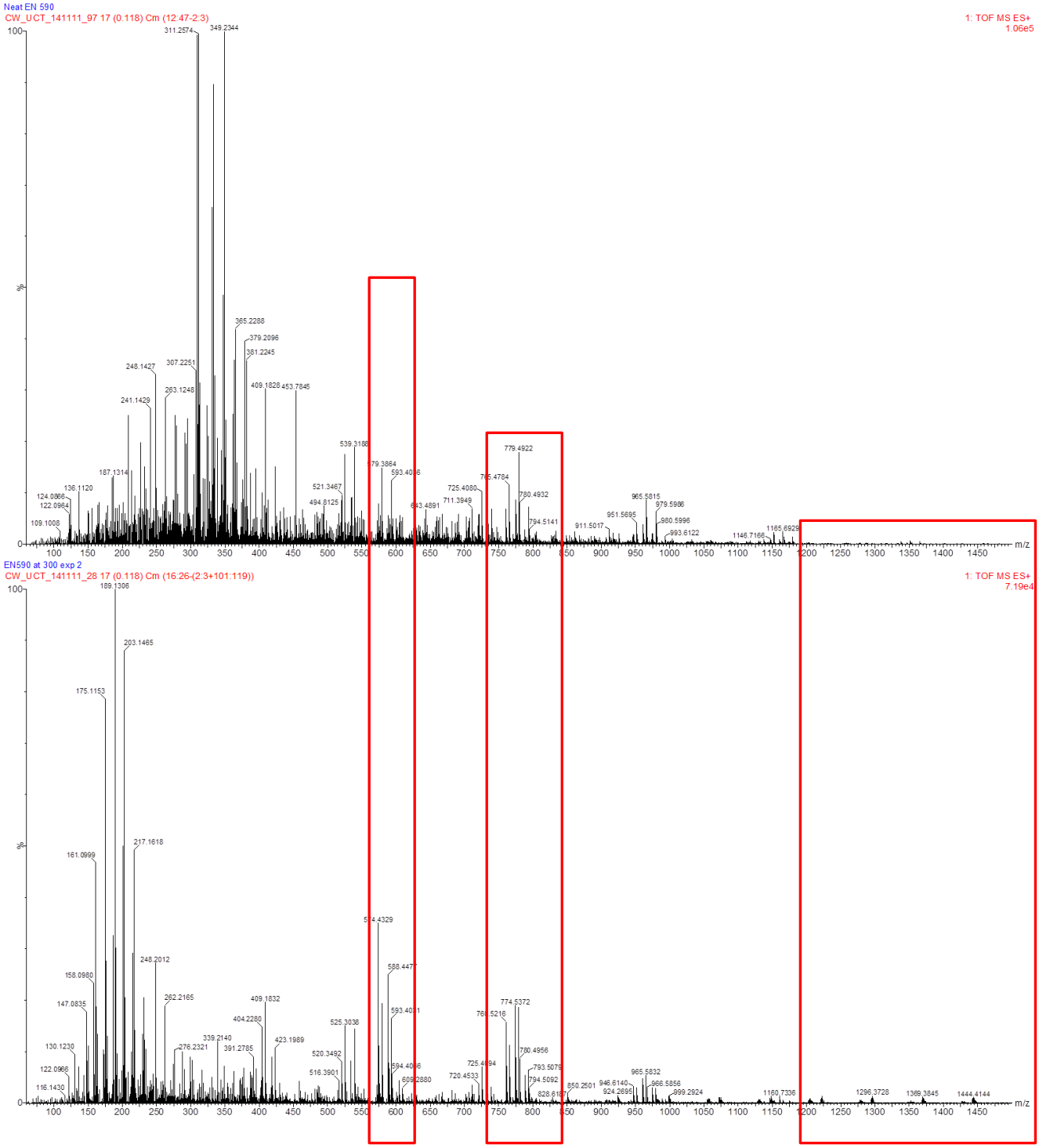

Figure 4-10: ESI (+) MS spectrum of EN 590 reference diesel before (top) and after (bottom) thermal oxidation at 300°C for 5h (0-1500 amu).

The presence of high molecular weight species was more evident in the ESI (-) MS shown in Figure 4-11. High molecular weight species suggest that during oxidation cross-linking of low molecular weight species to form high molecular weight dimers, trimers and even oligomers

took place. This would explain why there are relatively fewer low molecular peaks in the ESI (+) MS of the stressed fuel.

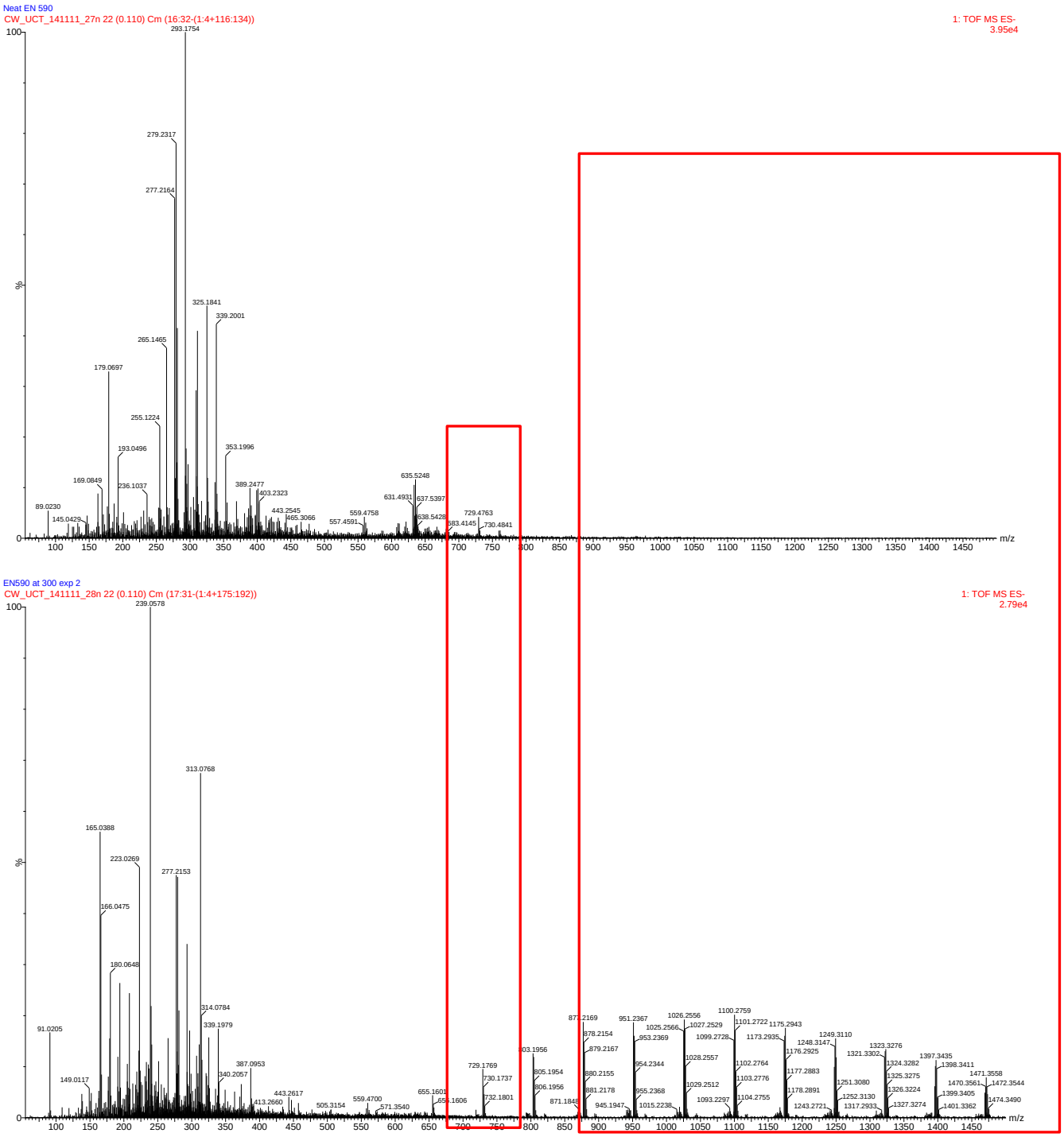

Figure 4-11:Negative ESI-MS of EN 590 diesel before and after thermal oxidation at 300°C for 5h.

4.4.2 RME100

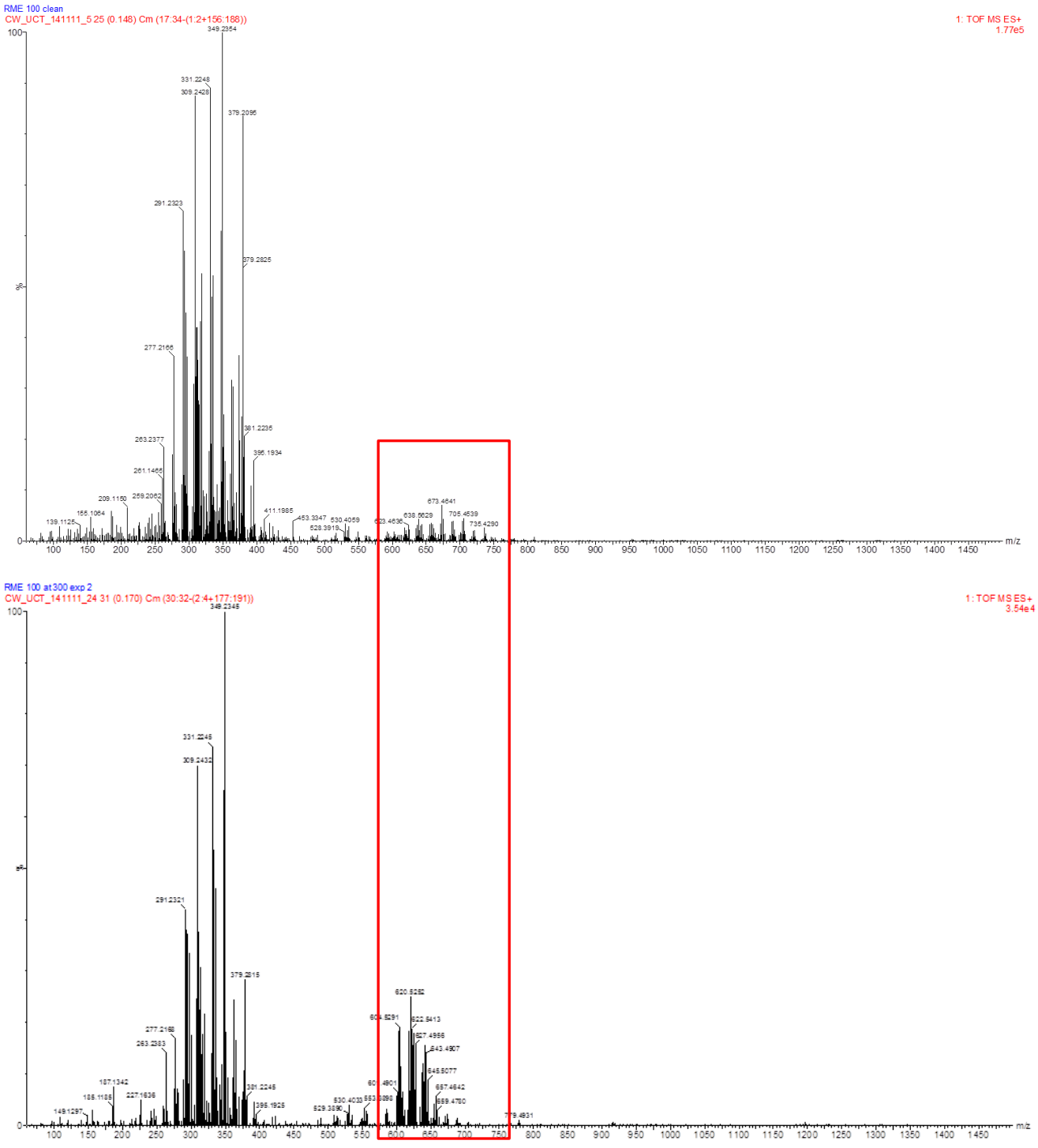

Figure 4-12: ESI (+) MS spectrum of RME100 before (top) and after (bottom) thermal oxidation at 300°C for 5h (0-1500).

The ESI (+) MS spectra of RME100, before and after thermal oxidation are shown in Figure 4-12. The majority of the peaks were observed in the range m/z 250-400 amu, with main

peaks observed at m/z 263, m/z 277, m/z 291, m/z 309, m/z 331, m/z 349 and m/z 379 for the unstressed fuel.

4.4.3 SME100

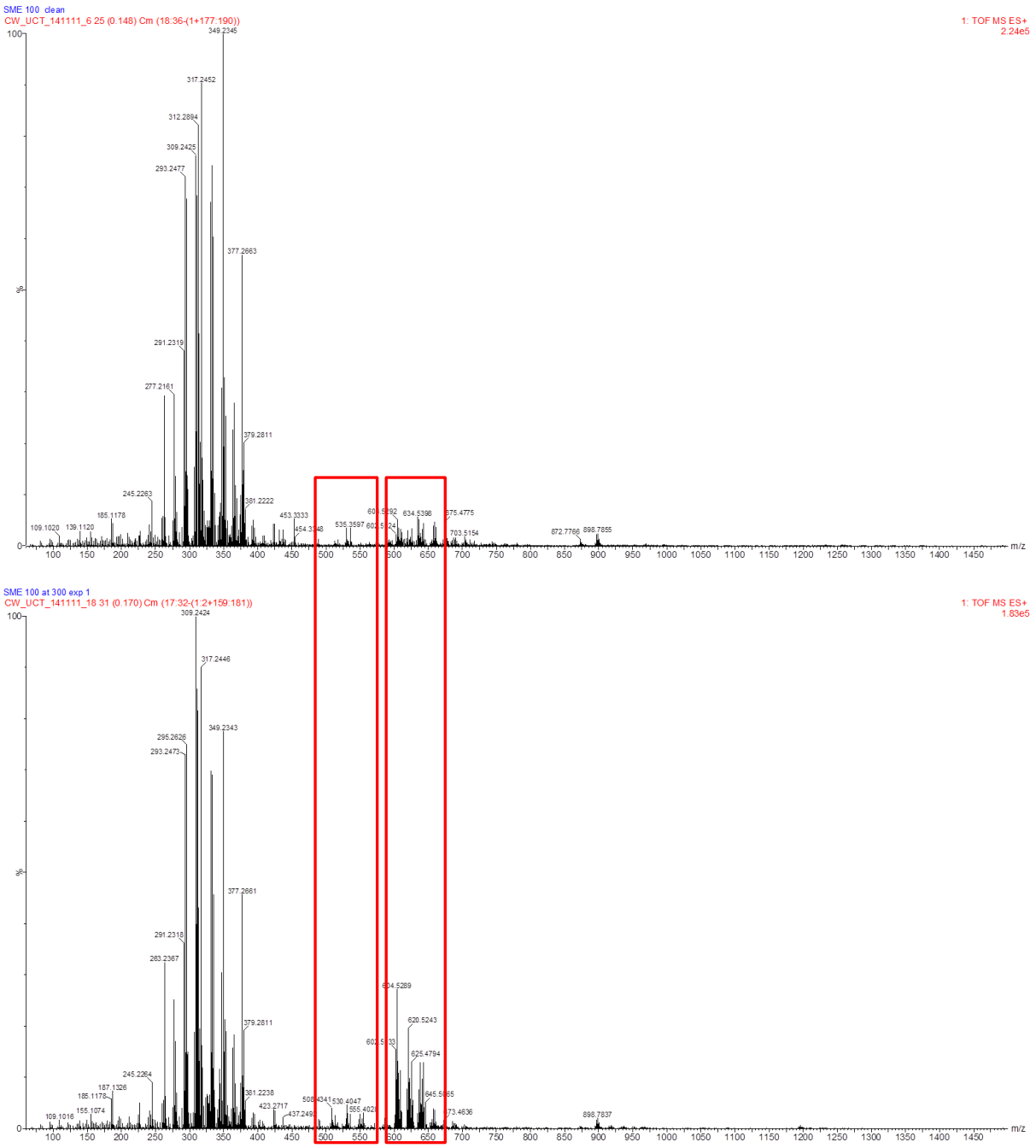

Figure 4-13: ESI (+) MS spectrum of SME100 before (top) and after (bottom) thermal oxidation at 300°C for 5h (0 -1500).

Upon thermal stressing there is an increase in peak intensity of peaks in range m/z 600-680 amu (highlighted by the red box in Figure 4-12). These peaks are likely due to the increased

concentration of dimers which are formed from reactions of low molecular weight species during thermal stressing (48). No high molecular weight species were observed in the spectra of the stressed fuel.

The ESI (+) MS spectrum of SME 100 before and after thermal oxidation are shown in Figure 4-13. The main peaks in the spectrum of the unstressed fuel were observed at m/z 277, m/z 291, m/z 293, m/z 309, m/z 312, m/z 317, m/z 349, m/z 377 and m/z 379. The peak at m/z 293 can be assigned to methyl linoleate; the stressed fuel also shows a peak at m/z 295 which is likely due to the presence of methyl linolenate.
Compared to the ESI (+) MS of the unstressed fuel, the stressed fuel shows peaks with a higher intensity in m/z range 600-680. In addition to this, relatively more peaks appeared in the m/z range 500-550 on the stressed fuel (see red box in Figure 4-13).

4.4.4 RME20

When comparing the ESI (+) MS of RME 100 to that of RME 20, the peaks that are due to the biodiesel (RME) portion in the blend can be identified. The peaks at m/z 277, m/z 291, m/z 309, m/z 349 and m/z 379 can be assigned to the biodiesel portion in the blend as these peaks were observed in ESI (+) MS of RME 100 and RME 20. There were no significant differences on the ESI (+) MS of RME20 before and after thermal oxidation in terms of peak intensity or peaks at higher molecular weight (Figure 10-5 in Appendix A).

4.4.5 SME 20

The biodiesel portion in the blend was also identified by comparing the major peaks present on the ESI (+) MS spectra of unstressed SME 20 and SME 100. The peaks at m/z 277, m/z 291, m/z 293, m/z 309, m/z 312, m/z 317, m/z 349, m/z 377 and m/z 379 can be attributed to the biodiesel portion in the blend as these peaks are present in both SME 20 and SME 100.

The intensity of the peaks in the range m/z 600-680 amu was relatively higher compared to the unstressed fuel (highlighted by the red box in Figure 10-6 in Appendix A); this suggests that thermal oxidation of SME 20 led to formation of high molecular weight dimers. The peak height was also accompanied by a decrease in concentration of species in the low molecular weight region.

4.5 Discussion

The darkening in colour after thermal oxidation has been associated with the extent of oxidation in previous studies (15,16,44). Compared to the other fuels, EN 590 showed a bigger colour change under conditions employed in this study. A possible reason may be that on the experimental time-scales of this study, the molecules of EN 590 diesel readily oxidised to form oxidation species which could lead to the formation of conjugated species (48). These conjugated species are suggested to be responsible for the deepening of the yellow fuel to orange after thermo-oxidative stressing. The presence of the conjugated oxidation products may also be responsible for the increase in UV absorption noted on the stressed fuel. Vukeya also noted an increase in the UV-absorption with the increase of oxygenated species in the stressed fuel (16).

The ESI (-) MS and ESI (+) MS results of stressed EN 590 fuel also demonstrated the presence of peaks at higher molecular weight > 800 amu. These peaks were absent in the unstressed fuel. These peaks may be attributed to the presence of trimers that formed from the cross-linking of low molecular weight species. The presence of this high molecular weight conjugated precursors could suggest that the deepening in colour observed maybe due to oxidation products present if the stressed fuel.

In contrast, RME100 and SME100 were lighter in colour after oxidation. The spectra of these fuel analysed in the visible region showed a decrease in absorption after thermal stressing. This decrease in absorption was likely due to decomposition in species which give FAME its orange colour (48). Some of the species responsible for the orange colour in the as received FAME fuels maybe be methyl linolenate, methyl linoleate and methyl oleate which have a yellow colour.

The FAME degradation mechanism proposed by Ogawa *et al.* suggests that the fatty acids methyl esters decompose to form short chain species such as alcohols, aldehydes and carboxylic acid (48). Evidence of the secondary oxidation products in the degraded fuel is provided by the UV-Vis spectra in the ultraviolet region. The stressed fuels displayed an increase in absorption in the wavelength from 270-320nm. Vukeya observed an increase in absorption in this wavelength and with the aid of FTIR, the increase in absorption was

attributed to the presence of oxygenated species such as carboxylic acid, alcohols and ketones (16).

4.6 Deposit Morphology

The thermal stressing temperature for this experiment was set to 300°C on the carbolite type TVS 12/60/900 three zone furnace. The average temperature readings from the three thermocouple place at different points along the furnace were 265°C at 15 cm, 298°C at 45 cm and 364°C at 75 cm. The exit fuel temperature varied slightly with fuel composition in the range of 280°C to 290°C.

The deposits that were analysed were taken from the following positions along the tube; 15 cm, 45 cm and 75 cm. These sections were chosen in order to assess the effect of the varying temperatures inside the furnace on the quantity and morphology of deposits formed at the three sections along the metal tube. The tube segment at 15 cm will be referred to as the bottom tube segment, that at 45 cm will be referred to as the middle tube segment and the tube at 75 cm will be referred to as the top tube section in the subsequent sections.

The carbon analyser was used to measure the amount of carbon deposited on the metal surface at the three points along the reactor. In addition to this, the TPO profiles of the deposits that had formed were examined to assess on their reactivity towards oxygen. SEM and TEM were used in order to give visual evidence of the differences in deposit morphology and internal structures in addition to the TPO profiles of the deposits.

4.6.1 EN 590 diesel

Figure 4-14 shows different sections from stressed tubes alongside an unstressed tube (blank) section that is useful as a reference. The tubes have been arranged in the following order; unstressed tube, tube from bottom section, tube from middle section and last tube on the right, tube segment from the top section.

When comparing the stressed tubes to the unstressed tubes, visible deposits were observed on the tubes from the top and middle sections. Furthermore the deposits were different in colour. The tube segment from the top section of the reactor formed black deposits,

whereas the tube segment from the middle section of the reactor formed deposits with a brown colour.

The tube segment from the bottom of the tube did not show any visible deposits, when compared to the blank tube (see Figure 4-14). However, a faint yellow staining was observed on the tube segment from the bottom section of the reactor. Kaminuza also observed yellow staining on tubes which were thermally stressed at 250°C for 24h. When Kaminuza analysed the tube sections using TGA- MS, negligible mass loss and no CO_2 evolution were noted (15). This though may well have been the result of the insensitivity of the TGA to the mass loss due to CO_2 evolution/fuel evaporation compared to the tube mass.

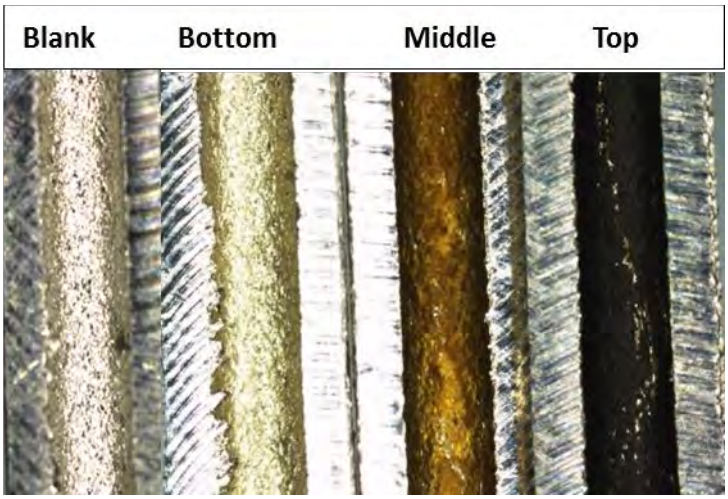

Figure 4-14: Digital microscope image of sectioned flow reactor tubes thermally stressed with EN 590 diesel over a SS 316 surface at 300°C for 5h.

Figure 4-15 shows the TPO profile of a tube section from the bottom section and the unstressed tube. The most notable difference between the TPO profiles of the two tubes was the low temperature peak at 100-200°C that was higher in the stressed tube. This was likely due to the yellow stain which is probably physisorbed fuel that was not removed by with n-hexane. It is important to note that although the tubes were thoroughly washed with *n*-hexane and dried, however some of the test fuel was still found adsorbed on the deposits.

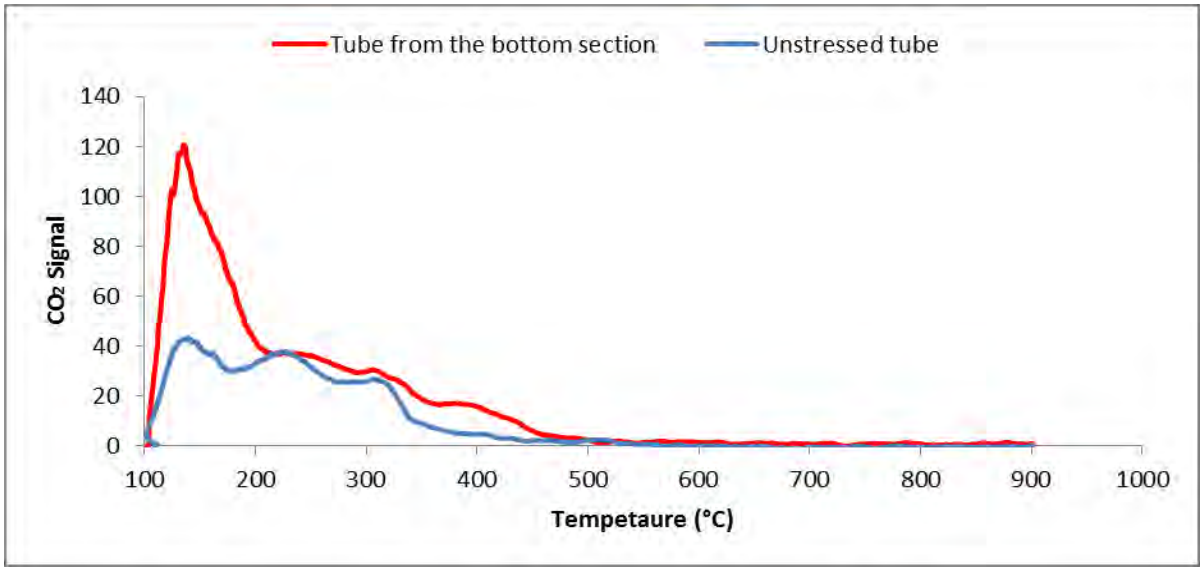

Figure 4-15: TPO profile of unstressed tube section (blue) and a tube section from the bottom of the reactor thermally stressed with EN 590 diesel.

The CO_2 evolution of the bottom section deposits between 200-450°C was not as significant relative to the CO_2 peak height from the blank tube. As a result only the top and middle tube sections which showed visible deposit and significantly high CO_2 peak intensity at high temperature were analysed.

Table 4-1 shows that the amount of carbon deposited on the middle tube section was relatively higher compared to the amount formed on the top section. These values are in the same range of magnitude as those reported by Ram Mohan and Eser (78). It is worth noting that, the total amount of deposits reported in Table 4-1, are an average of results from the two runs as each experiment was performed twice to assess the repeatability of the flow reactor. The deposit morphology of the top and middle section are analysed separately in the subsequent section.

Table 4-1: Quantity of deposit formed on different tube sections, results obtained by TPO.

Test Fuel	**Tube segment**	**Amount of deposit (µg C/cm^2)**
EN590 diesel	Middle section	74
	Top section	43

Middle Segment from flow Reactor: Figure 4-16a shows SEM images of unstressed SS316. The surface was not perfectly smooth. Instead there were some particles on the surface that could be dust particles that remained after the tube was cleaned. This image serves as a reference when examining deposits, in order to differentiate between dirt particles and carbon deposits.

Figure 4-16b shows SEM image of the stressed tube and what was apparent from this image was the present of carbon deposit with distinct structures that covered the metal surface. The deposits had a spherical morphology and appeared to be uneven. It is likely that as new particles form, old ones aggregate and this gave rise to the uneven cluster visible.

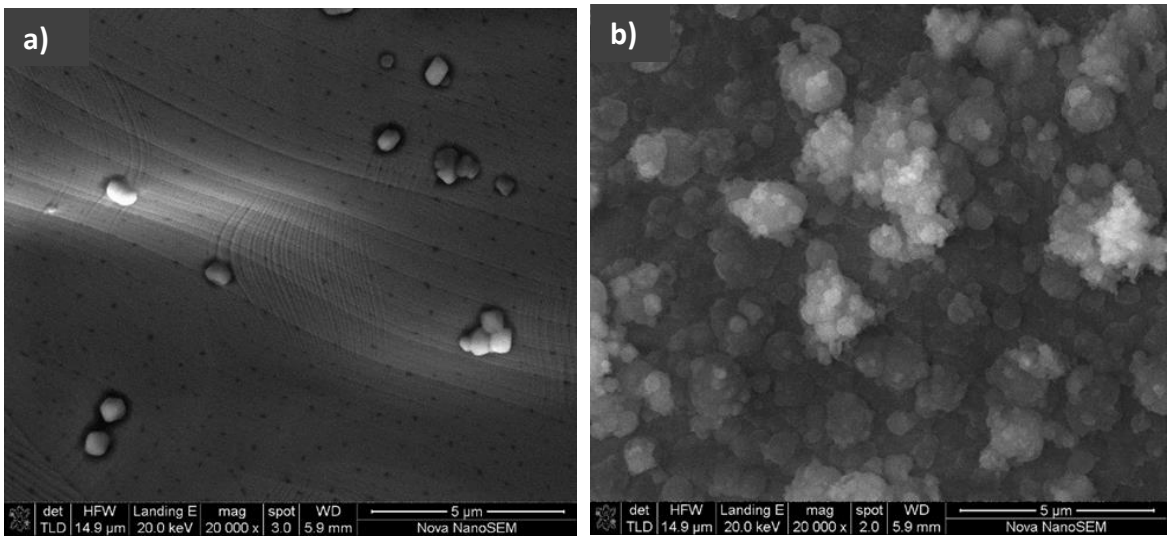

Figure 4-16: SEM images of (a) unstressed (b) stressed SS 316 tube segment from the middle section after thermal stressing of EN 590 diesel at 300°C for 5h.

Figure 4-17 illustrates two TEM micrographs of EN590 diesel deposits at different magnifications. The microstructure of deposits formed did not reveal the spherical particles that were observed in SEM images; instead the structures appeared to be amorphous with no regular diffraction patterns visible (10). In addition to the irregular shaped material, small spherical particles were also observed in the TEM micrographs. These particles had a uniform size distribution of approximately 3nm.

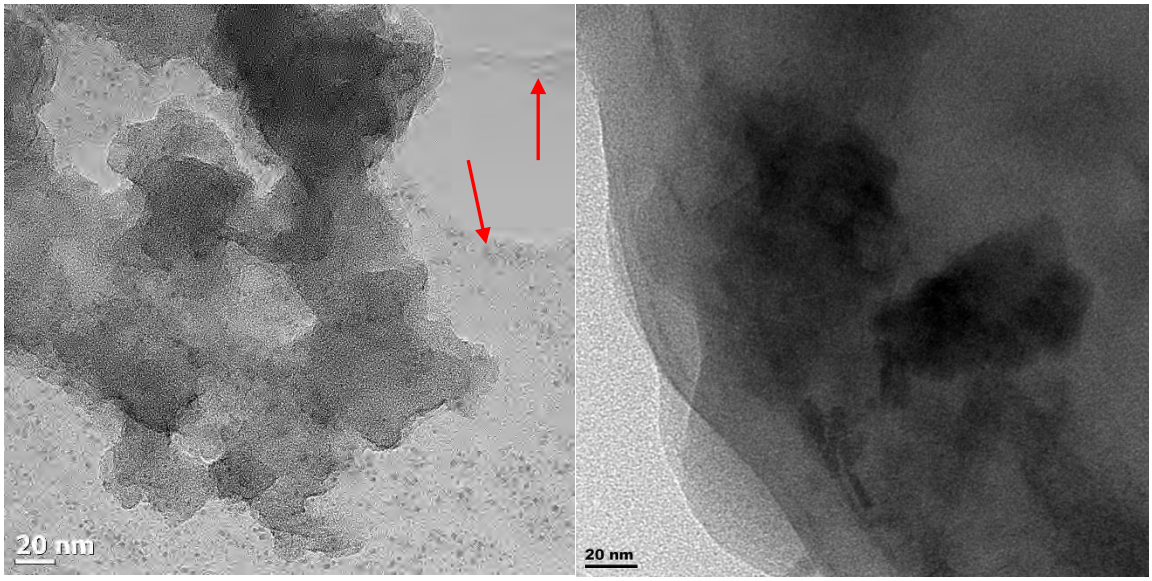

Figure 4-17: TEM images of deposits formed on a stressed SS 316 tube segment from the middle section after thermal stressing of EN 590 diesel at 300°C for 5h.

Both the small spherical particles and irregular shaped deposits seemed to be embedded in a gum-like material that also had no regular structure (highlighted by the red arrows in Figure 4-17). The morphology of these deposits was similar to what Kaminuza observed from deposits obtained from stressing fuel in a flask study and closed bomb reactor (15). Compared to the gum-like material the deposits are relatively darker in colour. This could be because the a) the material is thicker in these regions or b) it contains a higher oxygen content than the lighter areas. This is because the opacity of a TEM photo rises with increased atomic number and thickness. However, no interference patterns could be observed in the deposits.

Repeated experiments showed that the TPO profiles were repeatable with respect to individual peak positions and relative peak intensities as shown Figure 10-7 in Appendix A.

Figure 4-18 shows that the TPO profile of these deposits had three distinct peaks which evolved over a wide temperature range (100-510 °C). The first peak around 190°C is likely to oxidation/evaporation of hydrocarbon from the fuel that has been physisorbed on the deposit. A CO_2 peak at temperatures < 200°C was not observed by Venkataraman nor Roan. Altin and Eser, however, did observe a CO_2 peak at temperatures < 200°C (11) (12). Even though the tube segments in this study were washed with *n*-hexane and dried before analysis, the low temperature peak was still observed.

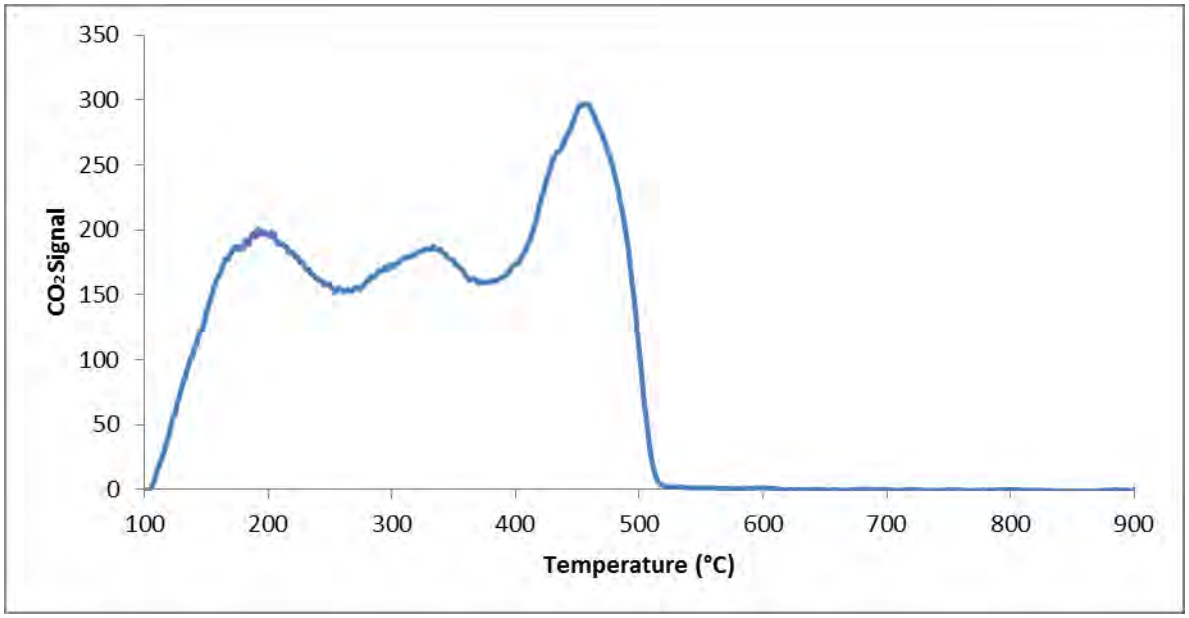

Figure 4-18: TPO profiles of carbon deposits formed on tube segment from middle section after thermal oxidation with EN 590 diesel at 300°C for 5h.

The second CO_2 peak evolved around 350°C. This peak can be attributed to oxidation of less ordered deposits. These deposits could be the darker deposits observed on TEM micrographs. The high oxygen content in this species would make them oxidise at lower temperatures (15). The last peak between 480°C and 510°C could be from the oxidation of relatively more ordered deposits with less oxygen content, which may be the spherical deposits observed in SEM or the amorphous deposits which were embedded in the carbonaceous layer.

Top Section from flow reactor: The SEM image of deposits from the top section did not show much detail with regards to the morphology. Spherical particles of different sizes, however, were visible in Figure 4-19. Some of the spherical particles seem to have agglomerated into clusters red arrows in Figure 4-23.

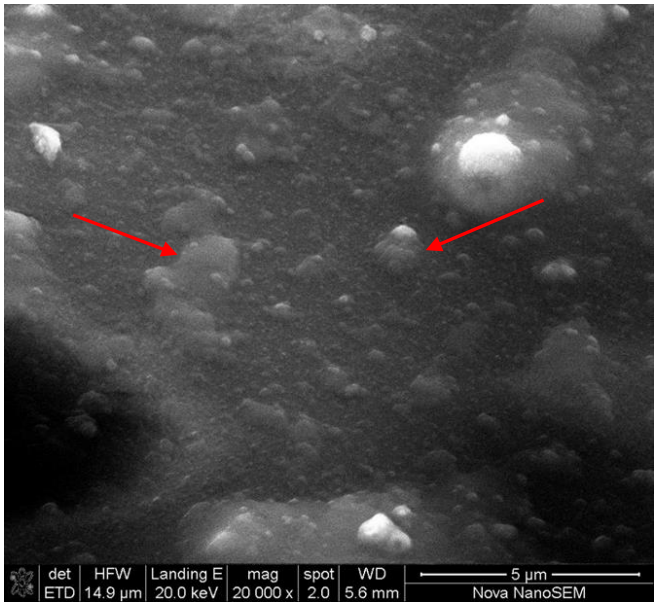

Figure 4-19: SEM images of deposits formed on SS 316 after thermal stressing of EN 590 reference diesel at 300°C for 5h (tube segments from top section of flow reactor).

The deposit morphology was more apparent when viewed under TEM. The two TEM micrographs in Figure 4-20a-b illustrate that the deposits had a spherical morphology. The size of the individual particles appeared to be uniform with a diameter of approximately 10nm. The particle size was significantly smaller compared to that reported by Venkataraman and Eser (8) and Kaminuza (15) which were 90nm and 100nm respectively.

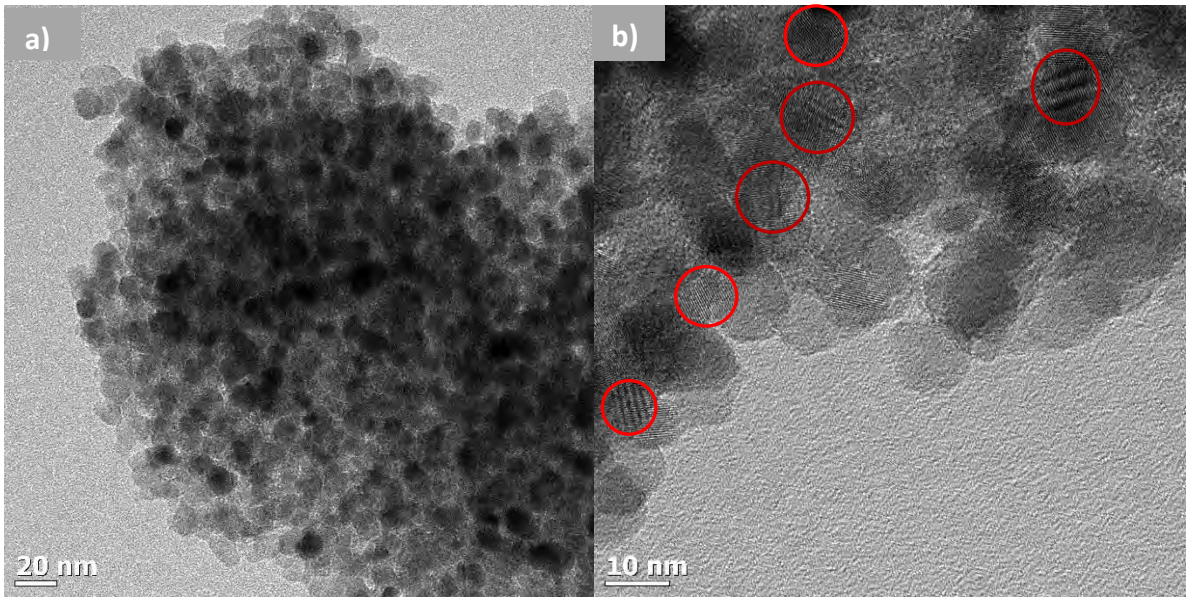

Figure 4-20: TEM images of deposits formed on SS 316 thermally (tube segments from top section of flow reactor).

The spherical deposits had different opacities. Some were darker than others. The increased colour intensity on certain particles might be because these particles contain higher oxygen content than lighter particles. When the spherical particles were observed at higher magnification, planar lattices were observed in the interior as highlighted by the red circles in Figure 4-20b. Inspection reveals that the spacing in each of the circles differs. This would suggest that the fringes are moiré fringe artefacts although it should be noted that overlapping sheets such as graphene may give rise to moiré fringes. Because crystallites have uniform crystal plane spacings, uniform fringes would be expected for 3-dimensional structures.

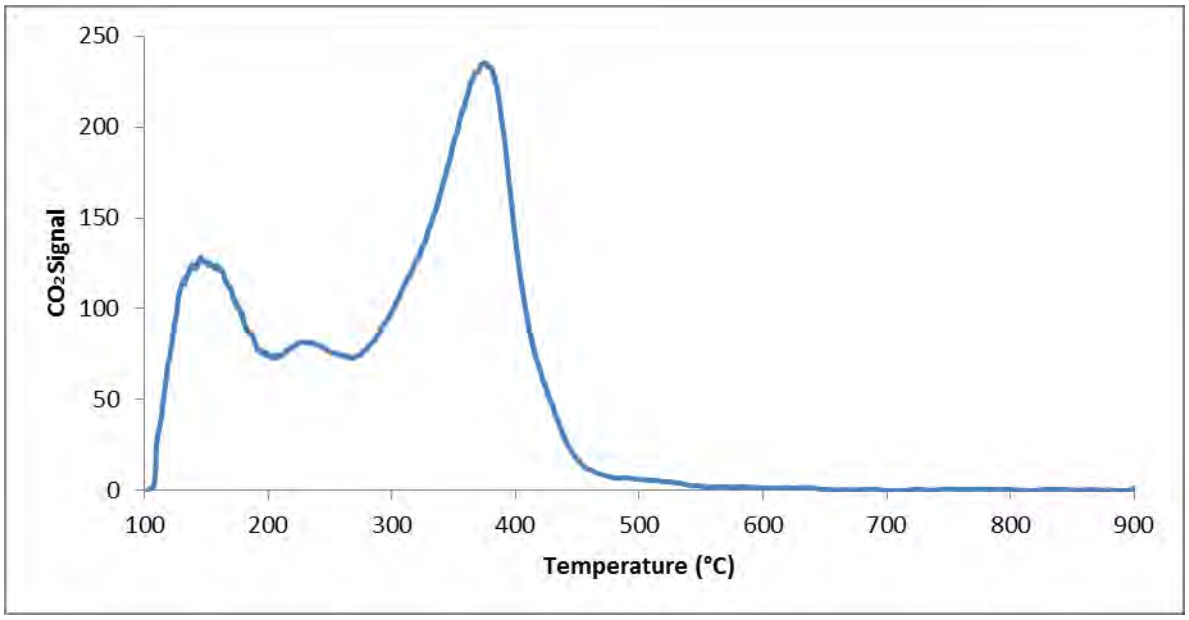

Figure 4-21: TPO profiles of carbon deposits formed on tube segment from top section after thermal oxidation with EN 590 diesel at 300°C for 5h.

The TPO profile of deposits from the top section was similar to that of deposits from the middle section. Three peaks were also observed from the TPO profile of these deposits with the major difference being the CO_2 intensity and the temperature at which the peak evolved.

Figure 4-21 illustrates CO_2 peaks evolving at 150°C, 220°C and 380°C. The peak evolving around 150°C is due to presence of fuel in the deposits. The second peak evolved around 220°C peak might be attributed to deposits that appear darker on the TEM micrographs because these deposits are likely high in oxygen. Venketaraman and Eser (8) suggested that

carbonaceous species bonded to oxygen functional groups are the most reactive and are most likely to oxidise/combust earliest. The third was peak evolved between 380°C and 460°C, and this is likely due to the oxidation of more ordered, less reactive spherical deposits. The peak size of the CO_2 signal at 380°C was higher than that observed at 220°C and 150°C. A shoulder can be observed between 460^{o}C and 530^{o}C.

1.1.1.1 Discussion

The results suggest that the position at which the fuel is stressed in the fuel reactor has an effect on the amount and nature of deposits formed. One would expect the deposits to increase with an increase in temperature along the tube. The results, however, show that this was not the case. The tube segment from the middle of the tube formed relatively more deposits compared to the tube from the top section. This may be because as the fuel travels up the reactor the oxygen concentration decreases and as a consequence the deposit-forming precursors are reduced.

The TPO profiles deposits from the top and the middle section were very similar. This was indicative that there might be some similarities in the mechanisms by which these deposits formed were formed. When SEM deposits from the middle section were viewed, spherical morphology was seen. A similar spherical morphology was observed with deposit from the top section when viewed under TEM and SEM. This supports the TPO results which suggest similarities in the mechanism in which the deposits were formed. The spherical profile of the deposits is significant as Venkataraman and Eser proposed that this is indicative of deposits formed by nucleation and growth in the liquid phase (8).

The height of the CO_2 signal was bigger at relatively higher temperature than at lower temperature for both top and middle section. The relative peak height of the CO_2 signal from deposits formed on the top section was significantly different as can be seen in Figure 4-21. This may be attributed to presence of relatively more ordered deposits present in the top section. The presence of lattice fringes observed on the TEM images supports the TPO results.

The TPO profiles from both tube segments showed peaks that evolved at relatively low temperature < 500°C. This is consistent with deposits that have been formed by polymerisation and condensation of hydrocarbons in the fluid phase. Even though lattice

fringes were observed on the top section deposits the TPO results do not that support the metal surface had a catalytic effect on the deposits forming mechanism.

4.6.2 Diesel/FAME blends

When the tube segments stressed with RME100, SME100, RME20 and SME20 were viewed under the Nikon microscope, the tube segment from top section of the reactor stressed with SME20 were the only ones that had visible deposits (see Figure 4-22d). Of the three tube segments stressed with SME20, the tube segment from the top section of the reactor was the one that had notable deposits that were brown in colour. The tubes from the middle and bottom only showed a yellow stain, similar to that observed on the tube segment from the bottom section that was stressed with EN 590 diesel. The tube segments, stressed with the other fuels, typically showed no deposits. A yellow staining, however, was observed as can be seen in Figure 4-22.

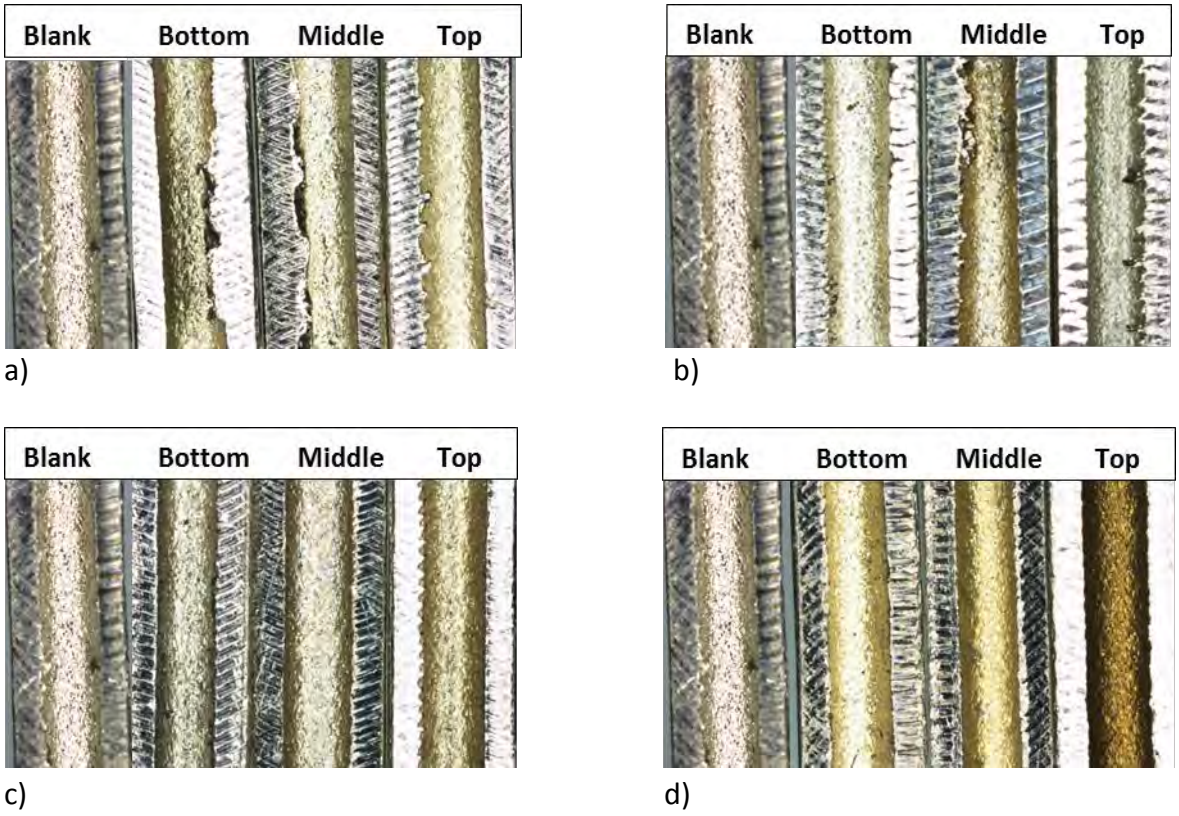

Figure 4-22: Digital microscope images of sectioned flow reactor tubes which were thermally stressed with a) RME100, b) SME100, c) RME20 and d) SME20 at 300°C for 5h.

Tube segments from the top section stressed with SME20 were analysed to obtain the amount of deposits that formed. The amount of deposits was 29 µg C/cm^2. This was lower than the amount of carbon deposits formed from stressing EN 590 diesel. This was not surprising as visually the deposits from EN 590 diesel were more intense compared to those formed from SME20.

SME20 formed a thin layer of deposit on the tube that could not be scrapped off the metal surface for TEM analysis. As a result the deposits were only examined under SEM. Figure 4-23a-b illustrates the SEM microstructure of deposits that formed on the top section of the tube stressed with SME20 along with a SEM micrograph of the unstressed tube. It is apparent when comparing the two micrographs that there is some surface roughening and more particles on the surface of the stressed fuel which have a different morphology to those observed on the unstressed tube. This is likely an indication of a small amount of deposits that have formed on the surface.

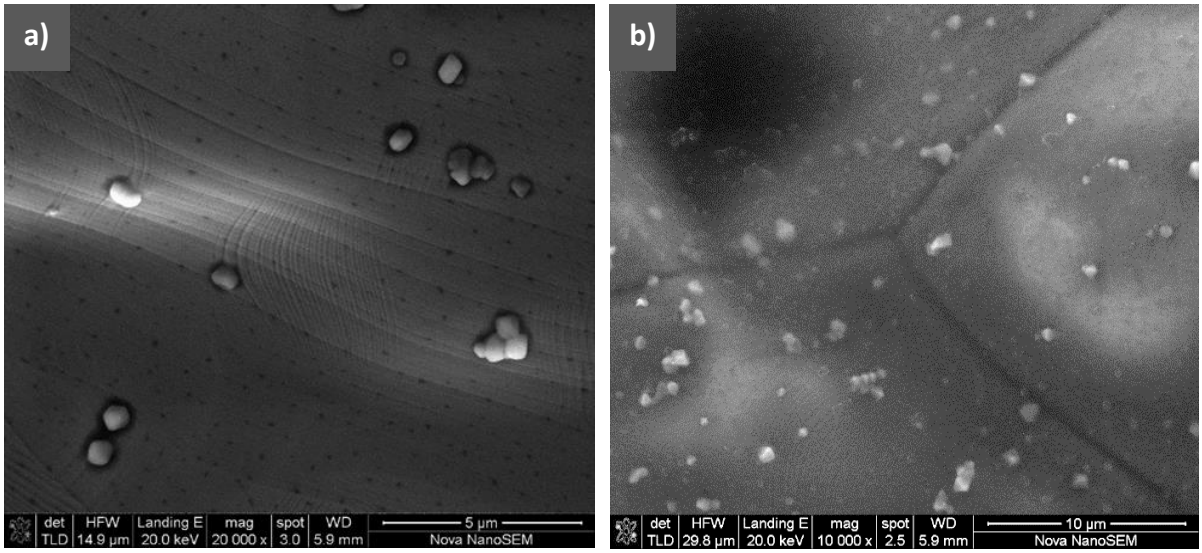

Figure 4-23: SEM images of (a) unstressed (b) stressed SS 316 tube segment from the top section after thermal stressing of SME20 at 300°C for 5h.

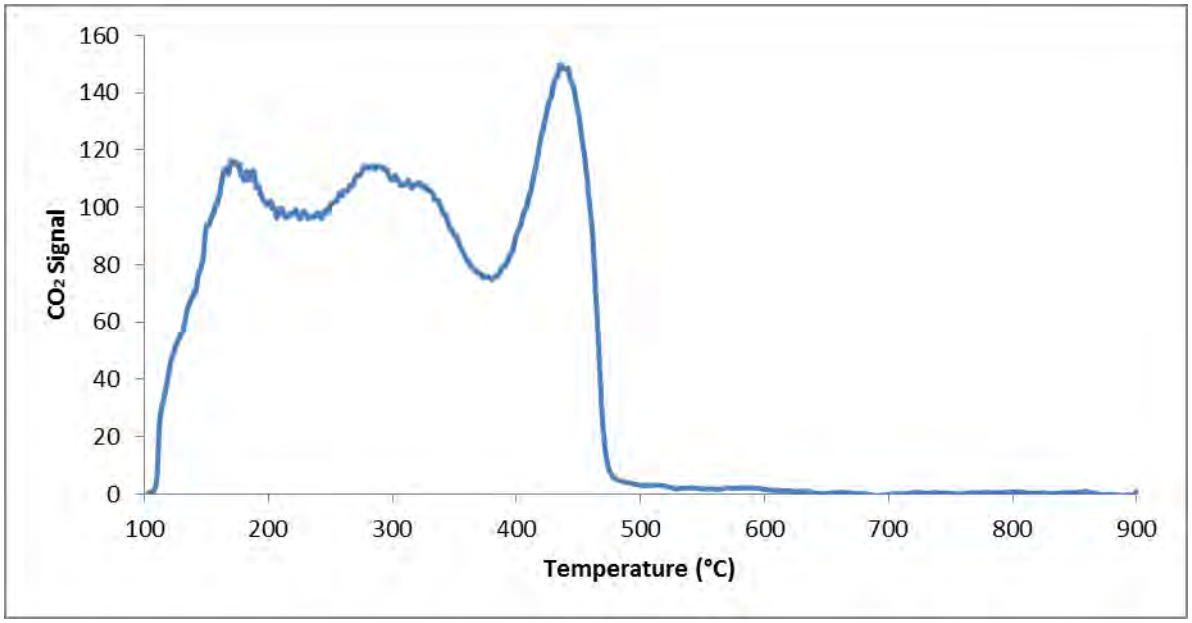

Figure 4-24: TPO profiles of carbon deposits from thermal stressing SME20 on SS 316 for 5h at 300°C compared to TPO profile of unstressed tube.

The TPO profile of these deposits depicted in Figure 4-24 has a shape similar to that observed with EN 590 diesel deposits. The CO_2 signal of the SME20 derived deposits was relatively lower compared to that of the EN 590 derived deposits from the same axial position (top tube segment).

The low temperature peak which has been attributed to the oxidation of fuel adsorbed on the deposits evolved around 170°C for these deposits. This was followed by CO_2 peaks at 300 and 450°C respectively. The SEM micrograph shows only a few particles with near spherical morphology. Even though the TPO results suggest that there is at least more than one structure in these deposits, it is difficult to correspond CO_2 peak to deposits morphologies observed from SEM.

4.6.2.1 Discussion

Few to no deposits were visible on the SS 316 metal tube segments that were examined after thermo-stressing where pure FAME or FAME blends were passed through the reactor. This was not expected. One might expect FAME and FAME/ diesel blend to form more deposits compared to EN 590 as this fuels are more prone to oxidation due to the presence of unsaturated fatty acid methyl esters (5,47,2). Kaminuza observed the level of deposits to

be SME20 > RME20 > EN 590 diesel after thermo-stressing in sand bath reactor at 250°C for 24h (15). Barker *et al.* also observed higher deposition on the injector tip from an engine running on SME 100 than that running on petro diesel. The engine had been for 1000 h and the temperature the fuel was exposed to was high (25).

The low or lack of deposition in this studies maybe because the fuel's residence time in the flow reactor is only 7.44 min versus 24h in the sand bath and 1000 h in a real engine. It could be that the deposit precursors that were formed did not have enough time in the reactor and the temperature in the reactor was not adequate to promote them to deposit on the metal surface. Another reason maybe that the solid deposits that were formed were soluble in the test fuel and as a result they did not precipitate out of solution and adhere on the surface.

It is suggested that the deposits that form contain oxygen, making them polar in nature (48). The oxygen-containing ester group in FAMEs makes this fuel inherently polar in nature. The polar deposits are easily soluble in the polar FAME fuel, which retains the deposits in solution. Blending EN 590 diesel with FAMEs reduces the polarity of the fuel. It is suggested that this in turn reduces the ability of the blend to keep the deposits in solution. This may explain why deposits formed from SME20 blend and not from SME100. The solvency of FAMEs is explored further in section 6.1.

Not all methyl ester have the same propensity to decrease fuel stability, as was evidenced by SME20 forming measurable solid deposits and RME20 forming very little under the same conditions. This can be attributed to the composition of the fatty acid composition of the soybean oil which is composed of 55% 18:2 (carbon number: double bond) fatty acids as opposed to 22% (18:2) for rapeseed oil (see Table 2-1) (22). The greater degree of unsaturation of SME makes it more prone to oxidation than RME since *bis*-allylic sites are extremely prone to hydrogen abstraction. This in turn leads to faster crosslinking reactions and thereby deposition.

The spherical morphology of the deposits and the absence of high temperature (> 500°C) CO_2 peaks suggest that the deposits formed from stressing SME20 were formed from nucleation and growth in the fluid. The similarity of the TPO profile shape to that observed from EN 590 diesel deposits also supports that the mechanism by which this deposit formed

is similar to the one by which EN 590 deposits were formed. This was not surprising as SME20 is composed of 80% EN 590 diesel.

4.7 Effect of zinc doping

Thermal stressing of pure FAME fuel stressed in a flow reactor at 300°C for 5h did not results in carbonaceous deposits that adhered to the metal surface. The objective of this study was also to analyse and compare the morphology and chemical nature of deposits formed from diesel fuel to those formed from FAME and FAME blends. In an attempt to drive the reaction to form solid deposits that would adhere to the surface, the fuel was doped with 10 ppm zinc because such doping has been shown to accelerate deposition (89).

This experiment was only conducted on SME100 since pure FAMEs were the fuels that appeared resistant to deposition on the metal surface.

4.7.1 Results and Discussions

Figure 4-25 shows even after doping the fuel with 10 ppm zinc, no deposits were observed when the sectioned tubes were viewed under an optical microscope. As a result no TEM and SEM analysis could be performed on the tubes to get an idea of their deposit's morphology. The TPO profile of middle section which showed some staining still showed negligible CO_2 peaks at high temperature. The most significant CO_2 signal in Figure 4-26 was that which has been suggested to be due to the oxidation of fuel that has physisorbed to the metal surface.

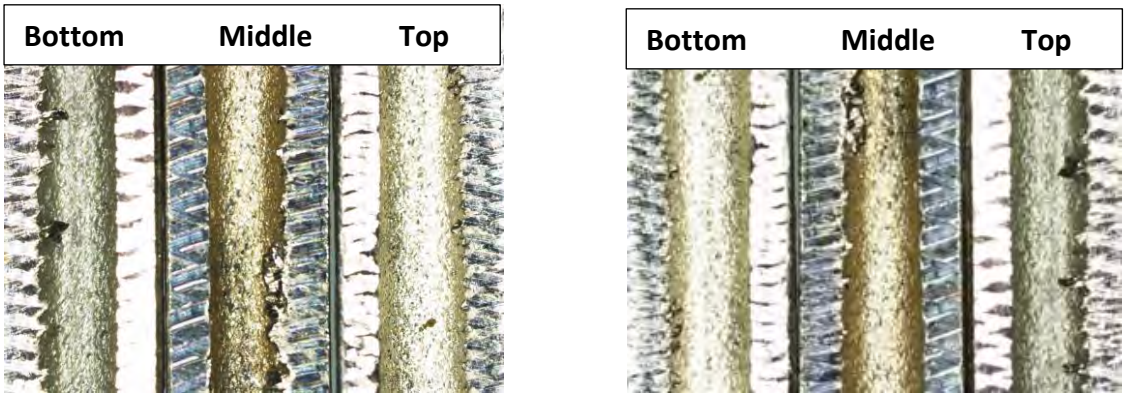

a) b)

Figure 4-25: Digital microscope image of sectioned flow reactor tubes which were thermally stressed with a) SME100 b) SME100 doped with 10 ppm zinc neodecanoate.

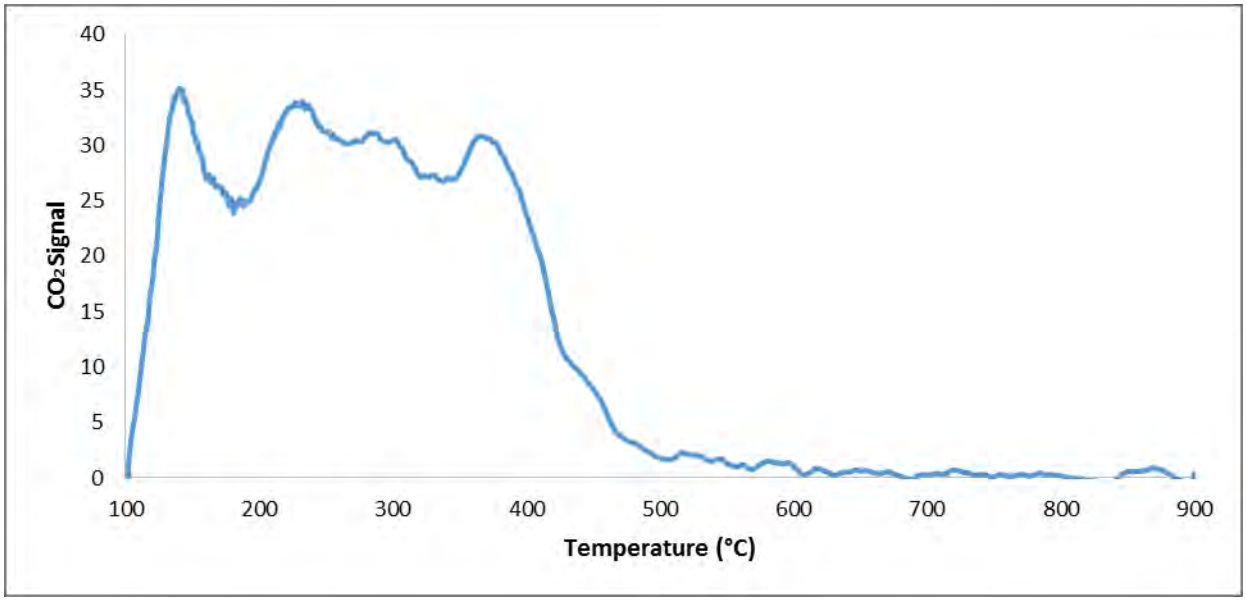

Figure 4-26: TPO profiles of carbon deposits formed on tube segment from middle section after thermal oxidation with SME100 at 300°C for 5h.

Very little deposits formed on the tube surface stressed with SME100 even after repeating the experiment several times. Therefore the thermal stressing procedure was not conducted with the other test fuels as the aim of this experiment was to form soluble deposits that adhere on the metal surface of tubes stressed with all five test fuels.

4.8 Pre-stressed fuel in glass flask reactor

Another approach was evaluated to drive the reaction to form deposits with a high molecular weight and polarity to precipitate out of the biodiesel and adhere on the metal surface.

500 mℓ of the test fuel was pre-stressed in a glass flask reactor for 6h at 140°C before they were thermally stressed in the flow reactor. This was done in order to expose the fuel to excess air in a batch system that would promote the formation of soluble deposit precursors that would be present in the fuel before it is stressed in a continuous flow system in the flow reactor. This experiment was conducted to simulate a real life situation where the fuel is stored for extended period of time. The fuel might be exposed to oxygen, light and moisture which may result in the fuel being unstable before it is used it the engine (1).

The presence of deposits precursors in the fuel would facilitate the formation of solid deposits that could adhere onto the flow reactor tube.

4.8.1 Results and discussions

No discernible deposits were formed on the sectioned flow reactor tubes stressed with pre-stressed SME 100 as can be seen in Figure 4-27. The tube section from the middle of the reactor was analysed in the carbon analyser. As expected the TPO profile of this tube did not show any high temperature peaks different to those observe in the blank tube section that would suggest that there were deposits that adhered on the tube section (Figure 4-28).

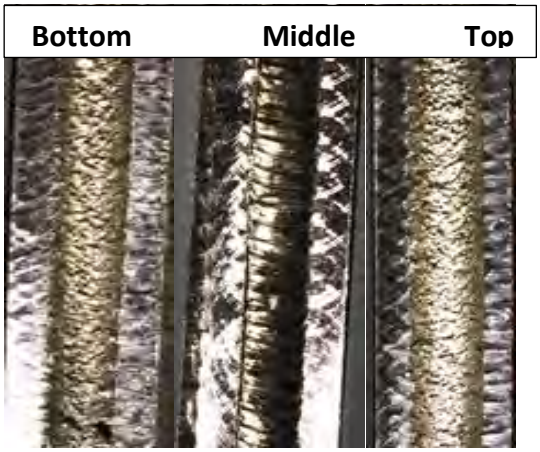

Figure 4-27: Digital microscope image of sectioned flow reactor tubes which were thermally pre - stressed SME 100.

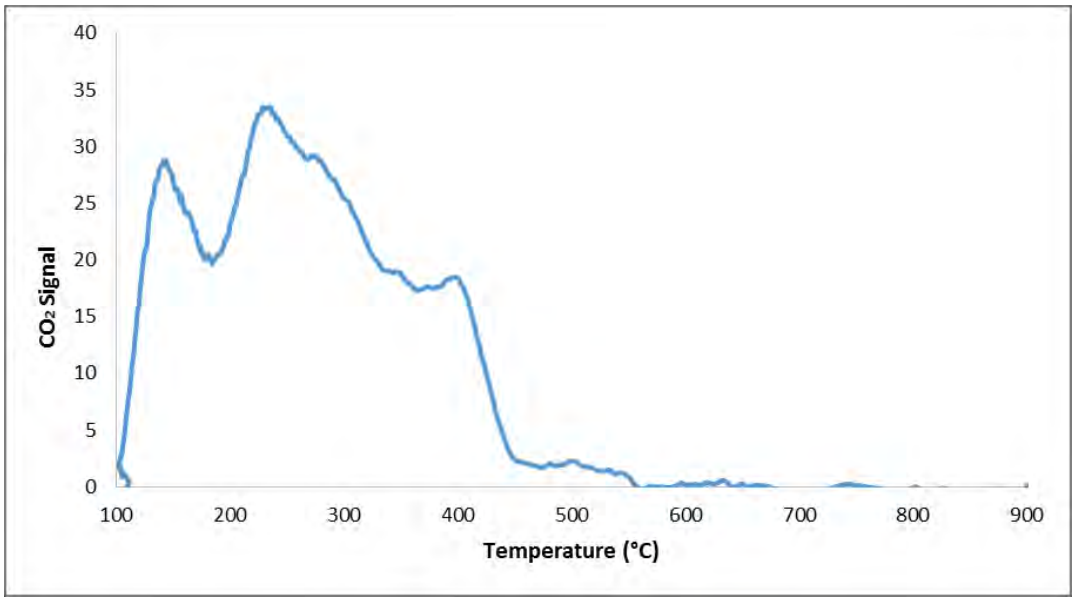

Figure 4-28: TPO profiles of carbon deposits formed on tube segment from middle section after thermal oxidation with SME100 at 300°C for 5h.

It may be that, even though precursor species were formed from thermal stressing the fuel in flask reactor, the conditions in the flow reactor are not sufficient to yield deposits with high molecular weight and polarity that could precipitate out of the polar SME100 and adhere onto the surface.

4.9 Conclusions

The use of a flow reactor to investigate the formation of deposits in biodiesel-containing systems was performed thoroughly for the first time. The results from this study showed that the composition of the fuel affects the deposits propensity of the fuel. Significantly more solid deposits formed from thermal stressing EN 590 over SS 316. This was ascribed to the non-polar nature of the fuel, which allows the deposits to easily precipitate out of solution and adhere on the metal surface. Pure FAMEs did not form discernible deposits on the metal surface. This was suggested to be because the oxygen containing ester in the FAME makes them highly polar. As a result the polar deposits are retained in the fuel.

Adding EN 590 diesel to pure FAME reduced the fuel's polarity and resulted in deposit formation in SME 20 diesel. Pre-stressing the pure FAME and doping FAME with 10 ppm zinc neodecanoate did not drive FAME to yield solid deposits. The results from this study are at odds with previous experiments. Under the conditions employed in this study, deposit formation has been shown to be very complex which would require further investigation beyond the scope of this study. It should also be noted that most previous experiments were flask/bomb experiments in which fuels were stressed for far longer than the time they were exposed to high temperatures in the flow reactor in this study.

The temperature regime which the metal tube was stressed in the flow reactor was found to have an effect on the amount and nature of deposits formed. The EN 590 derived deposits formed more deposits on the tube section from the middle than the top section of the tube; even though the top section was exposed to higher temperature. This was attributed to deposits precursors having being formed lower in the flow reactor and depleted.

The spherical morphology of the EN 590 derived deposits and the SME20-derived deposits suggest that the deposits are formed from nucleation and growth in the fluid.

5 DEPOSITS FORMED AT 400°C

The stressing temperature was increased to 400°C. This was done to investigate the effect of increasing stressing temperature on the stability of the test fuels. EN 590 diesel, RME100, SME100, RME20 and SME20 were thermally stressed in a flow reactor for 5h at 400°C. The thermal stressing temperature for this experiment was set to 400°C on the carbolite type TVS 12/60/900 three zone furnace. The average temperature readings from the three thermocouple placed at different points along the furnace were 320°C at 15 cm, 395°C at 45 cm and 470°C at 75 cm. The exit fuel temperature varied with fuel composition, and the temperature was in the range 350°C to 360°C. The results for the soluble deposit precursor for the test fuels are indicated in the Appendix B (Figure 10-8-Figure 10-13). The trend observed with the 300°C deposits for UV-Vis was the same at 400°C. The ESI-MS analysis on the stressed fuels was also conducted and the results are displayed in Figure 10-14-Figure 10-18 in appendix B.

5.1 Deposit morphology

Figure 5-1a-e indicates that increasing the stressing temperature to 400°C yielded discernible deposits on the top tube segment from all five test fuels. It is evident from Figure 5-1, that the deposits had varying pigmentation and texture. Deposits formed on the top tube segment from SME100 and RME20 degradation were brown in colour, whereas deposits from RME100, SME20 and EN 590 diesel were black in colour.

In order to quantify the observed deposits, the stressed tubes were analysed in the carbon analyser.

Table ***5-1*** shows the average masses of deposit of the different test fuels that displayed significant deposit when viewed under the optical microscope. The average masses were obtained from the two experimental runs. The individual results from each test run have been reported in appendix B Table 10-1.

EN 590 derived deposits were higher on the tube segment from the middle section that on the tube segment from the top. This trend was consistent with the results observed at 300°C. SME20-derived deposits were higher than the EN 590 deposits measured from the same tube segment along the reactor (the top segment). At 300°C the opposite was observed. The reactivity and the morphology of the deposits from all five fuels are reported separately in the succeeding sections.

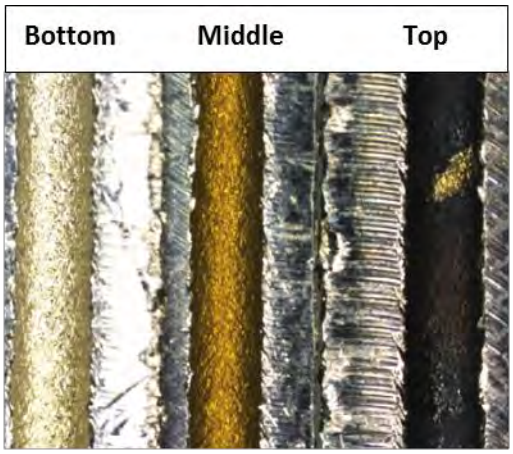

a)

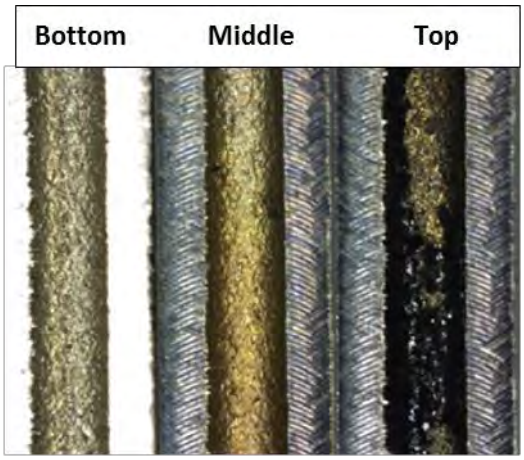

b)

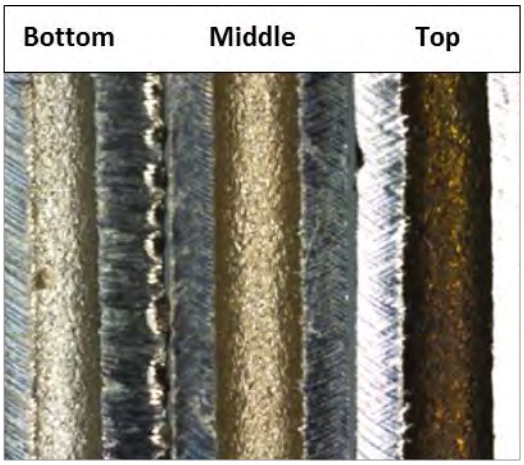

c)

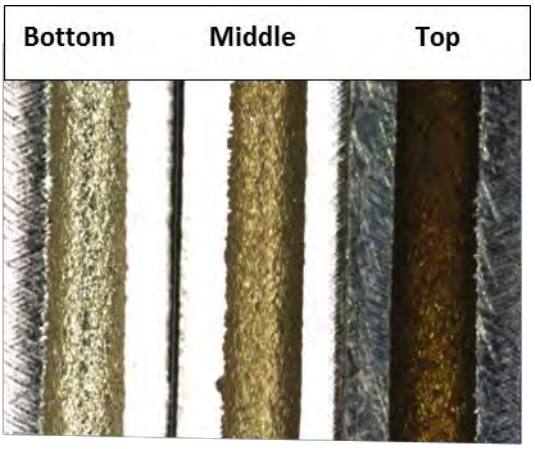

d)

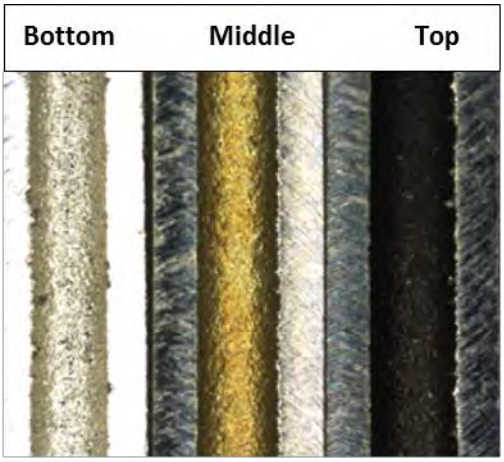

e)

Figure 5-1: Digital microscope images of sectioned flow reactor tubes which were thermally stressed with a) EN 590 diesel , b) RME100, c) SME100, d) RME20 and e) SME20 at 400°C for 5h.

Table 5-1: Average carbon deposit of different test fuels after stressing in flow reactor at 400°C for 5h.

Test Fuel	Average amount of carbon ($\mu gC/cm^2$)	Position of test tube along the axial distance in furnace
EN 590 diesel	68	Top
	131	Middle
RME100	112	Top
SME100	33	Top
RME20	212	Top
SME20	380	Top

5.1.1 EN 590 diesel

MIDDLE SECTION

The SEM micrograph depicted in Figure 5-2, shows that the deposits formed on the middle segment had a spherical morphology. The spherical particle had varying sizes. TEM results confirmed the presence of deposits with a spherical morphology as can be seen in Figure 5-3a. The varying particle size was also visible on the TEM results. The primary particle size of the spherical particles was 80-100nm in diameter; this was the same order of magnitude as the injector deposits reported by Venkataraman and Eser (8) .

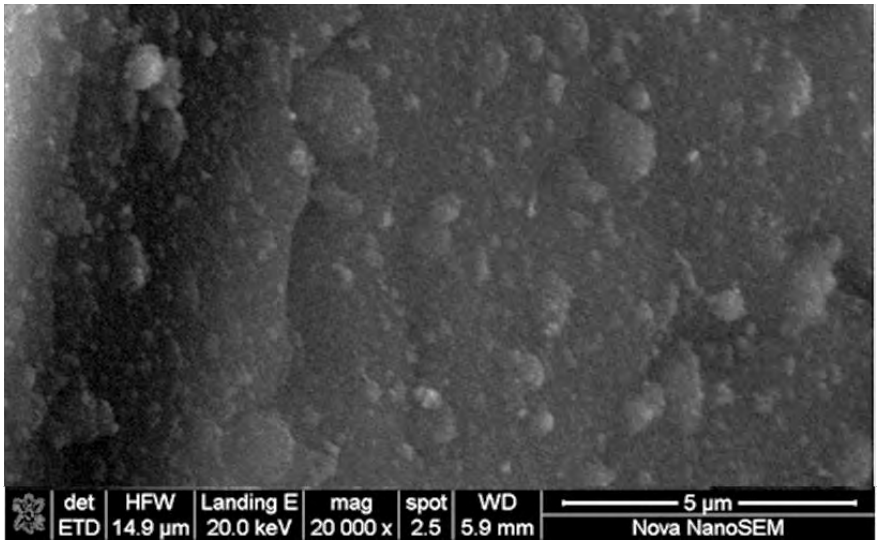

Figure 5-2: SEM images of carbon deposits formed on middle tube segment after thermal stressing with EN 590 diesel at 400°C for 5h.

The TEM micrograph also revealed a gum-like material (indicated by the red arrow in Figure 5-3b) around the spherical particles. The gum material was lighter compared to the dark spherical particles. When the spherical particles were viewed at a high magnification there were no diffraction patterns that were observed (see Figure 5-3b).

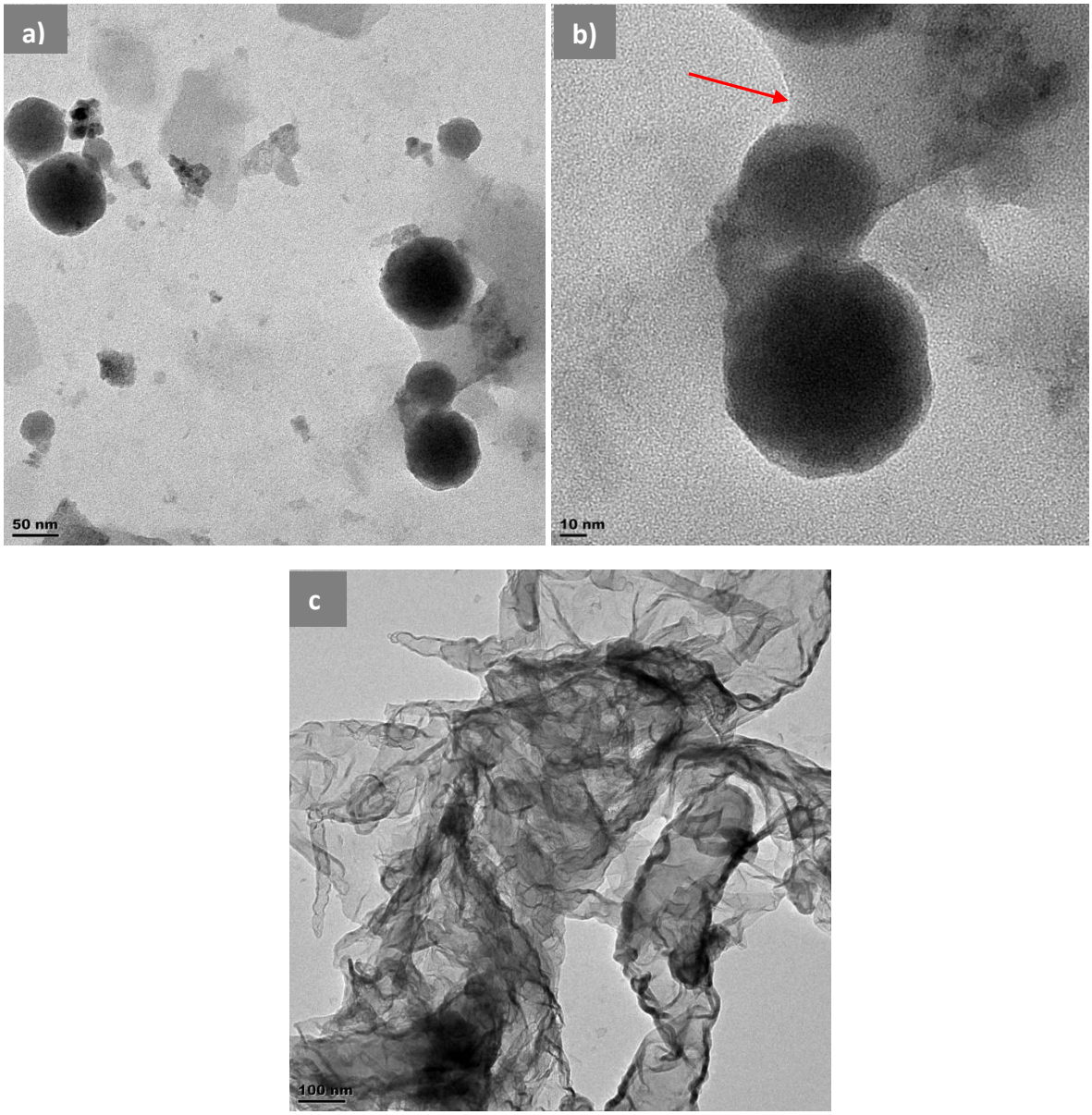

Figure 5-3: TEM images of carbon deposits formed on middle tube segment after thermal stressing with EN 590 diesel at 400°C for 5h; a) at low magnification) at high magnification c) at a different section on the grid.

In addition to spherical particles, a thin layer of material was observed when the deposits were viewed under TEM as can be seen in Figure 5-3c. The thin layers were overlapping and

in some region the layer was almost transparent. The periphery of the thin layer consisted of folded layers that were darker in colour compared to the flat layer. A closer inspection of the edges at high magnification revealed lattice fringes as indicated by Figure 5-4.

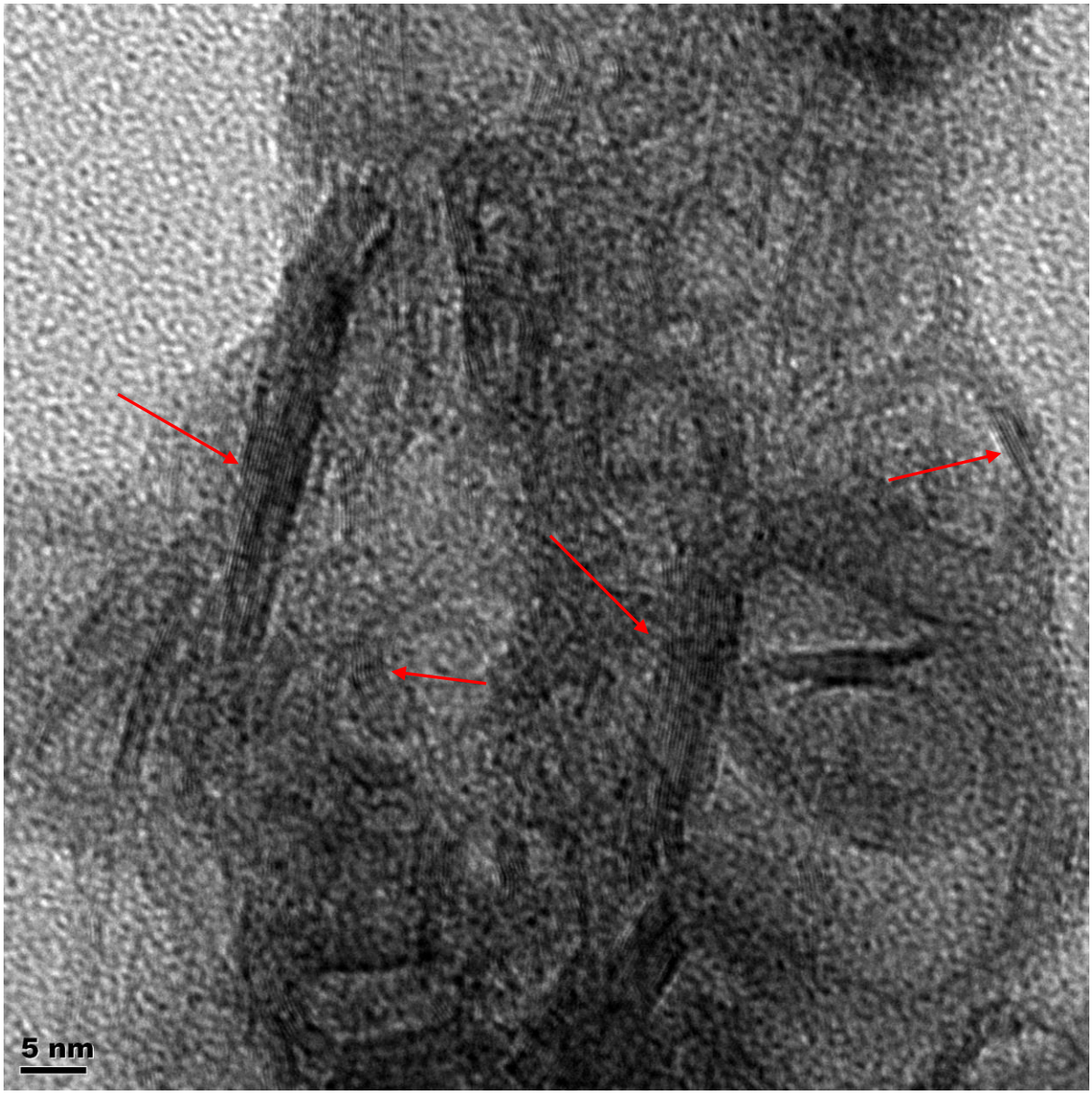

Figure 5-4: TEM micrograph of EN 590 derived deposits viewed at high magnification.

Figure 5-5 shows the TPO profile for deposits formed on the middle segment tube. The TPO shows three groups of peaks. The first peak evolving between 100-200°C is consistent with the oxidation of hydrocarbons adsorbed on the deposits. The second broad peak evolved in the temperature range between 250 and 350°C. The third sharp peak which had the highest peak size evolved around 450°C. The presence of different burn off temperature from the

middle segment deposits is indicative that more than one type of deposits formed. This is in agreement with the TEM results as two types of deposits were observed.

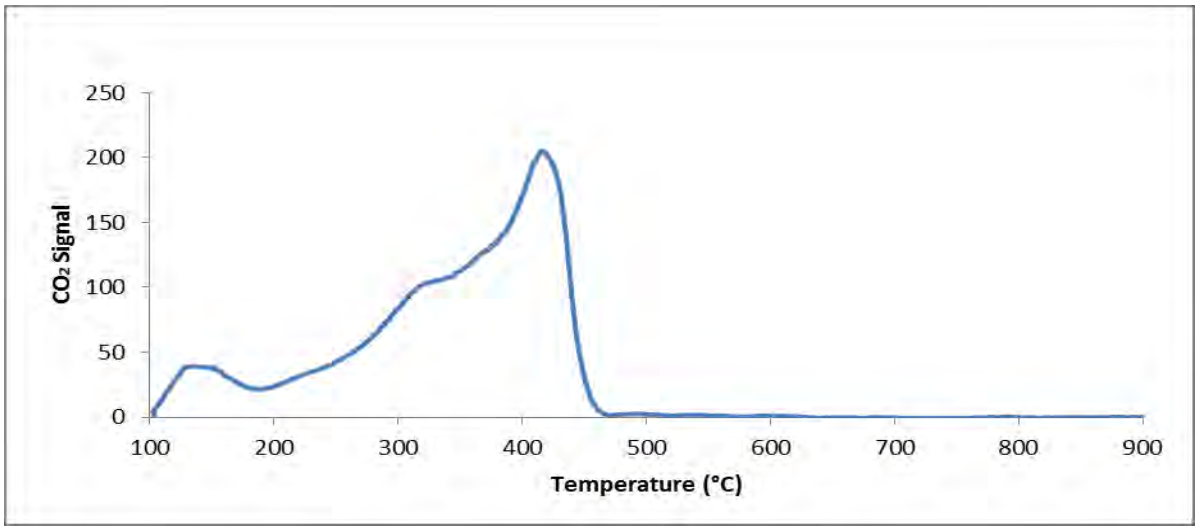

Figure 5-5: TPO profiles of carbon deposits formed on middle tube segment after thermal oxidation with EN 590 diesel at 400°C for 5h.

TOP SECTION:

The deposits formed from the top tube segment also had a spherical morphology. Figure 5-6a shows that these deposits were agglomerated, unlike the middle segment deposits. The individual particle size appeared to be uniform with an average particle size of 120nm in diameter. This was higher than the particle size of middle section deposits. At high magnification no diffraction patterns were observed on the spherical particles as can be seen in Figure 5-6b. The folded overlapped thin layers were also observed on the TEM micrographs of deposits from the top tube segment (see Figure 5-6c).

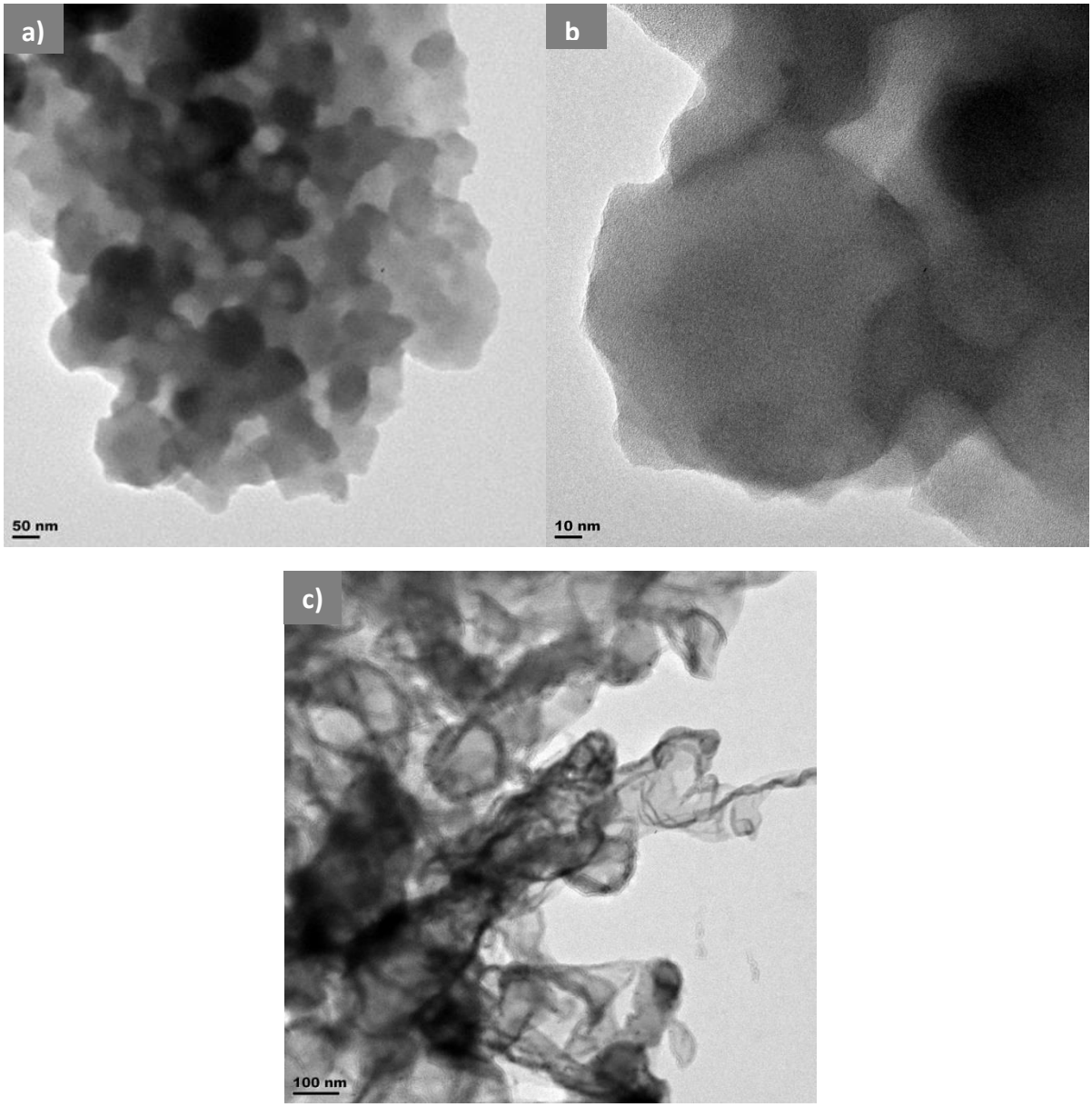

Figure 5-6: TEM images of deposits formed on top tube segment after thermal oxidation with EN 590 diesel at 400°C for 5h; a) at low magnification) at high magnification c) at a different section on the grid.

The TPO profile of deposits formed on the top tube segment contained three peaks around (150, 200-300 and 400°C) and a shoulder around 450°C (highlighted by the red arrow in Figure 5-7). The presence of peaks at different burn off temperatures is in agreement with the different carbonaceous structures noted on TEM images. The shoulder observed could be due to the presence of more ordered deposits forming, the presence of more deposits with lattice fringes observed under TEM corroborates this.

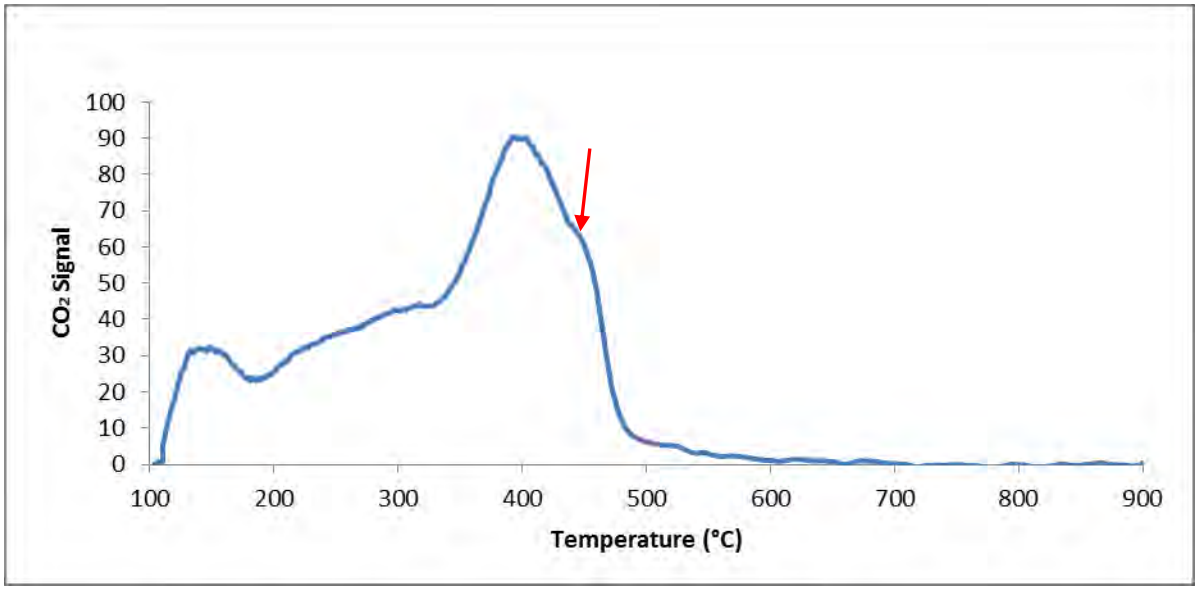

Figure 5-7: TPO profiles of carbon deposits formed on top tube segment after thermal stressing with EN 590 diesel at 400°C for 5h.

5.1.2 RME100

When the RME100-derived deposits were analysed under SEM, the microstructure showed densely packed aggregates with voids between the aggregates (Figure 5-8). This morphology was similar to that observed from diesel injector deposits (8) and thermal oxidative degradation of jet fuel (81).

Viewing the deposits under TEM also confirmed the presence of deposits with spherical morphology as indicated in Figure 5-9 a-b. The morphology of the spherical particles was different to that observed on EN 590 deposits. The particles in this deposits configured into agglomerates in a manner that is similar to carbonaceous soot. Kaminuza also observed a similar morphology on deposits produced from thermal oxidation of SME 20 in a closed bomb reactor (15). At high magnification, interference patterns highlighted by the red arrows were observed in these spherical particles as can be seen on Figure 5-9b. The patterns, however, were not perfectly circular. Figure 10-19 revealed that the thin tangled layers were also observed on these deposits. The TEM micrograph of these deposits at high magnification is depicted in Figure 5-10. Lattice fringes were also observed on the folded edges as indicated by the red arrows in Figure 5-10.

The primary particles size of the bigger spherical structure was 16-32nm in diameter. The primary spherical particles were significantly smaller than those reported by Kaminuza

which ranged from 50-70nm (15). Smaller spherical particles embedded on the bigger spherical material were also observed as can be seen in Figure 5-9a. Similar small spherical particles were observed on EN 590 deposits from the middle tube segment. These particles were relatively darker in colour and their individual particle size was in the same order of magnitude as those observed from EN 590-derived deposits (3nm).

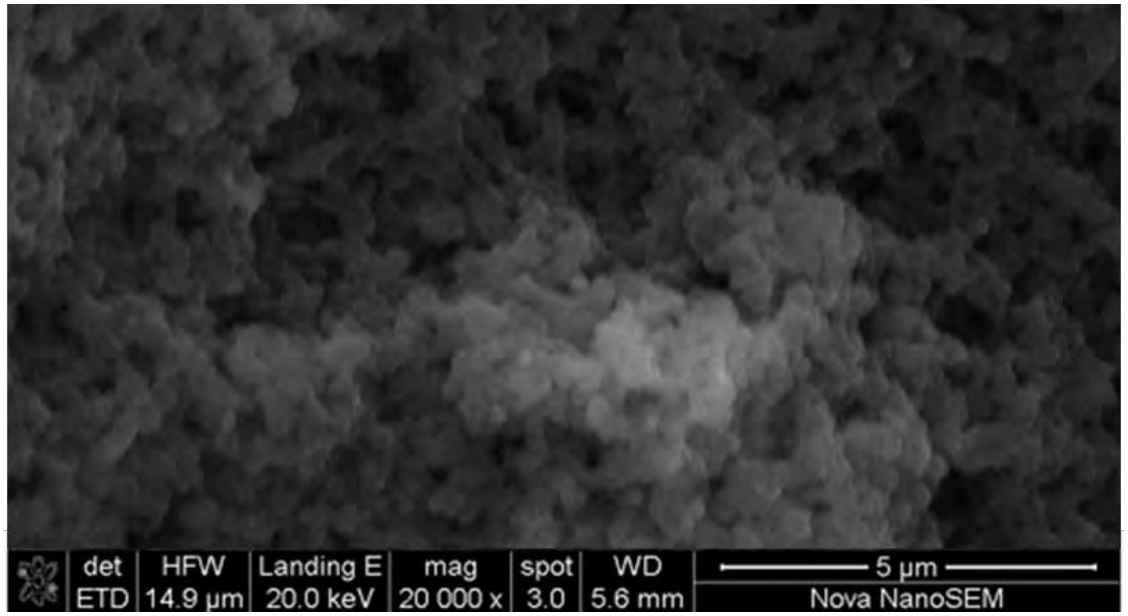

Figure 5-8: SEM image of carbon deposits formed on top tube segment after thermal stressing with RME100 at 400°C for 5h.

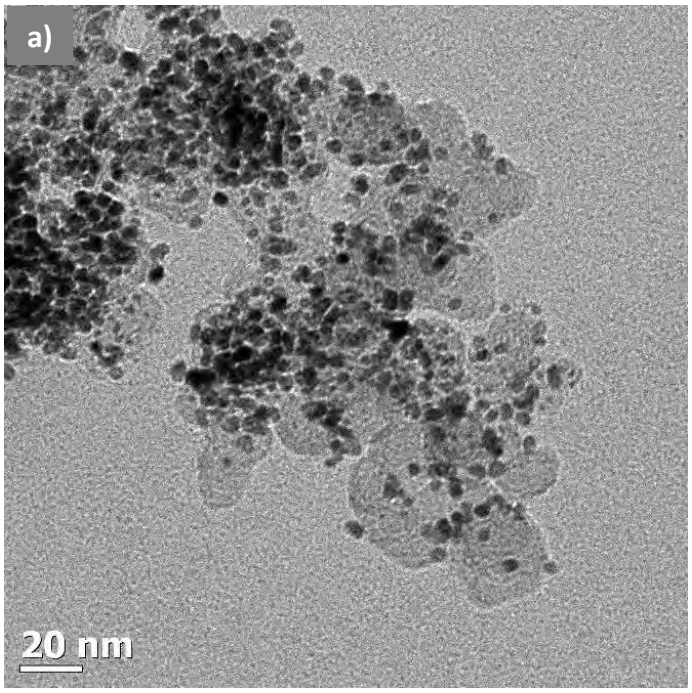

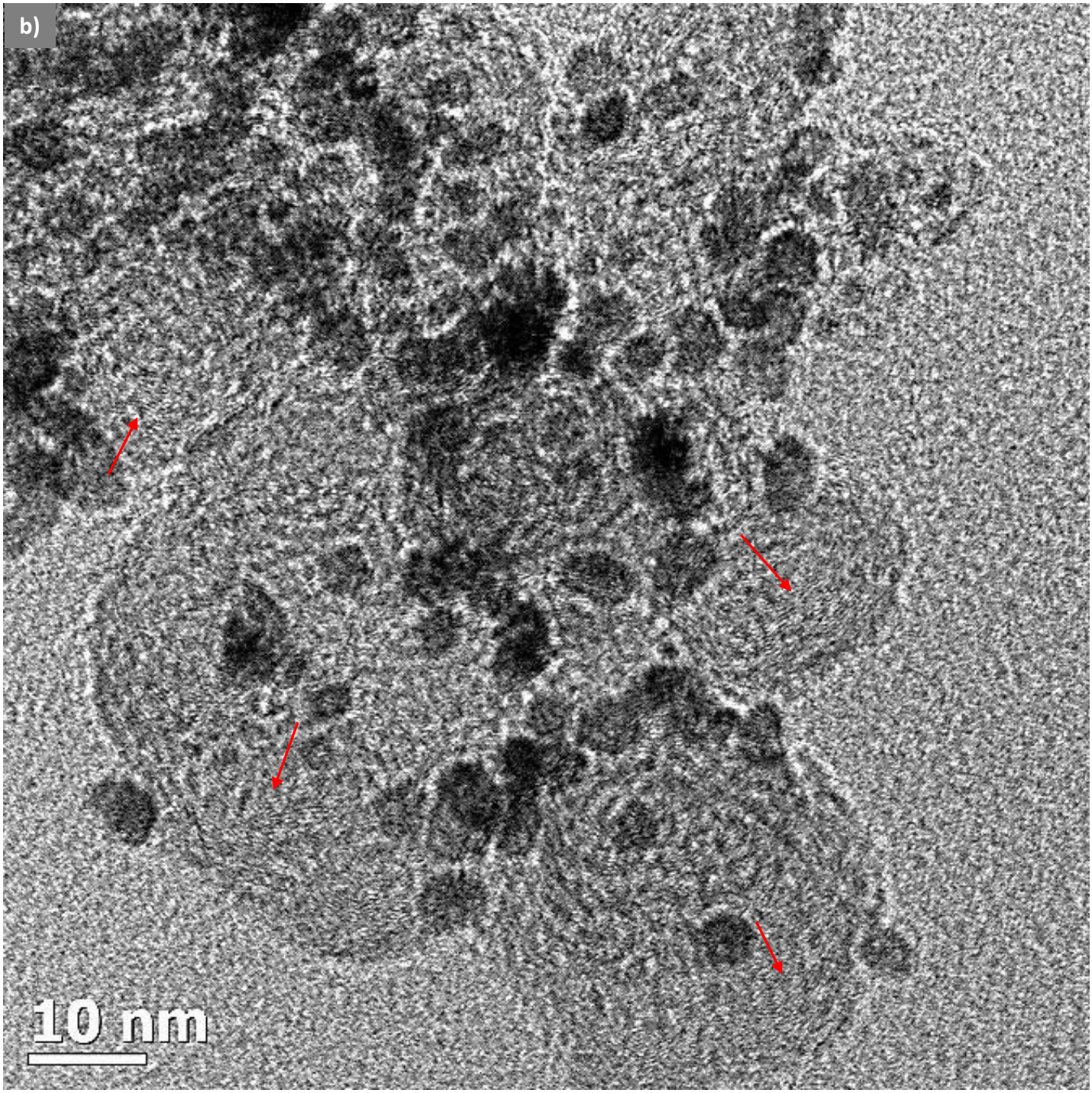

Figure 5-9: TEM images of carbon deposits formed on top tube segment after thermal stressing with RME100 at 400°C for 5h; a) at low magnification b) at high magnification.

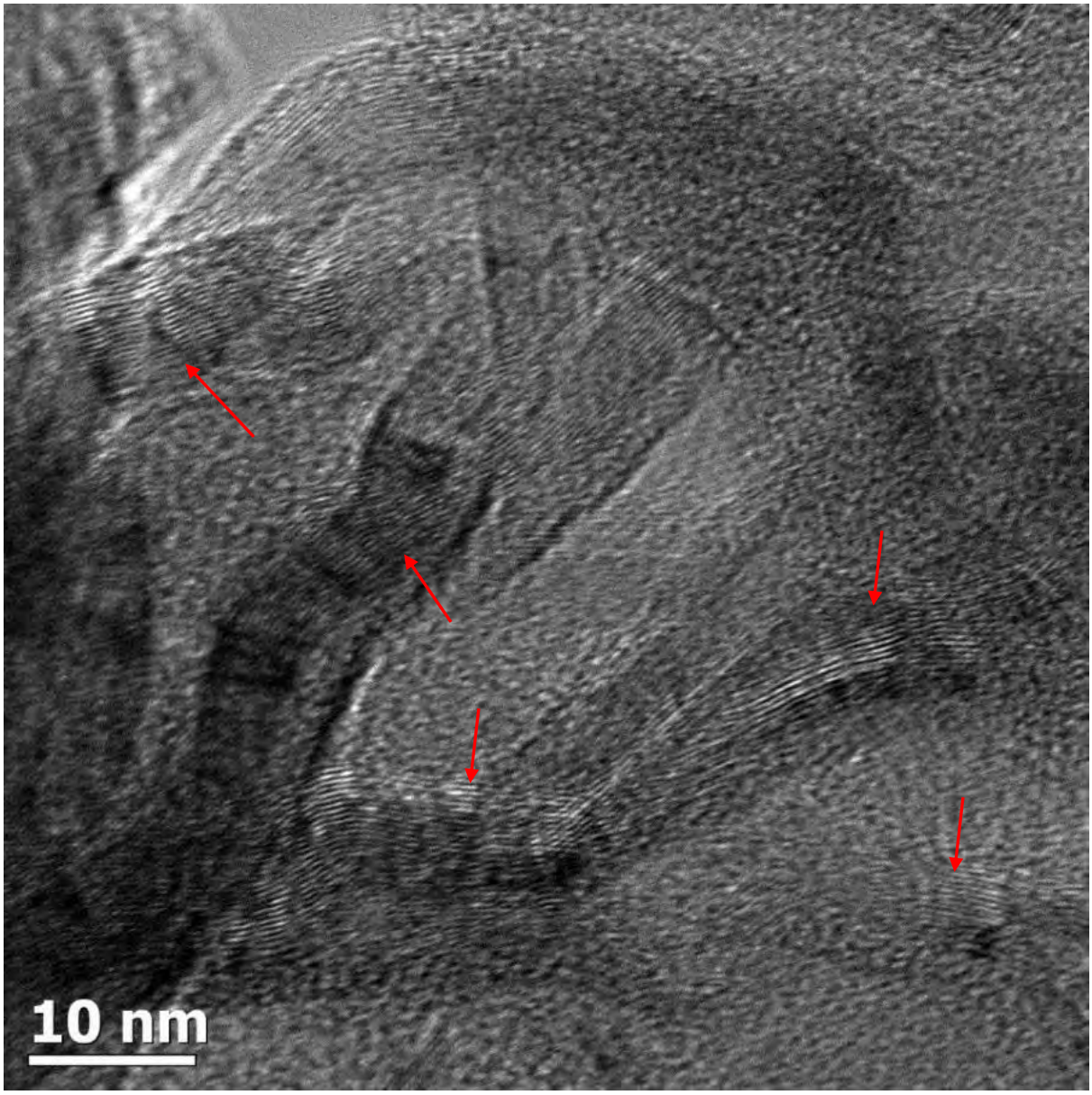

Figure 5-10: TEM images of carbon deposits formed on top tube segment after thermal stressing with RME100 at 400°C for 5h at a higher magnification.

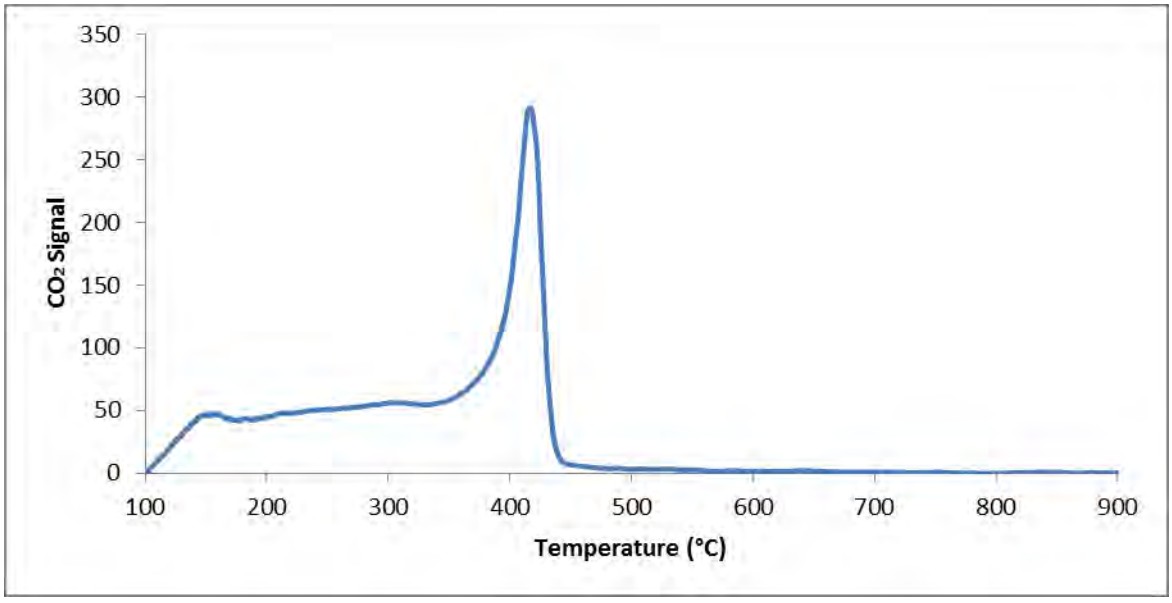

Figure 5-11:TPO profiles of carbon deposits formed on top tube segment after thermal tressing with RME100 at 400°C for 5h.

Figure 5-11 shows, three groups of peaks were also observed from the TPO profile RME100 deposits. The peaks evolved between 150-250°C, 250-350°C and 410°C respectively. The TPO profile of the deposits and the TEM results are consistent as they indicate the presence of more than one type of deposits. The shape of the TPO profile is different to that observed on EN 590 deposits. The high temperature peak is very sharp and narrow compared to the broad peak observed on the EN 590 deposits. In addition, the relative peak size of the peak at 410°C is higher compared to that which evolved between 250-350°C. This may be because at high thermal stressing temperature, more ordered deposits are formed. The presence of thin like film deposit with lattice fringes observed under TEM is corroborates the TPO results.

5.1.3 SME100

The morphology of the spherical particles from SME100 deposits was similar to those observed from EN 590 derived deposits from the middle section. Particles with varying sizes were also observed as can be seen in Figure 5-12a.

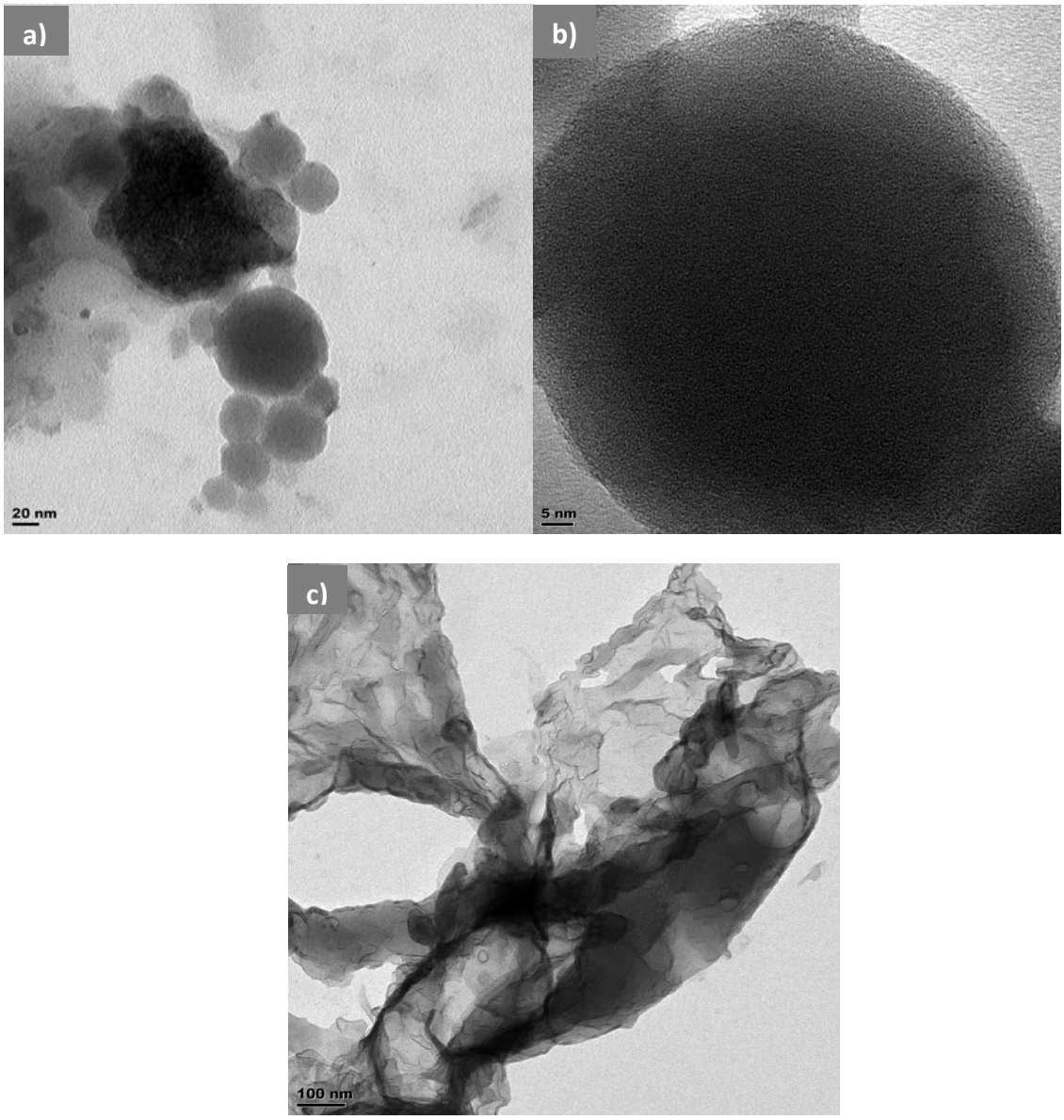

Figure 5-12: TEM micrographs of carbon deposits formed on top tube segment after thermal stressing with SME100 at 400°C for 5h; a) at low magnification) at high magnification c) at a different section on the grid.

The dimension of the individual particles was 20-85nm. Some of these particles were in the same order of magnitude as the deposits formed on the middle section of the tube stressed with EN 590 diesel. No diffraction patterns were perceived from high resolution TEM (see Figure 5-12b).

Deposits with overlapping thin layers were also noted from the TEM micrographs of SME100-derived deposits as indicated in Figure 5-12c. The lattice fringes observed at the edges were also present on this deposits as indicated by the red arrows in Figure 5-13.

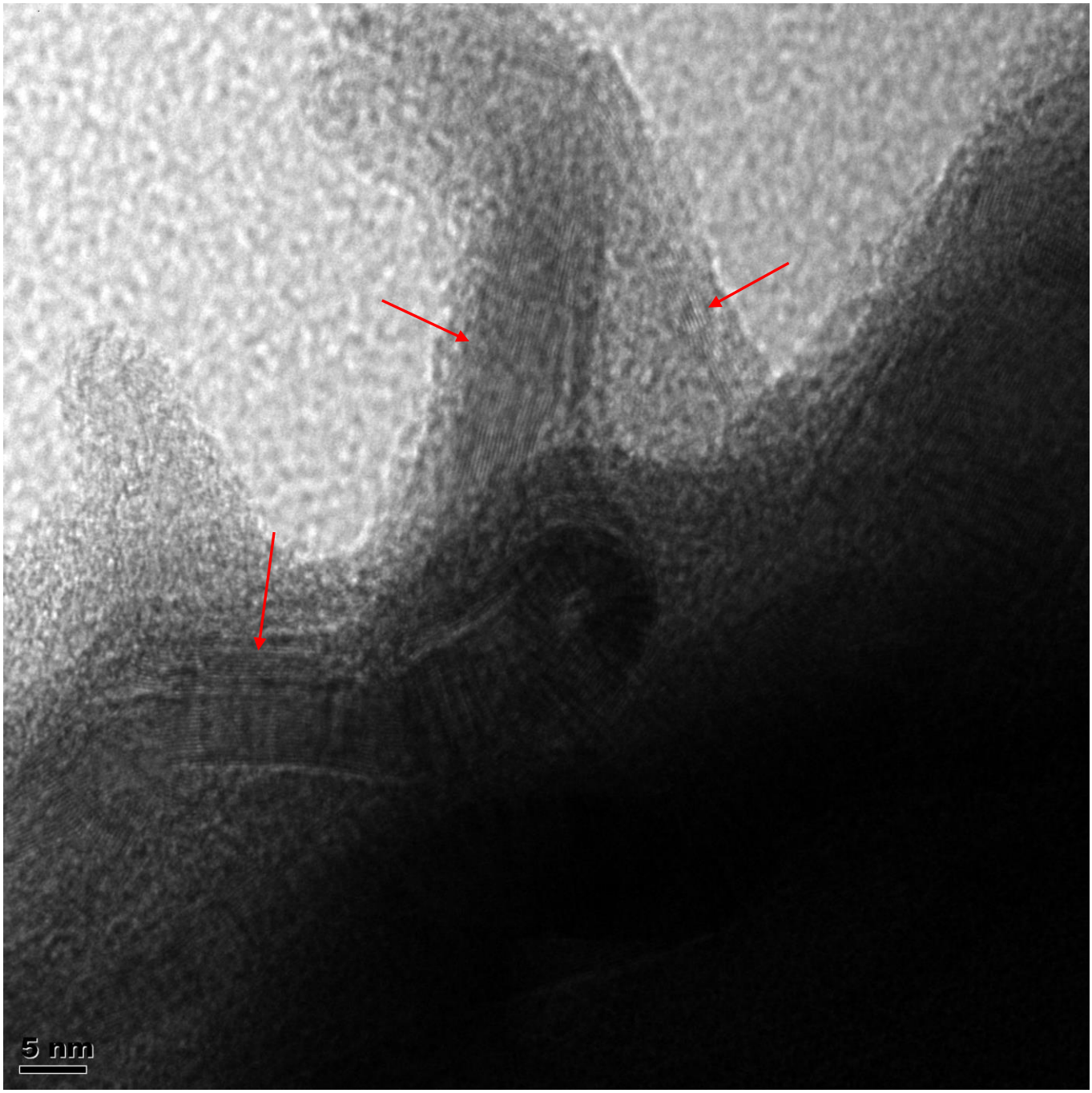

Figure 5-13: TEM micrograph of SME 100 derived deposits viewed at high magnification.

The TPO profile in Figure 5-14 showed CO_2 evolution at three temperatures; the first carbon signal evolved at 130°C, the second peak occurred approximately 250°C and the last peak which had the highest peak size was at 450°C. The TEM micrographs showed two types of deposits which are in accordance with the multiple peaks observed on the TPO profiles.

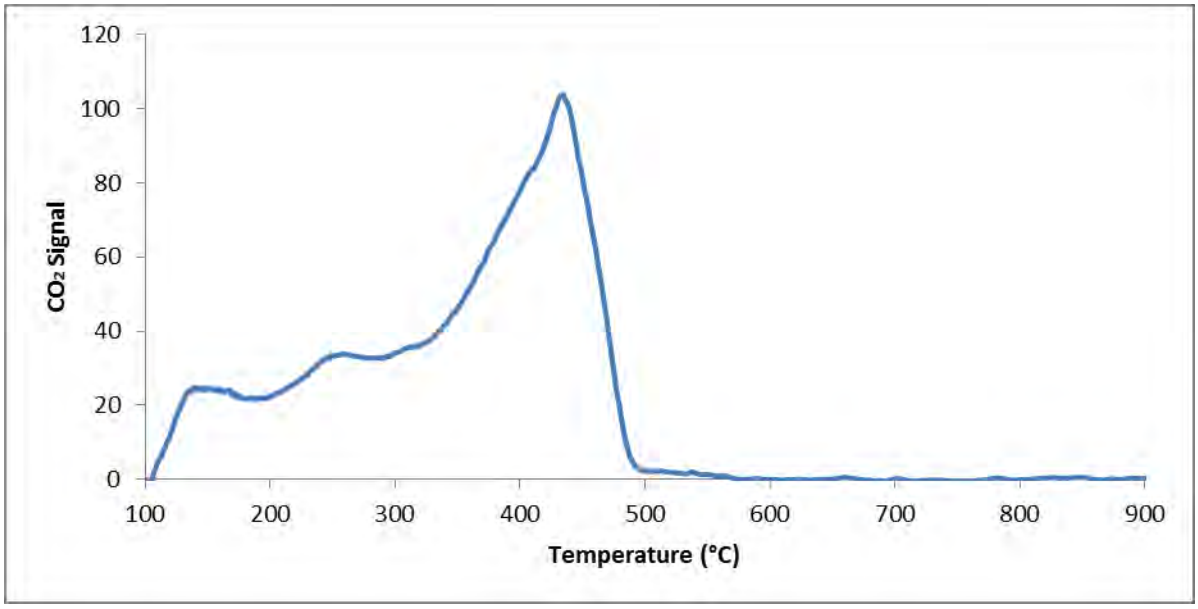

Figure 5-14:TPO profiles of carbon deposits formed on top tube segment after thermal stressing with SME100 at 400°C for 5h.

5.1.4 RME20

TEM images of RME20 deposits showed two types of deposits akin to the RME100 deposits as can be seen in Figure 5-15. The spherical deposits exist as agglomerates. The agglomerate has aggregates that are arranged like a chain of spherical particles (indicated by the red arrow in Figure 5-15a) and some aggregates that are clusters. Figure 5-15b revealed what appeared like short interference patterns in the spherical particles when examined at high magnification (highlighted by red arrows in Figure 5-15b. The deposits that appeared as overlapping thin layers with folded edges were also observed Figure 5-15c. The folded edges of these deposits revealed lattice fringes when viewed at a higher magnification (Figure 10-20).

Smaller spherical particles embedded on the bigger spherical material were also observed on these deposits. The individual particles size was in the same order of magnitude as those observed on EN 590 and RME 100 deposits (3nm).

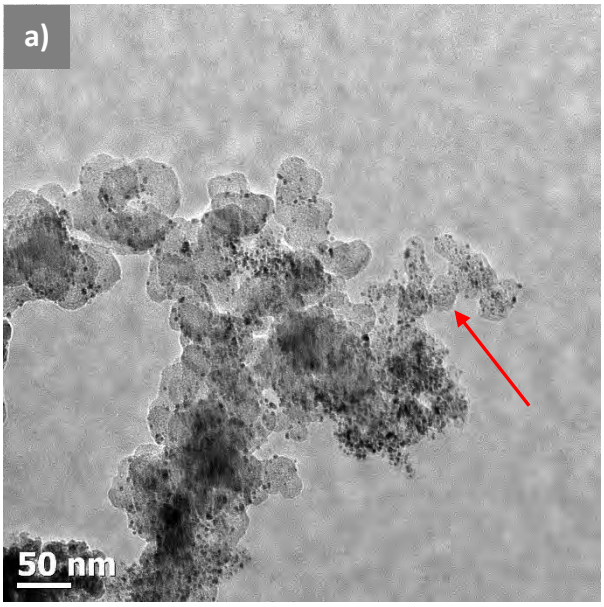
a)
50 nm

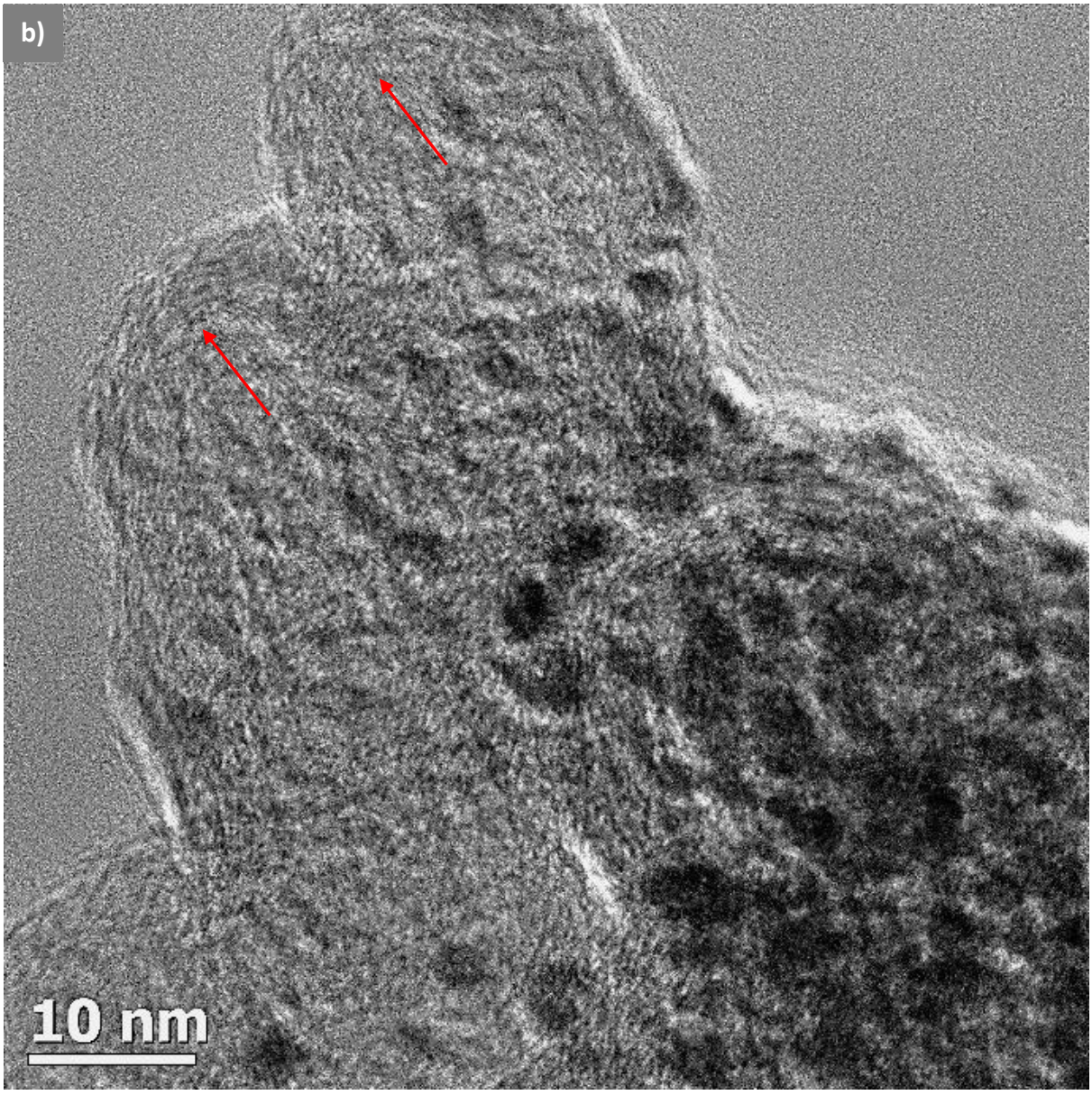
b)
10 nm

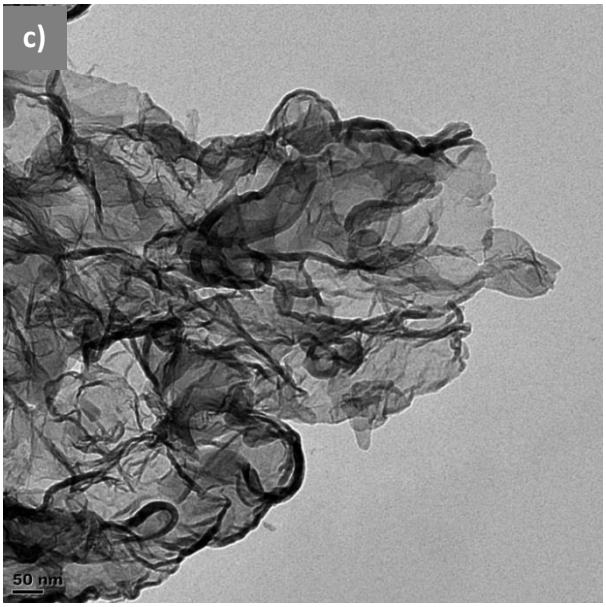

Figure 5-15: TEM micrograph of carbon deposits formed on top tube segment after thermal stressing with RME20 at 400°C for 5h; a) at low magnification) at high magnification c) at a different section.

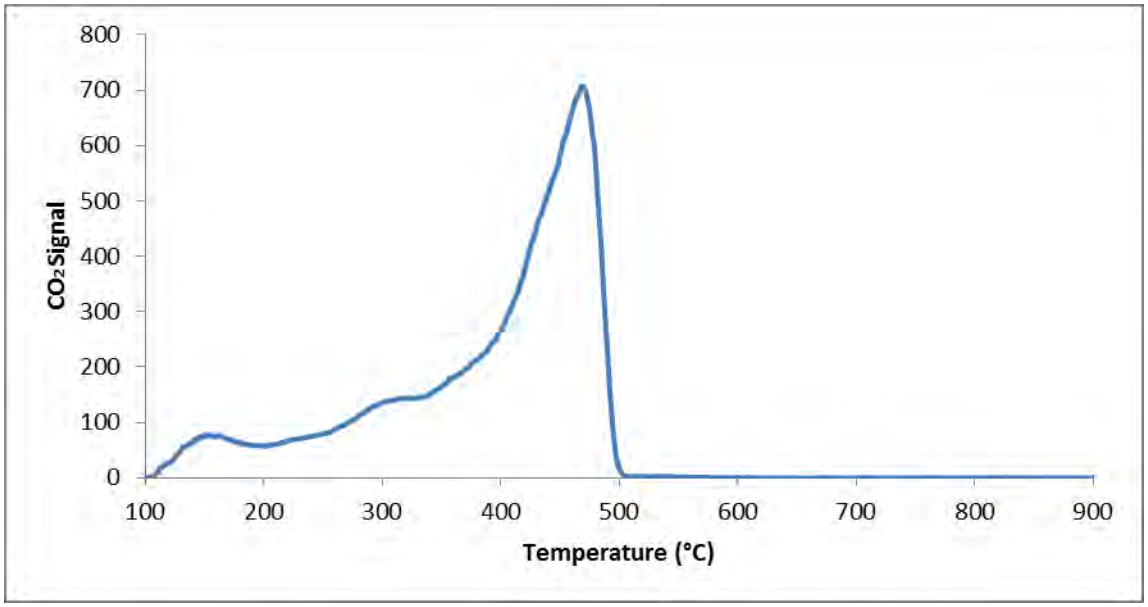

Figure 5-16:TPO profiles of carbon deposits formed on top tube segment after thermal stressing with RME20 at 400°C for 5h.

The TPO profile of these deposits also showed three peaks evolving at different temperatures (see Figure 5-16). This was consistent with the presence of different types of deposits as visually observed from the TEM results. The CO_2 peaks evolved between 100-200˚C, 250-350°C and at 470°C. The Peak at 470°C was very sharp compared to the other

two peaks and this peak also had the highest peak height. The shape of the TPO profile was similar to that observe from RME100-derived deposits.

5.1.5 SME20

The microstructure of SME20-derived deposits is displayed in Figure 5-17. The microstructure of these deposits had agglomerated clusters of spherical particles with voids similar to those observed with RME100 deposits. The spherical clusters appeared to protrude upwards. Underneath the clusters small spherical particles with a uniform size were also observed.

TEM micrographs of these deposits displayed in Figure 5-18 also showed spherical deposits. The spherical particles agglomerated in a manner which was similar to the RME100 and RME20 deposits. The spherical particles showed diffraction pattern near the periphery at high magnification (highlighted by a red arrow in Figure 5-18b). Smaller spherical particles similar to those observed on EN 590, RME100 and RME20 deposits were evident on the TEM micrographs of these deposits.

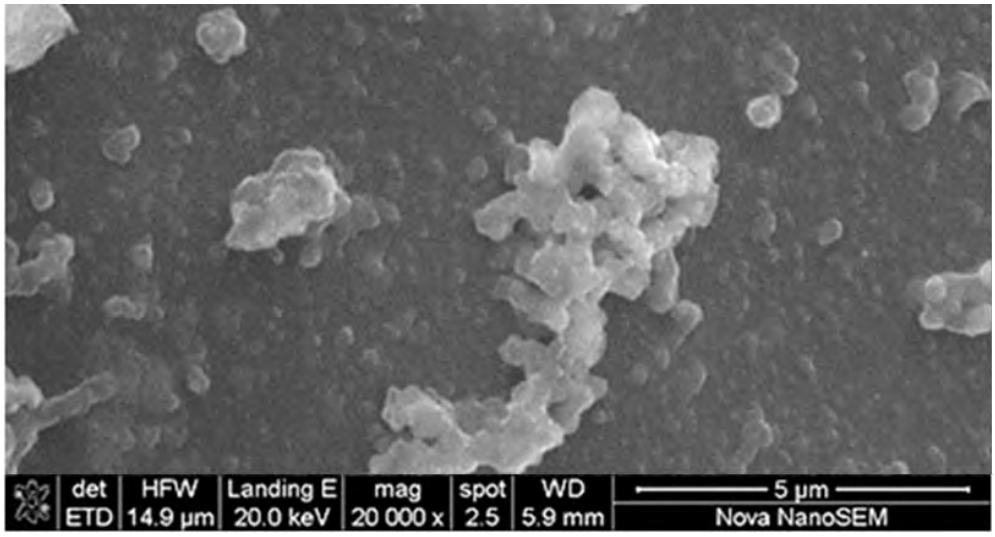

Figure 5-17: SEM image of carbon deposits formed on top tube segment after thermal stressing with SME20 at 400°C for 5h.

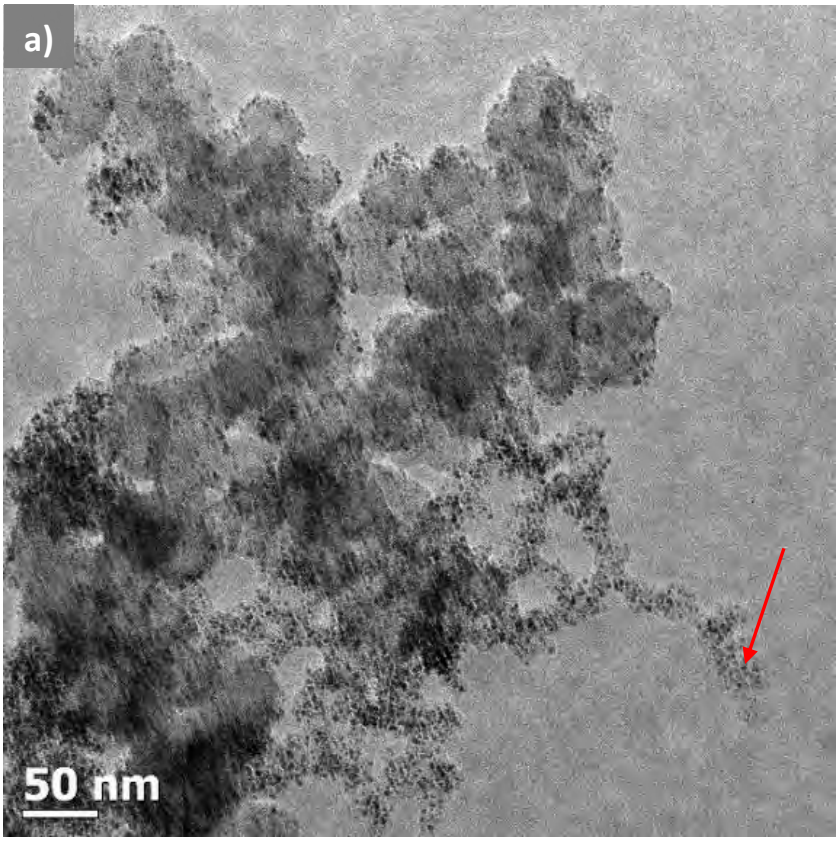
a)
50 nm

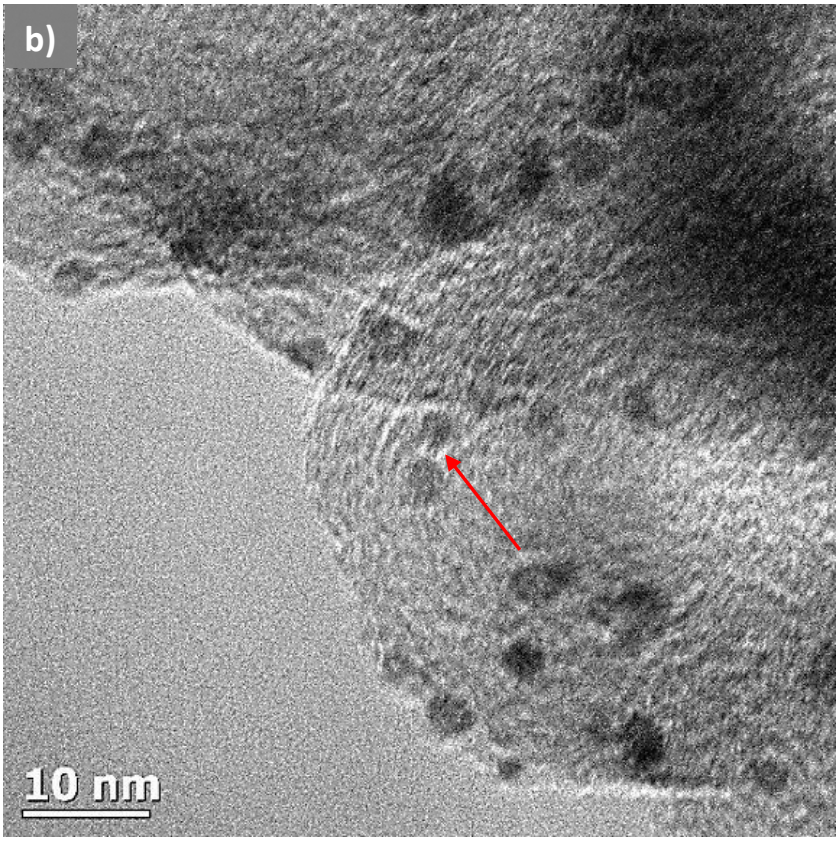
b)
10 nm

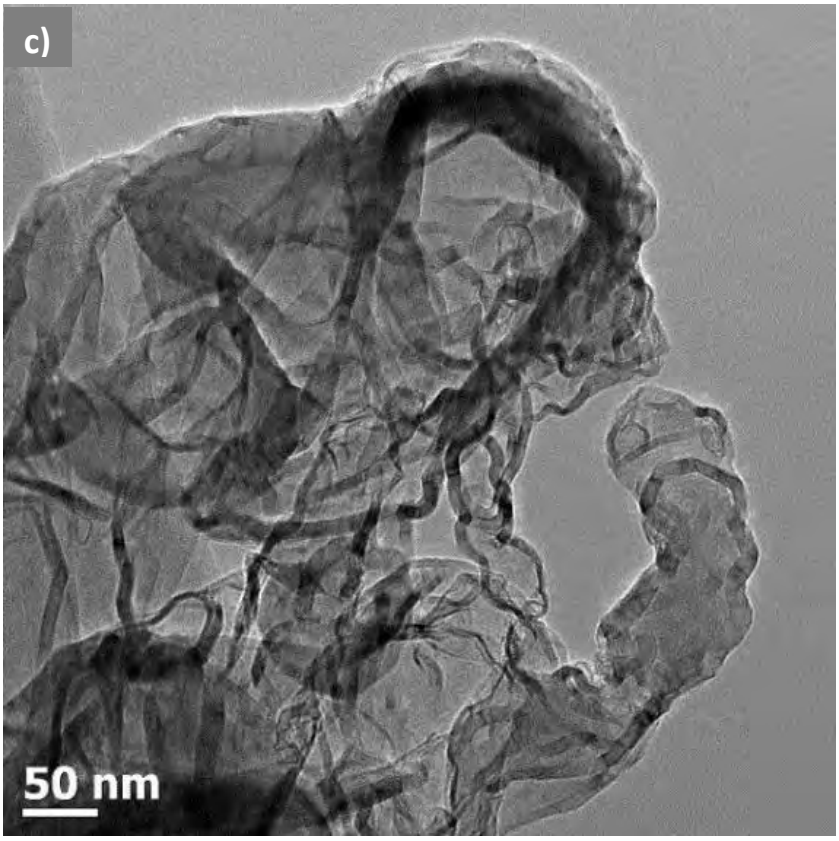

Figure 5-18: TEM images of carbon deposits formed on top tube segment after thermal stressing with SME20 at 400°C for 5h; a) at low magnification) at high magnification c) at a different section on the grid.

The deposits also had a diameter of 3nm. Deposit which has folded thin layers was also observed (Figure 5-18c); the folded edges showed lattice fringes that were parallel to each other as can be seen in Figure 10-21.

Figure 5-19 shows that the SME20-derived deposits also showed three groups of peaks. The first carbon signal was between 100-200°C, the second broad peak was between 200 and 400°C and the third carbon signal around 500°C. It is worth noting that the carbon signal at 500°C evolved at a relatively higher temperature compared to the other fuels. Furthermore, this peak had the highest carbon signal > 1000.

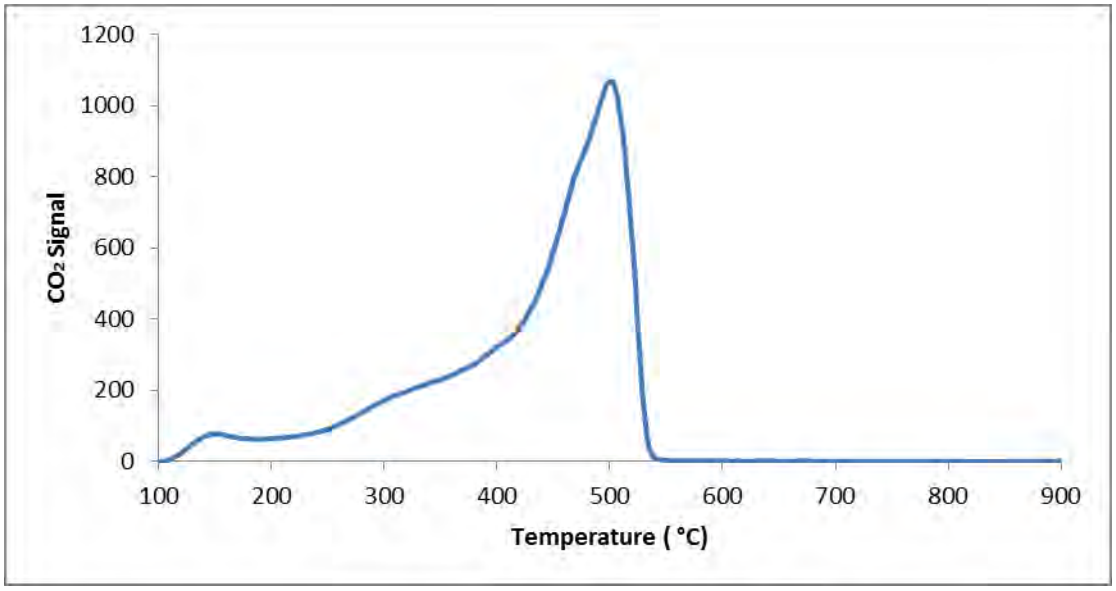

Figure 5-19:TPO profiles of carbon deposits formed on top tube segment after thermal stressing with SME20 at 400°C for 5h.

5.2 Discussion

The stability of EN 590 diesel and FAME blends was found to be influenced by the stressing temperature. Increasing the furnace temperature from 300°C to 400°C reduced the stability of the fuel and increased the formation of deposits. If one were to rank the fuels based on the amount of carbon formed on the top section of the tube, one would find the order SME20 > RME20 > RME100 > EN 590 diesel > SME100. The high amount of deposits from FAME blends than EN 590 diesel at this temperature was expected. Kaminuza observed a deposition trend of SME20 > RME20 > EN 590 diesel after thermo-stressing in a sand bath reactor at 250°C for 24h (15).

The high deposition of the blends can also be attributed to the fatty acid methyl esters with unsaturated hydrocarbon backbone (22,34). The unsaturated hydrocarbons are not conjugated but instead they are methyl-interrupted. The *bis*-allylic carbons in the backbone are the points of first attack during oxidation because the hydrogen located at these positions are weakly bonded and can easily be abstracted (49,52). This in turn leads to the rapid reaction between the radical and oxygen to form deposits precursors and ultimately solid deposits. This fuel composition of the blends in addition to the high temperature the fuel was exposed to resulted in more deposits

Not all methyl esters have the same deposition propensity. In this study, SME20 produced significantly more carbon deposits compared to RME20 under the same conditions. This can be attributed to the fatty acid composition of the soybean oil which is composed of 55% 18:2 (carbon number: double bond) fatty acids as opposed to 22% (18:2) for rapeseed oil (see Table 2-1). The high deposition in RME100 than SME100 was unexpected due to the reasons explained above. In this study, however, even in the duplicate experiment the same trend was observed. It is unclear, however, why RME100 formed more deposits that SME100.

The amount of deposits formed from blends was almost twice that of the pure FAME for RME and 11-fold more for SME. The high solvency of the pure FAME for the deposit precursors may be the reason for the notable decrease in amount of deposits in pure FAME. Osawa *et al.* showed that adding *n*-hexadecane (diesel component) to rapeseed methyl esters diesel and soybean methyl esters yielded a yellow precipitate which was not observed from the pure biodiesel component (56). A reason for this was that adding diesel component reduces the bulk polarity of FAME and as a consequence the solid deposits can precipitate out of solution.

EN 590 diesels, however, formed more deposit on the middle tube section than the top. The same trend was observed with deposits formed at 300°C. The high deposit in the middle tube than the one at the top which experienced higher temperature has been attributed to the depletion of deposit precursors as the fuel travels up the flow reactor.

FAME and FAME/blends, however, formed significantly more deposits on the top tube segment. It may be that as the FAME blends travels up the flow reactor more deposit precursors continue to form via the propagation reaction. At the top of the reactor, the formed deposits precursors have a higher molecular mass and higher polarity than the fuel. This results in them precipitating out of the fuel and depositing on the tube surface.

The deposits produced from all five test fuels consisted of a spherical morphology. This is consistent with deposit that have formed by the homogeneous reaction; which involves the polymerisation of hydrocarbon species to form larger polynuclear aromatic hydrocarbons (PAHs) which nucleate and grow into carbonaceous carbon in the fluid phase and then adhere onto the metal surface (8).

Two types of morphologies were observed in the spherical deposits. EN 590 diesel and SME100, formed spherical deposits with no interference patterns at high magnification. This suggests that these deposits have a highly amorphous structure. This is consistent with high pressure diesel deposits reported by Venkataraman and Eser (8) and the flask study deposits reported by Kaminuza (15) which were also found to be amorphous with no graphitic plane alignment.

The spherical deposits formed from RME100, RME20 and SME20 configured into agglomerates similar to those observed from SME 20 deposits by Kaminuza. The interference patterns observed on the spherical deposits were not perfectly circular and this was suggested to be a result of the disordered structure (81). These patterns are similar to those of jet fuel deposit reported by Venkataraman and Eser (81) and SME20 deposits reported by Kaminuza (15).

Deposits with overlapping nanosheets that appeared to be folded at the edges were consistent in all the fuels. The morphology of these deposits did not resemble any of the deposits reported in previous fuel stability studies. However, the morphology is similar to those of graphene nanosheets present on graphene oxide reported by Mungse *et al.* (91) (see Figure 5-20). The parallel lattice fringes at the edge of the nanosheets are indicative of multi-layers of graphene segments which are polyaromatic structures.

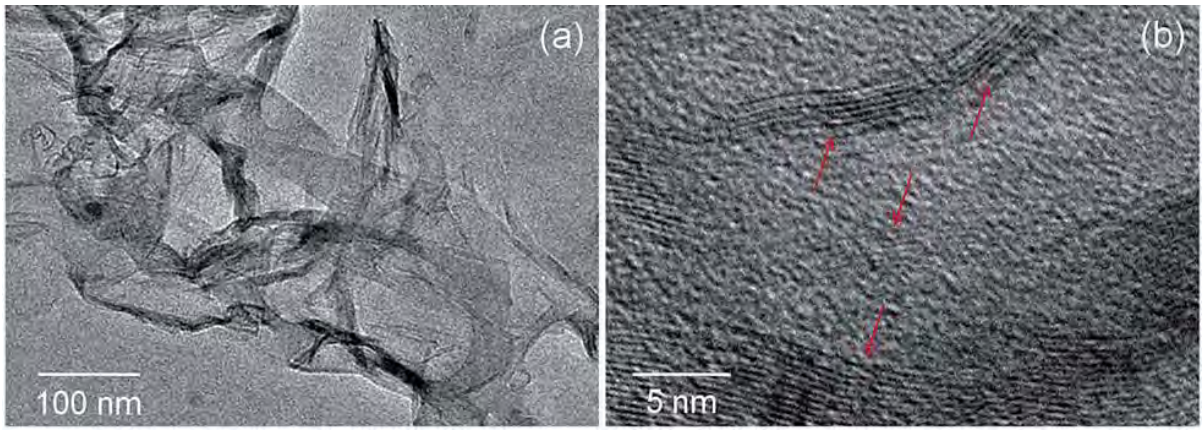

Figure 5-20: TEM images of graphene oxide at (a) low and (b) high resolutions **(91)**.

A study by Vander Wal (92) showed that the inference patterns observed on carbonaceous soot is due to the presence of graphene segments. It can be inferred from the morphology

observed on the deposits formed in this study that the spherical particles may have formed from the curvature or folding of graphene-like layers. The morphology of the deposits is indicative of deposits that formed by homogeneous reaction and not from catalytic process as there were no filaments or metal sulphides observed from the TEM micrographs.

The TPO profile of this deposits also suggest that the deposits might have formed by homogeneous reaction as there were no high temperature peaks (> 500˚C) observed. The TPO profile across all test fuels showed three groups of peaks; the first peak observed between 100 and 200°C is likely due to oxidation/evaporation of fuels physisorbed on the deposits. The second peak between 250 and 350°C may be attributed to the oxidation of more reactive, less ordered spherical deposits. Venkataraman and Eser (8) and Kaminuza (15) suggested that carbonaceous deposits associated with oxygen moieties are the most reactive and are likely to oxidise earlier. The EDS results of deposits in this study show the presence of oxygen associated with these deposits (see

Table ***10-2***).

The third CO_2 peak in these deposits evolved at relatively higher temperature (400-520°C) across all fuels. This was attributed to the oxidation of structurally more ordered graphene segments. The presence of parallel crystalline structure on these deposits suggests that they are structurally more ordered compared to the spherical deposits.

In order to characterise the deposits further the tube surfaces were inspected using PLOM. No change in the intensity of reflection of the coated surface and particles, with respect to each other, was observed when the polariser was rotated. This suggests that there was no structural anisotropy in the sample which would suggest that they are not mesophase spheres as observed by Eser (41). Such spheres would be expected to display polarisation texture when viewed using PLOM. It should be noted that Eser was investigating deposits formed under pyrolytic conditions at much higher temperatures. Venkataraman (10) also did not observe anisotropic mesophase carbon for jet fuel thermal stressing. Figure 10-22 in the Appendix contains representative PLOM micrographs of tube surfaces and particles for a variety of fuels.

When comparing the TPO profiles of EN 590 diesel (

Figure *4-18* and Figure 4-21) and SME20-derived deposits (Figure 4-24) formed at 300°C to those formed at 400°C (Figure 5-5, Figure 5-7 and Figure 5-19). The size of the third peak is higher for the 400°C deposits than the 300°C deposits. This is expected as more deposits have formed. Furthermore, the relative size of this peak was significantly higher compared to the second peak on deposits formed at 400°C. This could be because as the thermal stressing temperature increases more ordered deposits are formed. The presence of thin film like deposits with lattice fringes observed in TEM micrographs of 400°C corroborates the presence of more ordered deposits observed on TPO results.

Altin and Eser (12) also noted TPO profiles comprising three groups of peaks after thermal stressing jet fuel at 500°C for 5h. There were two low carbon signals at low temperature and a main carbon signal at relatively high temperature. The highest CO_2 signal peak for these deposits was observed between 500 and 575°C. This burn off temperature was higher than that observed in this study which was between 400-520°C. Altin and Eser attributed the

burn-off temperature to the oxidation of deposits catalysed by nickel and Iron. The relatively lower burn off temperature from deposits in this study corroborates the TEM and SEM results which suggest that the nickel and iron from the SS 316 metal did not catalyse the deposits that were formed. Ram Mohan and Eser (78) reported deposits which formed from a combination of homogenous and heterogeneous reaction under intermediate conditions (350°C, 5h, in the presence of oxygen). The results in this study indicate deposits were formed from homogeneous and heterogeneous reaction. It is likely that the structurally more ordered graphene segments were produced by surface catalysis.

5.3 Conclusions

The results in this study show that increasing the stressing temperature of the fuels accelerates the formation of deposits. At 400°C all test fuels produced discernible deposits in the flow reactor after 5h. The variation in temperature in the furnace along the axial distance was found to influence the amount of deposits formed. Most of the carbonaceous deposits adhered to the top section of the tube in the flow reactor which experienced the highest temperature.

The fuel composition had an effect on the amount of carbon deposits that formed. The highest amount of deposits was formed from SME20 whereas the lowest were formed from SME100. The morphology of the deposits formed consisted of two types of structure. Spherical deposits with varying degree of structural order and folded layers of graphene sheets.

The increase in thermal stressing temperature also had an effect on the chemical and morphological properties of the deposits. At 400°C, TEM and TPO results show that deposits that are more ordered are formed. Film like deposits with long lattice fringes were observed in this study. This was the first time such deposits were observed in fuel stability studies. The spherical morphology and chemical nature of the deposits formed at 400°C suggest that the deposits were formed from nucleation and growth in the liquid phase. The structurally more ordered graphene sheets are likely formed from the metal catalysis of dehydrogenation reactions.

6 THERMAL OXIDATION IN A FLOW REACTOR

6.1 The effect of solvency on deposit formation during oxidation in a flow reactor

The autoxidative and intermediate regime results showed that FAME blends had a higher deposition propensity compared to pure FAME. In an attempt to evaluate the effect of fuel solvency, 7, 20, 50 and 100 % SME blended with EN 590 diesel were thermally stressed in the flow reactor at 400°C for 5h in the presence of oxygen.

All test fuels formed discernible deposits on the tube segments from the top section of the flow reactor. The amount of carbon deposits measured using the carbon analyser for each test fuel is reported in Table 6-1. It is apparent that of all test fuels, SME7 formed the highest amount of deposits and SME100 formed the lowest amount of deposits. The amount of carbon deposits formed appears to have increased with a decrease in SME concentration in the blend.

Table 6-1: Amount of carbonaceous deposits formed from thermal stressing different SME blends in a flow reactor.

Test Fuel	Tube segment	Amount of deposit (µgC/cm^2)
SME7	Top	489
SME20	Top	379
SME50	Top	309
SME100	Top	33
EN 590	Top	68

6.1.1 Discussion

Figure 6-1 shows the amount of carbon deposit as a function of the percentage of SME in the blend. The first point in Figure 6-1 represent amount of carbonaceous deposits formed from stressing EN 590 diesel. It is clear from this graph that the addition of a small quantity of SME to a petroleum diesel greatly increased the extent of deposit formation.

It is also clear that with the increase in the quantity of SME the amount of carbonaceous deposits decrease. This may be because deposits and deposit precursors are polar in nature

and are likely to be more soluble in biodiesel which is also polar. Blending biodiesel and petroleum diesel decreases the bulk polarity of the fuel and consequently reduces the fuel's solvency for polar deposits (54,55).

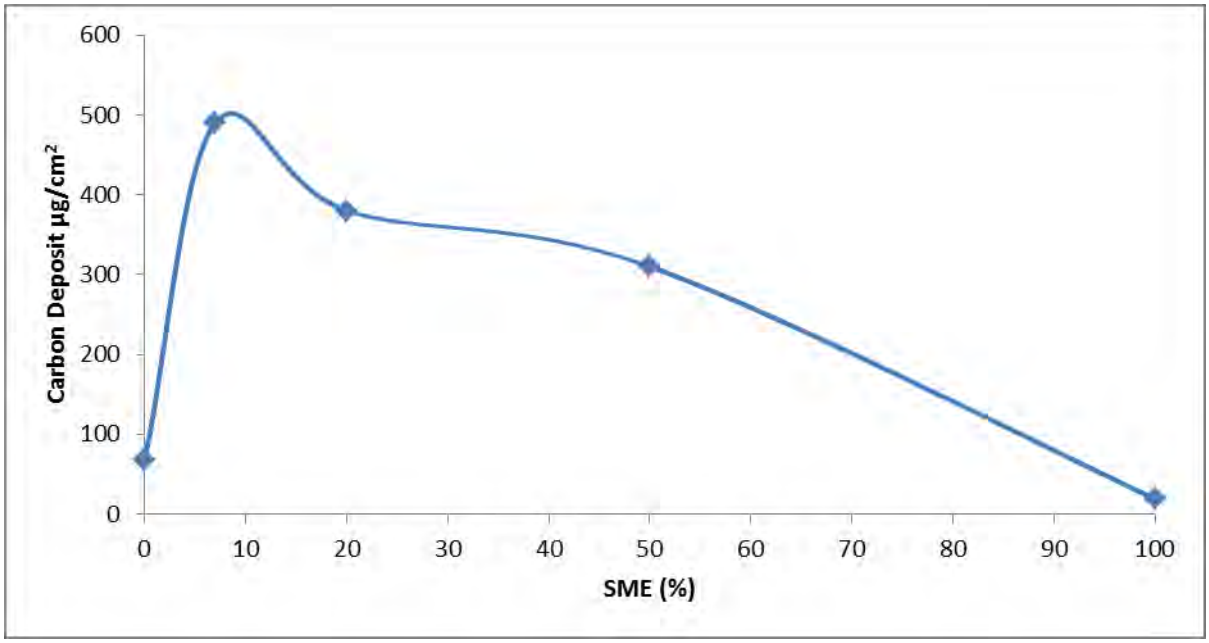

Figure 6-1: Effect of biodiesel content on mass accumulation for biodiesel/diesel blends.

Therefore, blends with low biodiesel content may form relatively more deposits due to their low polarity. This suggests that the polarity of the blend may be more important than the quantity of deposit precursor molecules in the blend.

A similar trend to that observed in this study was detected by Vukeya (16) who observed the amount of deposits accumulated from stressing a 80% n-hexadecane/20% tetralin blended with 10, 20, 30 and 65 % RME in a QCM at 140°C for 24h (see Figure 6-2). The highest deposits accumulated for 10 % blend.

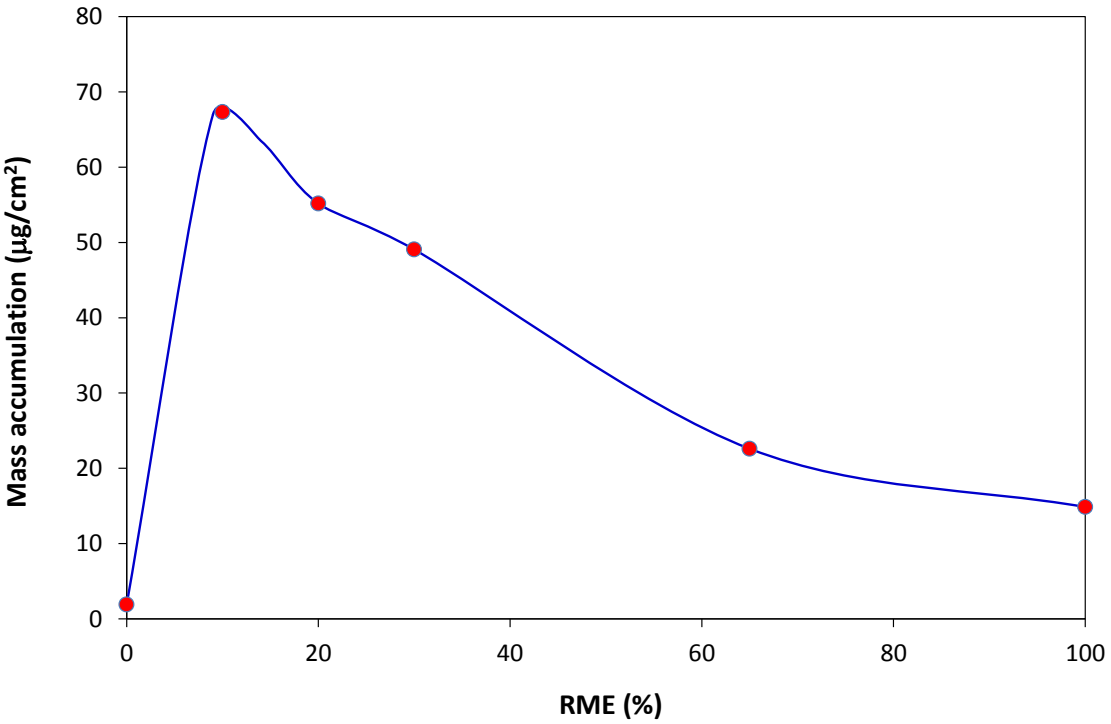

Figure 6-2: Effect of biodiesel content on mass accumulation for biodiesel/diesel model compounds blends.

Low FAME blends (< 10%) are already commercially available in the Europe (36), USA (37) and are expected to be commercially be available in the South African market by the end of 2015 (93). The results in this study show that these are the blends that are more prone to deposit formation. Deposition may be a serious issue when these blends are introduced into the South African market. It should, however, be noted that this study did not address the addition of deposit control additives (DCAs) which could address such a problem. The flow reactor methodology, however, has been demonstrated to provide a rapid, low fuel volume set of experiments to identify such problems. It could easily be extended to assess the performance of DCAs at costs well below those of full engine tests.

6.2 Effect of zinc doping

EN 590 diesel, RME100 and SME100 were doped with 10 ppm zinc neodecanoate in order to evaluate the effect of zinc on the deposition behaviour of diesel and biodiesel. Table 6-2 shows the amount of carbon deposits that formed from the doped fuels. It is evident that zinc doping significantly increased the amount of carbon deposits that formed. Zinc accelerated the deposition of FAME (RME100 and SME100) more than that of EN 590 diesel.

Table 6-2: Amount of carbon deposited from thermal stressing various fuels doped with 10 ppm zinc.

Test Fuel	**Amount of deposit (μg/cm^2)**
EN 590 Middle	377
EN 590 Top	425
RME 100	> 2970
SME 100	> 2625

In order to investigate the effect of zinc on the nature of deposits formed, the stressed tubes were analysed with the LECO carbon analyser to obtain TPO profile and their morphologies were investigated using TEM micrographs. Figure 6-3 illustrates degradation of deposits from stressed zinc doped EN 590 diesel, RME100 and SME100. These deposits had no regular structure. The deposits appeared to be made up of more than one layer of material. Furthermore the section with more layers appeared darker compared to those at the edges. When the deposits were examined at high magnification there were no regular interference patterns indicative of crystalline structure or plane alignment in this material (see Figure 6-4). This suggests that the deposits have a highly amorphous structure.

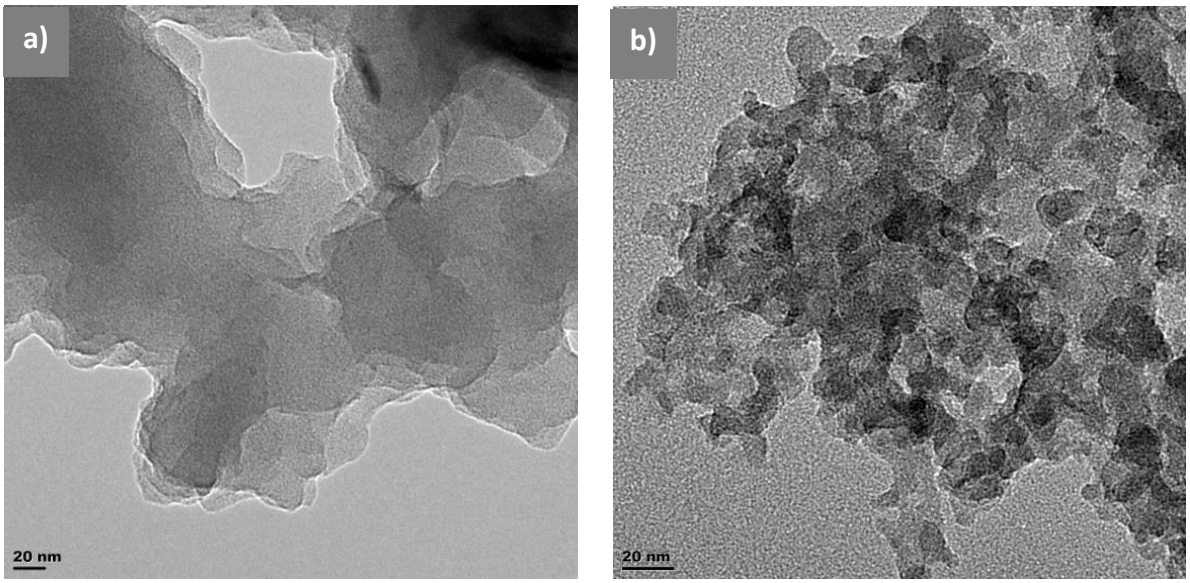

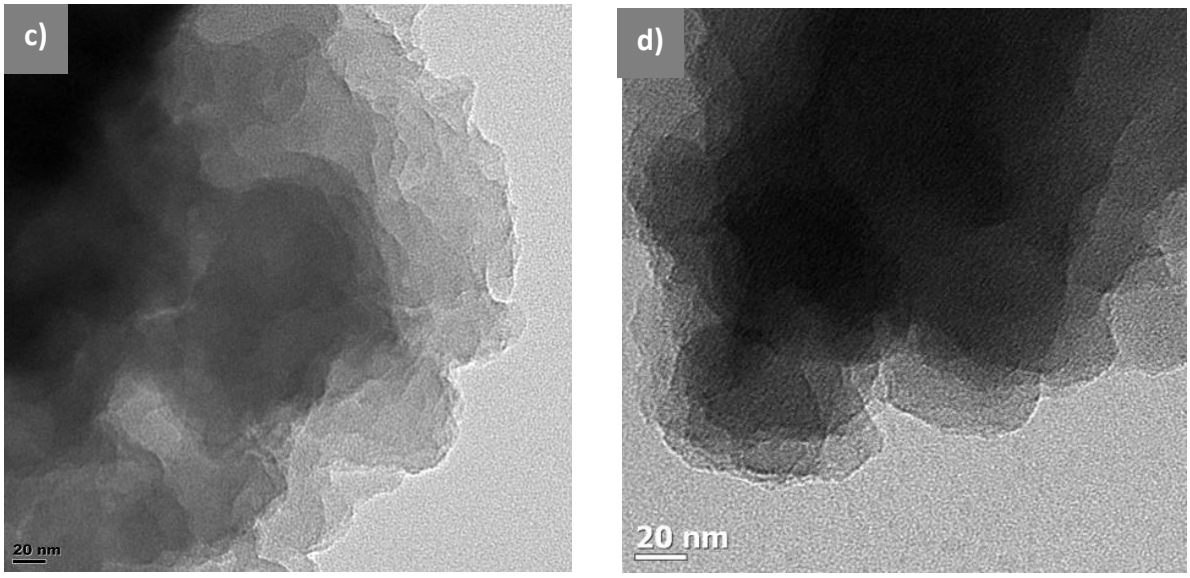

Figure 6-3: TEM micrographs stressed fuel deposits: a) EN 590 diesel-middle, b) EN590 diesel-top c) RME100 d) SME100.

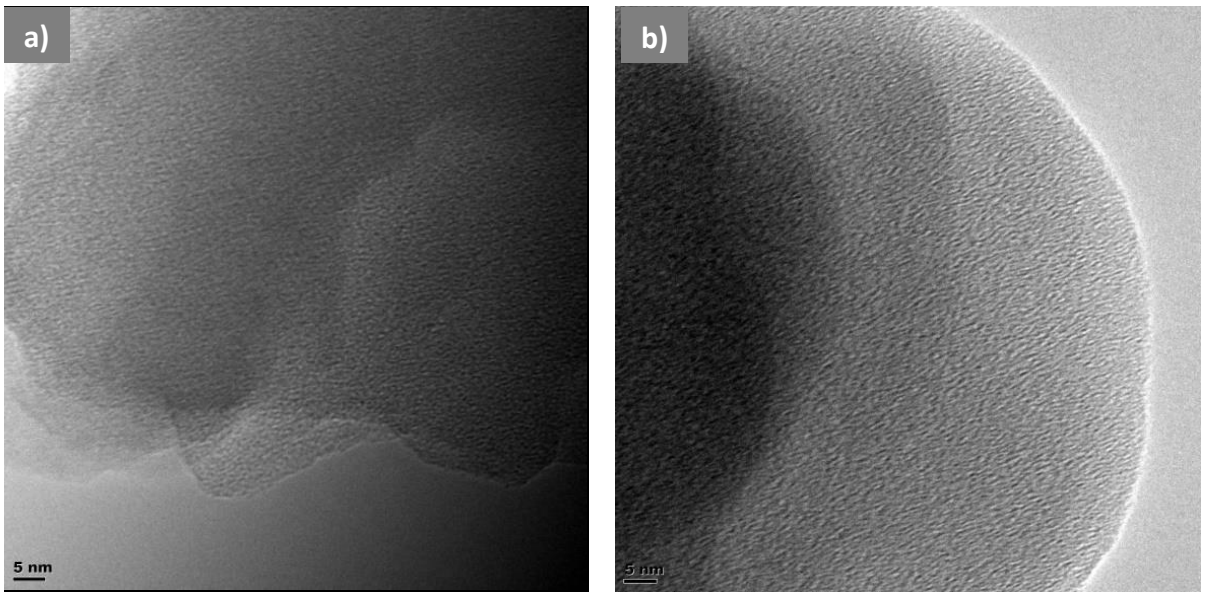

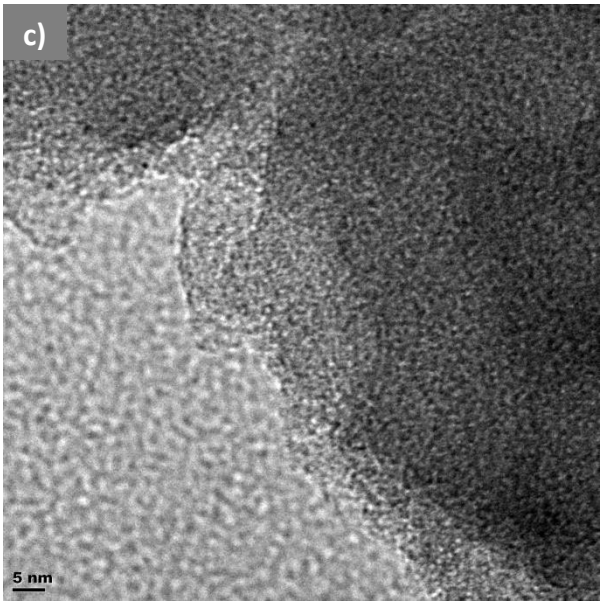

Figure 6-4: TEM micrographs stressed fuel deposits: a) EN 590 diesel b) RME100 c) SME100 at high magnification.

6.2.1 TPO profiles of the flow reactor deposits formed from zinc doped fuel

The TPO profile of the deposits formed from stressing the three test fuels are illustrated below. The TPO profiles of EN 590 diesel deposits showed three groups and a slight tail higher temperature > 500°C.

The temperature at which the carbon signal evolved was similar to the ones observed from the deposits formed from EN 590 diesel which has not been doped. The only significant difference is the increase in the intensity of the carbon signal. This is to be expected considering that the amount of deposits formed from the doped fuel was higher. The slight tail observed at high temperature may be indicative of highly ordered deposits present. However, since such deposits were not visible under TEM this was inconclusive.

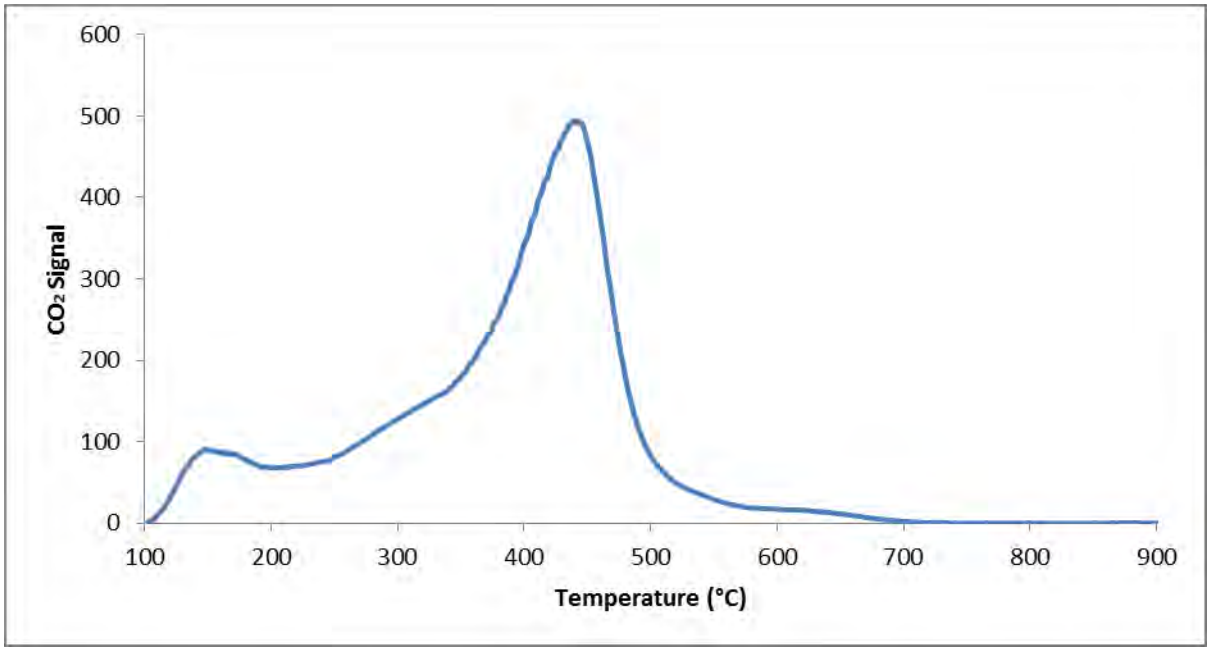

Figure 6-5: TPO profiles of carbon deposits formed on tube segment from middle section after thermal stressing EN 590 diesel doped with 10 ppm zinc on SS 316 for 5h at 400°C.

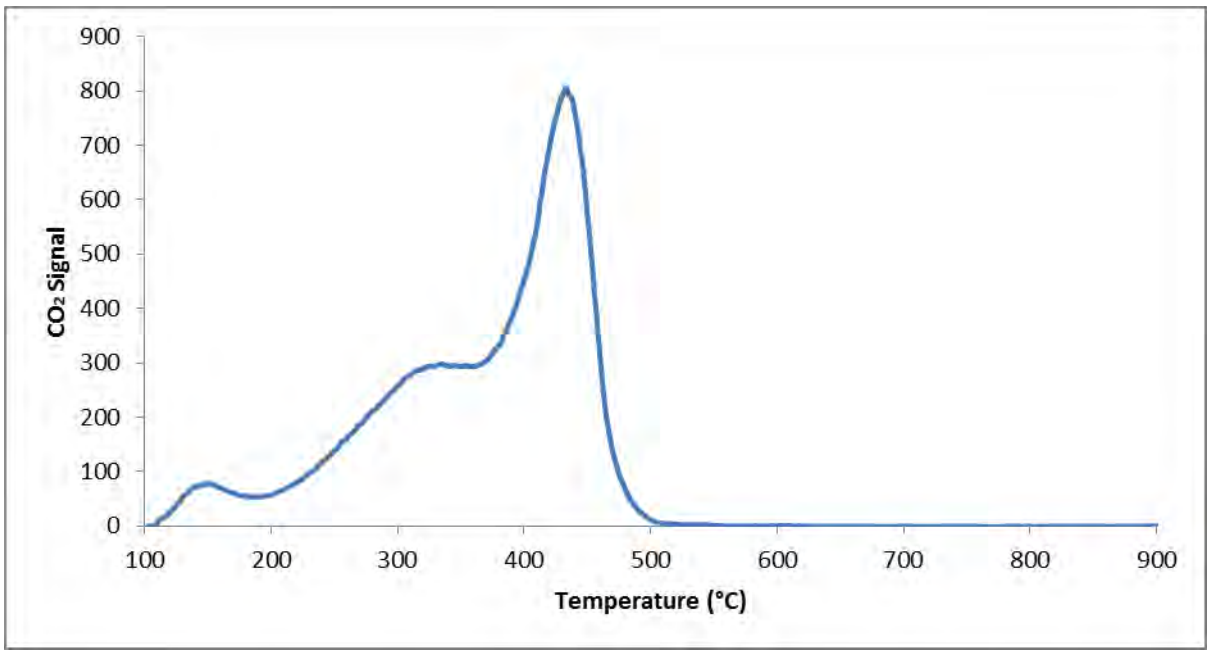

Figure 6-6:TPO profiles of carbon deposits formed on tube segment from top section after thermal stressing EN 590 diesel doped with 10 ppm zinc on SS 316 for 5h at 400°C.

The shape of the TPO profile of deposits from zinc doped RME 100 and SME 100 derived deposits (Figure 6-7 and Figure 6-8) was significantly different to that observed from the test fuel before zinc doping (see Figure 5-11 and Figure 5-14). Part of this shape change may

be the result of the high quantity of carbon that was burnt off. Thick layers will experience thermal lag with inner material reaching burn off temperature later than outer material causing an apparent delayed burn-off. TPO profiles of both RME and SME showed a sharp drop which has been highlighted by the red circles in Figure 6-7 and Figure 6-8. This is coincident with the maximum temperature at which data was recorded. Hence the reported deposition levels are minimal.

The TPO profile of RME-derived deposits had two groups of peaks, the first broad peak evolved between 150 and 350°C whereas the second broad peak evolved between 400 and 700°C. Similar behaviour was seen with SME100. The temperature at which the high intensity carbon signal evolved was higher compared to that of the deposits formed from RME and SME before zinc doping which were 410°C and 450°C respectively.

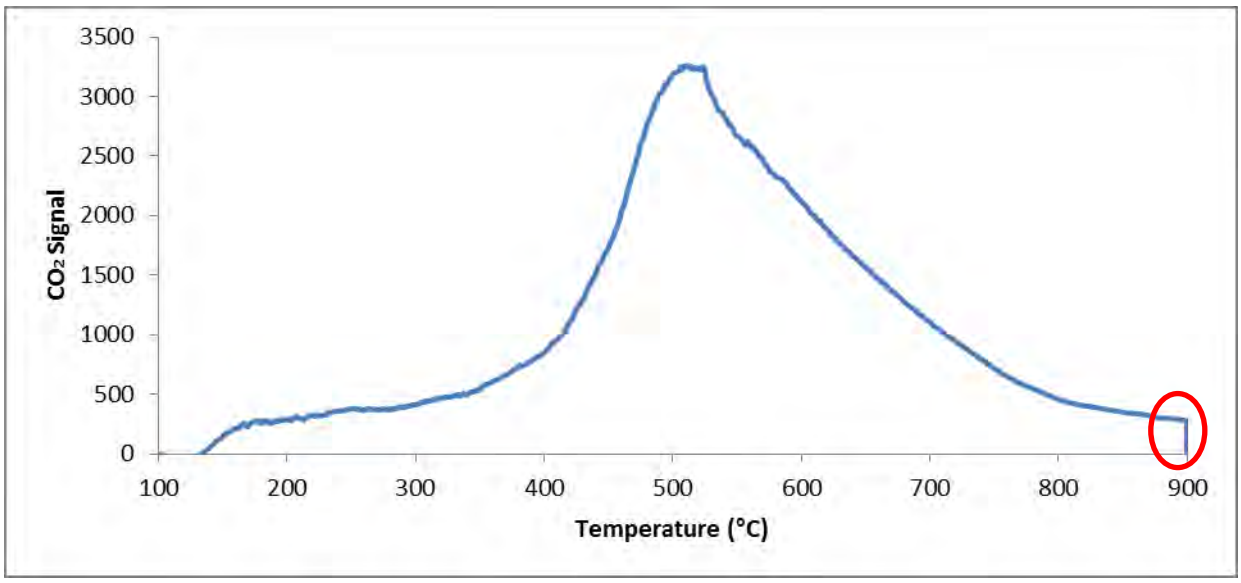

Figure 6-7: TPO profiles of carbon deposits from thermal stressing RME100 doped with 10 ppm zinc on SS 316 for 5h at 400°C.

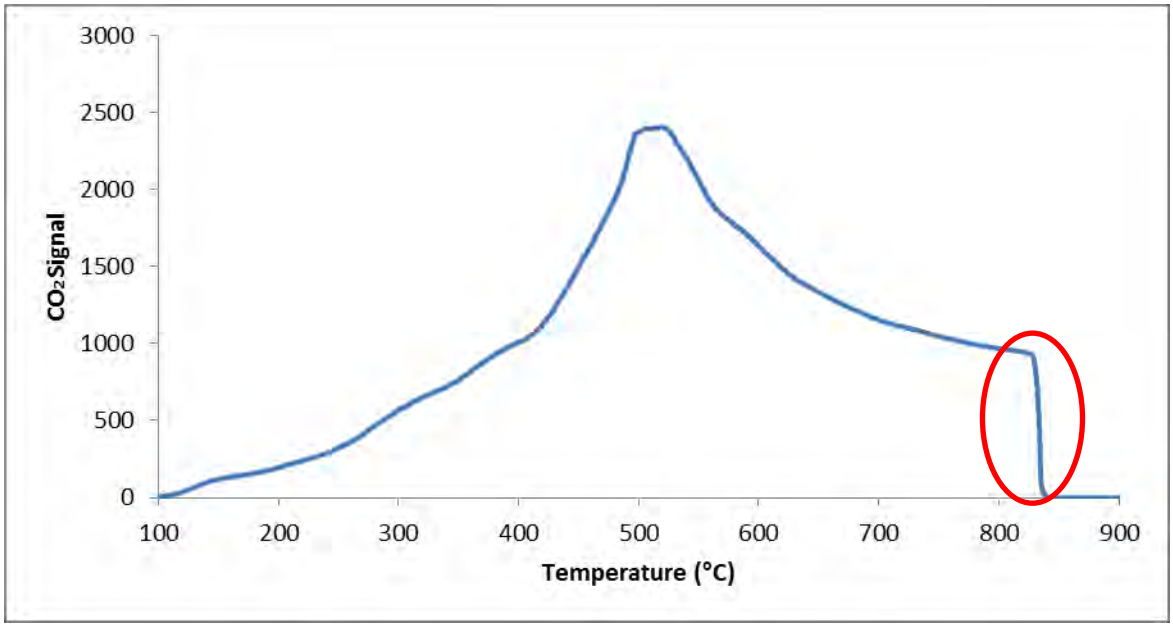

Figure 6-8: TPO profiles of carbon deposits from thermal stressing SME100 doped with 10 ppm zinc on SS 316 for 5h at 400°C.

6.2.2 Discussion

The results show that zinc accelerated the deposition behaviour of both B100 and EN 590 diesel. The presence of zinc in B100 dramatically increased the amount of deposits as can be seen in Table 6-3. A comparison of the deposits that formed from the zinc doped fuels showed that EN 590 derived deposits were lower, compared to B100 (RME100 and SME100) derived deposits. This trend was the inverse of what was observed from deposits formed from test fuels that were not doped which showed EN 590 diesel generating more deposits (see Table 6-3)).

Table 6-3: Comparison of the amount of deposits formed form various fuel before and after zinc doping.

Fuel composition	Deposits before zinc doping (µg/cm^2)	Deposits after zinc doping (µg/cm^2)
EN 590 diesel middle	131	377
EN 590 diesel top	68	425
RME 100	112	>2970
SME 100	33	>2625

The high amount of deposits observed on zinc doped B100 may be attributed to the catalytic effect of zinc on deposit formation. Metals have also been reported in numerous studies, to have a catalytic effect on the oxidation of biodiesel (47,94,95).

Velaers *et al.* (20) investigated the effect of zinc on paraffinic non-polar GTL, compared to relatively polar EN 590 diesel using a DW10 test procedure.Velaers *et al.* (20) suggested that in GTL which has a lower solvency compared to EN 590, zinc easily drops out of solution. The zinc that drops out of solution then readily reacts with combustion gases at high temperature to form deposits that are rich in zinc. This was suggested to be the reason for the increased fouling in GTL compared to EN 590 when zinc is added.

In this study, however, the EN 590 diesel that is less polar compared to B100 formed less deposits compared to B100 after zinc doping. Furthermore, the composition of EN 590 and B100 deposits examined using EDS did not show the presence of zinc in the deposits (see Table 10-3). All these results seem to suggest that the reaction of zinc that has dropped out of solution with combustion gases may not have been the reason for the increased fouling observed when the test fuels were stressed with zinc. The major reason for the high amount of deposits in B100 is likely due to catalytic effect of zinc on the oxidation of biodiesel.

6.3 Conclusions

Investigations into the effect of solvency on biodiesel/diesel blends using a flow reactor methodology has never been performed prior to this study. Blending small quantities of biodiesel with diesel was found to increase the amount of deposits that precipitate out of solution and adhere to the metal surface. The deposition potential trend in decreasing order was SME7 > SME20 > SME50 > SME100. The greater extent of deposit formation in low FAME-containing blends suggests that the ability of the fuel to keep deposits in solution is more important than the potential amount of deposit precursor molecules, *i.e.* percentage FAME.

The effect of zinc doping on diesel and biodiesel in the flow reactor for short duration was also invested. As far as it could be ascertained this is the first study to investigate effect of zinc doping using a flow reactor and yielded positive results. The study conducted by Kaminuza at 250°C for 24h, is the only other study that investigated zinc fouling in a flow

reactor. Results from Kaminuza's study were inconclusive as there were no visible deposits generated (15).

Significantly more deposits were formed when the test fuels were doped with zinc neodecanoate in this study. The effect of zinc had a greater effect on FAME-derived deposits than diesel derived deposits. This was attributed to catalytic effect of zinc on the oxidation of biodiesel.

It can be inferred from the results in this study that EN 590 and B100 are likely to pick up zinc when used in the market. The flow reactor technique can be used to test zinc pick up problems and asses the performance of DCA in zinc dosed fuels.

7 CONCLUSIONS

With the exception of the work conducted by Kaminuza that yielded no significant results, this study represents the first application of the flow reactor methodology to investigate the thermo-oxidative degradation of FAME and FAME/ diesel blends. The flow reactor methodology has been demonstrated to provide a rapid, low fuel volume set of experiments that can mimic the formation of deposits in diesel injectors and identify problems such as effect of temperature, fuel composition and metal contamination on the amount and nature of deposits formed.

The fuel's residence time in the flow reactor was only 7.44 min, nonetheless oxidation deposits precursors were observed on the stressed fuel and solid deposits were formed in such a short time. This shows that there is no need for very long experiments conditions which may be far removed from real systems.

The thermal stressing temperature, however, was found to have an impact on the amount of deposits that formed. Increasing the thermal stressing temperature from 300°C to 400°C resulted in an increase in the amount of deposits formed. Thermal stressing the deposits at 300°C only generated discernible deposits in EN 590 diesel and SME20. RME100, SME100 and RME20 did not yield any notable deposits and consequently the effect of fuel composition on the amount of deposits was inconclusive. Thermal stressing the test fuels at 400°C resulted in solid deposit in all five test fuels. This study shows FAMEs are more sensitive to temperature difference compared to EN 590 diesel.

The deposition tendency of the fuels in increasing order at 400°C for 5h was: SME20 > RME20 > EN 590 > RME100 > SME100. This study shows that the composition of the fuel has an effect on the quantity of carbonaceous deposits. The low stability of B20 (SME and RME) which resulted in higher deposition was attributed to the presence of double bond in the backbone of the fatty acids methyl esters which they are composed of. The double bond makes them more prone to oxidation; the higher concentration of di-unsaturated fatty acids in SME20 explains why it was more prone to oxidation.

The high solvency of B100 blends were found to retain polar deposits in solution resulting in less solid deposits adhering on the surface. The amount of solid deposit formed was found

to increase with a decrease in the concentration of FAME in FAME/diesel blend. Adding EN 590 reduces the bulk polarity of the fuels, which in turn promotes the precipitation of deposits from solution.

Adding zinc neodecanoate exacerbated the deposition potential of diesel and pure FAME. The effect of zinc doping was significantly higher in B100 blend than EN 590 diesel and this was attributed to the high catalytic effect of zinc to oxidation of FAME.

The nature of deposits that formed in all the experiments conducted in this study suggested that they were formed by nucleation and growth in the liquid phase as indicated by the spherical morphology of this deposits viewed under both SEM and TEM. The morphology of the deposits ranged from irregular shaped amorphous deposits to spherical deposits with varying degrees of order. In addition, the deposits at 400°C revealed thin film like deposits which were observed for the first time in this study. The film like deposits had lattice fringes along the edges which were attributed to graphene segments. The morphology and chemical nature of the deposits in this study did not indicate that the SS 316 tube had a significant effect on the type of deposits that formed.

The work in this study provides insight on the stability behaviour of FAME and its blends using the flow reactor methodology. FAME and FAME blends have been introduced into the market, and it is vital to understand the mechanism by which they form and factors that promotes their formation.

8 RECOMMENDATIONS

Because of the limited scope of this study and based on findings reported in this dissertation, a number of recommendations are made for future investigations. These are:

- The contradiction in the deposition trend observed at 300 °C and 400°C should be fully explored. This could be done with a broader range of temperature, including thermal stressing at 350°C and 450°C. On a broader thermal stressing temperature range, the flow reactor studies could be extended to a recirculating loop system which was not explored in this study as it was deemed beyond the scope of this study. In a loop system the fuel reservoir and waste fuel are in the same canister instead of each having their canister which was the case in this study. A comparison of the deposition trend in a recirculating loop to the non-recirculating loop would be of interest.
- The amount of carbon deposited at different section along the tube could be studied in more detail. The deposition profile of the FAME and FAME/diesel blends could be compared to the deposition profile observed by Roan using jet fuel. Furthermore, the deposition of diesel versus that of diesel and biodiesel could of interest and it would shed more light on the results observed in this study. In this study the highest amount of deposit was observed in the section for EN 590 diesel and at top section for pure FAME and FAME blends. The deposition profile can be obtained by cutting the whole stressed tube into equal 5cm segment and analysing each section in the carbon analyser.
- In order to investigate the effect of metals further, different metal surface could be evaluated. An inert metal such as alumina coated SS 316 could be used to shed more light on whether SS 316 had an effect on the amount of carbonaceous deposits. Other metal tube such as Inconel, brass and galvanized metals can also be used. Galvanized metal would provide a more market relevant source of zinc. As Quigley *et al.* (90) pointed out the only source of zinc in the market is galvanized components. The effect of dissolved metal traces could be explored further. Other metals besides zinc neodecanoate could be dissolved into the fuel. This would include Cu and Ni. The effect of trace metal should also be investigated on a broader

range of fuels, including RME 20 and SME 20. This would shed more light on the catalytic activity of trace metals on pure FAME, FAME blends and petro-diesel.

- The flow reactor experiments were only conducted on oxygenated fuels. Of interest would be experiments on FAME and FAME/diesel blend on deoxygenated fuels. To deoxygenate the fuels, they would be sparged with nitrogen following procedure described by Venkataraman (10). A comparison of results from fuels that were deoxygenated to those that were oxygenated would be of interest as the decomposition of FAME is strongly tied to oxygen.
- An oxygen sensor could be placed at the end of the fuel reactor to measure the amount of oxygen remaining in the fuel after the fuel's retention time in the reactor. This would help in understanding if the oxygen in the fuel is depleted as the fuel flows up the reactor and in turn explain why the deposits in EN 590 diesel decrease going up the flow reactor. This would require a modification of the flow reactor so that it incorporated these oxygen sensors.
- To obtain more information on the chemical composition of the deposits, more analytical techniques could be used as recommended by Venkataraman (10). X-ray photoelectron spectroscopy (XPS) and Diffuse Reflectance Infrared Fourier Transform Spectroscopy (DRIFTS) could be performed on the deposits to ascertain more information about the composition of the deposits. XPS would be used to obtain the chemical composition of the surface deposits up to a depth of ±100 Å (10). DRIFTS would provide information on the nature of hydrocarbon and heteroatom bonds in the deposits. DRIFTS analysis was not performed in this study because analysis is done on a powder sample. Getting enough powder for analysis proved to be difficult in this study.
- The formation of new film like deposits that had never been seen in previous studies needs to be explored further.
- To quantify the amount of deposits from the TPO profile the peaks could deconvoluted (81). This will quantify the relative % contribution from each of the three peaks observed on the TPO profile.

- Now that the suitability of a flow reactor to investigate fuel stability has been established, it is recommended that its potential be used to study the effect of the type and quantity of DCA on fuel stability.

9 REFERENCES

1. Batts BD, Fathoni ZA. A literature review on fuel stability studies with particular emphasis on diesel oil. Energy & Fuels. 1991; 5: p. 2-21.

2. Balat M, Balat H. A critical review of bio-diesel as a vehicular fuel. Energy Conversion and Management. 2008; 49: p. 2727-2741.

3. Lacey P, Gail S, Kientz JM, Milovanovic N, Gris C. Internal fuel injector deposits. SAE Technical Paper Series. 2011; 2011-01-1925.

4. Lacey P, Gail S, Kientz JM, Benoist G, Downes P, Daveau C. Fuel quality and diesel injector deposits. SAE Technical Paper Series. 2012; 2012-01-1693.

5. Karavalaks G, Stournas S, Karonis D. Evaluation of oxidation stability of diesel/biodiesel blends. Fuel. 2010; 89: p. 2483-2489.

6. Patrick J, Barranco R. Carbon Deposits: formation, nature and characterisation. In Coal Oven Manager Association/Coal Research Forum Meeting; 2006; Scunthorpe, United Kingdom. p. 1-7.

7. Commodo M, Fabris I, Groth CPT, Gulder OL. Analysis of aviation fuel from thermal oxidative stability by Electron Spray Ionisation Mass Spectroscopy (ESI-MS). Energy & Fuels. 2011; 25: p. 2142-2150.

8. Venkataraman R, Eser S. Characterization of deposits formed on diesel injectors in field test and form thermal oxidative degradation of n-hexadecane in a laboratory reactor. Chemistry Central Journal. 2008; 2: p. 1-11.

9. Omori T, Tanaka A, Yamada K, Bunne S. Biodiesel deposit formation mechanism and improvement of fuel injection equipment (FIE). SAE Technical Paper Series. 2011; 2011-01-1935.

10. Venkataraman R. Solid deposit formed from the pyrolytic and oxidative degradation of jet fuel and diesel fuel. PhD Thesis. USA: Pennsylvania State University; 2007.

11. Altin O, Eser S. Analysis of carboneceous deposits from thermal stressing of a JP-8 fuel on superalloy foils in a flow reactor. Industrial and Engineering Chemical Research. 2001; 40: p. 589-595.

12. Altin O, Eser S. Analysis of solid deposits from thermal stressing of a JP-8 fuel on different tube surface in a flow reactor. Industrial and Engineering Chemical Research. 2001; 40: p. 596-603.

13. Roan MA. The effect of disolved oxygen on the pyrolytic degradation of Jet fuels. PhD thesis. State College, USA: Pennsylvania State University; 2003.

14. Zabarnick S. Studies of jet fuel thermal stability and oxidation using a quartz crystal microbalance and pressure measurements. Industrial and Engineering Chemical Research. 1994; 33: p. 1348-1354.

15. Kaminuza I. Thermal and chemical analysis of carbonaceous materials: Diesel soot and diesel fuel reactor deposits. MSc dissertation. Cape Town, South Africa: University of Cape Town; 2013.

16. Vukeya HM. The use of model compounds to investigate the influence of fuel composition composition on the thermo-oxidative stability of FAME/diesel blends. MSc dissertation. Cape Town, South Africa: University of Cape Town; 2015.

17. Li J, Eser S. Surface effect of copper on deposit formation from jet fuel range hydrocarbons. In 23rd Biennial Conference on Carbon; American Carbon Society; 1997; USA: Carbon '97, Extended Abstracts. p. 290-291.

18. Sobkowiak M, Griffith JM, Wang B, Beaver B. Insight into the mechanisms of middle distillate fuel oxidative degradation. Part 1: On the role of phenol, indole, and carbazole derivatives in the thermal oxidative stability of fischer-tropsch/ petroleum jet fuel blends. Energy & Fuels. 2009; 23: p. 2041-2046.

19. Kabana CG, Botha S, Schmucker C, Woolard C, Beaver B. Oxidative stability of middle distillate fuels. Part 1: Exploring the soluble macromolecular oxidatively reactive species (SMORS) mechanism with jet fuels. Energy & Fuels. 2011; 25: p. 5145-5157.

20. Velaers AJ, de Goede S, Woolard C, Burnham R. Injector fouling performance and solubility of GTL diesel dosed with zinc. SAE Technical Paper Series. 2013; 2013-01-1697.

21. Stavinoha LL, Naegeli DW, McInnis L. The role of surface composition in fuel deposition. American Chemical Society. 1990; 35: p. 1315-1323.

22. Srivastava A, Prasad R. Triglycerides-based diesel fuels. Renewable and Sustainable Energy Reviews. 2000; 4: p. 111-133.

23. Bacha J, Freel J, Gibbs A, Gibbs L, Hemighaus G, Hoekman K, et al. Diesel Fuels Technical Review. San Ramon, CA: Chevron; 2007.

24. The International Council on Clean Transportation. An introduction to petroleum refining and the production of ulra low sulfur gasoline and diesel fuel. Bethesda, ML: MathsPro; 2011.

25. Barker J, Richards P, Snape C, W M. Diesel injector deposits - an issue that has evolved with engine technology. SAE Technical Paper Series. 2011; 2011-01-1923.

26. SAPIA Future Fuels Working Group. Petrol and diesel in South Africa and the impact on air quality. Sandton, South Africa: SAPIA; 2008.

27. Ullmann J, Geduldig M, Stutzenberger H, Caprotti R, Balfour G. Investigation into the formation and prevention of internal diesel injector deposits. SAE Technical Paper Series. 2008; 2008-01-0929.

28. Huhtala K, Vilenius M. Study of a common rail fuel injection system. SAE Technical Paper Series. 2001; 2001-01-3184.

29. Singer P, Rühe J. On the mechanism of deposit formation during thermal oxidation of mineral diesel and diesel/biodiesel blends under accelerated conditions. Fuel. 2014; 133: p. 245-252.

30. Tony Kitchen. Technical review of common rail diesel fuel system. [Online].: AK training; 2012 [cited 2013 July. Available from: http://www.docstoc.com/docs/68506505/Common-Rail-Injection-Training.

31. Barnwal BK, Sharma MP. Prospects of biodiesel production from vegetable oils in India. Renewable and Sustainable Energy Reviews. 2005; 9: p. 363-378.

32. Pinto AC, Guarieiroa LLN, Rezende MJC, Ribeiro NM, Torres EA, Lopes WA, et al. Biodiesel: An overview. J. Braz. Chem. Soc. 2005; 16: p. 1313-1330.

33. Li Y, Tian G, Xu H. Application of biodiesel in automotive diesel engines. In Biodiesel - Feedstocks, Production and Applications. Mountain View, CA: Creative commons licenses; 2013. p. 388-406.

34. Hoekman KS, Broch A, Robbins C, Ceniceros E, Natarajan M. Review of biodiesel composition, properties, and specifications. Renewable and Sustainable Energy Reviews. 2012; 16: p. 143-169.

35. Ullah K. Aging of polymer in diesel and biodiesel blended fuel. MSc Thesis. Gothenburg, Sweden: Chalmers University of Technology; 2013.

36. de Goede S, Roets P, Velaers A, Vermeulen J, Wilken C. The properties and injector nozzle fouling performance of GTL and EN590 Diesel with RME and SME biodiesel. SAE Technical Papers Series. 2013; 2013-01-1136.

37. Nair JN, Deepthi J, Kalyani SK. Study of biodiesel blends and emission characteristics of

biodiesel. International Journal of Innovative Research in Science Engineering and Technology. 2013; 2: p. 3710-3715.

38. Jain S, Sharma MP. Stability of biodiesel and its blends: A review. Renewable and Sustainable Energy Reviews. 2010; 14: p. 667-678.

39. Altin O, Eser S. Carbon deposit formation from thermal stressing of petroleum fuels. American Chemistry Society Divison of Fuel Chemistry. 2004; 49: p. 764-766.

40. Lin R, Tavlarides LL. Thermal stability and decomposition of diesel fuel under subcritical and supercritical conditions. Journal of Supercritical Fluids. 2013; 75: p. 101-111.

41. Eser S. Mesophase and pyrolytic carbon formation in aircraft fuel lines. Carbon. 1996; 34: p. 539-547.

42. Commodo M, Wong O, Fabris I, Groth CPT, Gulder OL. Spectroscopic study of aviation jet fuel thermal oxidative stability. Energy & Fuels. 2010; 24: p. 6437-6441.

43. Diaby M, Sablier M, Le Negrate A, El Fassi M, Bocqueta J. Understanding carbonaceous deposit formation resulting from engine oil degradation. Carbon. 2009; 47: p. 355-366.

44. Mayo FR, Lan BY. Gum and deposit formation from jet turbine and diesel fuels at 130°C. Industrial and Engineering Chemistry Production Reseach Development. 1986; 25: p. 333 - 348.

45. Aksoy P, Gul O, Cetiner R, Fonseca DA, Sobkowiak M, Falcone-Miller S, et al. Insight into the mechanisms of middle distillate fuel oxidative degradation. Part 2: On the relationship between jet fuel thermal oxidative deposit, soluble macromolecular oxidatively reactive species, and smoke point. Energy & Fuels. 2009; 23: p. 2047-2051.

46. Beaver B, Gao L, Burgess-Clifford C, Sobkowiak M. On the mechanisms of formation of thermal oxidative deposits in jet fuels. Are unified mechanisms possible for both storage and thermal oxidative deposit formation for middle distillate fuels?. Energy & Fuels. 2005; 19: p. 1574-1579.

47. Knothe G. Some aspects of biodiesel oxidative stability. Fuel Processing Technology. 2007; 88: p. 669-677.

48. Ogawa T, Kajiya S, Kosaka S, Tajima I, Yamamoto M, Okada M. Analysis of oxidative deterioration of biodiesel fuel. SAE Technical Paper Series. 2008; 2008-01-2502.

49. Arisoy K. Oxidative and thermal instability of biodeisel. Energy sources, Part A: Recovery,Utilization, and Environmental effects. 2008; 30: p. 1516-1522.

50. Kah B, Kay KH, Sally SN, Yasir SM. Study of biodiesel & biodiesel blends deterioration mechanism. International Journal of Chemical and Environmental Engineering. 2013; 4: p. 64-69.

51. Waynick AJ. Characterization of biodiesel oxidation and oxidation products. CRC Project No. AVFL-2b. San Antonio, Texas: Southwest Research Institute; 2005.

52. Fang HL, McCormick RL. Spectroscopic study of biodiesel degradation pathways. SAE Technical Paper Series. 2006; 2006-01-3300.

53. Lin R, Zhu Y, Tavlarides LL. Mechanism and kinetics of thermal decomposition of biodiesel fuel. Fuel. 2013; 106: p. 593-604.

54. McGinnis TP, Peyton KB. Analytical characterization of sediment formed in soy oil-based B20 biodiesel. Journal of ASTM International. 2010; 7: p. 1-17.

55. Plata V, Kafarova V, Castillob E. Improving the Low-temperature properties and filterability of biodiesel. Chemical Engineering Transactions. 2012; 29: p. 1243-1248.

56. Osawa M, Eninuma Y, Sasaki S, Takashiba T, Takaki Y, Jetter JJ, et al. Influence of base diesel fuel upon biodiesel sludge formation tendency. SAE Technical Paper Series. 2009; 2009-01-0482: p. 127-138.

57. Jiang W, Boshui C, Jianhua F, Jiu W. Spectroscopic analysis of structural transformation in biodiesel oxidation. China Petroleum Processing and Petrochemical Technology. 2013; 15: p. 28-32.

58. Silva VD, Conceição JN, Oliveira IP, Lescano CH, Muzzi RM, Filho OPS, et al. Oxidative stability of baru (Dipteryx alata Vogel) oil monitored by fluorescence and absorption spectroscopy. Journal of Spectroscopy. 2015; 803705: p. 1-6.

59. Kumar S. Spectroscopy of organic compounds. Amritsar, India: National Science Digital Library at NISCAIR; 2006.

60. Souza FHN, de Almeida LR, Batista FSCL. UV-Visible spectroscopy study of oxidative degradation of sunflower biodiesel. Energy Science and Technology. 2011; 2: p. 56-61.

61. Owen T. Fundamentals of modern UV-visible spectroscopy. Waldbronn, Germany: Agilent Technologies; 2000.

62. Gomez NA, Abonia R, Cadavid H, Vargas IH. Chemical and spectroscopic characterization of a vegetable oil used as dielectric coolant in distribution transformers. J. Braz. Chem. Soc. 2011; 22: p. 2292-2303.

63. Zawadzki A, Shrestha DS, He B. Biodiesel blend level detection using ultraviolet absorption spectra. American Society of Agricultural and Biological Engineers. 2007; 50: p. 1349-1353.

64. Dantas MB, Albuquerque AR, Barros AK, Filho MGR, Filho NRA, Sinfrônio FSM, et al. Evaluation of the oxidative stability of corn biodiesel. Fuel. 2011; 90: p. 773-778.

65. Li D, Fang W, Xing Y, Guo Y, Lin R. Spectroscopic studies on thermal-oxidation stability of hydrocarbon fuels. Fuel. 2008; 87: p. 3286-3291.

66. Tripathi KM, Sonker AK, Sonkar SK, Sarka S. Pollutant soot of diesel engine exhaust transformed to carbon dots for multicoloured imaging of E. coli and sensing cholesterol. Royal Society of Chemistry Advances. 2014; 4: p. 30100–30107.

67. Qian K, Edwards KE, Dieh JHl, Green LA. Fundamentals and applications of electrospray ionization mass spectrometry for petroleum characterization. Energy & Fuels. 2004; 18: p. 1784-1791.

68. Ho CS, K LCW, Chan MHM, Cheung RCK, Law LK, Lit LCW, et al. Electrospray ionisation mass spectrometry: principles and clinical applications. Clinical Biochemist Review. 2003; 24: p. 3-12.

69. Hughey CA, Hendrickson CL, Rodgers RP, Marshal AGl. Elemental composition analysis of processed and unprocessed diesel fuel by electrospray ionization fourier transform ion cyclotron resonance mass spectrometry. Energy & Fuels. 2001; 15: p. 1186-1193.

70. Rostad CE. Differentiation of commercial fuels based on polar pomponents using negative electrospray ionization/mass spectrometry. Environmental Forensics. 2006; 7: p. 5-14.

71. Adams RK, Zabarnick S, West ZJ, Striebich RC, Johnson DW. Chemical analysis of jet fuel polar, heteroatomic species via high-performance liquid chromatography with electrospray ionization-mass spectrometric detection. Energy & Fuels. 2013; 27: p. 2390−2398.

72. Catharino RR, Milagre HMS, Saraiva SA, Garcia CM, Schuchardt U, Eberlin MN. Biodiesel typification and quality control by direct Infusion electrospray ionization mass spectrometry fingerprinting. Energy & Fuels. 2007; 21: p. 3698-3701.

73. Abdelnur PV, Saraiva SA, Catharino RR, Coelho M, Schwab N, Garcia CM, et al. Blends of soybean biodiesel with petrodiesel: direct quantitation via mass spectrometry. Journal of Brazilian Chemistry Society. 2013; 24: p. 946-952.

74. Frankenfeld JW, Taylor WF. Deposit formation from deoxygenated hydrocarbons. 4. Studies in pure compound systems. Industrial and Engineering Chemistry Prodroduct Research and Development. 1980; 19: p. 65-70.

75. Gül Ö, Rudnick LR, Schobert HH. The Effect of chemical composition of coal-based jet fuels on the deposit tendency and morphology. Energy & Fuels. 2006; 20: p. 2478-2485.

76. Rudnick LR, Gül Ö, Schobert HH. The effect of chemical composition of coal-derived jet fuel on carbon deposits. American Chemical Society, Division of Fuel Chemistry. 2004; 49: p. 770-772.

77. Hallet H. Formation and characterization of carbon deposit from thermal stressing of gasoline and diesel fuels. B.S Thesis. State College, USA: Pennsylvania State University.

78. Ram Mohan A, Eser S. Analysis of carbonaceous solid deposits from thermal oxidative stressing of Jet-A fuel on iron- and nickel-based alloy surfaces. Industrial and Engineering Chemistry Research. 2010; 49: p. 272-2730.

79. Baker RTK, Yates CDJ. Filamentous carbon formation over iron surface. In Coke formation on metals surfaces. Washington DC, USA: American Chemical Society; 1982. p. 1-21.

80. Venkataraman R, Eser S. Characterization of solid deposits formed from short durations of jet fuel degradation: Carbonaceous solids. Industrial and Enginerering Chemistry Resources. 2008; 47: p. 9337-9350.

81. Venkataraman R, Eser S. Characterisation of solid deposits from the thermal-oxidative degradation of jet fuel. International Journal of Oil,Gas and Coal Technology. 2008; 1: p. 126-137.

82. Anastasi RF. An introduction to Moire methodswith applications in composite materials. Army Lab Command, Material Technology Lab. 1992; No. MTL TR 92-55.

83. Jasinski JB, Dumpala S, Sumanasekera GU, Sunkara MK, J OP. Observation and interpretation of adjacent Moire patterns of different shapes in bilayer graphene. Applied physics letters. 2011; 99.

84. Barker J, Richards P, Pinch D, Cheeseman B. Temperature programmed oxidation as a technique for understanding diesel fuel system deposits. SAE Technical Paper Series. 2010; 2010-01-1475.

85. Inorganic application note,surface carbon on steel sheet and rod samples. [Online].; 2008 [cited 2015 February 23. Available from: http://www.leco.co.za.

86. Eser S, Venkataraman R, Altin O. Utility of temperature-programmed oxidation for characterization of carbonaceous deposits from heated jet fuel. Journal of Industrial and Engineering Chemistry Research. 2006; 45: p. 8956 -8962.

87. Birgel A, Ladommatos N, Aleiferis P, Zülch S, Milovanovic N, Lafon V, et al. Deposit formation in the holes of diesel injector nozzles: A critical review. SAE Technical Paper Series. 2008; 2008-01-2383.

88. Konigsson F, Stalhammar P, Angstrom H. Controlling the injector tip temperature in a diesel dual fuel engine. SAE Technical Paper Series. 2012; 2012-01-0826.

89. Ikemoto M, Omae K, Nakai K, Ueda R, Kakehashi N, Sunami K. Injector nozzle coking mechanism in common rail diesel engine. SAE Technical Paper Series. 2011; 2011-01-1818.

90. Quigley R, Barbour R, G M. Trace metal contamination of diesel fuels. In TAE 6th International Fuels Colloquium; 2007; Technische Akademie Esslingen.

91. Mungse HP, Kumar N, Khatri OP. Synthesis, dispersion and lubrication potential of basal plane functionalized alkylated graphene nanosheets. Royal Society of Chemistry. 2015; 5: p. 25565-25571.

92. Vander Wal RL. Soot Nanostructure: definition, quantification and implications. SAE Technical Paper Series. 2005; 2005-01-0964.

93. Department of Energy. Draft position paper on the South African biofuels regulatory framework. [Online].; 2014. Available from: http://www.gov.za/sites/www.gov.za/files/37232gen24.pdf.

94. Dodos GS, Zannikos F, Stournas S. Effect of metals in the oxidation stability and lubricity of biodiesel fuel. SAE Technical Paper Series. 2009; 2009-01-1829.

95. Jain S, Sharma MP. Effect of metal contents on oxidation stability of biodiesel/diesel blends. Fuel. 2014; 116: p. 14-18.

10 APPENDICES

10.1 Appendix A : Autoxidative deposits

10.1.1 Visual observations

EN 590 diesel **RME100** **SME100** **RME20** **SME20**

Figure 10-1: Photographs of test fuel pre (top) and post (middle experiment 1: bottom experiment 2) thermal oxidation at 300°C for 5h.

10.1.2 FTIR results of test fuels before and after thermal oxidation

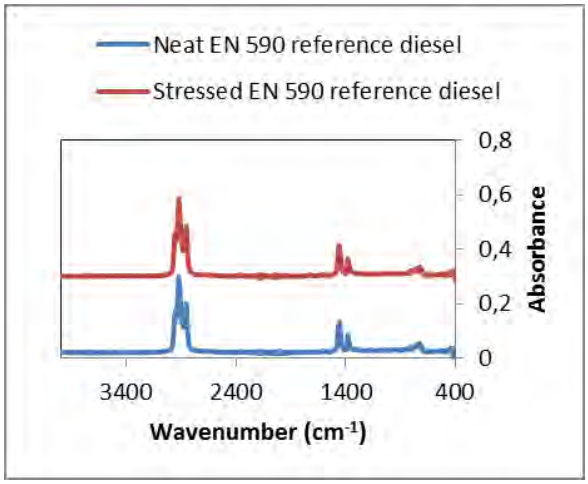

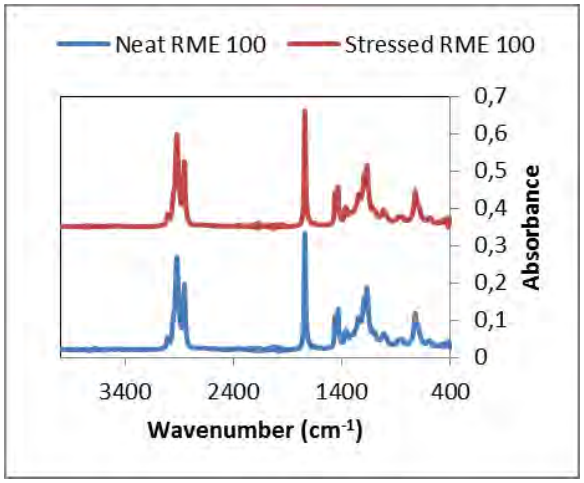

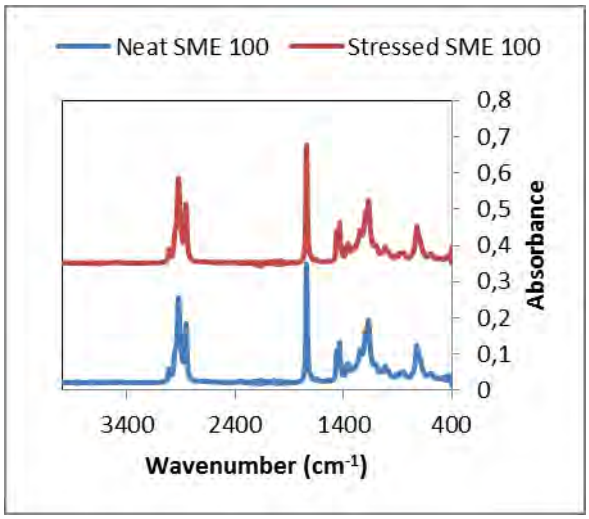

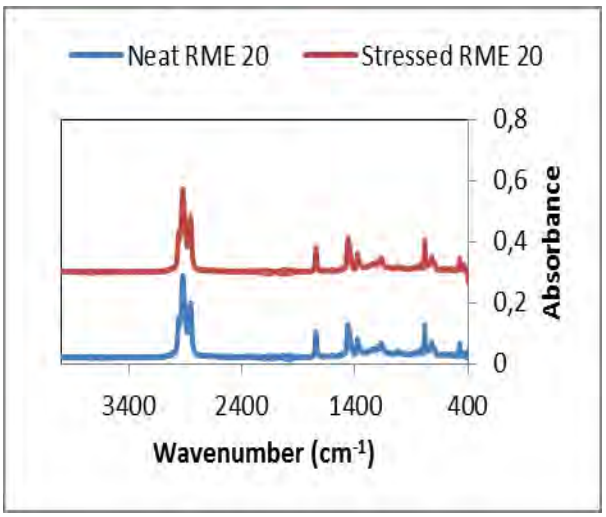

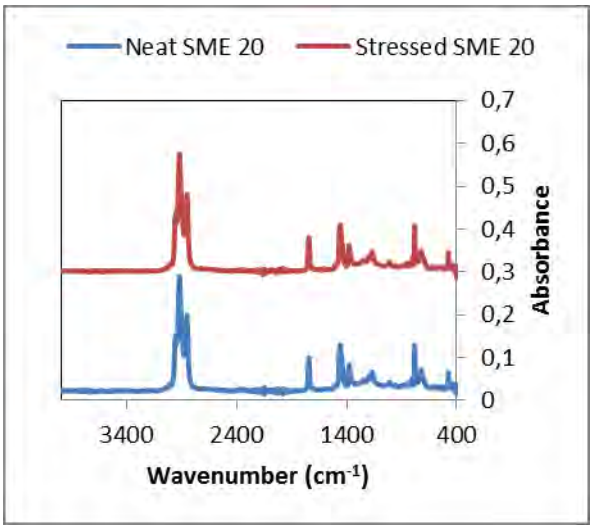

Figure 10-2: FTIR spectra of five different test fuels before (blue) and after (red) thermal oxidation at 300°C for 5h.

10.1.3 GC-MS results of test fuels before and after thermal oxidation

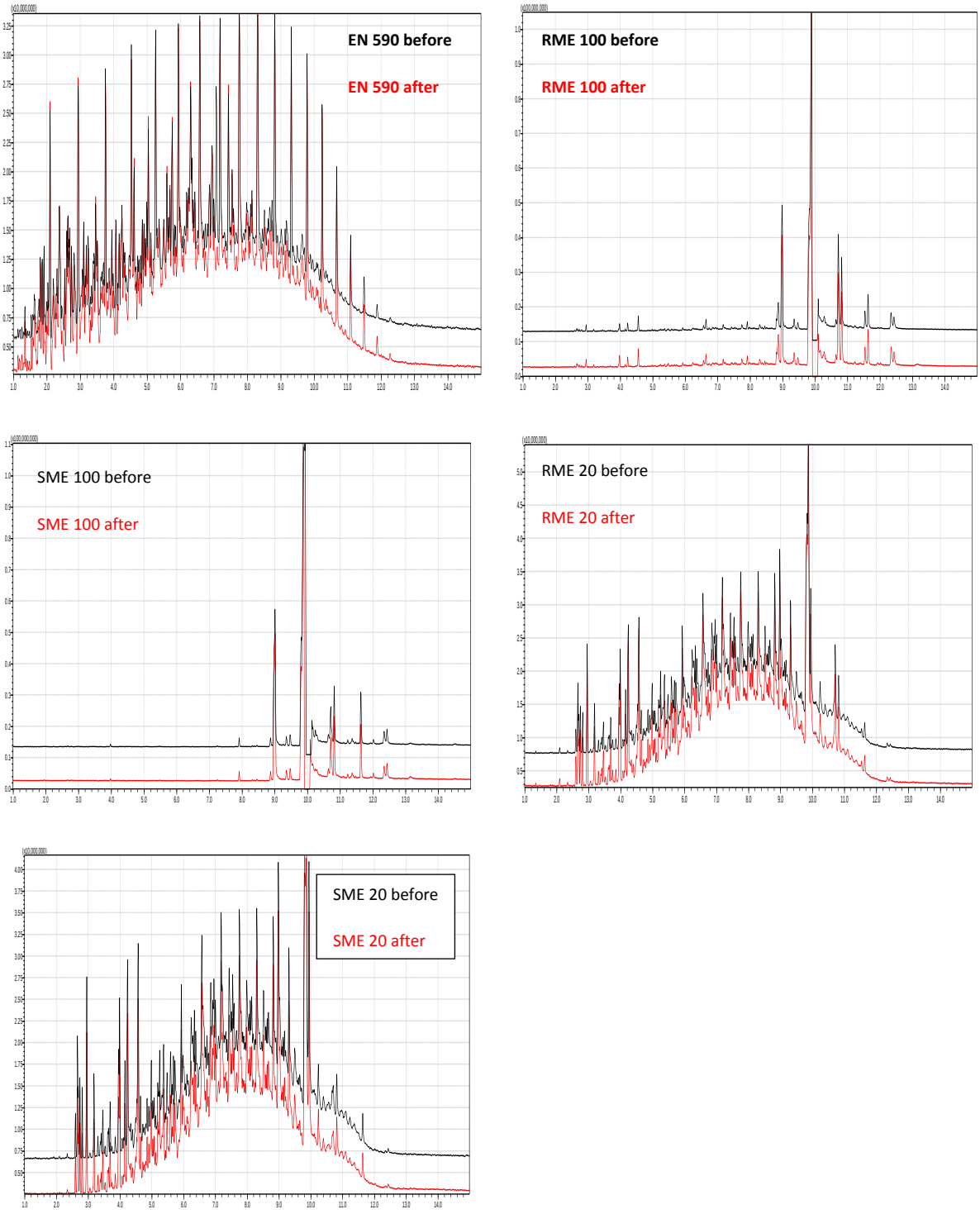

Figure 10-3: GC-MS chromatographs of five different test fuel before (black) and after (red) thermal oxidation at 300°C for 5h.

10.1.4 UV-Visible Spectroscopy

Repeat UV-Vis analysis showed that the wavelength at which the maximum absorbance of stressed and neat fuel was highly repeatable. The spectrums of the test fuels from the two runs are almost overlaid on top of each other as illustrated in Figure 10-4.

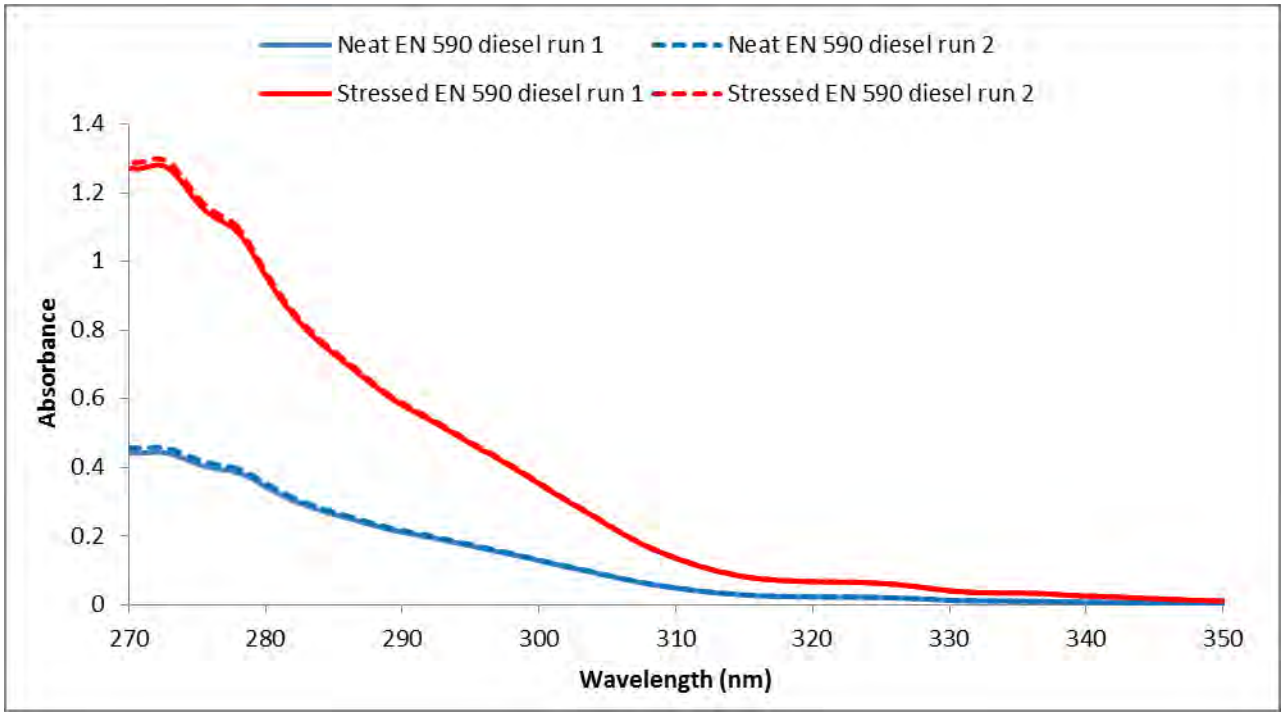

Figure 10-4: Repeat UV-Vis spectra of Neat EN 590 diesel and stressed EN 590 diesel. The stressed fuel was thermal stressed in a flow reactor at 400°C for 5h.

10.1.5 ESI-MS Results

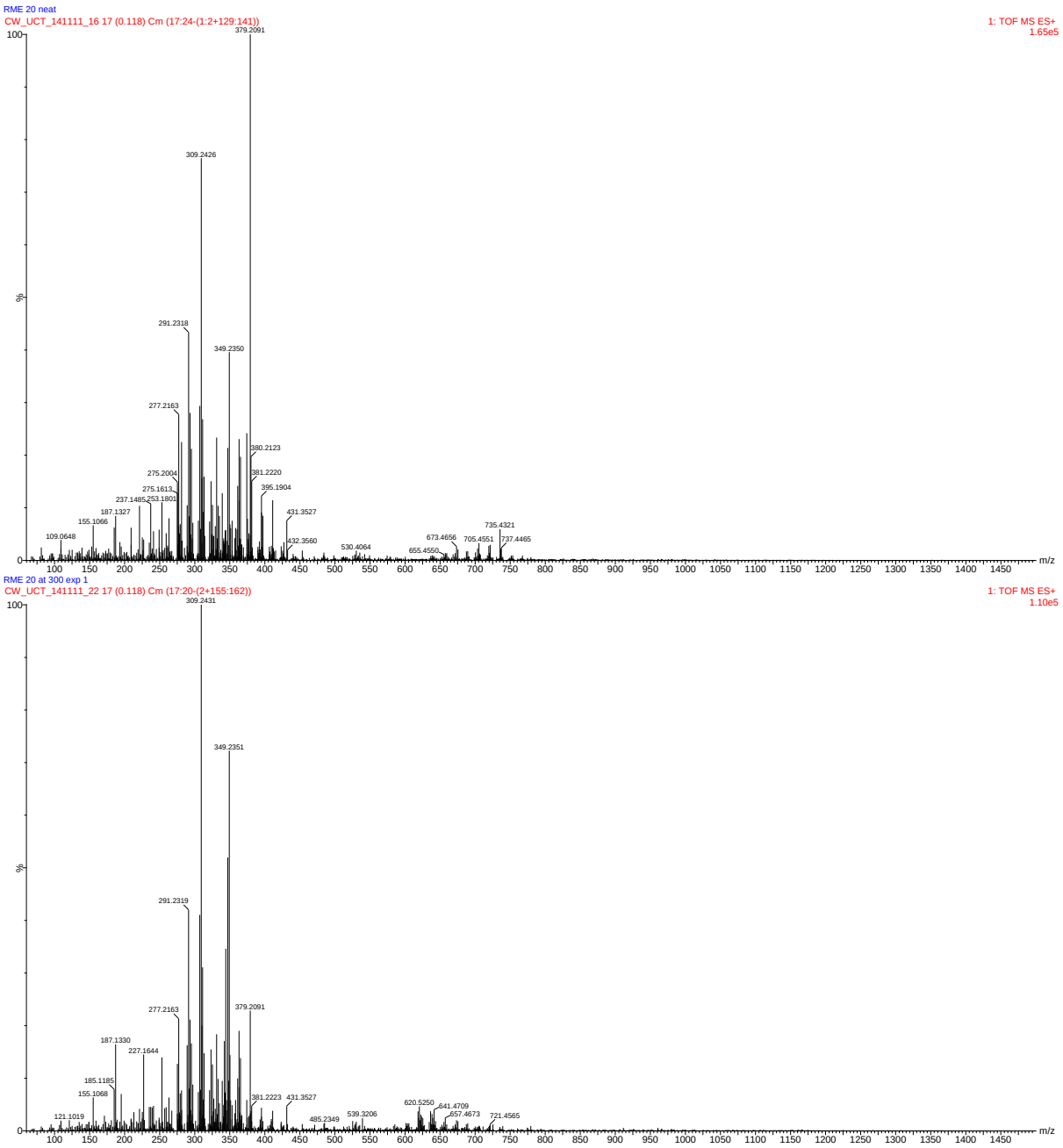

Figure 10-5: ESI (+) MS spectrum of RME20 before (top) and after (bottom) thermal oxidation at 300°C for 5h (0-1500).

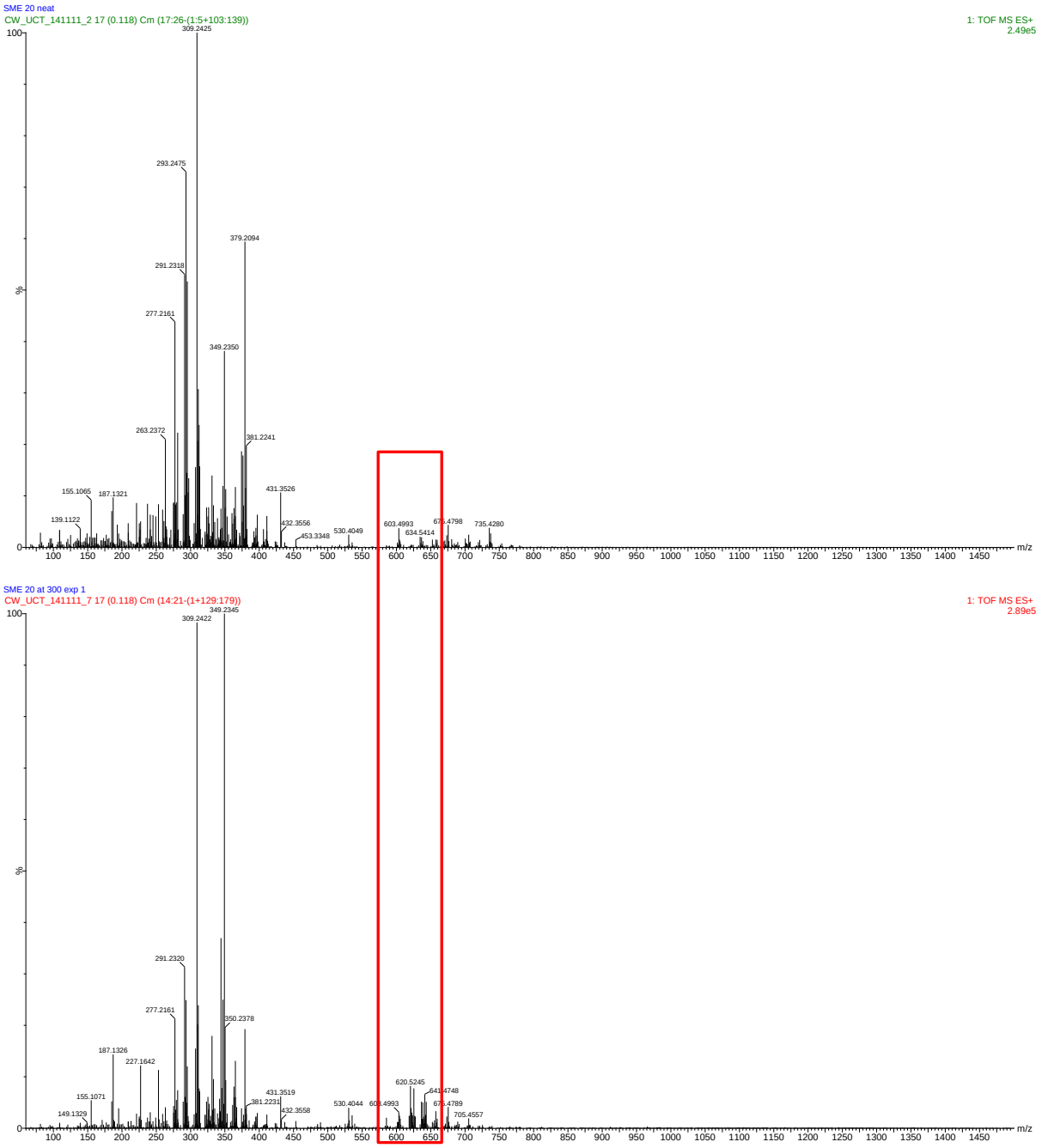

Figure 10-6: ESI (+) MS spectrum of SME20 before (top) and after (bottom) thermal oxidation at 300°C for 5h (0-1500).

10.1.6 TPO repeatability

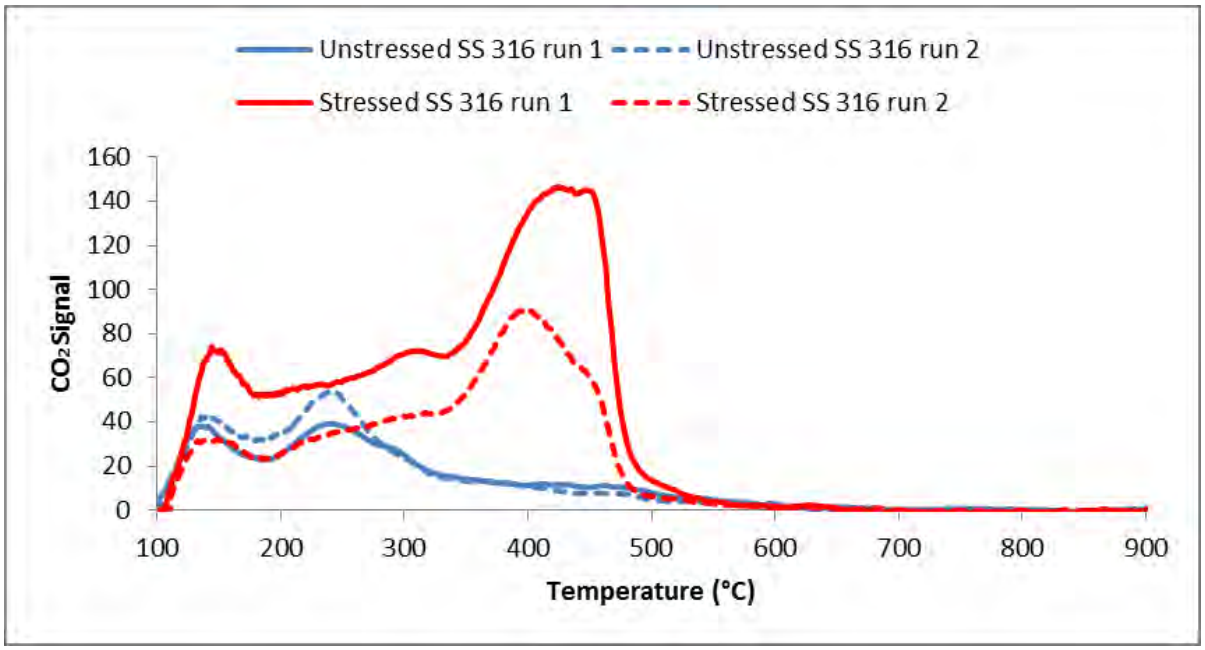

Figure 10-7: Repeat TPO profiles of unstressed tube section and tube section from the top of the reactor after thermal stressing EN 590 diesel at 400°C.

10.2 Appendix B: Intermediate deposits

10.2.1 Visual Observations

EN 590 diesel **RME 100** **SME 100** **RME 20** **SME 20**

Figure 10-8*: Photographs of test fuel pre (top) and post (bottom) thermal oxidation at 400°C for 5h.*

10.2.2 UV –Visible spectroscopy

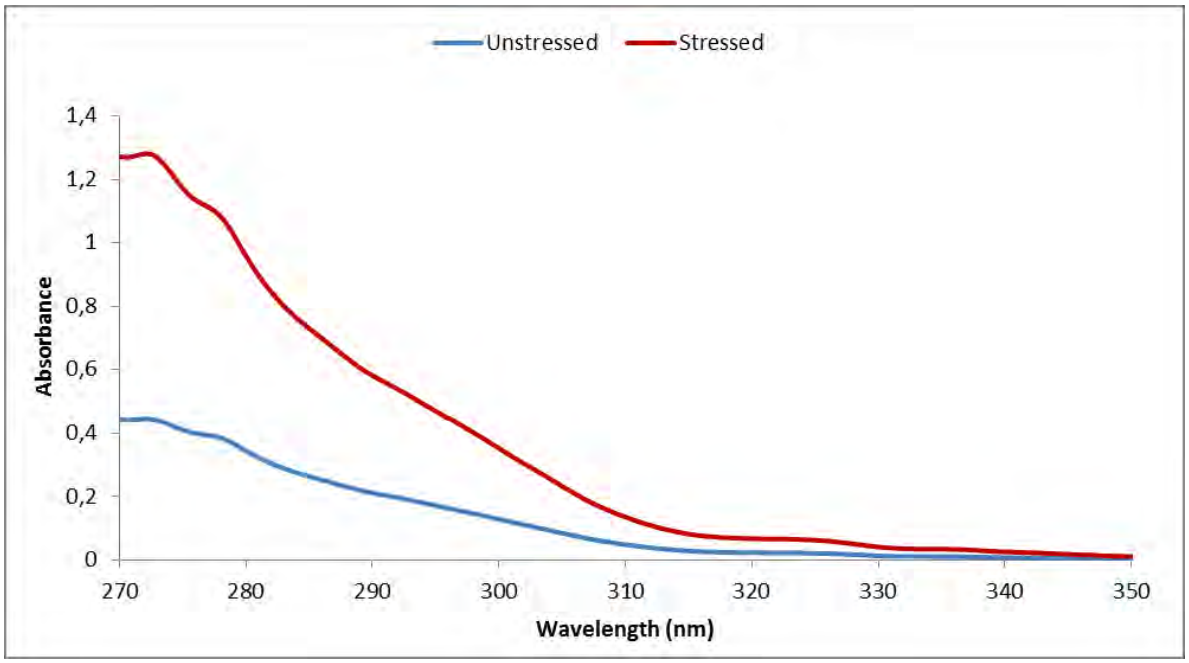

Figure 10-9: UV spectra of unstressed EN 590 reference diesel and stressed EN 590 reference diesel measured after 625× dilution in n-hexane.

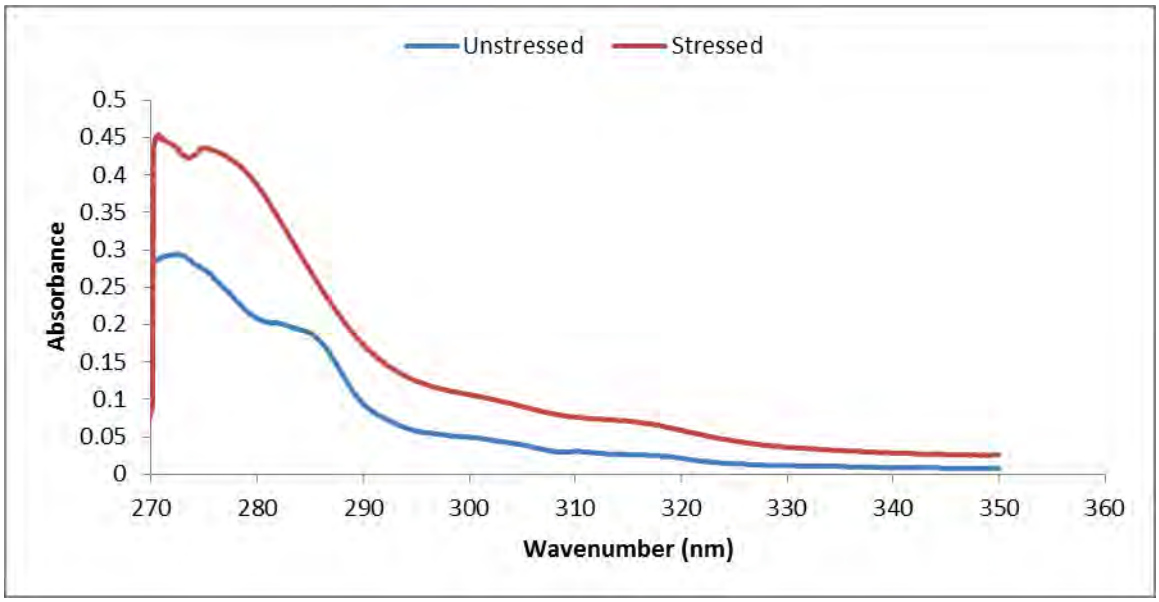

Figure 10-10: UV spectra of unstressed RME 100 and stressed RME 100 measured after 625× dilution in n-hexane.

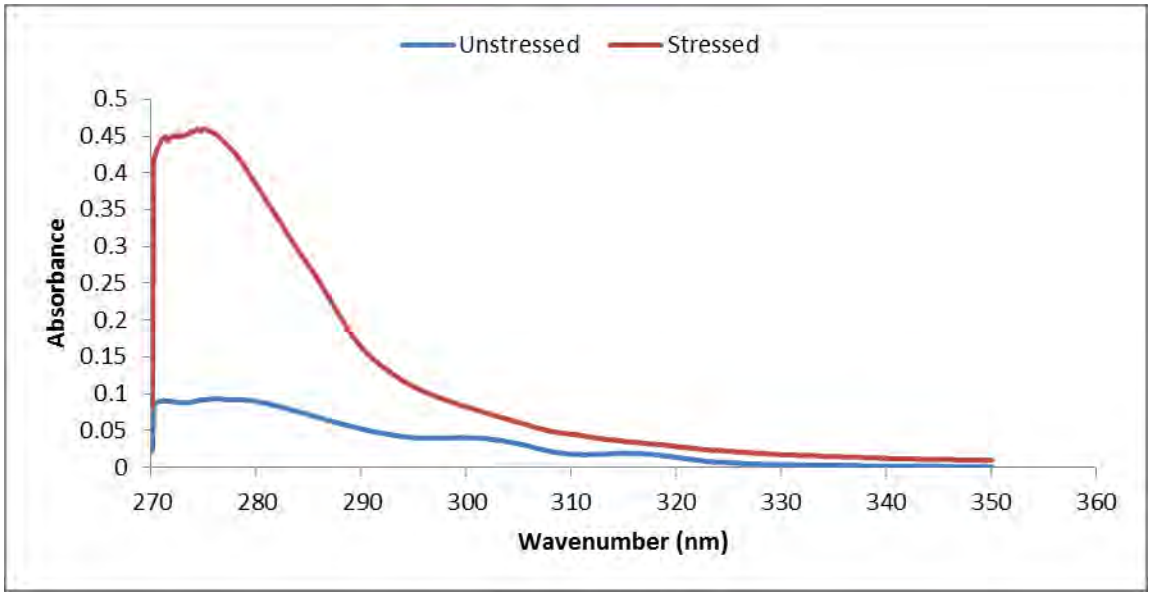

Figure 10-11: UV spectra of unstressed SME 100 and stressed SME 100 measured after 625× dilution in n-hexane.

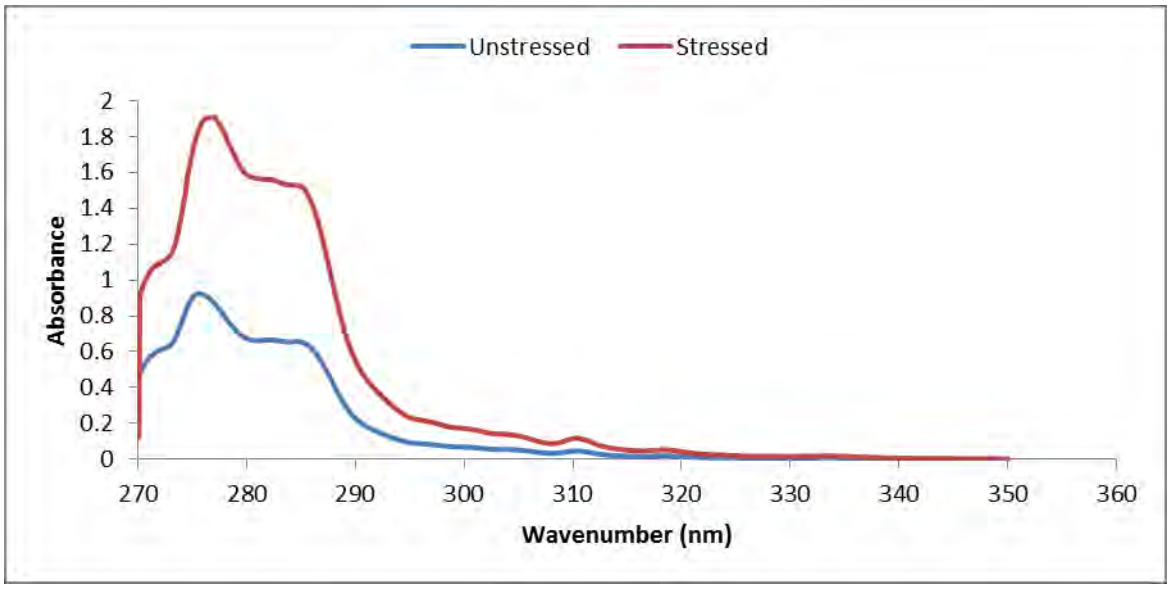

Figure 10-12: UV spectra of unstressed RME 20 and stressed RME 20 measured after 625× dilution in n-hexane.

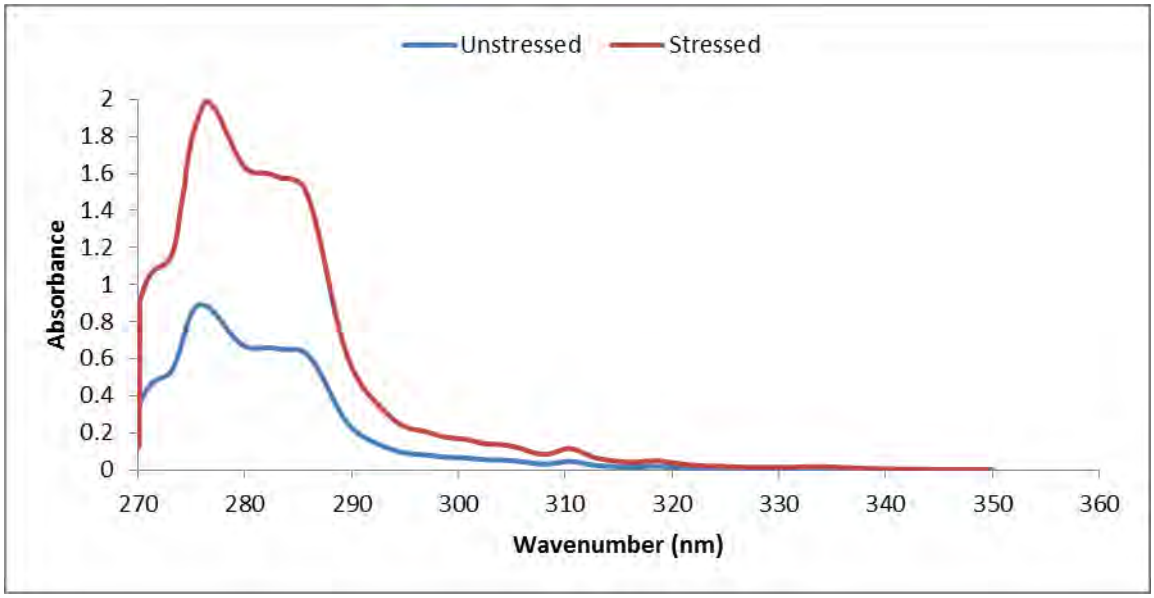

Figure 10-13: UV spectra of unstressed SME 20 and stressed SME 20 measured after 625× dilution in n-hexane.

10.2.3 ESI-MS

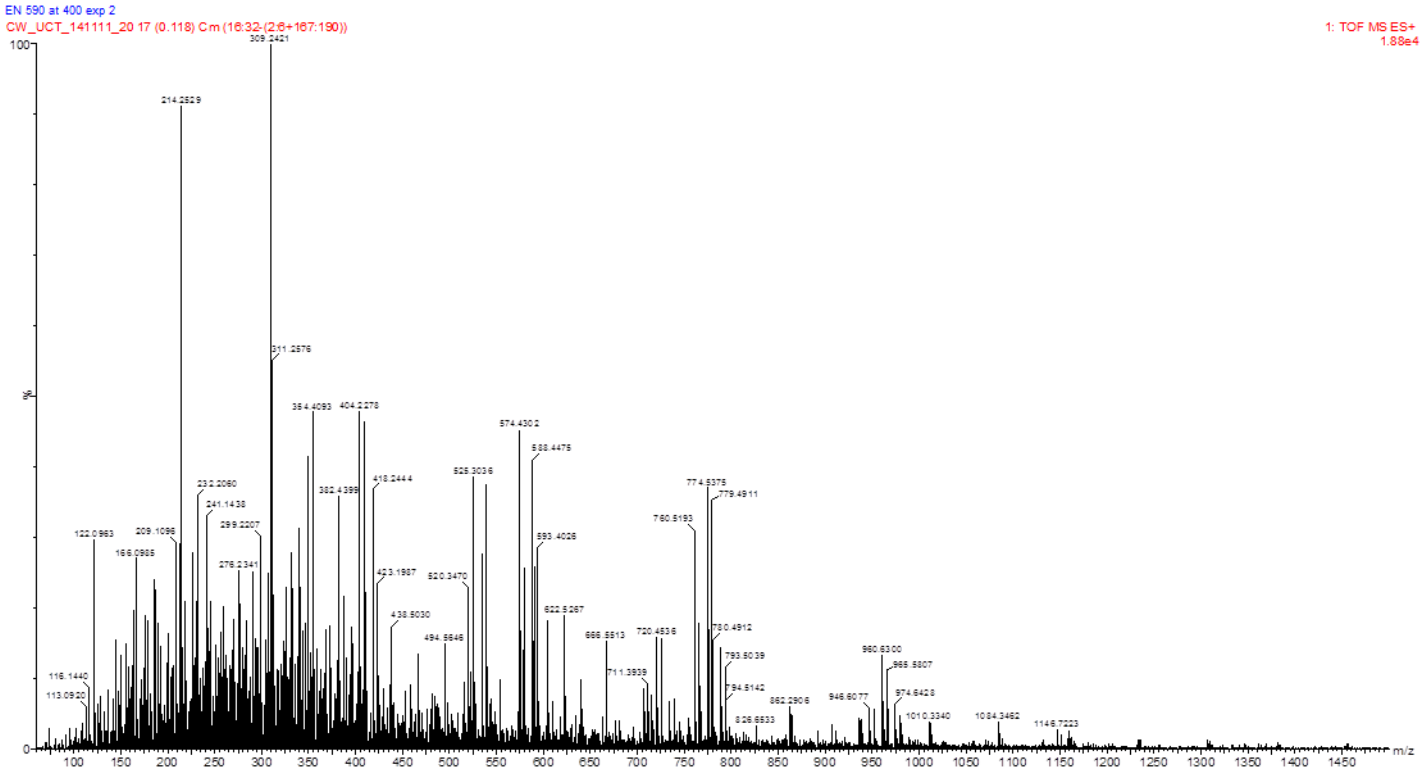

Figure 10-14: ESI (+) MS spectrum of EN 590 diesel after thermal oxidation at 400°C for 5h (0-1500).

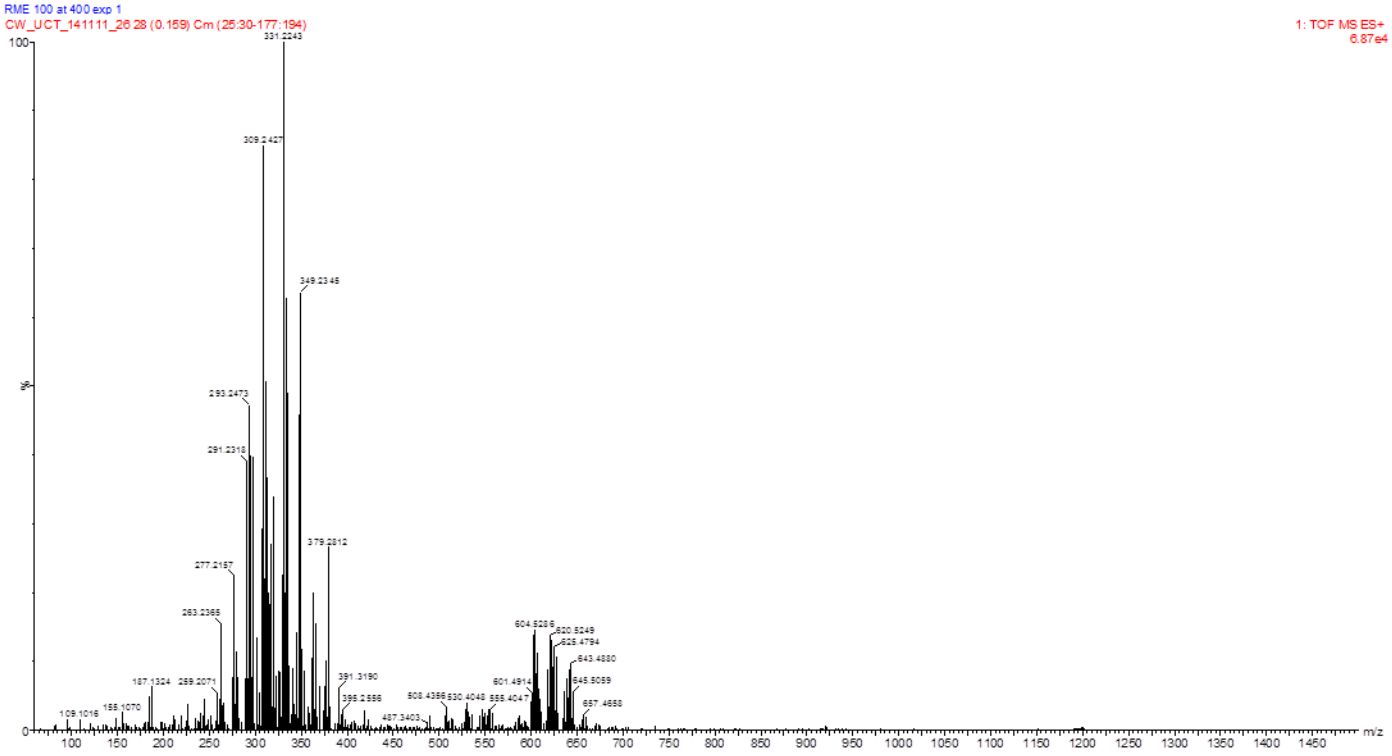

Figure 10-15: ESI (+) MS spectrum of RME100 after thermal oxidation at 400°C for 5h (0-1500).

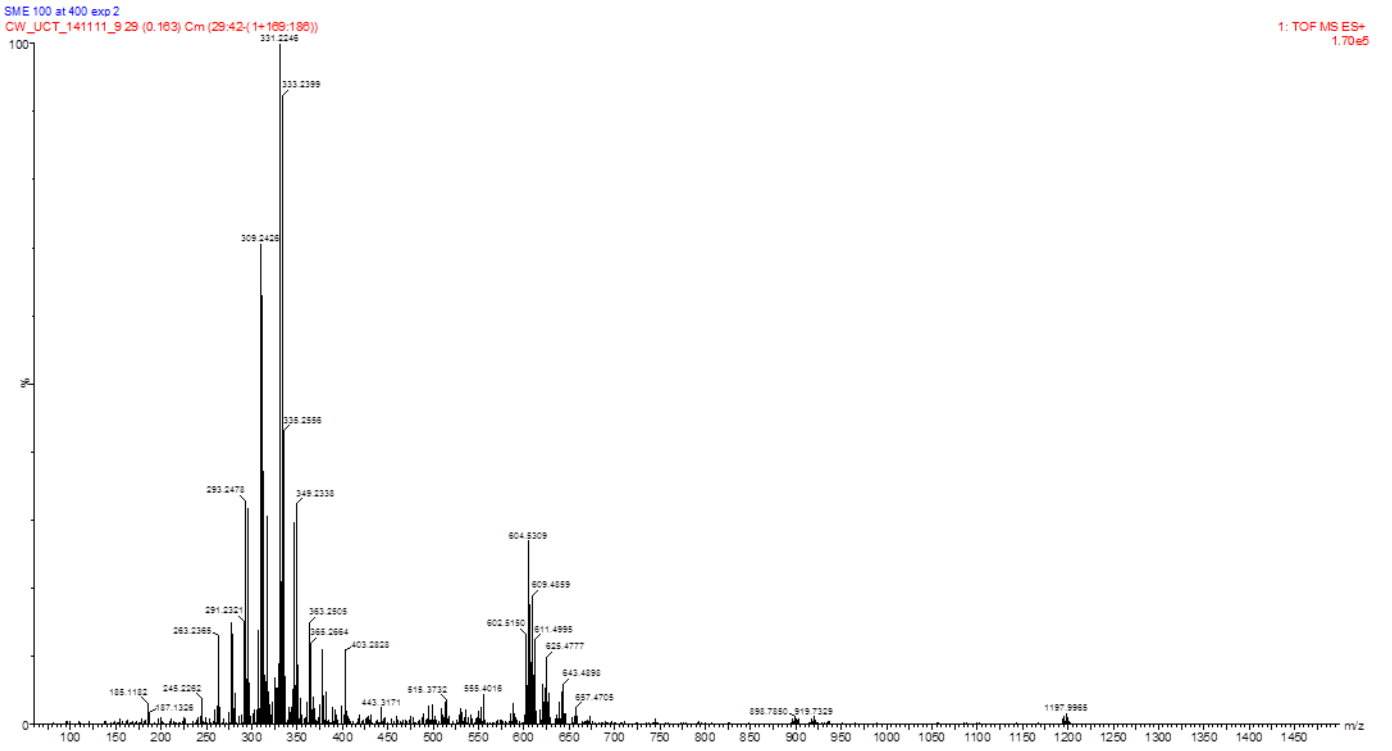

Figure 10-16: ESI (+) MS spectrum of SME100 after thermal oxidation at 400°C for 5h (0-1500).

Figure 10-17: ESI (+) MS spectrum of RME20 after thermal oxidation at 400°C for 5h (0-1500).

Figure 10-18: ESI (+) MS spectrum of SME100 after thermal oxidation at 400°C for 5h (0-1500).

10.2.4 Deposit Morphology

Table 10-1: Individual values from each test run and average carbon deposit of different test fuels after stressing in flow reactor at 400°C for 5h

	Run 1	**Run 2**	**Average**
EN 590 Top	67	69	68
MIDDLE	129	133	131
RME 100	99	125	112
SME 100	18	48	33
RME 20	194	230	212
SME 20	378	382	380

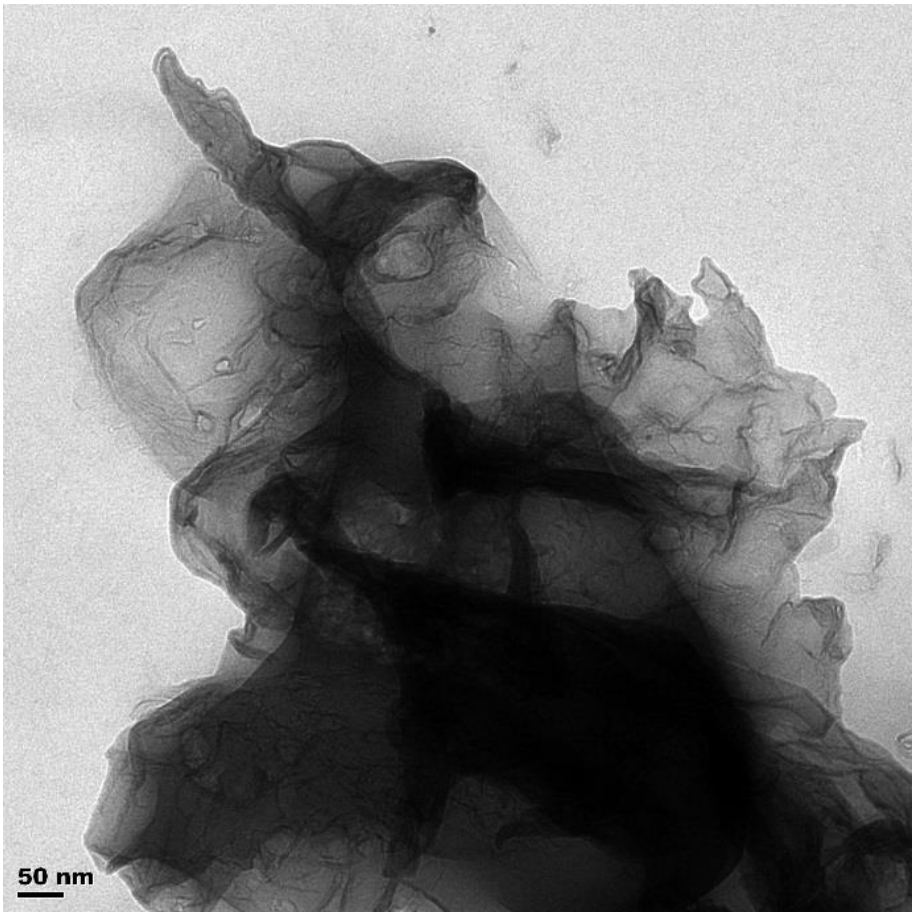

Figure 10-19: TEM micrograph of RME100-derived deposits viewed at a lower magnification.

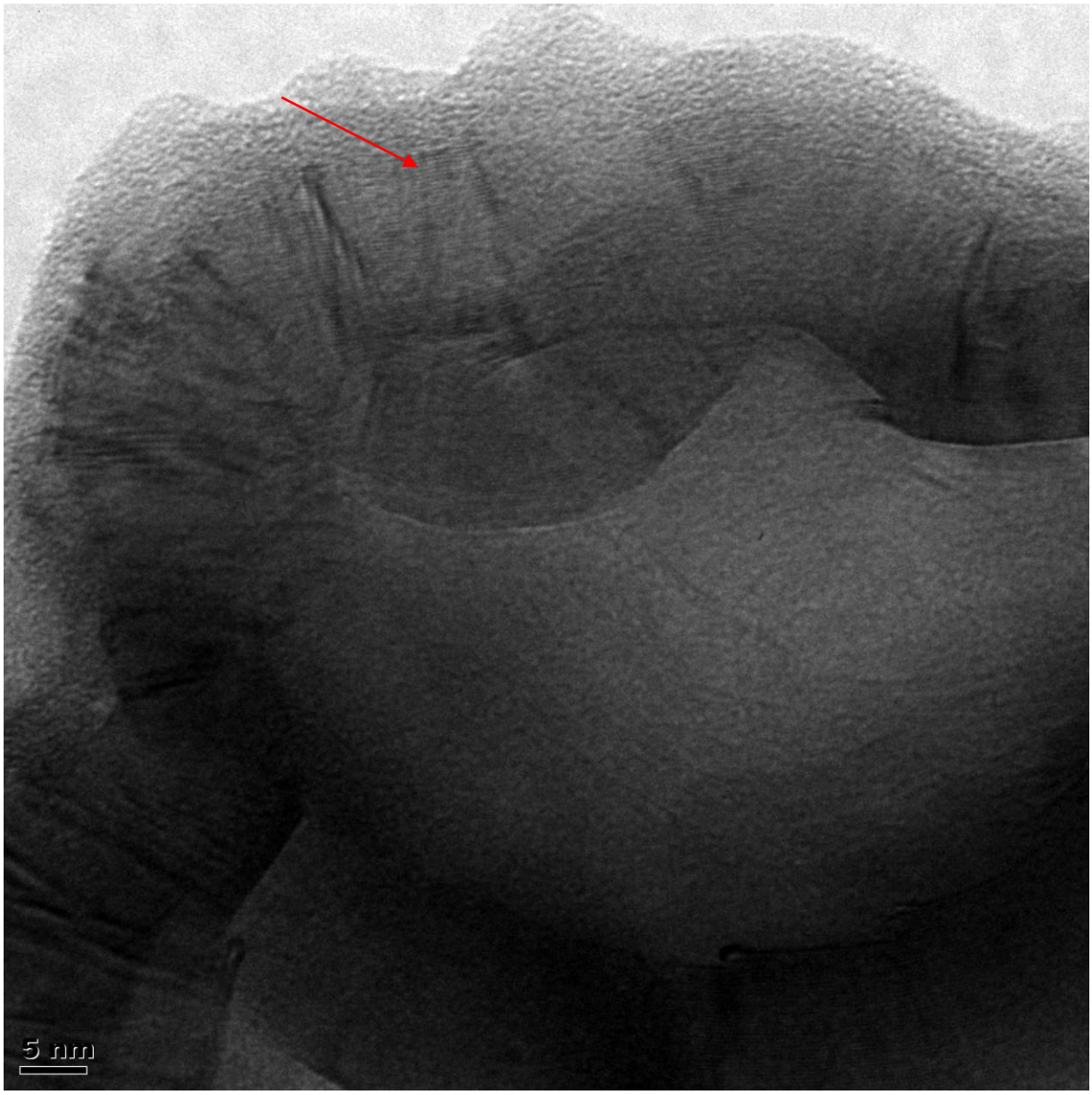

Figure 10-20: TEM micrograph of RME20- derived deposits viewed at high magnification.

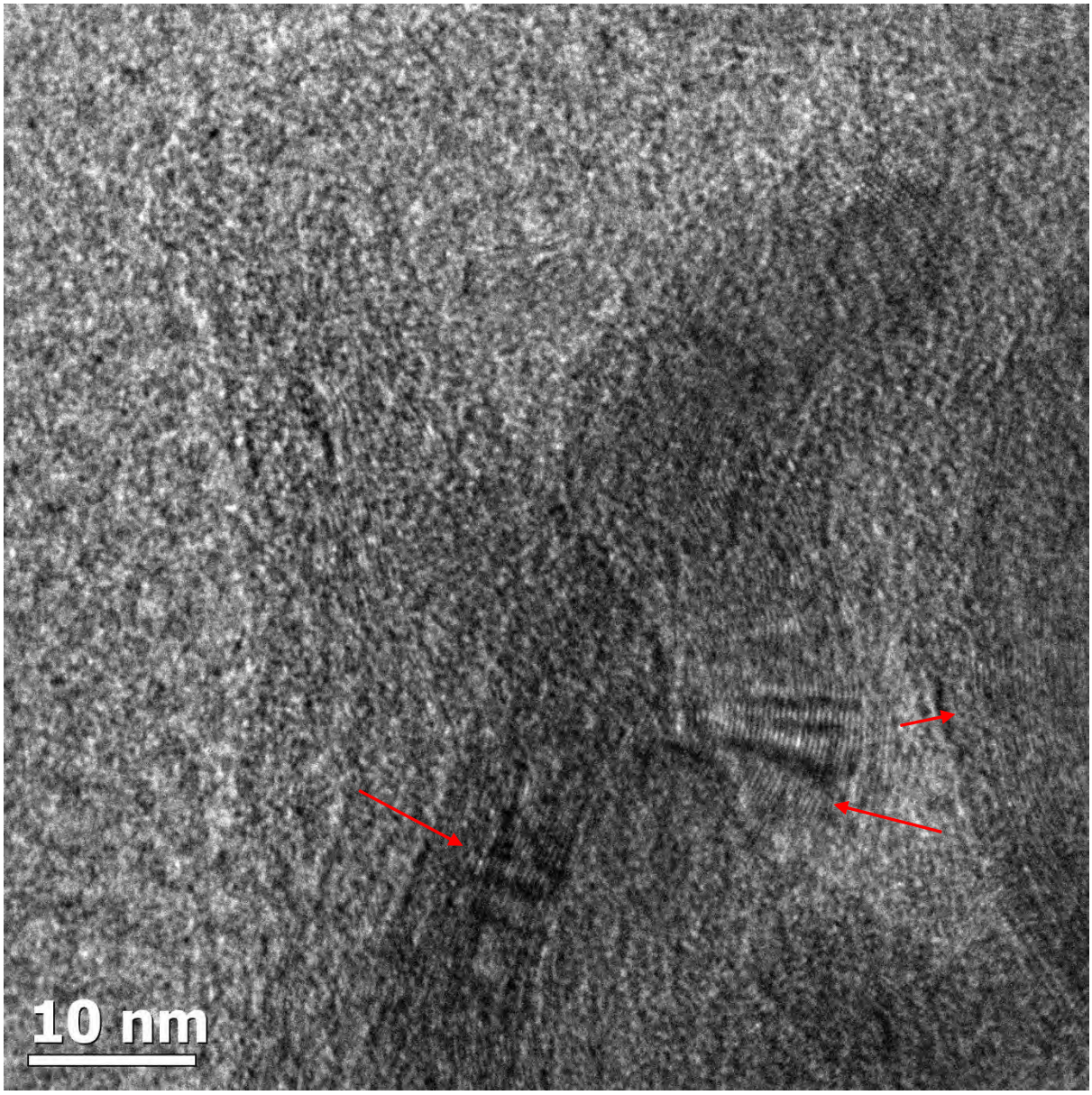

Figure 10-21: TEM micrograph of SME20- derived deposits viewed at high magnification.

a

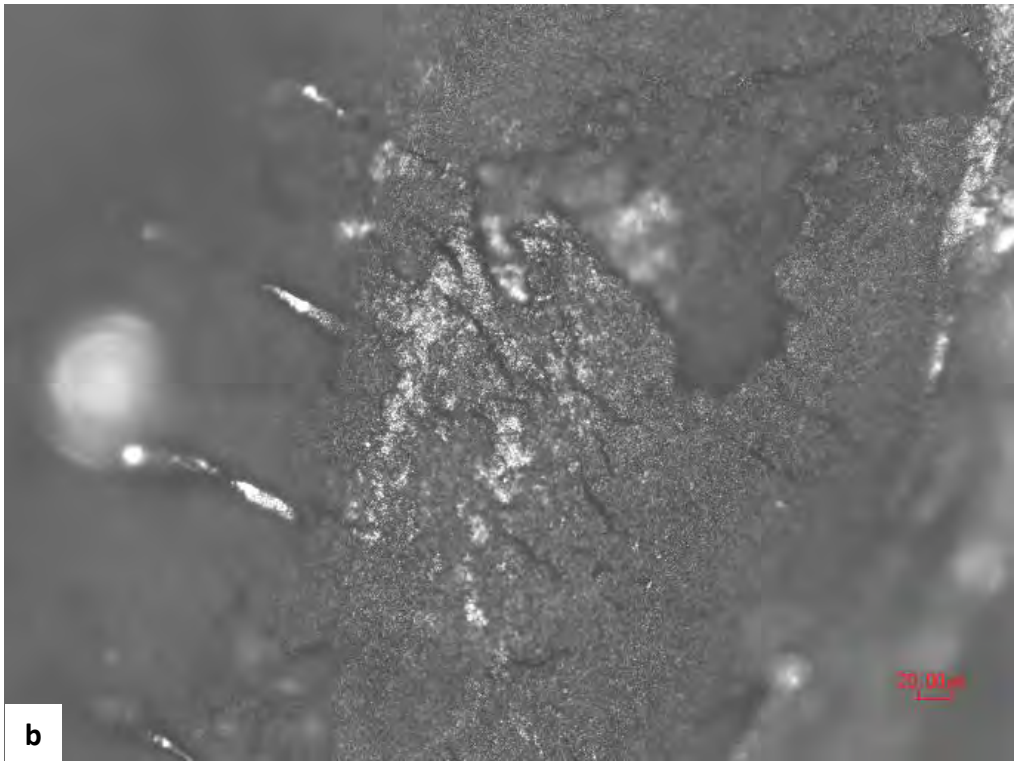

b

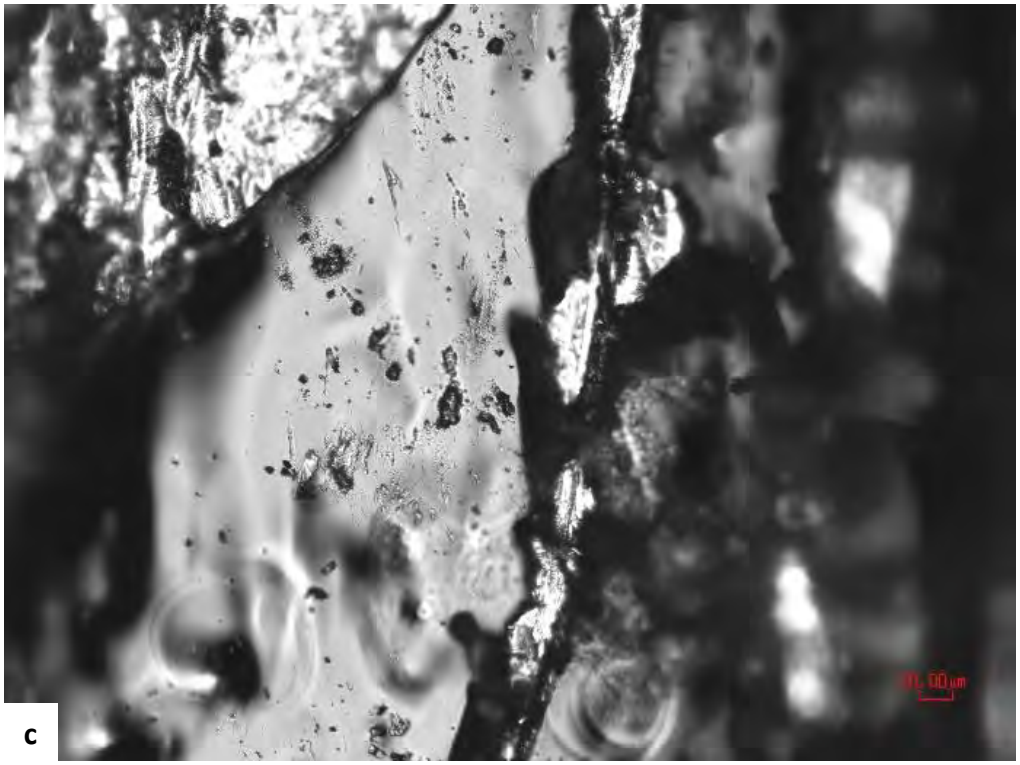

Figure 10-22: Polarised light micrographs of a) unstressed tube, b) tube stressed with RME 20, c) tube stressed with SME100 at 400^{o}C.

Table 10-2: EDS results of carbonaceous deposits formed at 400°C in flow reactor.

	C	**O**	**Cr**	**Fe**	**Ni**
EN 590 Top	32.81	9.12	14.97	34.73	7.05
EN 590 middle	68.06	4.3	5.68	18.56	3.40
RME 100	85.43	9.41			
SME 100	25.49	4.58	14.15	44.36	9.15
RME 20	22.3	10.72	15.22	38.24	7.19
SME 20	91.11	8.89			

Table 10-3: EDS results of deposits formed from various fuels doped with zinc neodecanoate.

	C	**O**	**Cr**	**Fe**	**Ni**
EN 590 diesel middle	35.90	6.31	10.03	40.22	7.54
EN 590 top	27.91	9.08	12.14	42.17	8.71
RME 100	100				
SME 100	67.69		9.4	23.09	

10.3 Appendix C: Sand bath deposits

10.3.1 Fuel degradation in closed bomb reactors

Closed bomb reactors were used to stress diesel and FAME/diesel blends under thermal-oxidative conditions (300°C, 5h) similar to those in the flow reactor for comparison purposes. A 5 cm SS 316 tube was inserted in the bomb reactor together with the test fuel in order to evaluate if deposit would adhere to the tube surface.

No discernible deposits were observed on the sliced metal tubes that were inserted in the closed bomb reactor. Furthermore there were no visible deposits on the walls of the closed bomb reactor. However, a notable colour difference was observed on the stressed fuel after thermal oxidation as can be seen in Figure 10-23. The stressed test fuels appeared darker compared to the unstressed fuels.

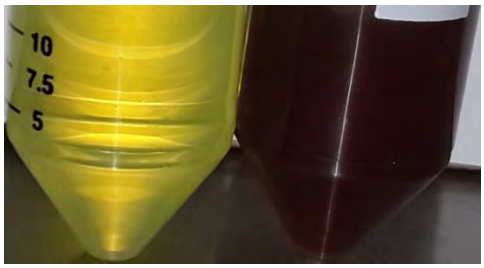

EN 590 diesel

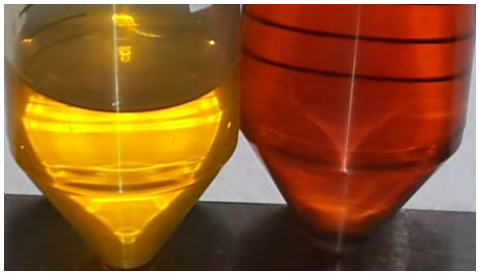

RME100

SME100

RME20

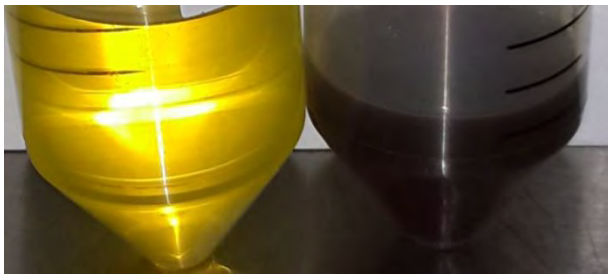

SME20

Figure 10-23: Photographs of neat fuels (left) and their corresponding stressed samples (right).

The colour of SME20, RME20 and EN 590 diesel changed to a dark brown colour after thermal oxidation whereas RME100 and SME100 changed to orange after thermal oxidation. To quantify the extent of degradation the neat and stressed test fuels were analysed by UV-Vis spectra.

The UV spectra of the stressed fuels showed an increase in absorbance after thermal oxidation across all test fuels (see Figure 10-25-Figure 10-29). This was consistent with the darkening in fuel colour after thermal oxidation observed visually. The UV spectra of some of the test fuels also showed a visible shift in wavelength after thermal degraded fuel. This was the case for RME20 and SME20.

10.3.2 Discussion

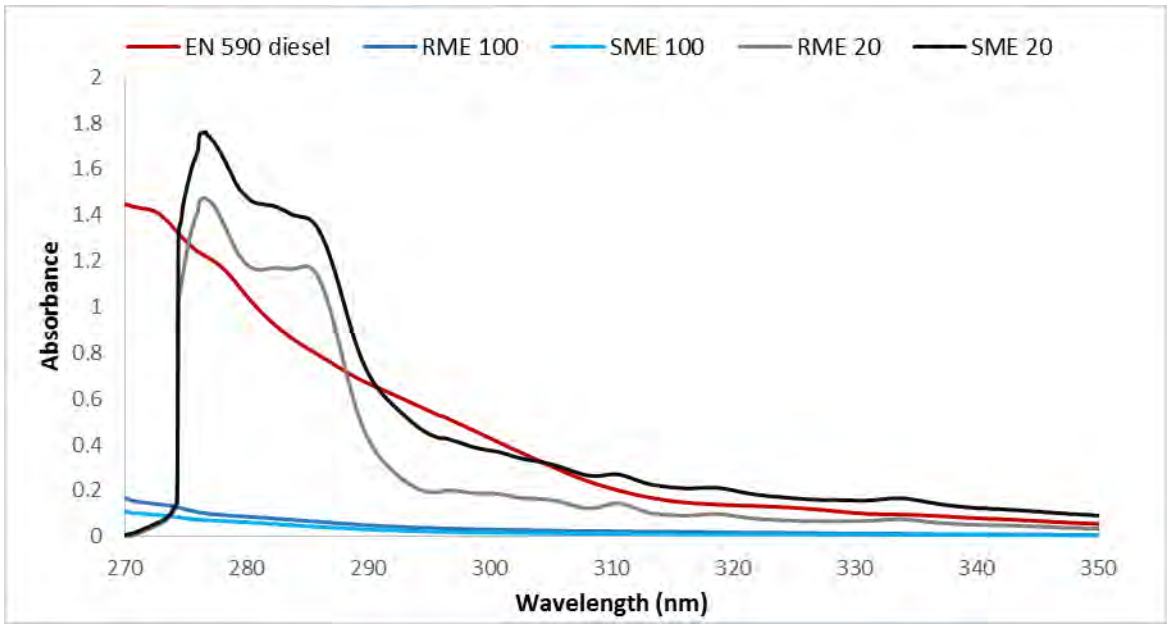

Figure 10-24: Comparison of the UV-Vis spectra of various stressed fuels.

A comparison of the UV-Vis spectra of the various fuels displayed in Figure 10-24 was used to shed more light on the stability of the fuels stressed in the bomb reactor. The results seem to suggest that SME20 was the least stable fuel as it showed the highest absorbance

compared to the other test fuels. The high absorbance can be attributed to the presence of more unsaturated deposit precursor in the stressed fuel. SME20 and RME20 also show a shift to a longer wavelength after thermal oxidation. This is likely due to the increase in the number of double bonds in the conjugated molecules (59).

If one were to rank the fuels according to the absorbance intensity observed after thermal degradation; the order would be SME20 > RME20 > EN 590 > RME100 > SME100. A similar trend was also observed from the flow reactor results. The trend SME20 > RME20 > EN 590 was also observed by Kaminuza from closed reactor deposits (15).

Significant colour changes observed from the fuels after thermo-stressing in the sand bath reactor was not observed when the fuels were stressed in the flow reactor under the same conditions. This could be because in the sand bath the temperature of the test fuel reaches 300°C. Furthermore the test fuel spends the whole five hours exposed to 300°C. In a flow reactor the fuel temperature does not reach 300°C only the furnace reaches this temperature. In addition to this the fuel's residence time in the reactor is only 7.44 min.

10.3.3 Conclusion

Thermal stressing the fuels in closed bomb reactors did not yield any discernible deposit on the metal tube inserted into the reactor or on the walls of the reactor bomb. The chemical and morphological properties of the deposits could not be compared to those that formed in the flow reactor.

The UV-Vis results seem to suggest that the differences in the setup of the closed sand bath reactor via that of the flow reactor have an effect on the extent at which the fuel degrades. The temperature, oxygen content and the residence time of the fuel in the reactor affect the degree at which the test fuel can degrade.

Stressing the test fuel in a closed reactor at 300°C resulted in the severe darkening of the fuel which can be used as an indicator of fuel stability; however, no discernible deposits were formed on the metal surface. The stability trend was SME20 > RME20 > EN 590 > RME100 > SME100. In the flow reactor only EN 590 diesel showed notable darkening in colour after thermal oxidation whereas FAME and FAME blends showed a lightening in fuel colour after thermal oxidation. These results suggest that the reaction was more extreme in

the sand bath, *i.e.* process has progressed further. The experimental set up of the two reactors is likely the reason for the difference. The fuel spends 5h exposed to high temperature in a sand bath and only 7.44 min in a flow reactor

When investigating injector deposits, the more ideal reactor would be the flow reactor as it simulates the conditions in the diesel engine better. The fuel comes into the reactor from a tank and is exposed to isothermal temperature and air. The fuel finally exits into a waste tank and new fuel is pumped in, similar to what happens in a diesel engine; whereas the closed bomb reactor has a batch of fuel exposed to the same temperature for the duration of the experiment.

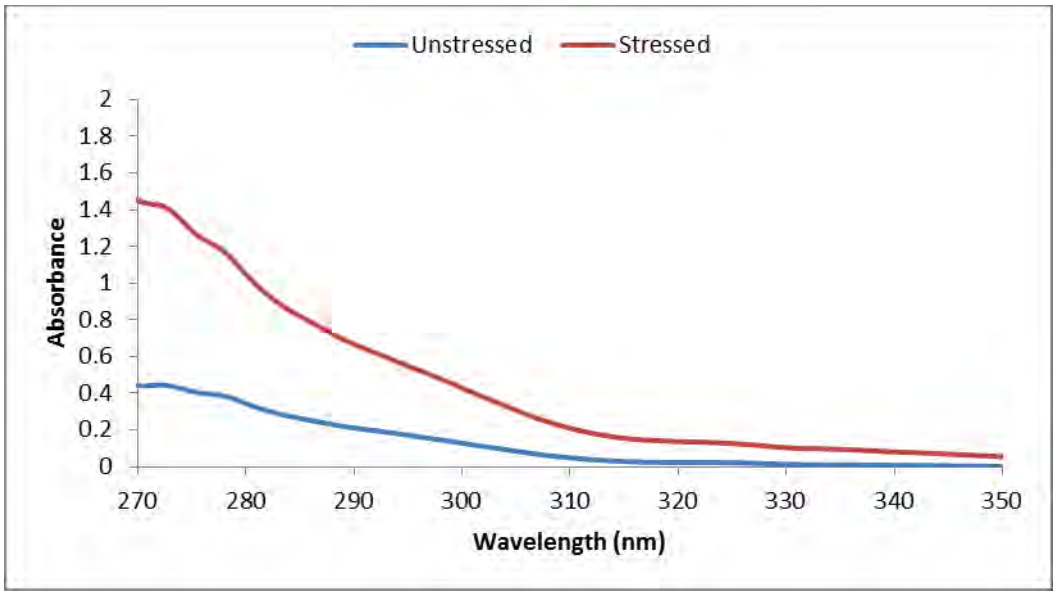

Figure 10-25: UV spectra of unstressed EN 590 reference diesel and stressed EN 590 reference diesel measured after 625× dilution in n-hexane.

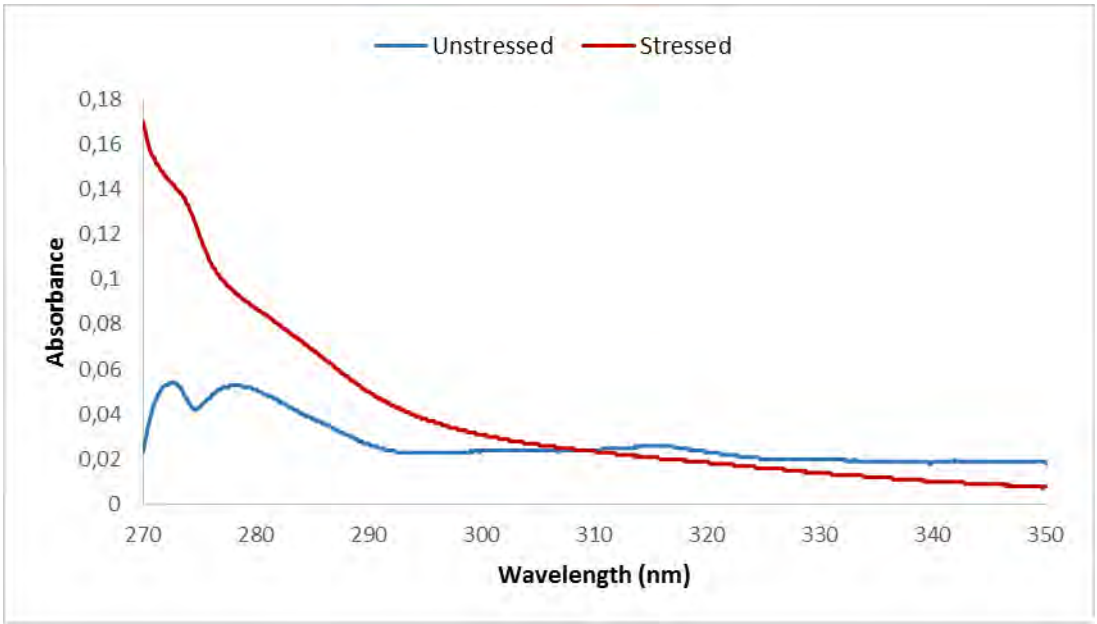

Figure 10-26: UV spectra of unstressed RME100 and stressed RME100 measured after 625× dilution in n-hexane.

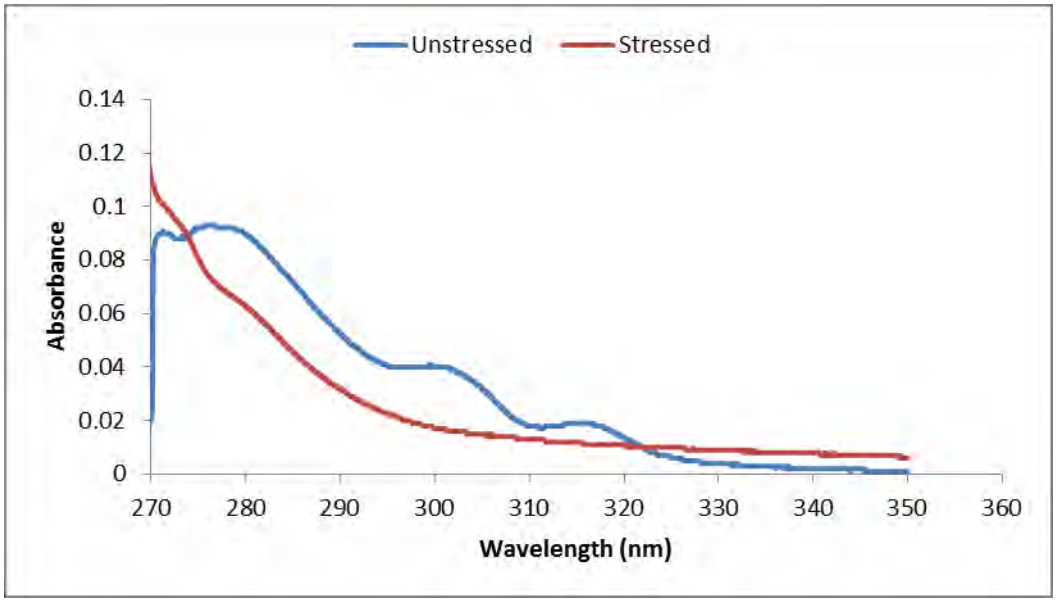

Figure 10-27: UV spectra of unstressed SME100 and stressed SME100 measured after 625× dilution in n-hexane.

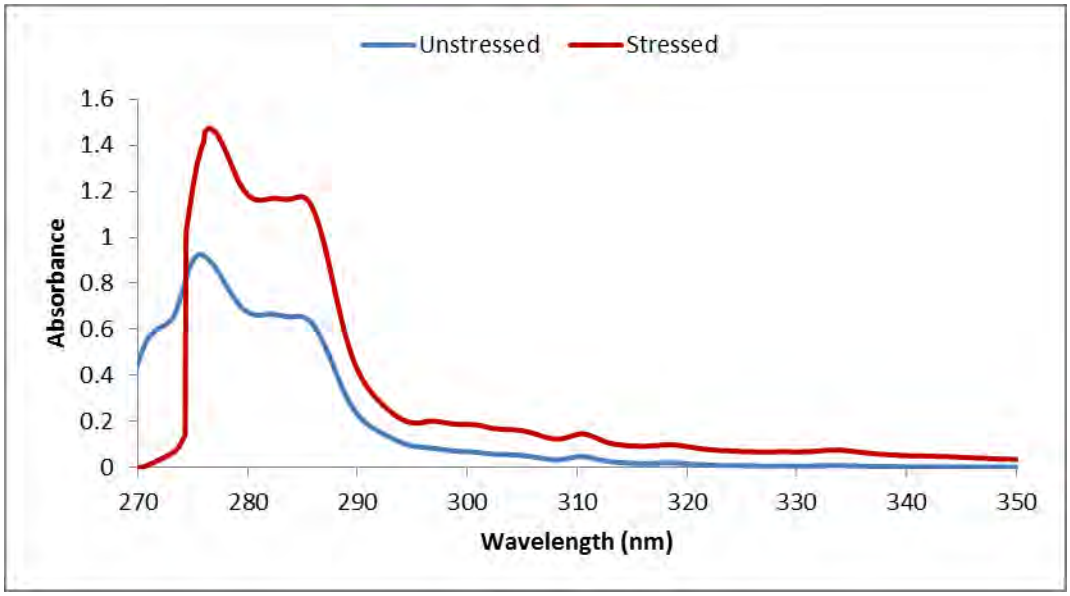

Figure 10-28: UV spectra of unstressed RME20 and stressed RME20 measured after 625× dilution in n-hexane.

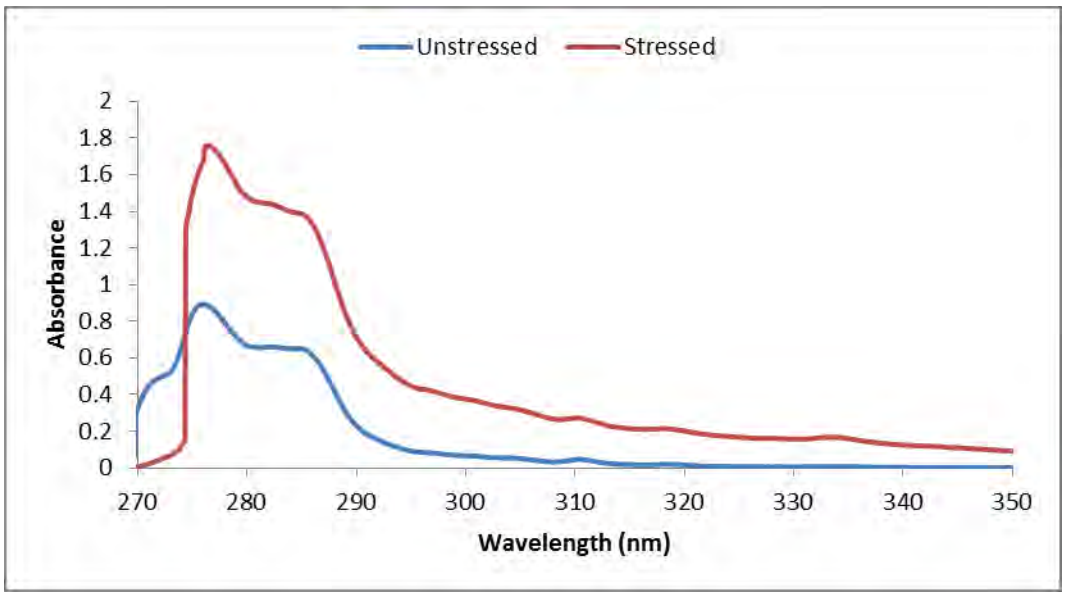

Figure 10-29: UV spectra of unstressed SME20 and stressed SME20 measured after 625× dilution in n-hexane.